

ฟลูออเรสเซนซ์เซ็นเซอร์จากการเกิดเอกไซเมอร์ของไพรีนและคัลเลอรีเมทริกเซ็นเซอร์จาก
ไนโตรเบนซีนสำหรับการตรวจวัดแอนไอออน

นางสาว ดวงรัตน์ ทองคำ

วิทยานิพนธ์นี้เป็นส่วนหนึ่งของการศึกษาตามหลักสูตรปริญญาวิทยาศาสตรดุษฎีบัณฑิต
สาขาวิชาเคมี ภาควิชาเคมี
คณะวิทยาศาสตร์ จุฬาลงกรณ์มหาวิทยาลัย
ปีการศึกษา 2553
ลิขสิทธิ์ของจุฬาลงกรณ์มหาวิทยาลัย

FLUORESCENT SENSORS FROM PYRENE EXCIMER FORMATION AND
COLORIMETRIC SENSORS FROM NITROBENZENE
FOR ANION DETECTION

Miss Duangrat Thongkum

A Dissertation Submitted in Partial Fulfillment of the Requirements
for the Degree of Doctor of Philosophy Program in Chemistry

Department of Chemistry

Faculty of Science

Chulalongkorn University

Academic year 2010

Copyright of Chulalongkorn University

Thesis Title FLUORESCENT SENSORS FROM PYRENE EXCIMER
FORMATION AND COLORIMETRIC SENSORS FROM
NITROBENZENE FOR ANION DETECTION
By Miss Duangrat Thongkum
Field of Study Chemistry
Thesis Advisor Professor Thawatchai Tuntulani, Ph.D.

Accepted by the Faculty of Science, Chulalongkorn University in Partial Fulfillment
of the Requirements for the Doctoral Degree

..... Dean of the Faculty of Science
(Professor Supot Hannongbua, Dr.rer.nat)

THESIS COMMITTEE

..... Chairman
(Assistant Professor Warinthorn Chavasiri, Ph.D.)

..... Thesis Advisor
(Professor Thawatchai Tuntulani, Ph.D.)

..... Examiner
(Associate Professor Sirirat Kokpol, Ph.D.)

..... Examiner
(Assistance Professor Soamwadee Chaianansutcharit, Ph.D.)

..... External Examiner
(Gamolwan Tumcharern, Ph.D.)

ดวงรัตน์ ทองคำ : ฟลูออเรสเซนต์เซ็นเซอร์จากการเกิดเอกไซเมอร์ของไพรีนและคัลเลอริเมตริกเซ็นเซอร์จากไนโตรเบนซีนสำหรับการตรวจวัดแอนไอออน.

(FLUORESCENT SENSORS FROM PYRENE EXCIMER FORMATION AND COLORIMETRIC SENSORS FROM NITROBENZENE FOR ANION DETECTION) อ. ที่ปรึกษาวิทยานิพนธ์หลัก

: ศ. ดร.ธวัชชัย ตันฑุลานี, 151 หน้า.

การทดลองส่วนแรกเป็นการสังเคราะห์พอลิเอทิลีนไกลคอลที่ปลายทั้งสองด้านประกอบด้วยไพรีนไทโอยูเรีย ได้แก่ **L1 – L3** และโมเลกุลเมทอกซีเบนซีนไพรีนไทโอยูเรีย **L4** เมื่อโมเลกุล **L1 – L3** จับกับฟลูออไรด์จะให้ความเข้มของการปล่อยแสงที่ตำแหน่งเอกไซเมอร์เพิ่มขึ้นและให้ความเข้มของการปล่อยแสงที่ตำแหน่งโมโนเมอร์ลดลง ในขณะที่โมเลกุล **L4** ให้ความเข้มของการปล่อยแสงใกล้เคียงกันทั้งสองตำแหน่ง โมเลกุล **L1** ให้ค่าคงที่การจับ (binding constant) สูงที่สุดเมื่อเทียบกับโมเลกุลอื่นเพราะการมีสายพอลิเอทิลีนไกลคอลที่ยาวช่วยลดผลของสเตอริกภายในโมเลกุล นอกจากนี้พบว่าสเปกตรัมของการปล่อยแสงของโมเลกุล **L1** ขณะที่ OH^- , AcO^- , BzO^- , H_2PO_4^- , Cl^- , Br^- และ I^- มีการเปลี่ยนแปลงน้อยหรือไม่มีการเปลี่ยนแปลง อัตราส่วนระหว่าง I_E (excimer intensity) และ I_M (monomer intensity) ของ **L1** ขึ้นอยู่กับความเข้มข้นของ **L1** ที่ใช้ แสดงว่าเป็นการเกิดไดเมอร์แบบระหว่างโมเลกุล (intermolecular excimer) ความเข้มข้นต่ำสุดของฟลูออไรด์ที่ทำให้เกิดเอกไซเมอร์ในโมเลกุล **L1** ได้คือ 2.3 ppm ในสารละลายคลอโรฟอร์ม

การทดลองส่วนที่สองเป็นการเปรียบเทียบสมบัติการเป็นเซ็นเซอร์สำหรับแอนไอออนระหว่างโมเลกุลที่มีความยืดหยุ่นสูง **R1** กับโมเลกุลที่มีความยืดหยุ่นเล็กน้อย **R2** โดยใช้เทคนิคการวัดการดูดกลืนแสงและเทคนิคนิวเคลียร์แมกเนติกเรโซแนนซ์สเปกโทรสโกปี พบว่าตัวรับทั้งสองมีความไวต่อ F^- , AcO^- , BzO^- และ H_2PO_4^- โดยมีแนวโน้มการเลือกจำเพาะตามลำดับ ดังนี้ $\text{F}^- > \text{BzO}^- > \text{AcO}^- > \text{H}_2\text{PO}_4^-$ ในอัตราส่วนระหว่างตัวรับและแอนไอออนเป็น 1:2 นอกจากนี้หากมีไอออนโซเดียมหรือโพแทสเซียม สมบัติการจับกับแอนไอออนจะแตกต่างกันออกไปซึ่งสามารถบอกความแตกต่างได้โดยใช้เทคนิคการวัดการดูดกลืนแสง

ภาควิชา.....เคมี.....ลายมือชื่อนิสิต.....
 สาขาวิชา.....เคมี.....ลายมือชื่อ อ.ที่ปรึกษาวิทยานิพนธ์หลัก.....
 ปีการศึกษา.....2553.....

4973817423 : MAJOR CHEMISTRY

KEYWORDS : PYRENE / EXCIMER / INTERMOLECULAR EXCIMER

DUANGRAT THONGKUM : FLUORESCENT SENSORS FROM
PYRENE EXCIMER FORMATION AND COLORIMETRIC SENSORS
FROM NITROBENZENE FOR ANION DETECTION. THESIS
ADVISOR : PROF. THAWATCHAI TUNTULANI, Ph.D., 151 pp.

In the first part, the polyethylene glycol (PEG) containing pyrene thioureas at both ends, **L1** – **L3**, and methoxy benzene pyrene thiourea, **L4**, were synthesized. Upon binding with F^- , **L1** – **L3** exhibited strong excimer emission bands and weak monomer emission bands, while **L4** displayed the same intensity of both bands. **L1** possessed the highest binding constant because a longer PEG chain may reduce steric hindrance on the receptor molecule. However, little or no change was observed in fluorescence spectra of **L1** upon adding OH^- , AcO^- , BzO^- , $H_2PO_4^-$, Cl^- , Br^- and I^- . Fluorescence intensity ratios of **L1**· F^- complex were dependent on the concentration of **L1**, implying that the dimerization of **L1** proceeded via intermolecular excimer interactions. Moreover, **L1** was able to give the excimer emission band even when the concentration of F^- was as low as 2.3 ppm in $CHCl_3$ solution.

The second part focused on the comparison of anion sensing properties between flexible and semi-rigid receptors of thiourea-nitrobenzene derivatives, **R1** and **R2**, by using UV-vis and 1H -NMR spectroscopy techniques. All the receptors were sensitive to F^- , AcO^- , BzO^- and $H_2PO_4^-$. The selectivity trends of **R1** and **R2** with anions were $F^- > BzO^- > AcO^- > H_2PO_4^-$ in 1: 2 ratios. In the presence of Na^+ and K^+ , receptors **R1** and **R2** were found to bind the mentioned anions to a different extent. Therefore, these anions can be distinctively detected by UV-vis spectrophotometry.

Department : Chemistry Student's Signature

Field of Study : Chemistry Advisor's Signature

Academic Year : 2010

ACKNOWLEDGEMENTS

I would like to thank my research advisor, Professor Dr. Thawatchai Tuntulani, for the opportunity he has given me to work in his laboratory and for his help in preparing this dissertation. He has spent with me discussing my research and also gives me a lot of great suggestions. Moreover, I would like also thank the thesis committee, Assistant Professor Dr. Warinthorn Chavasiri, Associate Professor Dr. Sirirat Kokpol, Assistance Professor Dr. Soamwadee Chaianansutcharit and Dr. Gamolwan Tumcharern for his/her valuable comments and suggestions regarding the revision.

I would like to thank Commission on Higher Education for supporting the grant under the program of Strategic Scholarships for Frontier Research Network. The Thailand Research Fund (RTA 5380003) is also acknowledged for financial support. I also thank Center for Petroleum, Petrochemicals, and Advanced Materials for their support.

Furthermore, I would like to thank Dr. Kanet Wongravee and Mr. Anusak Chaicham for MATLAB program and PCA calculation. I would like also thank my mentor, Ms. Matinee Jamkratoke, for her helpful. I have learnt many chemistry techniques from her. All members in Supramolecular Chemistry Research Unit (SCRU) have been pivotal in helping me complete my Ph.D. Their friendship during our graduate career has been invaluable.

Finally, I would like to appreciate my parents for their encouragement throughout my education.

CONTENTS

	Page
ABSTRACT (THAI)	IV
ABSTRACT (ENGLISH)	V
ACKNOWLEDGEMENTS	VI
CONTENTS	VII
LIST OF TABLES	IX
LIST OF FIGURES	XI
LIST OF ABBREVIATIONS	XVII
CHAPTER I INTRODUCTION	1
1.1 What is supramolecular chemistry?.....	1
1.2 Supramolecular interactions.....	1
1.3 Design of molecular sensors	2
1.4 Chromogenic sensors	2
1.5 Fluorescent molecular sensors.....	3
1.6 Formation of excimers.....	4
1.7 Principal Components Analysis (PCA).....	5
CHAPTER II LITERATURE REVIEWS	6
2.1 Literature reviews.....	6
2.2 Problems to be addressed.....	26
2.3 Objective and scope of research.....	28
CHAPTER III EXPERIMENTALS	31

	Page
3.1 Instruments, chemicals and general methods.....	31
3.2 Synthesis of receptor L1	31
3.3 Synthesis of receptor L2	36
3.4 Synthesis of receptor L3	39
3.5 Synthesis of receptor L4	41
3.6 Synthesis of receptor R1	43
3.7 Synthesis of receptor R2	44
3.8 Complexation studies of ligand L1 – L4	48
3.9 Complexation studies of ligand R1 and R2	52
3.10 Decomplexation studies of ligand L1 – L4	55
3.11 Decomplexation studies of ligand R1	58
3.12 Anion interference studies of ligand.....	59
3.13 Principal component analysis (PCA) for R1 with ions.....	60
CHAPTER IV RESULTS AND DISCUSSION	61
4.1 Fluorosensors L1 – L4	61
4.2 Chromogenic sensors R1 and R2	90
CHAPTER V CONCLUSIONS	106
REFERENCES	109
APPENDIX	114
VITAE	151

LIST OF TABLES

Table	Page
1.1 Description of the photophysical species	4
3.1 Amounts of anions (1.0×10^{-3} M) that added in 2 mL of ligands (L1 – L3 = 5.0×10^{-6} M) for complexation studies	49
3.2 Amounts of anions (1.0×10^{-2} M) that added in 2 mL of ligand L4 (5.0×10^{-5} M) for complexation studies	50
3.3 Amounts of fluoride (1.0×10^{-2} M) that added in 0.5 mL of ligands (L1 and L4 = 1.0×10^{-3} M) for complexation studies	51
3.4 Amounts of fluoride (5.0×10^{-5} M) and ligand L1 (5.0×10^{-5} M) that added in cuvette for Job's method	52
3.5 Amounts of anion or cation (5.0×10^{-3} M) that added in 2 mL of ligand (R1 and R2 = 2.5×10^{-5} M) for complexation studies	53
3.6 Amount of fluoride (0.1 M) that added in 0.35 mL of ligand R1 (1.0×10^{-2} M) for complexation studies	54
3.7 Amount of sodium (0.1 M) that added in 0.35 mL of ligand R1 (1.0×10^{-2} M) for complexation studies	54
3.8 Amounts of sodium that added in Ln ·100F solution for decomplexation studies	56
3.9 Amounts of fluoride that added in Ln ·10Na solution for decomplexation studies	57
3.10 Amounts of sodium that added in R1 ·4Anion solution for decomplexation studies	59
4.1 ^1H -NMR data for L1 – L4 in CDCl_3	64
4.2 ^{13}C -NMR data for L1 – L4 in d_6 -DMSO.....	64
4.3 The absorption and emission parameters for compound L1 – L4 in CHCl_3	66

Table	Page
4.4 The association constants (M^{-1}) of receptor L1 and various tetra-n-butylammonium anion salts in $CHCl_3$	72
4.5 The association constants (M^{-1}) for complexation of all receptors, L1 – L4 , with tetra-n-butylammonium fluoride in $CHCl_3$	75
4.6 Fluorescence intensity data of free L1 at 500 nm for repetition 10 times and its standard deviation.....	77
4.7 The absorption and emission parameters for compound R1 and R2 in DMSO.....	91
4.8 1H -NMR data for R1 and R2 in d_6 -DMSO.....	92
4.9 ^{13}C -NMR data for R1 and R2 in d_6 -DMSO.....	93
4.10 Association constants of all receptors with tetrabutylammonium anion salts in DMSO.....	98
4.11 Cations and anions response of compound R1	99
4.12 Cations and anions response of compound R2	99

LIST OF FIGURES

Figure	Page
1.1 Face-to-face and edge-to-face interactions between two benzene rings..	2
1.2 Perrin-Jablonski diagram	3
1.3 Fluorescence spectrum of monomer (400 nm) and excimer (500 nm) bands	4
2.1 The proposed binding mode of compound 1 and 2 upon addition fluoride	7
2.2 The proposed binding mode of 3 and fluoride.....	8
2.3 Structures of compound 4a – 4d	8
2.4 The proposed binding mode of compound 5 ·F ⁻ in aqueous media.....	9
2.5 Structure of receptor 6	10
2.6 Intermolecular proton transfer between 7 and the fluoride ion.....	11
2.7 Structure of compound 8	12
2.8 Structure of compound 9 (X = O) and 10 (X = S).....	12
2.9 Proposed $\pi - \pi$ interaction between two naphthyl moieties of compound.....	13
2.10 Structure of Imidazolium-functionalized fluoride binding receptor 12 .	14
2.11 Structures of chemosensor 13 – 14 and its proposed structures.....	15
2.12 Structures of compound 15 – 18	16
2.13 Structure of compound 19 and its metal chelation.....	17
2.14 Structure of sensor 20 – 24 and theirs proposed structures.....	18
2.15 Proposed binding mode of chemosensor 25	19

Figure	Page
2.16 Structures of the 26·Zn and 26·Zn·Na	20
2.17 Structures of oligo(ethylene glycols) 27b-h and compound 27a as a reference molecule.....	21
2.18 Proposed structures of oligo(ethylene glycols) 27b-h	21
2.19 Structure of compound 28	22
2.20 Interaction of tetrabutylammonium fluoride with compound 28 self-assembly which justifies the enhancement in fluorescence.....	22
2.21 Structure of N-P_n-N and CB[8].....	23
2.22 Cucurbit[8]uril-templated intramolecular photocycloaddition of N-P_n-N in aqueous solution.....	23
2.23 The concentration independence of I_e/I_m of CB[8] with various concentration of N-P₄-N (I_e : excimer intensity at 433 nm; I_m : monomer intensity at 373 nm).....	23
2.24 Eight-sensor structures and PCA score plot for four toothpaste brands and NaF.....	24
2.25 Six-sensor structures and PCA score plot of the first two PCs of the S1 – S6 array for eight-drinking water.....	25
2.26 Main classes of fluorescence molecular sensors of ions or molecules..	27
2.27 Structure of receptor 1 that was synthesized by Rittikulsittichai	28
2.28 Structures of fluorescence sensors L1 – L4	29
2.29 Structures of chromogenic sensors R1 and R2	30
4.1 Syntheses of fluorescence sensor L1 – L3	61
4.2 Syntheses of fluorescence sensor L4	62
4.3 UV-vis absorption spectra of fluorescence sensor L1 and L4	63
4.4 Fluorescence emission spectra of fluorescence sensor L1 – L4	63

Figure	Page
4.5 Linear plot for anthracene standard in EtOH.....	65
4.6 Linear plots for all synthesized ligands in CHCl ₃	66
4.7 Fluorescence changes of L1 with 100 equiv. of tetrabutylammonium anion salts in CHCl ₃	67
4.8 Plot of I _E /I _M (I _E : excimer fluorescence intensity at 500 nm; I _M : monomer fluorescence intensity at 398 nm).....	67
4.9 (a) Color changes of L1 (5.0×10 ⁻⁵ M) in the presence and absence of 500 equiv. of anions (from left to right: L1 , L1 +F ⁻ , L1 +BzO ⁻ , L1 +AcO ⁻ , L1 +H ₂ PO ₄ ⁻ , L1 +Cl ⁻ , L1 +Br ⁻ , and L1 +I ⁻) (b) Fluorescence changes of L1 after addition fluoride (from left to right: L1 , L1 +F ⁻) in CHCl ₃	68
4.10 Fluorescence titration of L1 with tetra-n-butylammonium fluoride in CHCl ₃	69
4.11 Job's plot of L1 (5.0×10 ⁻⁶ M) with tetra-n-butylammonium fluoride in CHCl ₃	70
4.12 Proposed conformations of L1 with fluoride ions in solution.....	70
4.13 (a) Fluorescence emission of various concentration of L1 (b) various concentration of L1 with fluoride (100 equiv.) (c) Plot of I _E /I _M of various concentration of L1 (b) various concentration of L1 with fluoride (100 equiv.).....	71
4.14 Example of Benesi-Hidebrand plot for calculation the association constant of L1 with fluoride anion.....	72
4.15 Fluorescence titration spectra of L2 with tetra-n-butylammonium fluoride in CHCl ₃	73
4.16 Fluorescence titration spectra of L3 with tetra-n-butylammonium fluoride in CHCl ₃	73
4.17 Fluorescence titration spectra of L4 with tetra-n-butylammonium fluoride in CHCl ₃	74
4.18 Fluorescence spectra of (a) L1 – L4 with 100 equiv. of tetra-n-butylammonium fluoride in CHCl ₃ (b) plot of I _E /I _M	75

Figure	Page
4.19 Fluorescence emission spectra of various concentrations of (a) L1 and (b) L4 with 100 equiv. of TBAF in CHCl_3	76
4.20 Plot of fluorescence intensity of L1 · F^- complex at 500 nm.....	77
4.21 Fluorescence spectra of L1 · F^- in different mixtures of methanol or hexane in chloroform solution.....	78
4.22 ^1H -NMR titration spectra of L1 · F^- in CDCl_3 at 400 MHz.....	79
4.23 (a) Full 2D NOESY spectrum (b) zoom-in on the range of polyethylene glycol (c) zoom-in on the range of aromatic of L1 · F^- in CDCl_3 at 400 MHz.....	80
4.24 ^1H -NMR spectra of L1 in the presence of 4 equiv. of tetrabutylammonium F^- , AcO^- , BzO^- and H_2PO_4^- in CDCl_3 at 400 MHz.....	81
4.25 Unfolded structure of L1 · F^- complex.....	82
4.26 ^1H -NMR titration of all the synthesized receptors with F^- in CDCl_3 at 400 MHz.....	82
4.27 Expected structures of L1 · F^- · Na^+ or L1 · Na^+ · F^-	83
4.28 Fluorescence titration spectra of L1 · F^- complex with sodium perchlorate in CHCl_3 : CH_3CN (9:1 v/v).....	84
4.29 Fluorescence titration spectra of L1 · 30Na^+ complex with tetra-n-butylammonium fluoride in CHCl_3 : CH_3CN (9:1 v/v).....	84
4.30 Fluorescence titration spectra of L4 · F^- complex with sodium perchlorate in CHCl_3 : CH_3CN (9:1 v/v).....	85
4.31 ^1H -NMR titration spectra of L1 · F^- with sodium perchlorate monohydrate in CHCl_3 : CH_3CN (9:1 v/v) at 400 MHz.....	86
4.32 ^1H -NMR titration spectra of L4 · F^- with sodium perchlorate monohydrate in CHCl_3 : CH_3CN (9:1 v/v) at 400 MHz.....	86
4.33 Proposed binding modes of L1 with fluoride and sodium.....	87
4.34 Selectivity of all the synthesized ligands toward each anion (100 equiv.) and the mixture of all anions.....	88

Figure	Page
4.35 Fluorescence changes of L1 (5.0×10^{-6} M) after addition 2.3 ppm fluoride.....	88
4.36 Syntheses of chemosensor R1 and R2	90
4.37 UV-vis titration spectra of R1 (2.7×10^{-6} M) with fluoride in DMSO...	94
4.38 UV-vis titration spectra of R2 (2.5×10^{-5} M) with fluoride in DMSO...	95
4.39 UV-vis titration spectra of R1 (2.5×10^{-5} M) with AcO^- in DMSO.....	95
4.40 UV-vis titration spectra of R2 (2.5×10^{-5} M) with AcO^- in DMSO.....	96
4.41 Titration profile of R1 · F^- at the wavelength 369 nm and 473 nm in DMSO.....	97
4.42 Titration profile of R2 · F^- at the wavelength 365 nm and 471 nm.....	97
4.43 Proposed structures of the R1 and R2 complexes.....	98
4.44 ^1H -NMR spectra of a) free R1 b) R1 + 4 equiv. F^- c) R1 + 4 equiv. F^- + 10 equiv. Na^+ in d_6 -DMSO at 400 MHz.....	100
4.45 ^1H -NMR spectra of a) free R1 b) R1 + 4 equiv. AcO^- c) R1 + 4 equiv. AcO^- + 10 equiv. Na^+ in d_6 -DMSO at 400 MHz.....	100
4.46 PCA score plot of the first two PCs for 25 samples of R1 and 4 anions.....	101
4.47 PCA score plot of the first two PCs for 10 samples of R1 and 2 metal ions.....	102
4.48 PCA score plot of the first two PCs for 10 samples of R1 · F^- sensor and 2 metal ions.....	103
4.49 PCA score plot of the first two PCs for 10 samples of R1 · AcO^- sensor and 2 metal ions.....	103
4.50 PCA score plot of the first two PCs for 10 samples of R1 · BzO^- sensor and 2 metal ions.....	104
4.51 PCA score plot of the first two PCs for 10 samples of R1 · H_2PO_4^- sensor and 2 metal ions.....	104

Figure	Page
4.52 PCA score plot of the first two PCs for 10 samples of 4 sensors and 2 metal ions.....	105

LIST OF ABBREVIATIONS

AcO ⁻	Acetate ion
CH ₃ CN	Acetonitrile
BzO ⁻	Benzoate ion
K _{ass}	Binding constant
Br ⁻	Bromide ion
¹³ C-NMR	Carbon Nuclear Magnetic Resonance
δ	Chemical shift
Cl ⁻	Chloride ion
CHCl ₃	Chloroform
COSY	Correlation Spectroscopy
<i>J</i>	Coupling constant
°C	Degree Celsius
CH ₂ Cl ₂	Dichloromethane
H ₂ PO ₄ ⁻	Dihydrogen phosphate
DMSO	Dimethylsulfoxide
equiv.	Equivalent
EtOAc	Ethyl acetate
F ⁻	Fluoride ion
g	gram
Hz	Hertz
HMBC	Heteronuclear Multiple Bond Correlation

HMQC	Heteronuclear Multiple Quantum Coherence
I_E	Intensity of excimer
I_M	Intensity of monomer
Γ	Iodide ion
K_2CO_3	Potassium carbonate
1H -NMR	Proton Nuclear Magnetic Resonance
μL	Microliter
mmol	Millimole
mL	Milliliter
M	Molar
NOESY	Nuclear Overhauser Enhancement Spectroscopy
M^{-1}	Per Molar
ppm	Part per million
s, d, t, m	singlet, doublet, triplet, multiplet
TBAF	Tetra-n-butylammonium fluoride
TLC	Thin-layer chromatography

CHAPTER I

INTRODUCTION

1.1 What is supramolecular chemistry?

Supramolecular chemistry is chemistry beyond the molecule, whereby a supermolecule is species that are held together by non-covalent interactions between two or more covalent molecules or ions. These interactions include electrostatic interactions, hydrogen bonding interactions, $\pi - \pi$ stacking interactions, van der Waals and hydrophobic effects [1].

Supramolecular chemistry can be divided into two main categories; host-guest chemistry and self-assembly. The difference between these two areas is a question of size and shape. If one molecule is significantly larger than another and can wrap around it then it is termed the host and the smaller molecule is its guest, which becomes enveloped by the host. Where there is no significant difference in size and no species is acting as a host for another, the non-covalent joining of two or more species is termed self-assembly [1].

1.2 Supramolecular interactions

Non-covalent interactions are the energies that hold supramolecular species together. The *hydrogen bond* is the most important non-covalent interaction in the design of supramolecular architectures, due to its strength and high degree of directionality. There are many non-covalent interactions such as dipole-dipole interactions between a proton donor (D) and a proton acceptor (A). Hydrogen bond donors are groups with a hydrogen atom attached to an electronegative atom (such as nitrogen or oxygen), therefore forming a dipole with the hydrogen atom carrying a small positive charge. Hydrogen bond acceptors are dipoles with electron-withdrawing atoms by which the positively charge hydrogen atom can interact (such as carbonyl moiety) [1].

The $\pi - \pi$ stacking interaction is also one type of non-covalent interactions that occur via a stacked arrangement of often aromatic molecules (such as benzene,

pyrene). The $\pi - \pi$ stacking interactions are caused by intermolecular overlapping of p-orbitals in π -conjugated systems. They become stronger as the number of π -electron increases. There are two types of $\pi - \pi$ stacking interactions, face-to-face and edge-to-face interactions as shown in Figure 1.1. The former is the interaction between the center of one ring and the corner of another, while the latter is the interaction between a hydrogen atom of one ring which is perpendicular to the center of another ring [1].

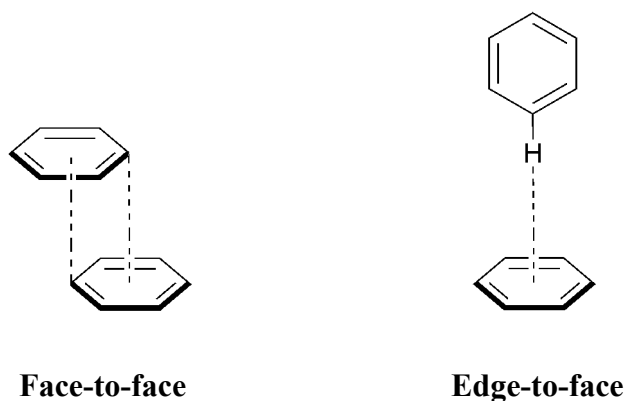


Figure 1.1 Face-to-face and edge-to-face interactions between two benzene rings

1.3 Design of molecular sensors

The development of molecular sensors for recognition of ions is one of the most challenging fields in supramolecular chemistry due to its implications in analytical applications [2]. The design of such molecular systems normally consists of two parts. The first part is a macrocyclic receptor unit or ionophore, which is responsible for coordination with selective ions via non-covalent interactions. The other part is an organic signaling unit, which is in charge of converting the binding event into easy-to-follow signal changes such as changes of color, electrochemical or fluorescence signals [3].

1.4 Chromogenic sensors

UV-visible absorption is an electronic transition from the promotion of an electron from the ground state to an unoccupied orbital by absorption of a UV-visible light. For example in $\pi \rightarrow \pi^*$ transition, the absorption of a photon of appropriate energy can promote one of the π electrons to the antibonding orbital denoted by π^* [4].

Chromogenic sensors or colorimetric sensors can be divided into two main parts: a receptor part for binding an analyte and the chromophore for giving a different color. When the interaction between the analyte and the receptor occurs, the receptor will definitely change its electronic properties. This results in an observable color change [5].

1.5 Fluorescent molecular sensors

The Perrin-Jablonski diagram in Figure 1.2 is convenient for visualizing the fluorescence process and other processes (such as photon absorption, phosphorescence) in a simple way. The singlet electronic states are denoted S_0 , S_1 , S_2 , ... and the triplet states, T_1 , T_2 , ... Fluorescence is an emission of photons accompanying the $S_1 \rightarrow S_0$ relaxation. Normally, the fluorescence spectrum is located at higher wavelengths than the absorption spectrum because of the energy loss in the excited state due to vibrational relaxation [4, 6-10].

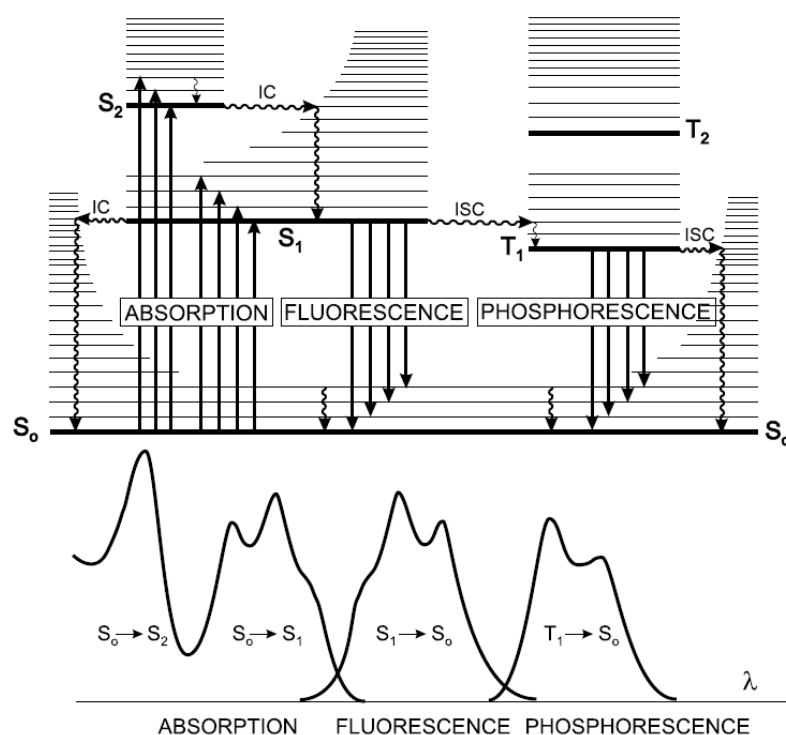


Figure 1.2 Perrin-Jablonski diagram [4]

In fluorescent molecular sensors, the fluorophore is the signaling unit that acts as a signal transducer to convert the event of ion recognition into fluorescence

signal. This sensor is particularly attractive because of sensitivity and fast response time.

1.6 Formation of excimers

An excimer is a dimer in an electronic excited state. This term results from the contraction of excited dimer. The formation of excimer requires the collision between an excited molecule and an identical unexcited molecule. For example, the pyrene excimer formed by the interaction of an electronically excited pyrene with a second pyrene in its ground electronic state (Figure 1.3) [4, 11].



Table 1.1 Description of the photophysical species

Symbol	Description
M	Fluorophore in the ground state
M*	Monomer in the excited singlet state
(MM)*	Excimer in the excited singlet state

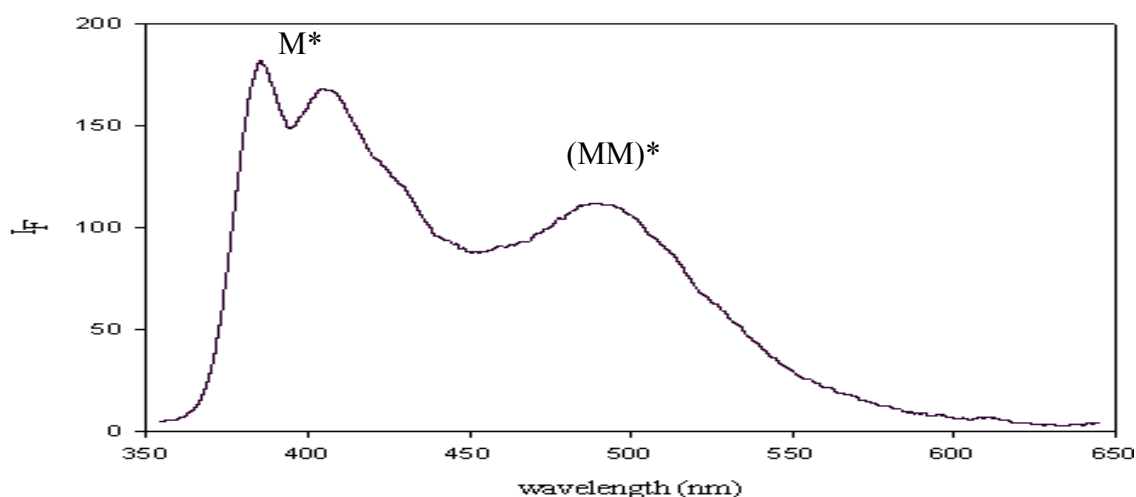


Figure 1.3 Fluorescence spectrum of monomer (400 nm) and excimer (500 nm) bands

1.7 Principal Components Analysis (PCA)

Chemical analysis can be handled more clearly by integration with mathematical and computation methods. This discipline is called Chemometrics, which is to analyze experimental results obtained by chemical measurements. In general, chemometrics includes mathematics, statistics and computer science to interpret and predict chemical results. Normally, there are many data for analysis from chemical measurements. For example, a UV-vis spectrum contains hundreds of wavelengths on a single sample. This means that there are multivariate data from one UV-vis spectrum. PCA is one of several mathematical methods that used a statistical treatment (calculating orthogonal eigenvectors) to explore patterns or reduce a multivariate data for easier interpretation. The aims of PCA are also to determine underlying information from multivariate raw data [12, 13].

CHAPTER II

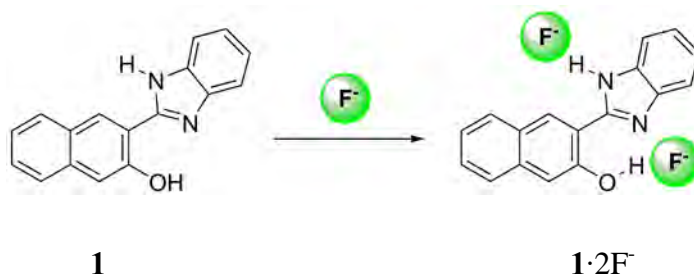
LITERATURE REVIEWS

2.1 Literature reviews

2.1.1 Chromogenic fluoride sensors

The selective sensing of fluoride has gained attention due to its significance in clinical treatment for osteoporosis and the detection of fluoride as a result of its over-accumulation in bones. A chromogenic sensor is particular interest due to its simplicity. Its molecule allowed naked-eye detection of an analyte without resort to any spectroscopic instrumentation [14].

In 2007, Kumar *et al.* synthesized receptors **1** and **2** containing naphthal and binaphthal for colorimetric and ratiometric fluorescence sensing of fluoride anion (Figure 2.1) [15]. On addition of fluoride anions, the appearance of a new absorption band between 400 and 440 nm in the case of **2** (but not in receptor **1**) resulted in visible change in colorless to yellow. The spectral fitting of the absorbance data showed the formation of LF_2 in the case of **1** and LF , LF_2 and LF_3 of **2**. The absorbance and emission titration data showed that monomeric receptor **1** simultaneously interacted with two fluoride ions to form LF_2 complex but the dimeric receptor **2** underwent stepwise complexation to form LF and LF_3 complexes. The 1H -NMR results showed that for **1** both the OH and NH proton interacted with fluoride simultaneously. However, in the case of **2**, at lower concentrations of fluoride ions the OH protons preferentially hydrogen bonded with fluoride and at higher concentrations of fluoride, stronger H-bonds between the benzene NH and fluoride ions took place.



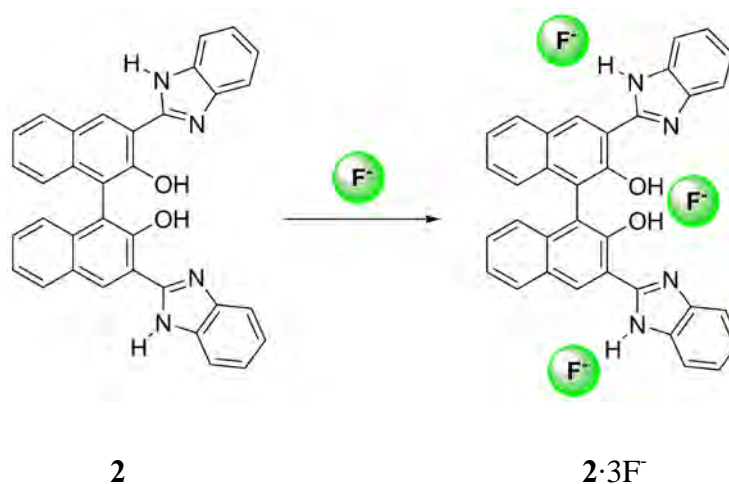
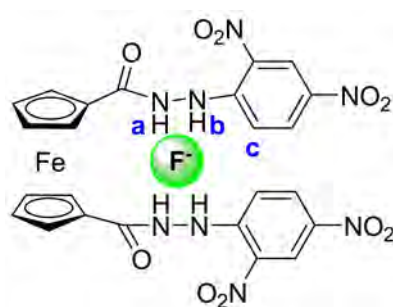


Figure 2.1 The proposed binding mode of compound **1** and **2** upon addition fluoride

In 2008, Lin *et al.* reported the colorimetric and electrochemical sensor for fluoride anion based on ferrocene and nitrophenylhydrazine or receptor **3** (Figure 2.2) [16]. The naked-eye detection provided the dramatic change from brown to red by addition of fluoride anion, whereas the acetate, dihydrogenphosphate, chloride, bromine or iodine resulted in slightly change in color. The UV-vis spectrum displayed the original peak at 345 and 496 nm due to the nitrophenylhydrazine. The titration spectra with fluoride showed the decrease of absorption intensity at 345 nm and the increase of absorption intensity at 496 nm, whereas these changes were insignificant in the other anions. Receptor **3** may have a proper cavity for fluoride, a spherical anion, which can match the receptor better than trigonal (AcO^-) and tetrahedral ($H_2PO_4^-$) anions. Furthermore, fluoride ion can form five-membered chelate ring with the carbonylhydrazine derivatives that is steadier than seven-membered chelate ring form by AcO^- or $H_2PO_4^-$. Finally, the stronger basicity of fluoride binding $-NH$ is much stronger than weaker base Cl^- , Br^- and I^- . 1H -NMR titration of **1** with fluoride displayed the broadened and amalgamated peaks of NH_a and NH_b due to fluoride combined with the receptor **3** by hydrogen bondings. Similarly, the H_c also shifted downfield because the $C-H_c$ bonds were polarized through ring effects and then partial positive charge on proton was created (through-space effect). On the other hand, the other aromatic protons were shifted to highfield due to the NH -fluoride hydrogen bond formations which increased the electron density of the phenyl ring (through-bond effect). The electrochemical response of receptor **3** showed the irreversible oxidation during the course of experiment, which was indicative of an EC

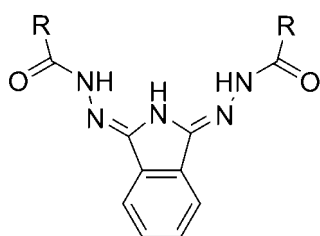
mechanism. The addition of fluoride caused the oxidation moving to more negative potentials.



3·F⁻

Figure 2.2 The proposed binding mode of **3** and fluoride

In 2008, Jurczak *et al.* synthesized bishydrazide derivatives of isoindoline scaffold (Figure 2.3) [17]. Pyrrole could act as a hydrogen bond donor and a risk of formation of unfavorable intermolecular hydrogen bond was diminished. These ligands contained **R** groups of various acids: caproic, benzoic, picoline, and 2-pyrrolicarboxylic acid. Therefore, aliphatic derivative, **4a**, should have the least acidic NH protons, thus being the weakest binder in the series. Compound **4d** possessed two additional anchoring points and its enhanced affinity toward anions could be expected. For all ligands, the most spectacular color changes were detected for highly basic anions (i.e. fluoride), it is likely that the color changes were mainly an effect of ligand deprotonation, rather than the anion complexation. To check this hypothesis, the UV-vis spectra of ligands and TBA salts were compared with TBA hydroxide.



4a – 4d

4a R = n-C₆H₁₁

4b R = Ph

4c R = 2-Pyridine

4d R = 2-Pyrrole

Figure 2.3 Structures of compound **4a – 4d**

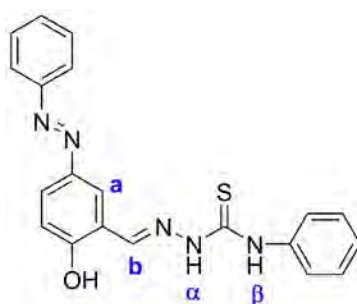
In 2009, Lin *et al.* synthesized a simple salicylaldehyde-based receptor **5** (Figure 2.4), which is an organic colorimetric chemosensor for recognition of fluoride anion by naked-eye detection in aqueous solution (DMSO: H₂O 9:1 v/v) [18]. Upon the addition of fluoride, the absorption peak at 430 nm decreased but that at 502 nm increased, which was ascribed to the charge transfer (CT) between the fluoride bound –NH and –OH units and the electron deficient –NO₂ moiety. The color of the sensor solution changed from yellow to red at the same time. ¹H-NMR titration data showed the downfield shift of aniline –NH and phenol –OH upon addition of 0.5 equiv. of fluoride. This indicated the formation of a hydrogen bonding complex. With further adding 2 equiv. of fluoride, the signals of these protons were disappeared and the phenyl protons, a and b, positions moved upfield, which indicated the increase of the electron density on the phenyl ring.



Figure 2.4 The proposed binding mode of compound **5·F⁻** in aqueous media

In 2009, Lin *et al.* synthesized an anion receptor containing azobenzene with hybrid –OH. UV-vis titrations were carried out in DMSO (Figure 2.5) [19]. This receptor exhibited strong absorption at 340 nm with a shoulder at 470 nm, which was assigned to the charge transfer of the azo moiety. The UV-vis spectra of **6** with F⁻, AcO⁻ showed similar effect with H₂PO₄⁻. As the concentration of H₂PO₄⁻ was increased, the absorption intensity at 340 nm gradually decreased and a new absorption peak at 480 nm increased, which was accompanied by a visual color change from light yellow to orange. The selectivity trend of binding affinity of **6** for anions followed the order: H₂PO₄⁻ > AcO⁻ > F⁻ > Cl⁻ ≈ Br⁻ ≈ I⁻. The multiple hydrogen bond interactions of H₂PO₄⁻ with receptor **6** and its configuration may well match **6** in terms of shape. As expected from their basicity, H₂PO₄⁻, AcO⁻ and F⁻ would bind

more strongly than the other halide anions. Two effects would be expected to result from the formation of hydrogen bond between the binding sites and the fluoride anion: (1) through-bond effects, which increase the electron density of phenyl ring (H_a and H_b) and promote upfield shifts in 1H -NMR spectrum and (2) through-space effects, which polarize C-H bond in proximity to hydrogen bond, create the partial positive charge on the proton and cause the downfield shift. The peak of $-OH$ disappeared upon addition of fluoride and at the same time a new peak of $[HF_2^-]$ at 16.10 ppm was observed. The signals of NH_α and NH_β exhibited the broadened peak and the downfield shift due to the hydrogen bonding interaction with fluoride.



6

Figure 2.5 Structure of receptor **6**

In 2010, Tian *et al.* designed and synthesized the diketopyrrolopyrrole (DCM) compound **7** which was a colorimetric and a ratiometric red fluorescent sensor for fluoride anion (Figure 2.6) [20]. When TBAF was added to the DCM solution of **7**, an apparent color changed from orange to purple in ambient light and can be observed by naked-eye. The UV-vis spectra at 497 nm of $7 \cdot F^-$ were gradually decreased and showed a large bathochromic shift following a new band at 594 nm was developed. The emission spectra also displayed a decrease of the emission at 563 nm and the emergence of a red shift band at 635 nm was observed. A possible explanation for the ratiometric absorption changes was IPT (intermolecular proton transfer) process between the amide moiety and fluoride ion and its change from electronically neutral without fluoride to negatively charged with fluoride ($Ar-DPP-NH-Ar \rightarrow Ar-DPP-N^--Ar$). In the presence of fluoride, the ICT (internal charge transfer) effect from the amide to the electro-withdrawing moiety was enhanced, which was facilitated by deprotonation of amide moiety. This enhancement in ICT

effect also afforded the reduced intensity and bathochromic shift of fluorescence as a function of fluoride concentration. The $^1\text{H-NMR}$ titration confirmed the breaking of hydrogen bonding when fluoride ion was added by the decrease and disappearance of the amide proton signal.

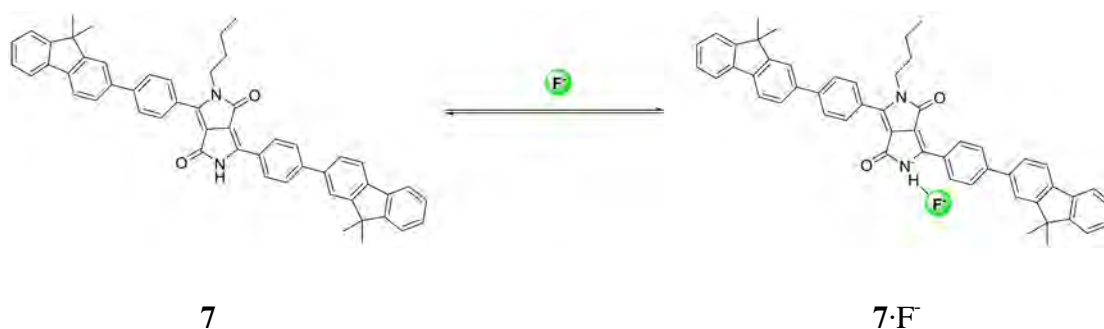


Figure 2.6 Intermolecular proton transfer (ICP) between **7** and the fluoride ion

2.1.2 Fluorescence fluoride sensors

Many excellent fluorescent sensors for fluoride ion detection had been reported [21]. The recognition unit of these sensors normally contains the polarized NH fragment, which act as H-bond donors towards fluoride ion [22]. Hydrogen-bonding sites typically used are urea, thiourea, amide, phenol, or pyrrole moieties. Among them, the thiourea group often chosen as anion binding site because it gives strongly hydrogen-bonded complexes with different anions such as acetate, phosphate and fluoride [23].

In 2007, Lin *et al.* synthesized the multiple hydrogen bond receptor **8** based on guanidinium group (Figure 2.7) [24]. Interactions of **8** with halide and benzoate anions were studied by NMR spectroscopy, fluorescence spectroscopy, and calorimetry experiments. Introduction of fluoride ion caused broadening of the $^1\text{H-NMR}$ signals. This may result from rapid proton exchange due to deprotonation. The emission spectrum of **8** with increasing concentrations of fluoride ion displayed little change upon addition of initial increments of fluoride. However, a dramatic change began as the ratio of fluoride anion to receptor reached 1 equiv. Therefore, the noncovalent complex with fluoride ion was initially formed. Fluoride ion acted as a base to deprotonate **8** with formation of the FHF^- ion. The result from isothermal titration calorimetry (ITC) indicates that as ΔH was much greater for reaction with 2

equiv of fluoride, the initial binding step must be more entropically favorable than the deprotonation step under these conditions.

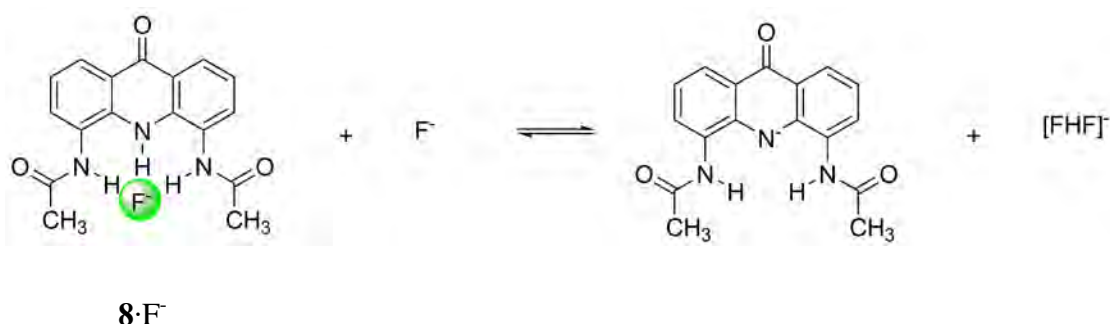


Figure 2.7 Structure of compound **8**

In 2008, Chauhan *et al.* developed simple sensors **9** and **10** having urea/thiourea binding sites based on phenazine signaling unit (Figure 2.8) [25]. The fluoride interacted with receptors **9** and **10** more strongly due to its high electronegativity and small size compared to other halides. However, the color change of thiourea **10** was much more sensitive to fluoride than that of urea **9**. The color changes were probably due to the formation of hydrogen bond interactions between the urea or thiourea groups and the fluoride anion. On addition of fluoride ion, the characteristic absorption peaks of **9** and **10** at 400 nm decreased gradually with a strong red shift and the new peaks at 500 nm were observed. The absorption intensity of **10·F⁻** complex at 500 nm was greater than the intensity of **9·F⁻**. This result showed that fluoride bound more tightly with thiourea than with urea, indicating the formation of stronger hydrogen bonds between the acidic N-H groups of thiourea **10** and fluoride.

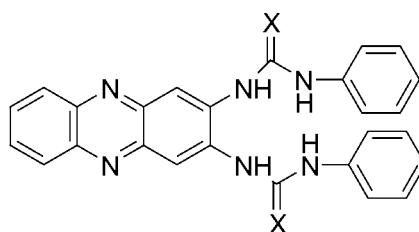
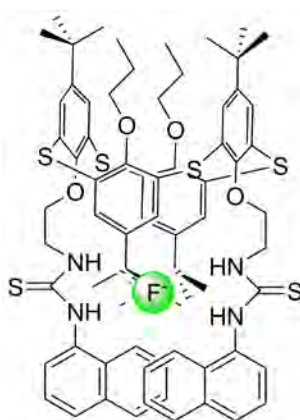


Figure 2.8 Structures of compound **9** (X = O) and **10** (X = S)

In 2009, Kumar *et al.* reported a selective fluorescent sensor **11** for fluoride ion based on thiacalix[4]arene with two naphthyl moieties (Figure 2.9) [22].

This compound did not show any fluorescence emission band when excited at 310 nm. Upon addition of fluoride ion to the solution of compound **11**, a significant increase in fluorescence emission at 385 nm was observed. The increase in fluorescence emission was attributed to the intermolecular binding interactions of fluoride ion with NH protons of thiourea moieties trigger the intramolecular $\pi - \pi$ interactions of naphthyl group, which led to excimer formation. From $^1\text{H-NMR}$ study, there were remarkable downfield shifts in NH proton due to the hydrogen bond formed between thiourea NH protons and fluoride ion.



11

Figure 2.9 Proposed $\pi - \pi$ interaction between two naphthyl moieties of compound **11** and hydrogen bond interaction between thiourea groups and fluoride ion

In 2009, Yu *et al.* have developed the multifunctional receptor for both chromogenic and chiral anion recognition [26]. The receptor **12** contained OH groups and imidazolium rings that linked with the binaphthyl backbone for the construction of the unique chiral (Figure 2.10) and provided the interesting fluorescence signals. When the receptor **12** was excited, the new intense peak was observed in the presence of F^- or CH_3CO_2^- . Therefore, the receptor **12** displayed the F^- and CH_3CO_2^- recognition selectivity due to the excited state intermolecular proton transfer in the sensor-anion complexes. The most obvious $^1\text{H-NMR}$ spectral changes were observed by treatment with F^- . The imidazolium C(2)-H displayed a large downfield shift due to the strong hydrogen bond between C(2)-H of imidazolium ring and F^- . Moreover, a triplet peak of FHF was found at 16.1 ppm. While several aromatic peaks displayed the strong highfield shifts because the F^- induced the change of electronic distribution

in naphthyl and imidazolium rings. In addition, the host receptor **12** was examined for chiral recognition with various amino acid derivatives and displayed a remarkable binding ability for *t*-Boc alanine anion.

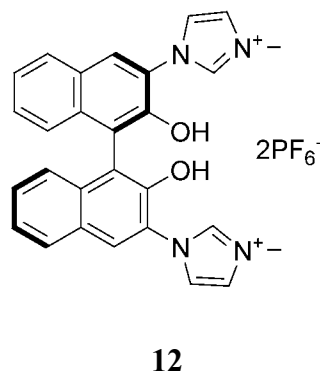


Figure 2.10 Structure of Imidazolium-functionalized fluoride binding receptor **12**

2.1.3 Intermolecular pyrene stacking

A molecule with two reactive groups separated by a flexible link may undergo either *intramolecular* or *intermolecular* reactions. Intramolecular reaction gives macrocyclic ring-closure products, while intermolecular reaction results in dimers, oligomers and polymers. Thus cyclization suffers from intermolecular reactions. The rates of intermolecular reactions are dependent on the substrate concentration or monomer concentration, while those of the intramolecular reactions are not, since the effective concentration for intramolecular reaction is constant by virtue of tether between the two functional groups [27].

In 2007, Gozin *et al.* synthesized the pseudocyclic trithiourea chemosensor **13** and a model of folded monomeric structure or chemosensor **14** (Figure 2.11) [28]. In DMSO or chloroform, chemosensor **13** formed folded and/or dimeric structures in solution. There was a very similar anion-binding pattern for chemosensor **13** in both solvents, $\text{H}_2\text{PO}_4^- > \text{F}^- > \text{CH}_3\text{CO}_2^-$. The highest affinity of dihydrogenphosphate was due to its geometry and ability to form hydrogen bond with more than one thiourea group. Therefore, chemosensor **13** preferred binding with larger dihydrogenphosphate to smaller fluoride and acetate anions. However, the amount of excimer and the polarity of a solvent affected the molecular structure. Chloroform strongly influenced hydrogen bonding between thiourea groups and DMSO gave the stronger excimer emission. In contrast to **13**, chemosensor **14**

Py* formation to show an intense static excimer band. Density function theory calculations were executed for energy minimized structures of **15** – **17**. In the case of free **15**, the H-bond is fairly weak due to the steric hindrance between the proximate pyrene groups. However, in the case of free **16** and **17**, stable H-bonding between two amide groups was available to form stable dimers. Therefore, the binding energy for the free dimer **17** with two H-bonds was found to be higher than that of **16** and **15**, respectively. Addition of Cu^{2+} to the dimers of **16** and **17** disrupted this stable H-bonding, which would perturb stable electrostatic interactions between two monomer units. The interaction of Cu^{2+} with **16** or **17** may be thermodynamically less favorable compared to addition of Cu^{2+} to the dimer of **15**.

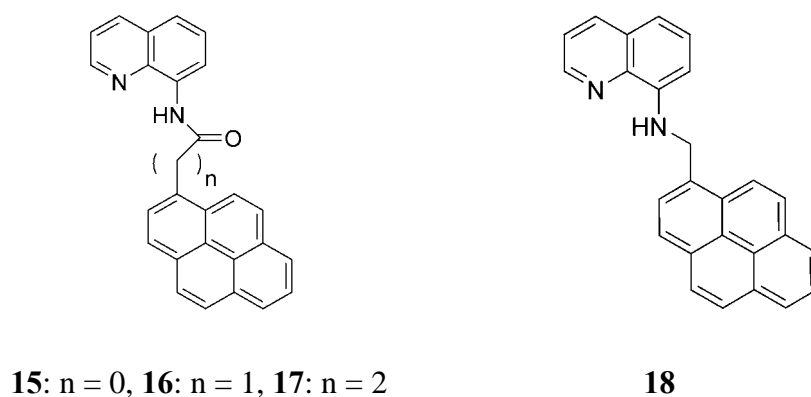


Figure 2.12 Structures of compounds **15** – **18**

2.1.4 Intramolecular pyrene stacking

In 2006, Koskinen *et al.* described the metal (Zn^{2+} and Li^+) chelation of the molecular pincer based on crown ether and salen ligand or compound **19** (Figure 2.13) [30]. By monitoring with fluorescence spectroscopy, compound **19** gave only weak fluorescence when excited at 347 nm. When solution was titrated with $\text{Zn}(\text{ClO}_4)_2$, the emission intensity increased at 475 nm and then stayed stable at 100 mole%. The fluorescence intensity returned to the level of nonchelated compound **19** by adding 100 mole% of EDTA, which was known to trap transition metal. The ditopic chelation ability was studied by adding LiCl to the **19**· Zn solution. The intensity dropped and then remained stable until 100 mole% of Li^+ because of the Li^+ coordination to the crown ether causing a disturbance in the pyrene excimer. Moreover, titration of **19** with Li^+ indicated the chelation also possible with single metal ion.

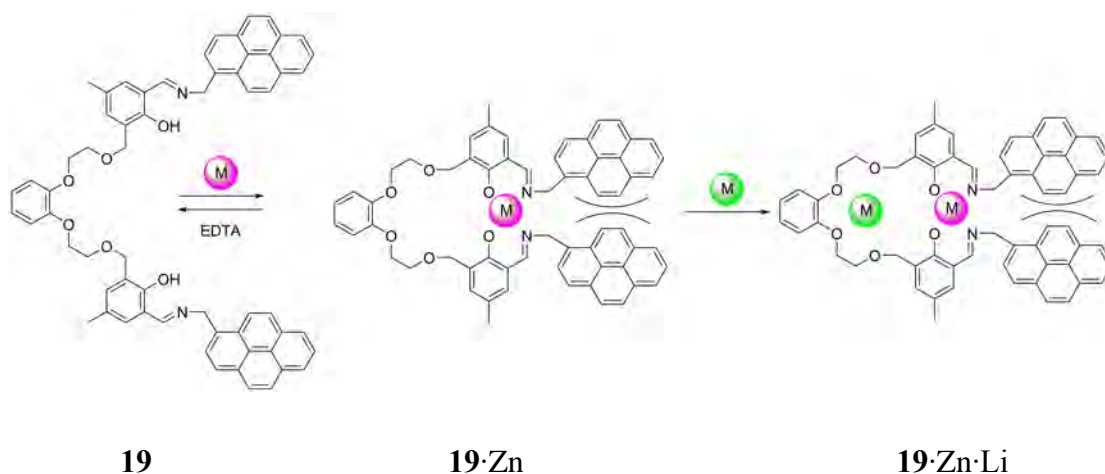


Figure 2.13 Structure of compound **19** and its metal chelation

In 2009, Chung *et al.* reported the synthesis of many fluorescent sensors with variable methylene chain lengths as spacer between the two triazole methyl ether units (Figure 2.14) [31]. All of them showed a strong excimer emission around 482 nm due to the overlap of two pyrene units in an intramolecular $\pi \rightarrow \pi$ stacking and displayed weak monomer emission around 376 and 396 nm. The fluorescence quenching of monomer emission was observed by the addition of Cu^{2+} , Hg^{2+} , and Cr^{3+} ions in the solution of **20**. This result was similar to the data from the mono-triazole model compound **24**. Therefore, metal ions may be complexed by both the triazole group(s) and the oxygen atom(s). The quenching of monomer emission can be explained as a reverse PET as well as a heavy atom effect, that is, the pyrene units behaved as a PET donor and the metal ion bound triazole groups acted as an electron acceptor. The quenching of excimer emission resulted from the conformational change caused by the two outward-facing triazole groups that turned inward upon binding with metal ions. Similar fluorescence quenching by these metal ions was also observed in compound **21** – **23**. However, the fluorescence of compound **23** revealed two different types of binding modes: (1) for Cu^{2+} , Hg^{2+} , Cr^{3+} , Pb^{2+} , and Ni^{2+} , the monomer and excimer emissions were both quenched, and (2) for Cd^{2+} and Zn^{2+} ions, the monomer emission was enhanced but the excimer emissions was quenched. In the $^1\text{H-NMR}$ titration of **23** with Hg^{2+} or Pb^{2+} , the methylene protons exhibited upfield shifts. Normally, the complexation is expected to reduce the electron density of the coordination sites and induce a downfield shift of the nearby protons; however, upfield shift was observed. There must be a change of conformation which causes the methylene protons to be shielded by the pyrene rings (Cu^{2+} , Cr^{2+} , Ni^{2+} ions were not

analyzed due to the high spin states). Upon addition of Cd^{2+} , the H_b and H_c protons were slightly upfield shift but H_d , H_e , and H_f were more upfield shift. Therefore, the chemical shift of H_b was affected more strongly by Pb^{2+} than by Cd^{2+} . This implied that compound **23** complexed were in a different mode.

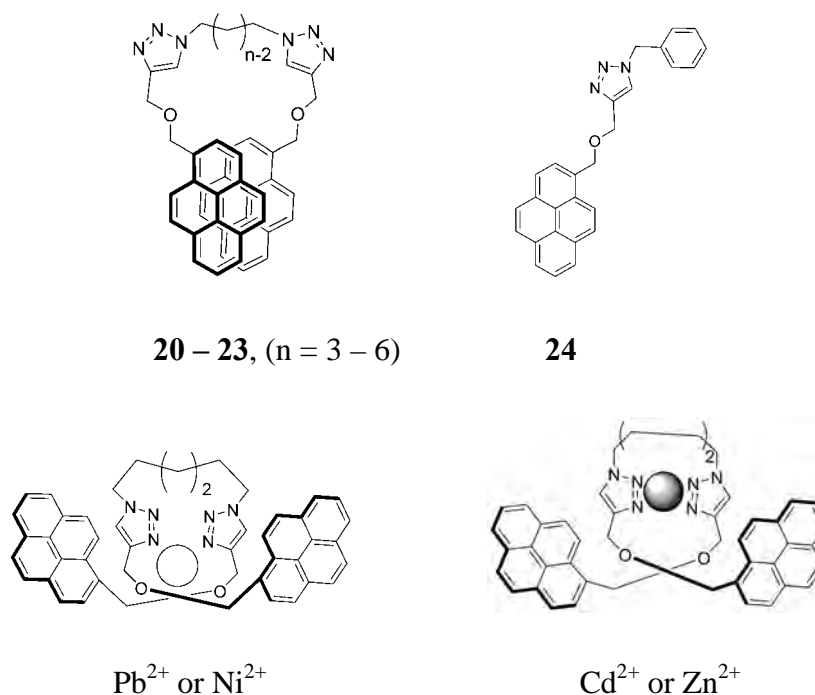


Figure 2.14 Structure of sensor **20 – 24** and theirs proposed structures

In 2010, Yao *et al.* synthesized a pyrene-based derivative bearing an azadiene group or chemosensor **25** as a ratiometric chemosensor for Hg^{2+} (Figure 2.15) [32]. The absorption spectrum of **25** with Hg^{2+} displayed the formation of the new low-energy band. This attributed to the interaction of Hg^{2+} with the imino nitrogens leading to the intramolecular charge transfer from the pyrene moieties to the imino groups. The fluorescence characteristics of **25**· Hg^{2+} were found to be strongly dependent on the medium. The pyrene excimer band increased significantly as the water content in acetonitrile increased. This observation implied that complexation structure of **25** with Hg^{2+} ions changed from its chair conformation to stacked or folded conformation resulting in the switch of the pyrene monomer emission to an excimer emission. The $^1\text{H-NMR}$ results suggest that Hg^{2+} coordinated with the imino forms $\text{Hg} - \text{N}$ bonding and that O atoms form $\text{Hg} - \text{O}$ bonding, which force the two pyrene moieties to become folded. The conformational changes result in the weak pyrene monomer emission to strong pyrene excimer emission switch.

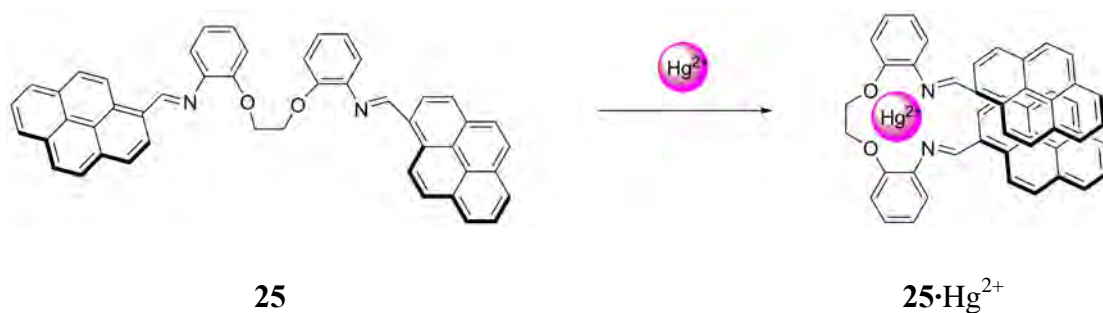


Figure 2.15 Proposed binding mode of chemosensor **25**

2.1.5 Ions or molecules induced conformational changes

In general, host flexibility is a key importance, especially in biological systems, in which recognition of a substrate results in a conformational change, for example, in a protein's biochemical role [1]. In most cases, the driving forces to induce conformational change come from varying intramolecular interactions. Example for this approach includes the folded backbone of oligomeric arylamide to recognize small organic molecule. Another approach makes use of external interaction. In this case, the backbones themselves are structurally flexible but may fold to convergent conformations through binding a neutral or ionic template [33].

In 2001, Monti *et al.* studied the effect of the inclusion of sodium on the binding features of the oligooxaethylene diporphyrin receptor or compound **26** (Figure 2.16) [34]. The **26**·Zn was a good receptor for several ditopic amines such as 4, 4'-bipyridine (bpy) and trans-1, 2-diaminocyclohexane (1, 2-DACy). However, the receptor **26**·Zn bound to bpy more strongly than 1, 2-DACy. This may indicated that the shorter N – N distance of 1, 2-DACy produced some degree of ring strain. The complexation studies were also performed in the presence of added Na⁺, which known to promote a conformational change toward a pseudo-cyclic structure (**26**·Zn·Na). The case for 1, 2-DACy showed the increase of the binding constant. Conversely, in case of bpy which was a longer guest, the decrease of binding constant was observed. This can be interpreted in term of a less favorable interaction of bpy with in the less flexible cavity of the host.

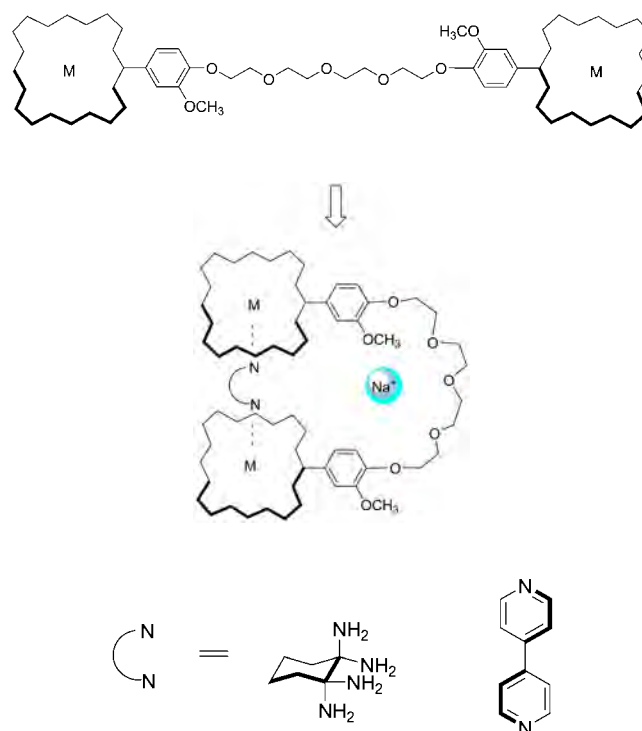


Figure 2.16 Structures of the **26·Zn** and **26·Zn·Na**

In 2004, Chen *et al.* described that the oligo(ethylene glycols) incorporating with 2,3-naphthalene unit or **27b-h** (Figure 2.17) could spontaneously form stable helical foldamer conformation in polar solvent such as acetonitrile and DMSO (Figure 2.18) [35]. It has been established that in polar solvents the non polar aromatic units of linear molecule tend to aggregate or stack intermolecularly or intramolecularly as a result of hydrophobic interactions. The UV-vis study was first performed in acetonitrile or chloroform to exclude intermolecular interaction. All oligomers displayed similar results in both solvents that were the absorbance dependence on the concentration range which followed Beer's law. Therefore, the experiment ruled out any important intermolecular interactions. Moreover, hypochromic effect occurred at lower concentration of acetonitrile (binary solvent system, CH₃CN:CHCl₃) for the longer oligomers suggesting that the longer oligomers had greater folding ability because their increased hydrophobicity and implied that the stacking was cooperative. ¹H-NMR spectra showed the upfield shift of all peaks of **27b-h** compared to **27a** due to intramolecular naphthalene stacking and oligo(ethylene glycol) folding. The lower resolution and the higher upfield shifting of the aromatic proton peaks of the longer oligomers also supported more folding state of the skeleton. The fluorescent study also supported the folded conformations

for long oligomers (**27d-h**) in polar solvent, which increased the excimer emission with the lengthening of the oligomers. In addition, the NOEs experiment in CD_3CN revealed the correlation between the ethylene protons of **27f** and some methylene protons.

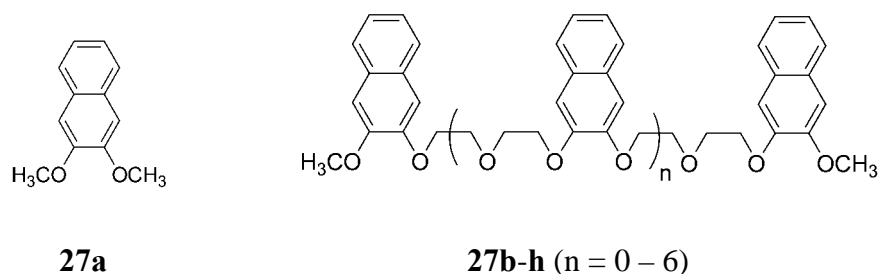


Figure 2.17 Structures of oligo(ethylene glycols) **27b-h** and compound **27a** as a reference molecule

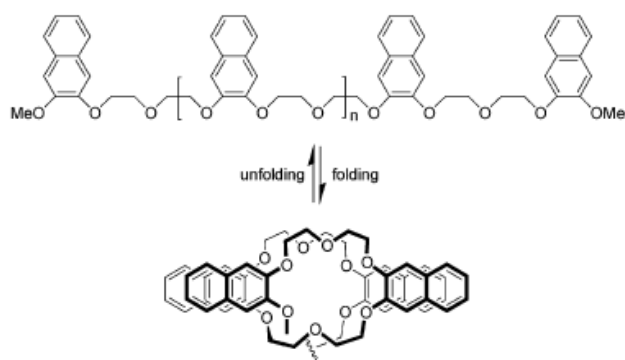
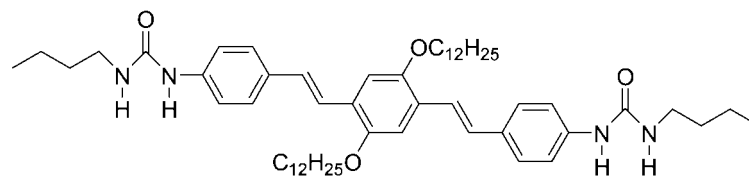


Figure 2.18 Proposed structures of oligo(ethylene glycols) **27b-h** [35]

In 2005, Ajayaghosh *et al.* reported the anion controlled modulation of oligo(phenylenevinylene) or compound **28** architectures with tunable optical properties (Figure 2.19) [36]. This molecule formed a stable one-dimensional assembly by the cooperative interaction of H-bonding between the urea groups and π -stacking between the aromatic moieties (Figure 2.20). Moreover, this molecule was sensitive to solvents such as chloroform, the absorption spectrum showed the characteristics of molecule **28** and showed a strong emission indicating that they were not aggregated. However, in cyclohexane (non-polar solvent), the UV-vis spectrum was broad and the fluorescence was significantly quenched indicating strong intermolecular interactions between molecules. Since halide anions are known to compete with urea H-bonds, non-emissive molecule of urea oligo(p-phenylenevinylene) fluorophore turned strongly emissive in the presence of

tetrabutylammonium fluoride due to fluoride induced the breaking of H-bond and π stack assisted self-assembly of molecule thereby reinstating the strong emission of the oligo(p-phenylenevinylene) unit.



28

Figure 2.19 Structure of compound 28

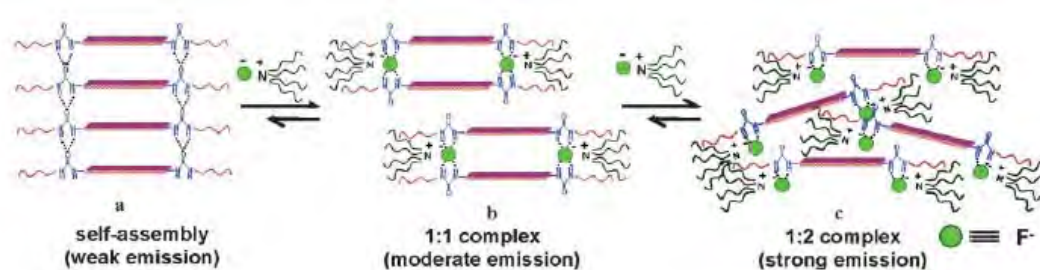


Figure 2.20 Interaction of tetrabutylammonium fluoride with compound 28 self-assembly [36]

In 2008, Wu *et al.* reported the photocycloaddition of 2-naphthalene poly(ethyleneglycol) or N-P_n-N by using cucurbit[8]uril or CB[8] templates (Figure 2.21) [37]. There are hydrophobic cavity and polar carbonyl group surrounding the portal of CB[8]. Therefore, the CB[8] can encapsulate the hydrophobic or/and positively charged guest molecule in aqueous solution such as the naphthalene of N-P_n-N molecule. More importantly, N-P_n-N may undergo either intramolecular or intermolecular reactions. The former produces a macrocyclic ring-closure, while the latter results in dimer and oligomers. Generally, the intramolecular reaction can proceed in good chemical yields only at very low concentrations in solution since it suffers from the competition of polymerization. However, CB[8] can capture the two naphthalene groups of N-P_n-N to make a 1:1 inclusion complex like a molecular loop (Figure 2.22). As a result, the intermolecular reaction might be prohibited. The fluorescence spectrum of N-P_n-N exhibited the monomer emission at 370 nm. The addition of CB[8] into N-P_n-N led to a growth of excimer emission at 430 nm. In

addition, the ratio of fluorescence intensities of excimer to monomer was independent of the concentration used, suggesting that the excimer occurred intramolecularly (Figure 2.23).

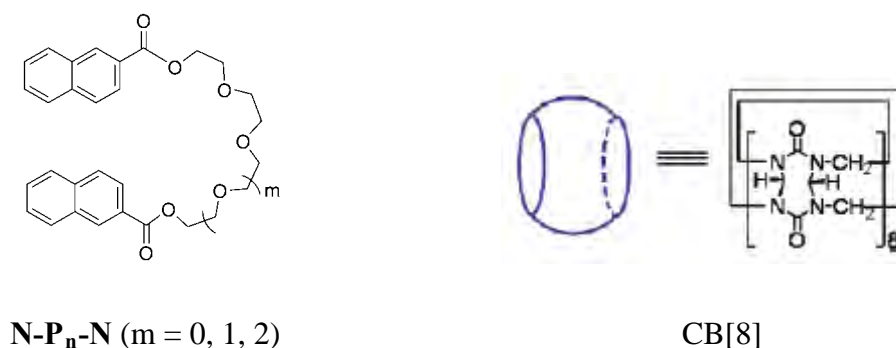


Figure 2.21 Structure of $\text{N-P}_n\text{-N}$ and $\text{CB}[8]$

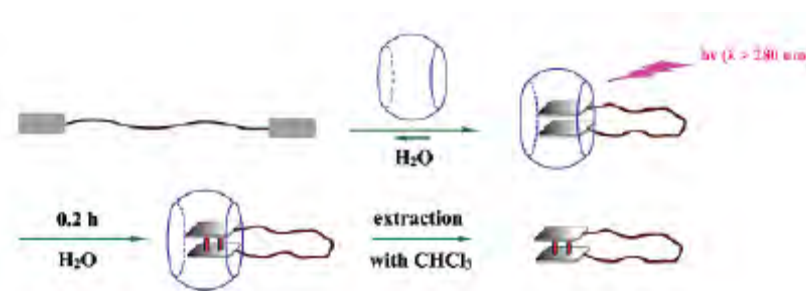


Figure 2.22 Cucurbit[8]uril-templated intramolecular photocycloaddition of $\text{N-P}_n\text{-N}$ in aqueous solution [37]

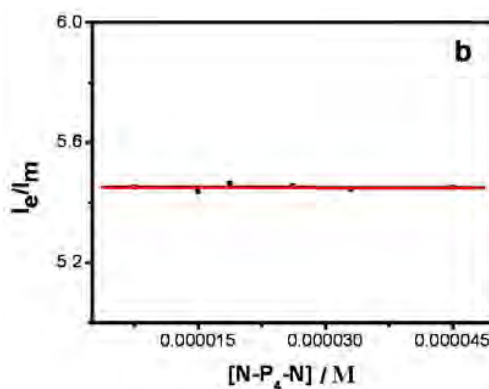


Figure 2.23 The concentration independence of I_e/I_m of $\text{CB}[8]$ with various concentration of $\text{N-P}_4\text{-N}$ (I_e : excimer intensity at 433 nm; I_m : monomer intensity at 373 nm) [37]

2.1.6 Principal Components Analysis (PCA)

In 2007, Anzenbacher *et al.* reported the applicability of eight-sensor array for analysis ten inorganic anions (AcO^- , BzO^- , Br^- , Cl^- , F^- , NO_3^- , H_2PO_4^- , $\text{HP}_2\text{O}_7^{3-}$, HSO_4^- , HS^-) and four toothpaste brands using image that was recorded by scanning the array slides [13]. The array showed good separation in PCA score plot. Figure 2.24 represented an example of the score plot obtained after performing PCA for four toothpaste brands and NaF with eight sensors. Here, the PCA score plot shows 81.1% of the certain level of discrimination, and it displays clear clustering. The PC1 (52.4%) is higher than PC2 (28.7%). From the plot, Aquafresh, Colgate, and Crest appear to be more similar than Fluoridex and NaF. This approach could be applied for other analytes and applications.

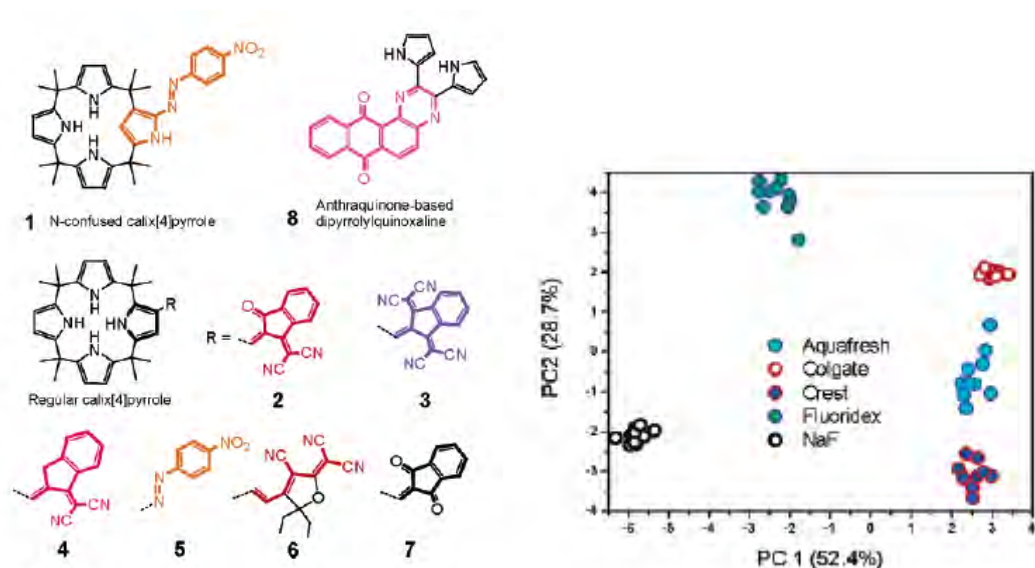


Figure 2.24 Eight-sensor structures and PCA score plot for four toothpaste brands and NaF [13]

In 2008, they designed fluorescent sensor arrays (**S1** – **S6**) for cations using chromophore attached to 8-hydroxyquinoline [38]. This array could discriminate 10 cations (Ca^{2+} , Mg^{2+} , Cd^{2+} , Hg^{2+} , Co^{2+} , Zn^{2+} , Cu^{2+} , Ni^{2+} , Al^{3+} , and Ga^{3+}). Moreover, this approach was applied to analyze these metals in drinking water. From Figure 2.25 PCA score plot showed clear separation of all clusters. Thus, electrolyte waters that did not contain significant amounts of Ca^{2+} and were free of Mg^{2+} and Zn^{2+} (Dasani Lemon, Powerade Option, and Propel Lemon) appeared close to the nanopure water. The Ca^{2+} enhanced waters (Propel Calcium and Owater) were

together in the left upper corners, whereas the Ca^{2+} , Mg^{2+} , and Zn^{2+} supplemented waters (Vitaminwater and Antioxidant Water Snapple) displayed together in the lower center of the PCA score plot. This pattern was highly consistent with the metal cation content and with the bias of the array sensors elements.

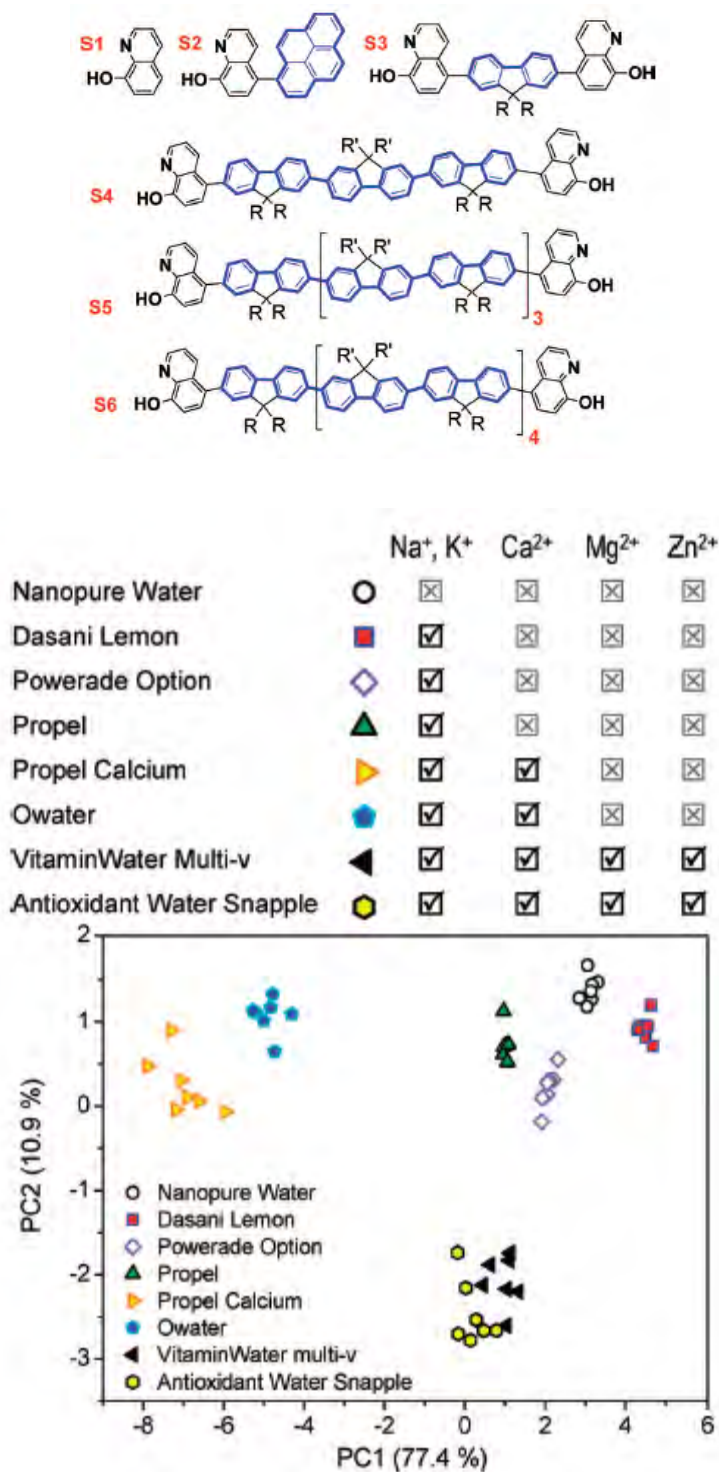
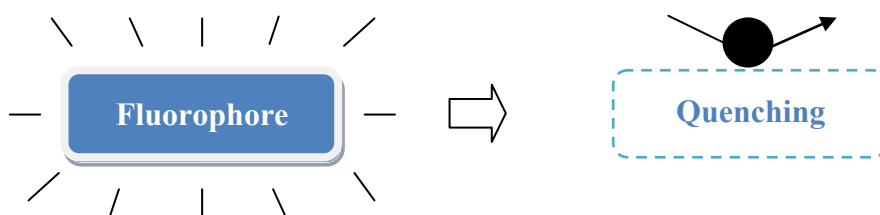


Figure 2.25 Six-sensor structures and PCA score plot of the first two PCs of the S1 – S6 array for eight-drinking water [38]

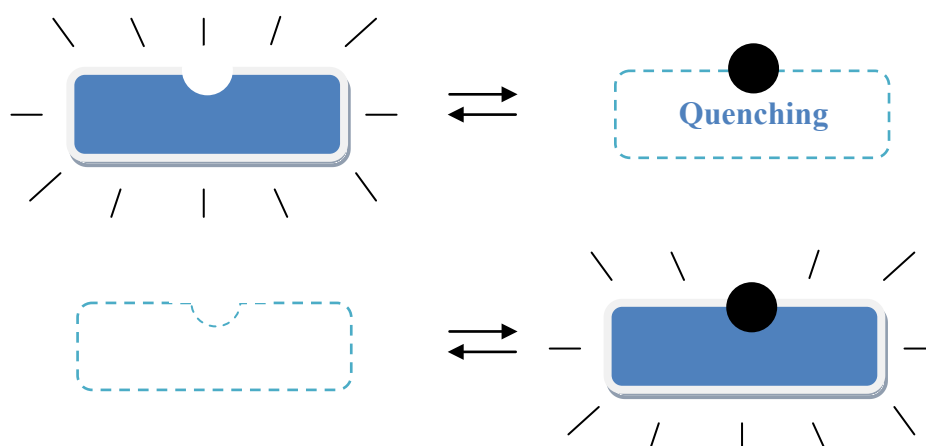
2.2 Problems to be addressed

The design of fluorescence and chromogenic sensor is quite important due to demand in medical and environmental detection of ions and molecules. The distinct advantage of fluorescence spectrophotometry is its high sensitivity, high selectivity and instantaneous response. Normally, the fluorescence molecular sensors contain fluorophores with signal transducer that converts the information into an optical signal. There are three classes of these sensors: fluorophores that undergo quenching upon collision with analytes (**class 1**), complexing fluorophores (**class 2**) and fluorophores linked to acceptor (**class 3**) as show in Figure 2.26. In our research, the fluorescent sensor possesses pyrene fluorophore that linked to thiourea and polyethylene glycol groups in **class 3** [4]. The interactions between host and guest are monitored by the change in fluorescence spectra.

CLASS 1: No association



CLASS 2: Complexing fluorophores



CLASS 3: Fluorophores linked to a receptor

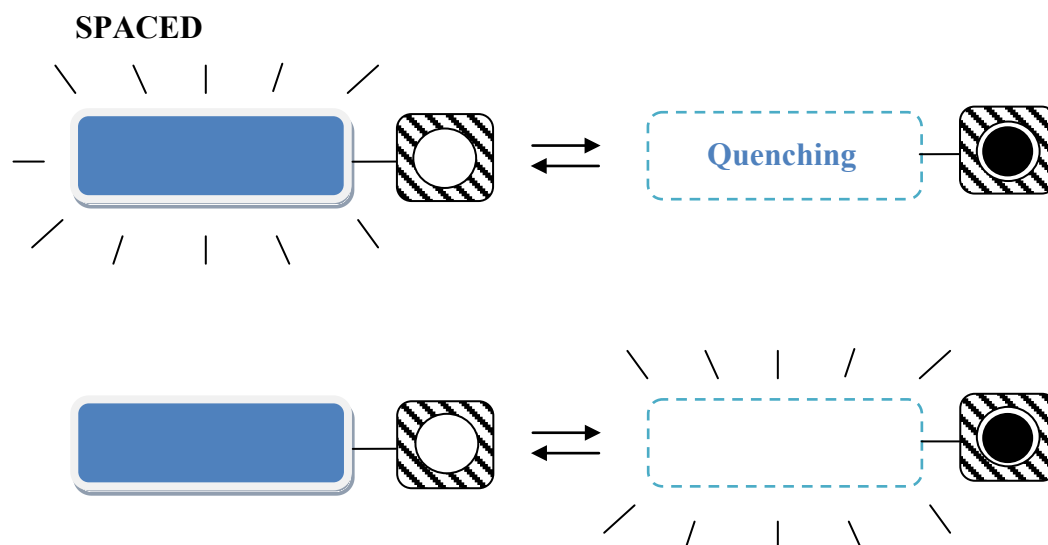
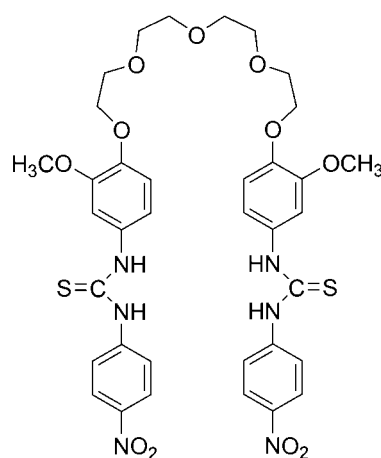


Figure 2.26 Main classes of fluorescence molecular sensors of ions or molecules

In 2003, Supachai synthesized a chromogenic anion receptor **1** using polyethylene glycol connecting to nitrobenzene thiourea (Figure 2.27) [39]. He found that this receptor was selective for fluoride and the decomplexation of this anion occurred upon addition of sodium or potassium ion. However, their complex structures had not been identified because there were two possible structures to form in solution, a folded and/or unfolded structure. The 1D and 2D NMR techniques had been chosen to explain the conformational structure of synthesized compounds in the presence and absence of ion. Moreover, this preferred configuration could not be easily determined by the technique such as UV-vis or fluorescence spectrophotometry measurements. It is known that the most efficient technique for finding the structure of a molecule is the single crystal X-ray diffraction. However, it is not easy to obtain a single crystal. Since our synthesized receptors consist of a flexible polyethylene glycol chain and the limitation of their solubility properties. Therefore in the first part of this research, new receptors containing pyrene fluorophore, **L1 – L4**, were synthesized to resolve the conformation problems. The binding properties and the selectivity trends with various ions were compared between the synthesized compounds by using the spectroscopic techniques. The fluorescence intensity ratios of excimer to monomer emission by varying concentration of receptors were used to

assess the preferred arrangement of the synthesized receptors between intramolecular and intermolecular excimer interactions, folded and unfolded structures.



Receptor 1

Figure 2.27 Structure of receptor **1** that was synthesized by Rittikulsittichai [39]

Chromogenic sensors allow naked-eye detection of ions without resorting to any spectroscopic instrumentation [40]. Moreover, these sensors have an edge over others in views of their cost effectiveness and easy handling [41]. In general, such a system consists of two parts. One part is the receptor unit which is being linked covalently or noncovalently to one or more optical signaling groups. The other is the chromophore part which converts the binding events to optical signals [42].

Therefore, the second part of this research is about the extended study of the chromogenic anion receptor **1** by varying the length and the rigidity of the polyethylene glycol chain connecting to nitrobenzene thiourea, **R1** and **R2**. The electron withdrawing nitro (NO_2) groups can enhance acidity of thiourea protons and stabilize the negative deprotonated species to have stronger binding with basic anions [43].

2.3 Objective and scope of research

1. To synthesize new fluorescent sensors based on pyrene fluorophores and chromogenic sensors based on nitrobenzene thiourea.

2. To study sensing properties of the synthesized compounds toward anions and cations.

In the first part, our study focused on synthesis and characterization of a heteroditopic receptor which involved a separate binding unit for the cation and anion together with a fluorogenic unit (Figure 2.28). It is well known that the polyethylene glycol chains can complex alkali metal salts and the conformation of this compound changed from a linear chain to pseudocrown structure [44-46]. Thiourea is frequently used as a neutral receptor for binding of anions since the thiourea group is a strong hydrogen bond donor and forms quite stable complexes with a variety of anions [47]. Pyrene is often used as fluorogenic unit which causes a molecule to be fluoresced because of its relatively efficient excimer formation via $\pi - \pi$ stacking between two pyrene units [48, 49]. Two important informations are intensity ratio of excimer to monomer emission (I_E/I_M) and maximum wavelength of excimer emission (λ_E). The I_E/I_M ratio is sensitive to the structure change while the λ_E is much less variable and usually locates at 475 – 500 nm [50]. The binding properties of anions with thiourea receptors **L1** – **L3** which varying the length of polyethylene glycol chains were studied by fluorescence spectrophotometry and $^1\text{H-NMR}$ spectroscopy. We supposed that the spectroscopic properties could be affected by complexation with anions. Moreover, the conformational structure in solution of various chain lengths of the polyethylene glycol was also examined. The reverse binding property of the **L1-F** and **L4-F** in the presence of Na^+ was also tested by fluorescence and $^1\text{H-NMR}$ spectroscopy. The 2D NOESY and $^1\text{H-NMR}$ spectra were also used to support the preferred arrangement of the complexation structures.

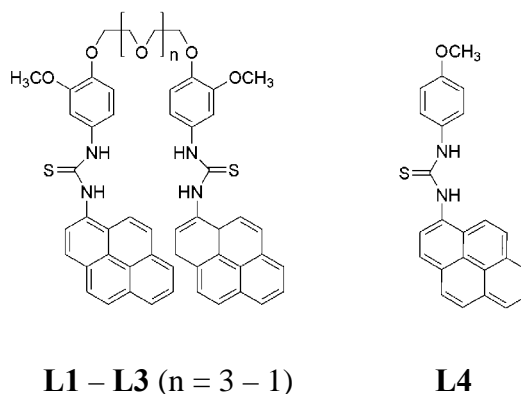


Figure 2.28 Structures of fluorescent sensors **L1** – **L4**

In the second part we focused on the comparison of anion sensing properties between flexible and semi-rigid receptors of thiourea-nitrobenzene derivatives (Figure 2.29). Receptors **R1** contained the flexible chain of polyethylene glycol. Receptor **R2** consisted of the benzene ring to increase the rigidity of the polyethylene glycol moiety. The colorimetric sensing properties with various anions and the selectivity trend were investigated by naked eyes, UV-vis spectrophotometry and principal component analysis (PCA).

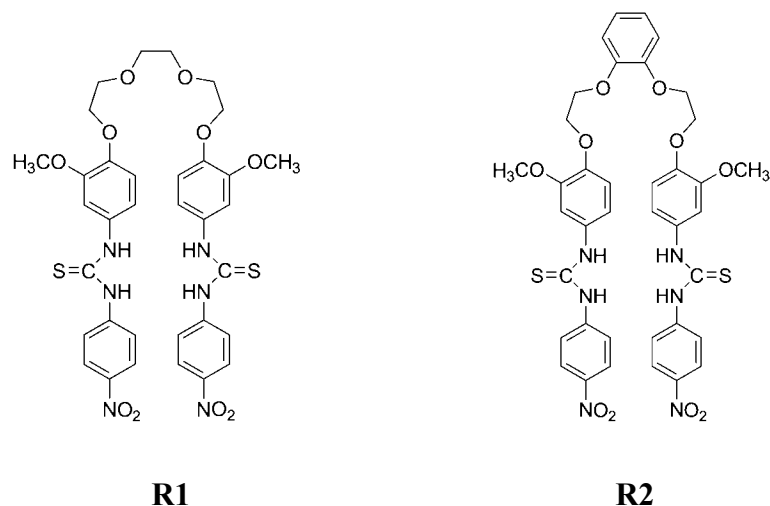


Figure 2.29 Structures of chromogenic sensors **R1** and **R2**

CHAPTER III

EXPERIMENTALS

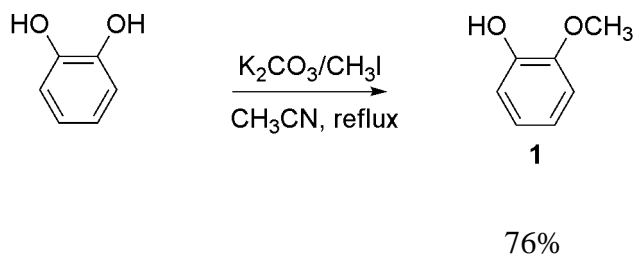
3.1 Instruments, chemicals and general methods

The melting points were recorded on a Electrothermal 9100. MS spectra were obtained on Bruker Daltonics MalDI-TOF. Elemental analysis data were recorded with a CHNS/O Analyzer Perkin Elmer PE2400 Series II. IR spectra were obtained on a Nicolet Impact 410 FT-IR spectrometer. ¹H-NMR (400 MHz), ¹³C-NMR (100 MHz), COSY, HMBC, HMQC spectra were recorded with a Varian Mercury Plus 400 NMR spectrometer and a Bruker Ultrashield™ Plus 400 NMR spectrometer. 2D NOESY spectrum was recorded on a Varian INOVA 500 NMR spectrophotometer. UV-Vis spectra were obtained on a Varian Cary 50 Probe UV-Visible spectrometer. Fluorescence spectra were obtained on a Varian Cary Eclipse Fluorescence spectrophotometer.

All materials and reagents were standard analytical grade, and used without further purification. Commercial grade solvents, methanol, dichloromethane, hexane, ethyl acetate, were distilled before use. CDCl₃, CD₃CN and DMSO-d₆ were used as solvents for NMR experiments. In complexation studies, added anions and cations were tetrabutylammonium and perchlorate salts, respectively. The progress of the reactions was monitored by TLC on silica gel and visualized by UV light. The chromatographic separations were carried out on silica gel columns (0.063-0.200 mm).

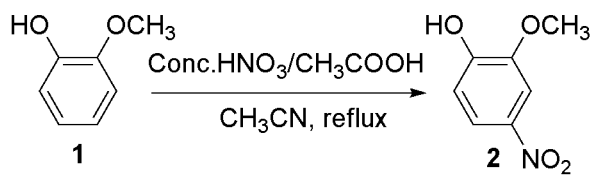
3.2 Synthesis of receptor L1

3.2.1 Synthesis of 2-Methoxyphenol (1)



The mixture of pyrocatechol (5.50 g, 0.050 mol), anhydrous K_2CO_3 (3.46 g, 0.025 mol) in 50 mL of CH_3CN was refluxed under nitrogen. CH_3I (4.80 mL, 0.075 mol) was dissolved in CH_3CN 50 mL and was added dropwise to the mixture. After 24 hours, the reaction color was changed from gray to brown-red. The solvent was removed under reduced pressure. The residue was dissolved in CH_2Cl_2 , and 3M HCl was added to adjust pH=1. The resulting residue was extracted with CH_2Cl_2 (25 mL \times 3) and water. The organic phase was dried over anhydrous Na_2SO_4 , filtered and evaporated. The crude residue was purified by column chromatograp (SiO_2 , CH_2Cl_2) to yield yellow oil (4.69 g, 76%). 1H -NMR (400 MHz, $CDCl_3$) δ 6.97-6.88 (m, 4H), 5.78 (s, 1H), 3.88 (s, 3H).

3.2.2 Synthesis of 2-methoxy-4-nitrophenol (**2**)

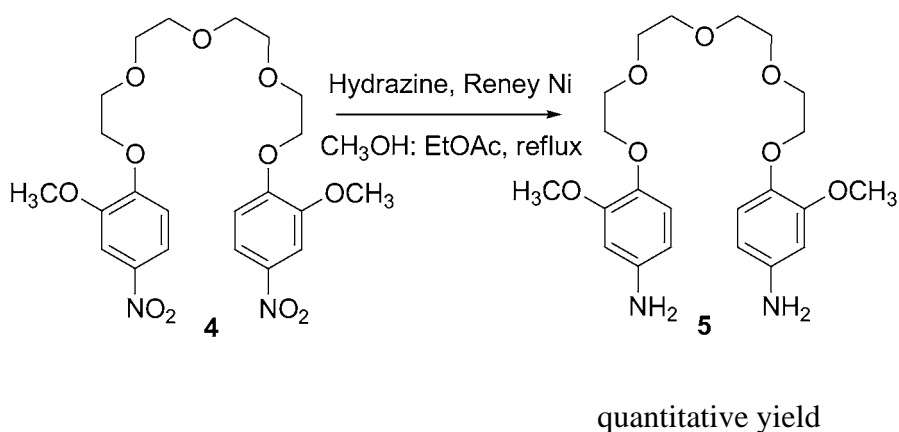


16%

The mixture of **1** (2.12 g, 0.017 mol) in CH_3CN 30 mL and CH_3COOH 15 mL was stirred under nitrogen. A solution of concentrated HNO_3 1.20 mL in 15 mL of CH_3CN was then added dropwise and refluxed. After 5 hours, this reaction was stirred at room temperature about 12 hours. After that reaction temperature was controlled at 0 °C in an ice bath and then adjusted to pH 7-8 by saturated HCO_3^- solution (900 mL). The resulting residue was extracted with CH_2Cl_2 and water. The organic phase was isolated and dried over anhydrous Na_2SO_4 . The solvent was removed and purified by column chromatograp on silica gel with CH_2Cl_2 as eluent. The second band was collected and recrystallized with hexane: CH_2Cl_2 to give final product as yellow solid in 0.05 g (16%). Mp: 121.0-122.0 °C. IR (KBr) 3372, 1513, 1342, 870, 789 cm^{-1} . 1H -NMR (400 MHz, $CDCl_3$) δ 7.88 (dd, $J = 8.8, 2.4$ Hz, 1H), 7.76 (d, $J = 2.4$ Hz, 1H), 6.98 (d, $J = 8.8$ Hz, 1H), 6.43 (s, 1H), 3.99 (s, 3H). ^{13}C -NMR (100 MHz, $CDCl_3$) δ 151.7, 146.1, 141.2, 118.6, 114.0, 106.4, 56.5 ppm.

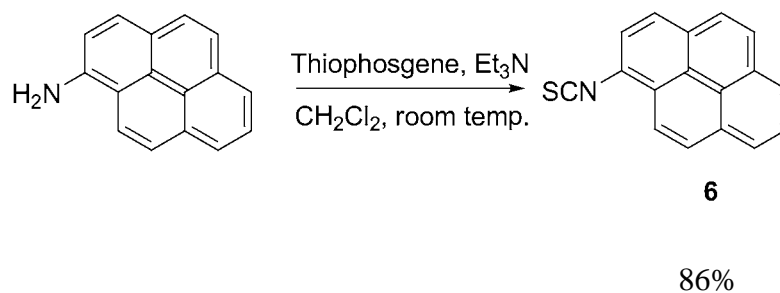
(50 mL) was stirred and refluxed under nitrogen. After 2 days, the solvent was removed and pH of the mixture was adjusted to 1 with 3M HCl. The residue was extracted with CH₂Cl₂ (25×3 mL) and H₂O. The organic phase was collected and dried over anhydrous Na₂SO₄. The solvent was removed and then recrystallized with CH₃OH to yield a yellow solid 0.27 g (76%). Mp: 114.0-116.0 °C. IR (KBr): 2902, 1516, 1336, 1278, 859, 787 cm⁻¹. ¹H-NMR (400 MHz, CDCl₃) δ 7.86 (d, *J* = 8.4 Hz, 1H), 7.71 (s, 1H), 6.94 (d, *J* = 8.8, 1H), 4.26 (s, 2H), 3.92 (s, 5H), 3.72 (s, 2H), 3.66 (s, 2H). ¹³C-NMR (100 MHz, CDCl₃) δ 153.8, 149.0, 141.5, 117.6, 111.3, 106.6, 70.9, 70.6, 69.3, 68.7, 56.2 ppm.

3.2.5 Synthesis of 2,2-[oxabis(4-oxapentaethyleneoxy)]bis(2-methoxy-4-aminophenol) (5)



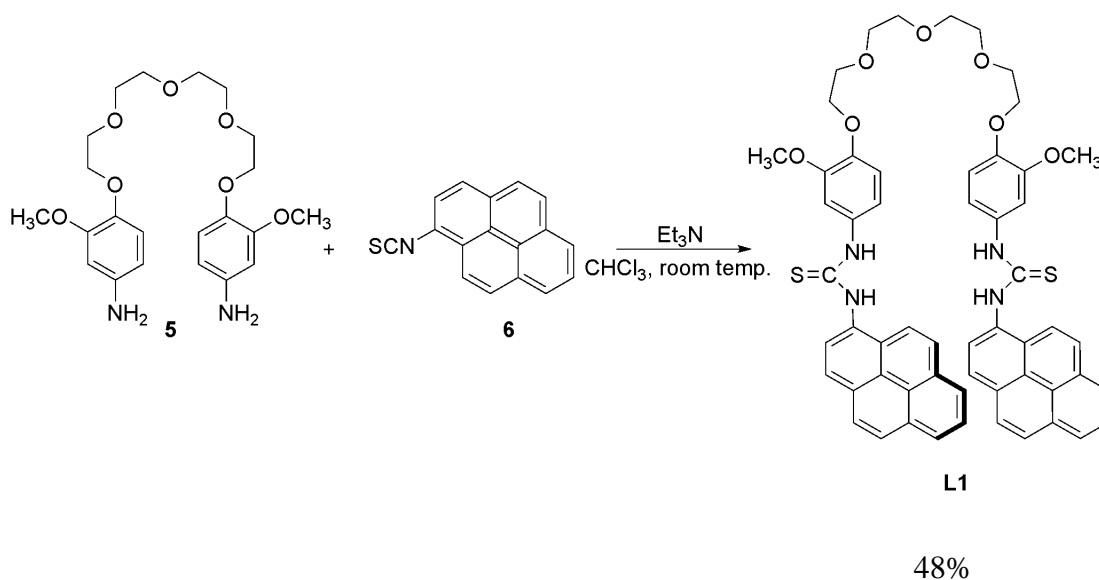
A mixture of **4** (0.10 g, 0.201 mmol) in CH₃OH (5 mL) and EtOAc (10 mL) was stirred with molecular sieve under nitrogen. After 15 min, Raney Ni (1/4 spoon) and 2 mL of hydrazine hydrate were added and refluxed for 1 hour. The color of the reaction was changed from yellow to colorless solution. The molecular sieve and Raney Ni were removed by filtration. The residue was evaporated to dryness and extracted with CH₂Cl₂ and H₂O. The organic phase was collected and dried over anhydrous Na₂SO₄. Solvent was evaporated to give yellow oil product in a quantitative yield, and the product was used in the next step.

3.2.6 Synthesis of 1-Isothiocyanatopyrene (6)



A mixture of 1-aminopyrene (0.55 g, 2.5 mmol) and triethylamine (0.70 mL, 5.02 mmol) in CH_2Cl_2 (40 mL) was stirred under nitrogen at room temperature for 30 minutes. A solution of thiophosgene (0.20 mL, 2.6 mmol) in CH_2Cl_2 (20 mL) was added dropwise to the reaction mixture and stirred for 4 hours to give a brown solution. The reaction mixture was extracted with H_2O and CH_2Cl_2 (25 mL \times 3). The organic phase was collected and dried over anhydrous Na_2SO_4 . The residue was evaporated to dryness and purified by column chromatography on silica gel with CH_2Cl_2 as eluent to give 0.57 g (86%) of compound **6** as red-orange solid. Mp: 144.7- 144.8 °C. MS (m/z) calcd 259.3, found 259.6. IR (KBr): 2114, 839 cm^{-1} . $^1\text{H-NMR}$ (400 MHz, CDCl_3) δ 8.3 (d, $J = 9.2$ Hz, 1H), 8.2 (m, 3H), 8.0 (m, 4H), 7.9 (d, $J = 8$ Hz, 1H). $^{13}\text{C-NMR}$ (100 MHz, CDCl_3) δ 136.1, 131.0, 130.7, 130.0, 128.8, 128.0, 126.8, 126.6, 126.5, 125.9, 125.8, 124.8, 124.7, 123.9, 123.8, 123.6, 121.4 ppm.

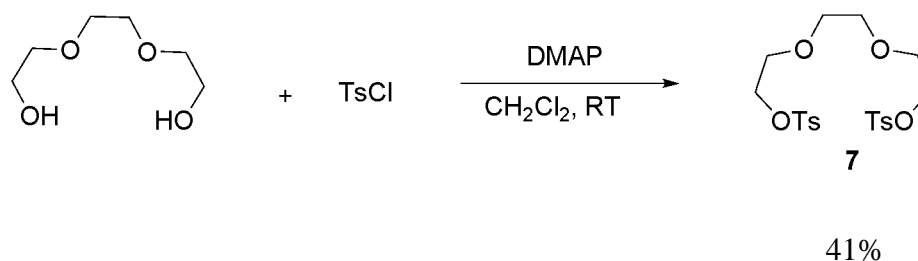
3.2.7 Synthesis of receptor L1



A solution of **5** (0.100 mmol) and triethylamine (0.10 mL, 0.717 mmol) in CHCl_3 (10 mL) was stirred under nitrogen at room temperature for 30 minutes and then **6** (0.07 g, 0.255 mmol) in CHCl_3 (20 mL) was added to the reaction. The reaction mixture was stirred for 3 days and then evaporated to dryness. The residue was extracted with CH_2Cl_2 and H_2O . The organic phase was collected and evaporated to dryness and purified by column chromatography on silica gel with EtOAc as eluent. The final product was recrystallized with $\text{CH}_2\text{Cl}_2:\text{CH}_3\text{OH}$ to give yellow solid in 0.05 g (48%). Mp: 140.0-142.8 °C. MALDI-TOF (m/z) $[\text{M}^+]$: calcd 954.31, found 953.0. Elemental Analysis for $\text{C}_{56}\text{H}_{50}\text{N}_4\text{O}_7\text{S}_2$: calcd C, 70.42; H, 5.28; N, 5.87; S, 6.71, found C, 70.40; H, 5.23; N, 5.82; S, 6.68. IR (KBr): 3235, 2924, 1513, 1229, 1131, 847 cm^{-1} . $^1\text{H-NMR}$ (400 MHz, CDCl_3) δ 8.0 (m, 22H), 7.0 (s, 2H), 6.8 (s, 4H), 4.1 (s, 4H), 3.8 (s, 10H), 3.6 (d, $J = 8.8$ Hz, 8H). $^{13}\text{C-NMR}$ (100 MHz, d_6 -DMSO) δ 181.2, 148.5, 145.3, 133.2, 132.6, 130.6, 130.4, 129.2, 127.3, 127.1, 127.0, 126.7, 126.4, 126.3, 125.3, 125.1, 124.8, 124.4, 123.8, 122.7, 116.7, 113.0, 109.7, 69.8, 69.7, 68.9, 68.0, 55.4 ppm.

3.3 Synthesis of receptor L2

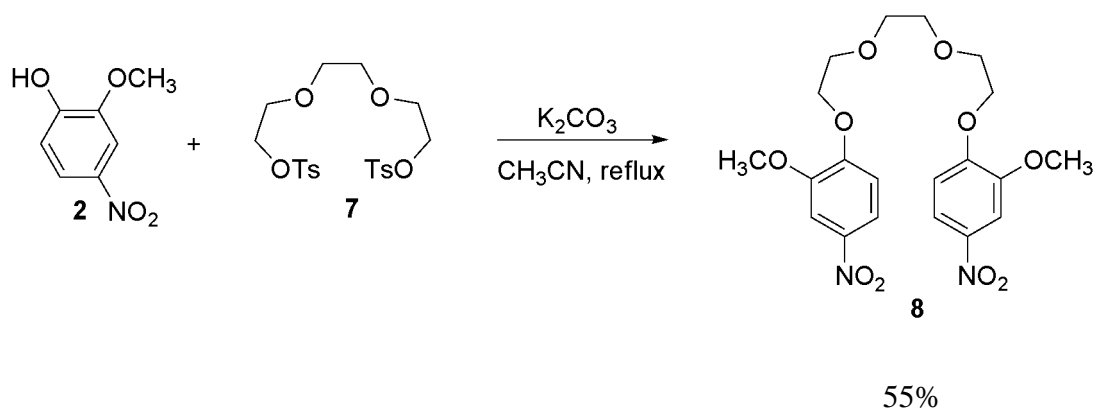
3.3.1 Synthesis of Triethyleneglycolditosilate (7)



The mixture of triethylene glycol (3.35 mL, 0.025 mol), triethylamine (7.00 mL, 0.050 mol) in CH_2Cl_2 (100 mL) was stirred at 0 °C for 30 min under nitrogen. A catalytic amount of DMAP was added. The TsCl (10.00 g, 0.052 mol) was dissolved in CH_2Cl_2 and added dropwise in the reaction. The mixture was stirred overnight at room temperature. The solvent was removed, and the 3 M HCl was added to adjust pH to 1. The residue was extracted with CH_2Cl_2 (50 mL \times 3) and H_2O . The organic phase was collected and dried over anhydrous Na_2SO_4 . The reaction mixture was filtered, and the filtrate was evaporated. The crude product was purified by column chromatography using CH_2Cl_2 to obtain a white solid in 5.30 g (41%). $^1\text{H-NMR}$

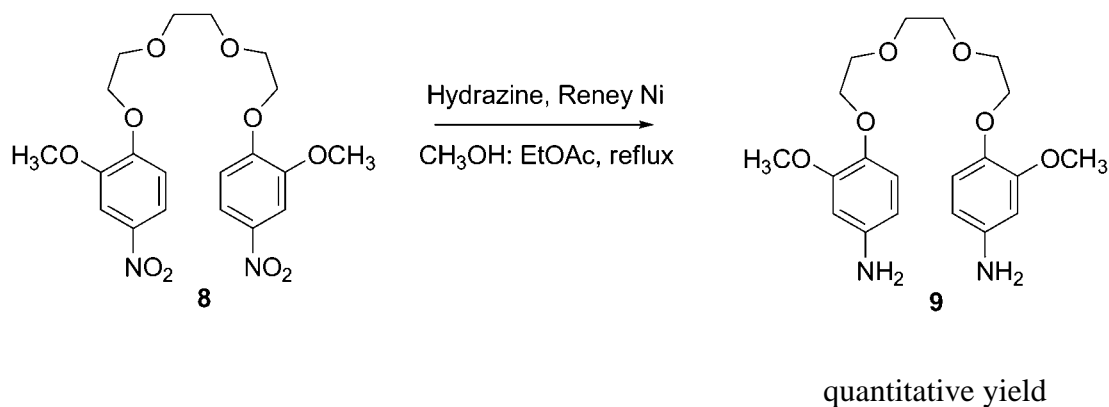
(400 MHz, CDCl₃) δ 7.79 (d, J = 8.0 Hz, 4H), 7.34 (d, J = 8 Hz, 4H), 4.14 (t, J = 4.8, 4.8 Hz, 4H), 3.65 (t, J = 5.2, 4.4 Hz, 4H), 3.53 (s, 4H), 2.45 (s, 6H). ¹³C-NMR (100 MHz, CDCl₃) δ 144.9, 133.0, 129.9, 128.0, 70.7, 69.2, 68.8, 21.6 ppm.

3.3.2 Synthesis of 1,2-bis(2-(2-methoxy-4-nitrophenoxy)ethoxy)ethane (8)



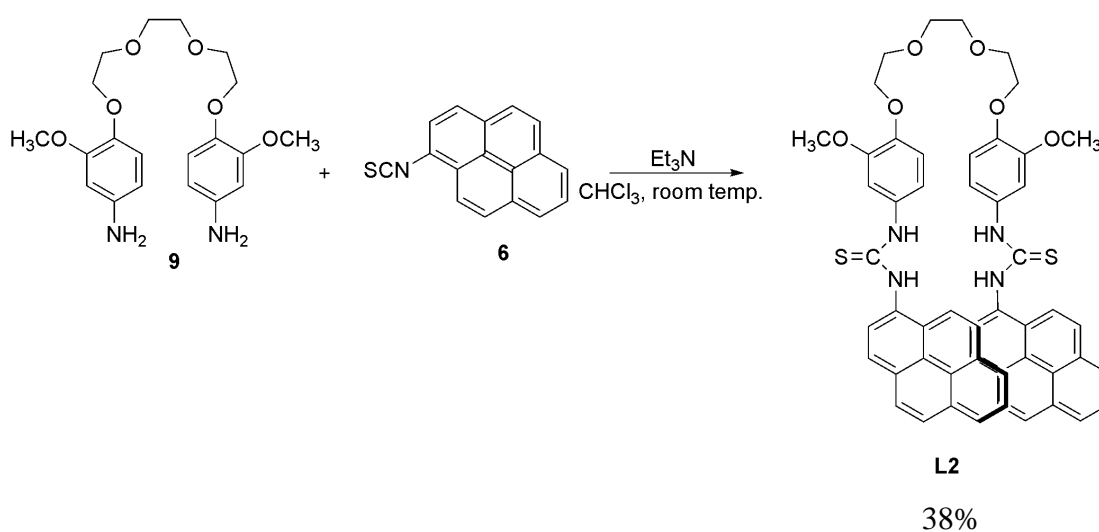
The mixture of compound 7 (0.30 g, 0.0007 mol), compound 2 (0.22 g, 0.0013 mol), K₂CO₃ (0.90 g, 0.007 mol), tetrabutylammonium bromide in CH₃CN (50 mL) was stirred and refluxed under nitrogen. After 3 days, the solvent was removed, and pH of the reaction mixture was adjusted to 1 with 3M HCl. The residue was extracted with CH₂Cl₂ (25×3 mL) and H₂O. The organic phase was collected and dried over anhydrous Na₂SO₄. The solvent was removed and then recrystallized with CH₃OH to yield 0.16 g (55%) as yellow solid. ¹H-NMR (400 MHz, CDCl₃) δ 7.87 (dd, J = 8.8, 2.8 Hz, 2H), 7.73 (d, J = 2.8 Hz, 2H), 6.94 (d, J = 8.8 Hz, 2H), 4.27 (t, J = 4.8, 5.2 Hz, 4H), 3.93 (t, J = 5.2, 4.4 Hz, 10H), 3.75 (s, 4H). ¹³C-NMR (100 MHz, CDCl₃) δ 153.9, 149.2, 141.7, 117.6, 111.4, 106.8, 71.0, 69.4, 68.9, 56.3 ppm.

3.3.3 Synthesis of 1,2-bis(2-(2-methoxy-4-aminophenoxy)ethoxy)ethane (9)



A mixture of **8** (0.05 g, 0.102 mmol) in CH₃OH (2.5 mL) and EtOAc (8 mL) was stirred with molecular sieve under nitrogen. After 15 min, Raney Ni (1/4 spoon) and 1 mL of hydrazine hydrate were added and refluxed for 1 hour. The color of the reaction was changed from yellow to colorless solution. The molecular sieve and Raney Ni were removed by filtration. The residue was evaporated to dryness and extracted with CH₂Cl₂ (25 mL×2) and H₂O. The organic phase was collected and dried over anhydrous Na₂SO₄. Solvent was evaporated to give yellow oil in quantitative yield and was used in the next step without further purification.

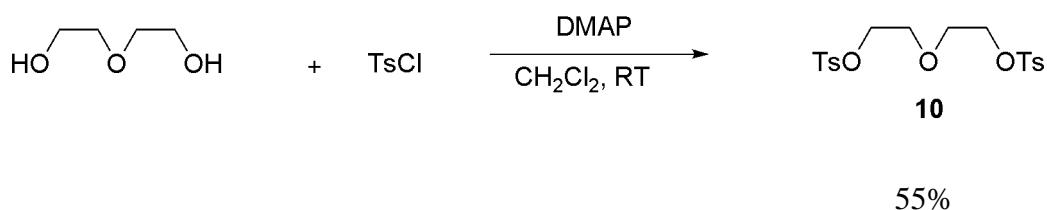
3.3.4 Synthesis of receptor L2



A similar procedure to the preparation of **L1**, **L2** was synthesized from compound **9** and 1-isothiocyanatopyrene and was obtained as yellow powder in 0.04 g (38%). MALDI-TOF (m/z) [M]⁺: calcd 910.290, found 909.407. Elemental Analysis for C₅₄H₄₆N₄O₆S₂: calcd C, 71.19; H, 5.09; N, 6.15. found C, 71.05; H, 4.99; N, 6.23. ¹H-NMR (400 MHz, d₆-DMSO) δ 10.07 (s, 2H), 9.73 (s, 2H), 8.31-8.06 (m, 18H), 7.20 (d, J = 2 Hz, 2H), 6.97 (dd, J = 27, 8.8 Hz, 4H), 4.04 (t, J = 4 Hz, 4H), 3.74 (m, 10H), 3.60 (s, 4H). ¹³C-NMR (100 MHz, d₆-DMSO) δ 181.2, 148.5, 145.3, 133.2, 132.6, 130.6, 130.4, 129.2, 127.3, 127.2, 127.0, 126.7, 126.4, 126.4, 125.3, 125.1, 124.9, 124.4, 123.8, 122.7, 116.8, 113.0, 109.7, 69.9, 68.9, 68.0, 55.4 ppm.

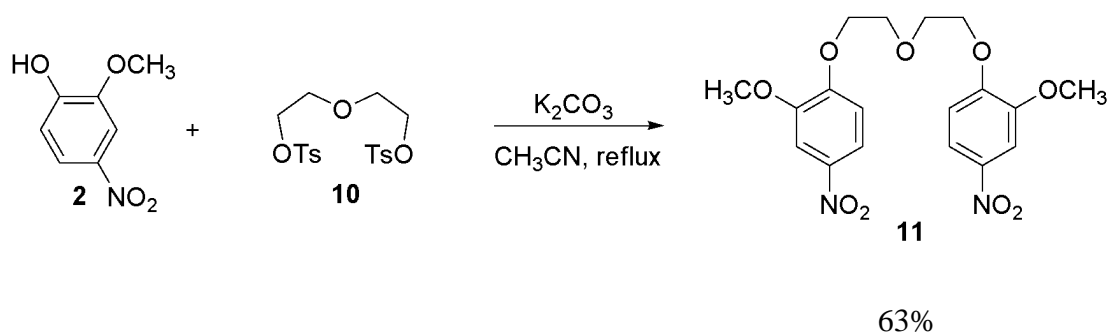
3.4 Synthesis of receptor L3

3.4.1 Synthesis of diethyleneglycolditisylate (10)



The mixture of diethylene glycol (2.45 mL, 0.025 mol), triethylamine (7.00 mL, 0.050 mol) in CH_2Cl_2 (100 mL) was stirred at 0 °C for 30 min under nitrogen. A catalyze amount of DMAP was added. TsCl (10.34 g, 0.054 mol) was dissolved in CH_2Cl_2 and added dropwise to the reaction. The mixture was stirred overnight at room temperature. The solvent was removed, and the 3 M HCl was added to adjust pH to 1. The residue was extracted with CH_2Cl_2 (50 mL \times 3) and H_2O . The organic phase was collected and dried over anhydrous Na_2SO_4 . The reaction mixture was filtered, and the filtrate was evaporated. The crude product was purified by column chromatograp using CH_2Cl_2 and gave a white solid in 5.69 g (55%). $^1\text{H-NMR}$ (400 MHz, CDCl_3) δ 7.78 (d, $J = 8.4$ Hz, 4H), 7.35 (d, $J = 8.4$ Hz, 4H), 4.09 (t, $J = 4.4, 4.8$ Hz, 4H), 3.61 (t, $J = 4.8, 4.8$ Hz, 4H), 2.45 (s, 6H). $^{13}\text{C-NMR}$ (100 MHz, CDCl_3) δ 145.0, 132.9, 129.9, 128.0, 69.0, 68.8, 21.7 ppm.

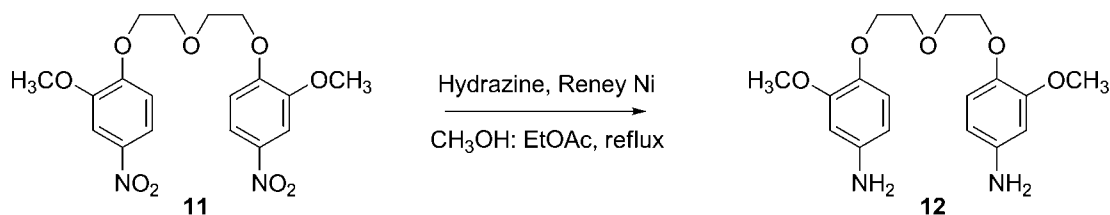
3.4.2 Synthesis of compound 11



The mixture of compound **10** (0.23 g, 0.0006 mol), compound **2** (0.19 g, 0.0011 mol), K_2CO_3 (0.76 g, 0.006 mol), tetrabutylammonium bromide in CH_3CN (50 mL) solution was stirred and refluxed under nitrogen. After 3 days, the solvent was removed, and pH of the reaction mixture was adjusted to 1 with 3M HCl. The residue was extracted with CH_2Cl_2 (25 \times 3 mL) and H_2O . The organic phase was

collected and dried over anhydrous Na_2SO_4 . The solvent was removed and then recrystallized with CH_3OH to yield yellow solid 0.14 g (63%). $^1\text{H-NMR}$ (400 MHz, CDCl_3) δ 7.87 (dd, $J = 8.8, 2.8$ Hz, 2H), 7.73 (d, $J = 2.8$ Hz, 2H), 6.94 (d, $J = 8.8$ Hz, 2H), 4.30 (t, $J = 4.4, 5.2$ Hz, 4H), 4.01 (t, $J = 4.4, 4.8$ Hz, 4H), 3.93 (s, 6H). $^{13}\text{C-NMR}$ (100 MHz, CDCl_3) δ 153.7, 149.1, 141.6, 117.5, 111.3, 106.6, 69.6, 68.8, 56.2 ppm.

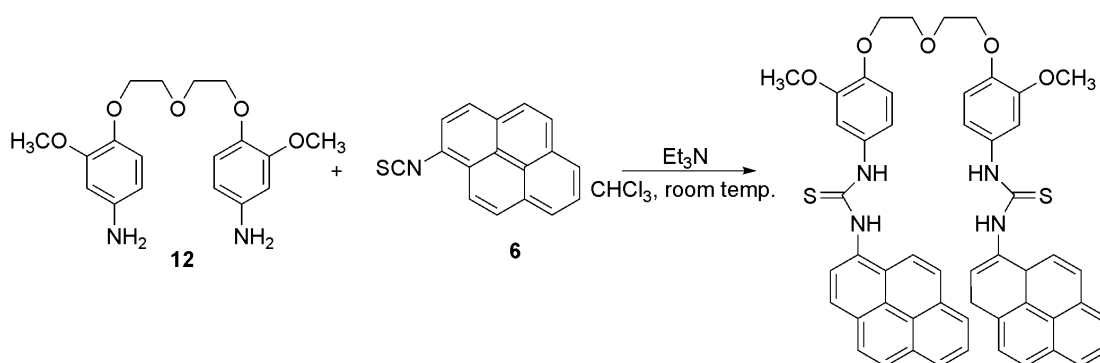
3.4.3 Synthesis of compound 12



quantitative yield

A mixture of **11** (0.04 g, 0.100 mmol) in CH_3OH (2.5 mL) and EtOAc (5 mL) was stirred with molecular sieve under nitrogen. After 15 min, Raney Ni (1/4 spoon) and 1 mL of hydrazine hydrate were added and refluxed for 1 hour. The color of reaction was changed from yellow to colorless solution. The molecular sieve and Raney Ni were removed by filtration. The residue was evaporated to dryness and extracted with CH_2Cl_2 (25 mL \times 2) and H_2O . The organic phase was collected and dried over anhydrous Na_2SO_4 . Solvent was evaporated to give yellow oil product in a quantitative yield and was used in the next step without further purification.

3.4.4 Synthesis of receptor L3



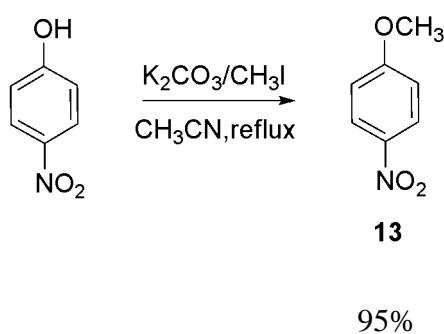
L3

52%

A similar procedure to the preparation of **L1**, the **L3** was used to synthesize from **12** and 1-isothiocyanatopyrene. The **L3** was obtained as yellow powders in 0.05 g (52%). MALDI-TOF (m/z) $[M]^+$: calcd 866.26, found 865.07. Elemental Analysis for $C_{52}H_{42}N_4O_5S_2$: calcd C, 72.03; H, 4.88; N, 6.46. found C, 72.25; H, 4.86; N, 6.42. 1H -NMR (400 MHz, $CDCl_3$) δ 8.20-8.00 (m, 18H), 7.00 (s, 2H), 6.85-6.84 (m, 4H), 4.14 (t, $J = 4.8$ Hz, 4H), 3.88 (t, $J = 4.4$ Hz, 4H), 3.80 (s, 6H). ^{13}C -NMR (100 MHz, d_6 -DMSO) δ 181.0, 148.4, 145.1, 133.0, 132.5, 130.4, 130.2, 129.0, 127.2, 127.0, 126.8, 126.5, 126.3, 126.2, 125.1, 124.9, 124.7, 124.2, 123.6, 122.5, 116.6, 113.0, 109.5, 68.8, 67.9, 55.2 ppm.

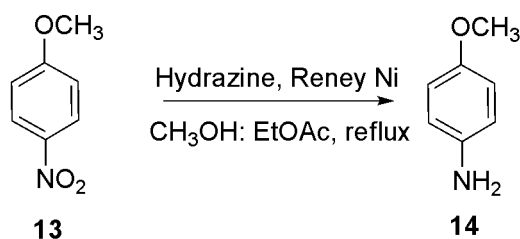
3.5 Synthesis of receptor L4

3.5.1 Synthesis of 1-Methoxy-4-nitrobenzene (**13**)



A mixture of 4-nitrophenol (3.48 g, 0.025 mol), anhydrous K_2CO_3 (1.73 g, 0.0125 mol) in 25 mL of CH_3CN solution was refluxed under nitrogen. CH_3I (3 mL, 0.0375 mol) was dissolved in CH_3CN (25 mL) and was added dropwise to the mixture. After 5 hours, the solvent was removed under reduced pressure. The residue was dissolved in CH_2Cl_2 and 3M HCl was added to adjust pH = 1. The resulting residue was extracted with CH_2Cl_2 (25 mL \times 3) and water. The organic phase was dried over anhydrous $NaSO_4$, filtered and evaporated. The crude residue was purified by column chromatography (SiO_2 , CH_2Cl_2) to yield compound **6** as yellow-green solid (3.65 g, 95%). IR (KBr): 3116, 2944, 1606, 1590, 1500, 1332, 1107, 847 cm^{-1} . 1H -NMR (400 MHz, $CDCl_3$) δ 8.19 (dd, $J = 7.2, 2.0$ Hz, 2H), 6.95 (dd, $J = 7.2, 2.0$ Hz, 2H), 3.9 (s, 3H). ^{13}C -NMR (100 MHz, $CDCl_3$) δ 164.6, 141.6, 125.9, 114.0, 56.0 ppm.

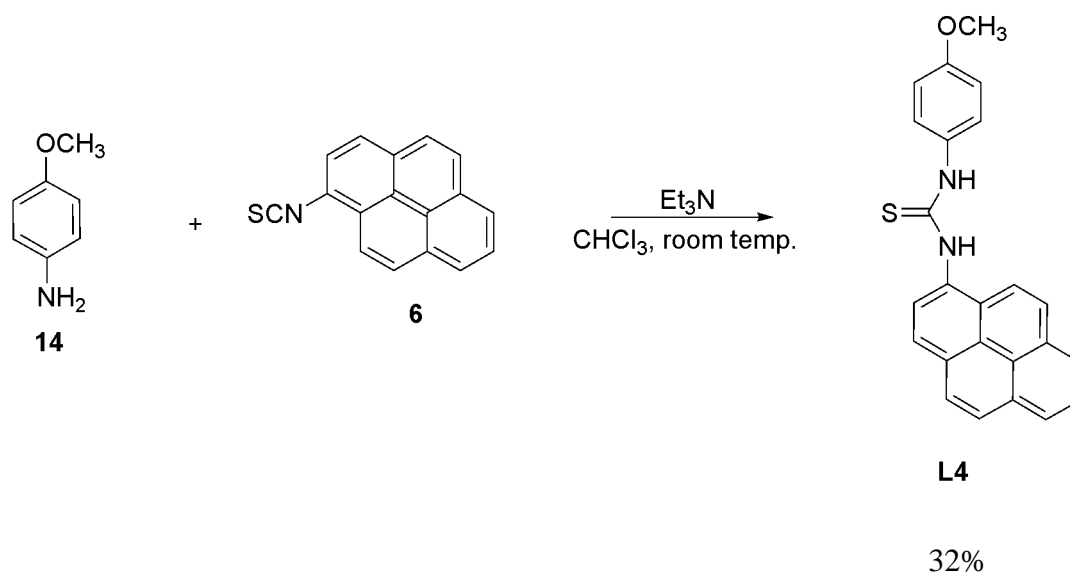
3.5.2 Synthesis of 4-Methoxyaniline (**14**)



quantitative yield

A mixture of **13** (0.05 g, 0.3 mmol) in CH₃OH (1 mL) and EtOAc (20 mL) was stirred with molecular sieve under nitrogen. After 15 min, Raney Ni (1/4 spoon) and 2 mL of hydrazine hydrate were added and refluxed for 1 hour. The color of the reaction was changed from yellow to colorless. The molecular sieve and Raney Ni were removed by filtration. The residue was evaporated to dryness and extracted with CH₂Cl₂ and H₂O. The organic phase was collected and dried over anhydrous NaSO₄. Solvent was evaporated to give yellow oil and the product was used in the next step without purification.

3.5.3 Synthesis of receptor L4

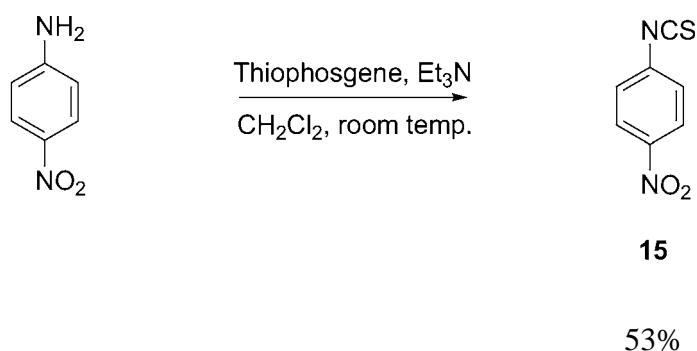


A solution of compound **14** (0.300 mmol) and triethylamine (0.20 mL, 1.5 mmol) in CHCl₃ (10 mL) was stirred under nitrogen at room temperature for 30 minutes and then 1-isothiocyanatopyrene (0.09 g, 0.360 mmol) in CHCl₃ (20 mL) was added to the reaction. The reaction mixture was stirred for 3 days and then

evaporated to dryness. The residue was extracted with CH_2Cl_2 and H_2O . The organic phase was collected and evaporated to dryness and purified by recrystallization with CH_2Cl_2 : EtOAc to give a white solid in 0.04 g (32%). MALDI-TOF (m/z) $[\text{M}]^+$: calcd 382.11, found 382.70. Elemental Analysis: for $\text{C}_{24}\text{H}_{18}\text{N}_2\text{OS}$: calcd C, 75.37; H, 4.74; N, 7.32 found C, 75.40; H, 4.83; N, 7.41. IR (KBr): 3356, 3293, 3129, 2959, 1511, 1244, 844 cm^{-1} . $^1\text{H-NMR}$ (400 MHz, CDCl_3) δ 8.05 (m, 11H), 7.32 (d, $J = 8$ Hz, 2H), 6.90 (d, $J = 8$ Hz, 2H), 3.79 (s, 3H). $^{13}\text{C-NMR}$ (100 MHz, d_6 -DMSO) 181.6, 156.6, 133.0, 132.2, 130.6, 130.4, 129.2, 127.3, 127.1, 126.9, 126.6, 126.4, 126.3, 125.3, 125.1, 124.8, 124.4, 123.8, 122.6, 113.5, 55.1 ppm.

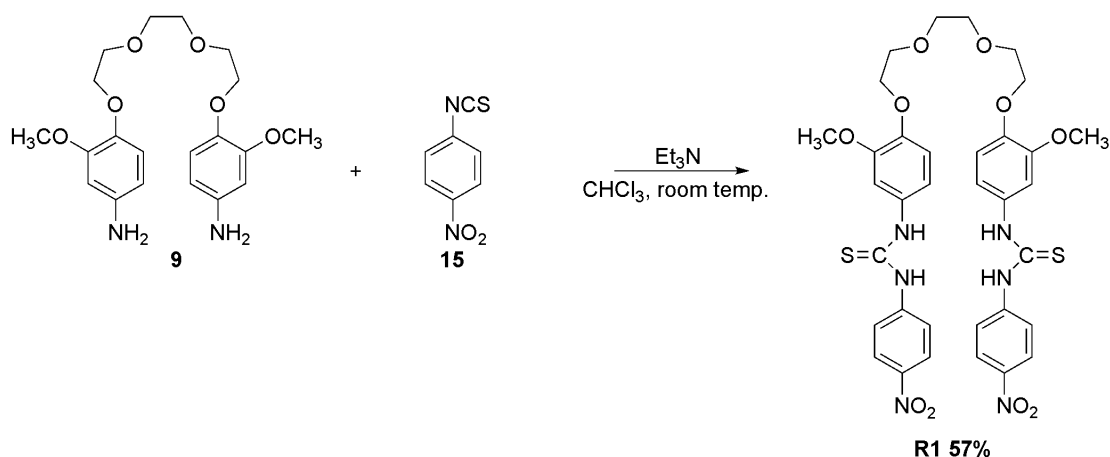
3.6 Synthesis of receptor R1

3.6.1 Synthesis of 1-Isothiocyanato-4-nitrobenzene (**15**)



A mixture of 4-nitroaniline (0.35 g, 2.55 mmol) and triethylamine (0.70 mL, 5.05 mmol) in CH_2Cl_2 (40 mL) was stirred under nitrogen at room temperature for 30 minutes. A solution of thiophosgene (0.20 mL, 2.61 mmol) in CH_2Cl_2 (20 mL) was added dropwise to the reaction mixture and stirred for a day to give a red brown solution. The reaction was extracted with H_2O and CH_2Cl_2 (25 mL \times 3). The organic phase was collected and dried over anhydrous Na_2SO_4 . The residue was evaporated to dryness and purified by column chromatography on silica gel with CH_2Cl_2 as eluent to give 0.24 g (53%) of compound **15** as orange solid. $^1\text{H-NMR}$ (400 MHz, CDCl_3) δ 8.25 (d, $J = 9.2$ Hz, 2H), 7.35 (d, $J = 8.8$ Hz, 2H). $^{13}\text{C-NMR}$ (100 MHz, CDCl_3) δ 145.8, 140.4, 137.9, 126.4, 125.5 ppm.

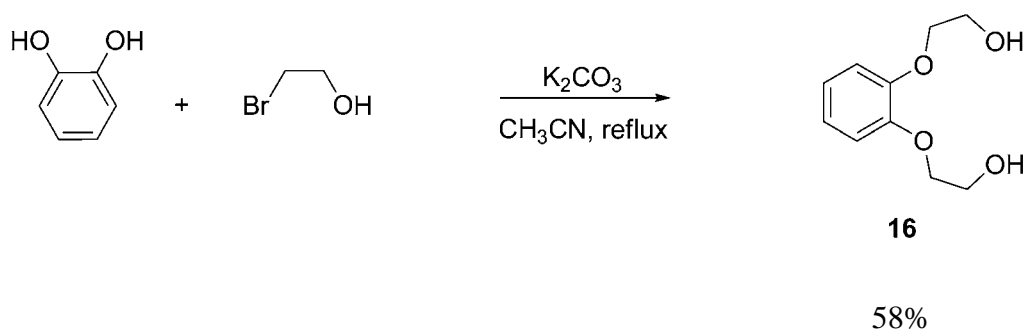
3.6.2 Synthesis of receptor R1



A similar procedure to the preparation of **L1**, the **R1** was synthesized from compound **9** and 1-isothiocyanato-4-nitrobenzene. The **R1** was obtained as yellow powders in 0.04 g (57%). MALDI-TOF (m/z) $[M]^+$: calcd 752.19, found 753.41. Elemental Analysis for $C_{34}H_{36}N_6O_{10}S_2 \cdot H_2O$: calcd C, 52.98; H, 4.97; N, 10.90. found C, 52.14; H, 4.39; N, 11.18. 1H -NMR (400 MHz, d_6 -DMSO) δ 10.16 (s, 4H), 8.18 (d, $J = 9.2$ Hz, 4H), 7.82 (d, $J = 9.2$ Hz, 4H), 7.14 (s, 2H), 6.94 (s, 4H), 4.07 (t, $J = 4.4, 4.4$ Hz, 4H), 3.73 (m, 10H), 3.62 (s, 4H). ^{13}C -NMR (100 MHz, d_6 -DMSO) δ 179.0, 148.6, 146.4, 142.1, 132.1, 124.3, 121.5, 116.3, 113.0, 109.1, 69.9, 69.0, 68.0, 55.5 ppm.

3.7 Synthesis of receptor R2

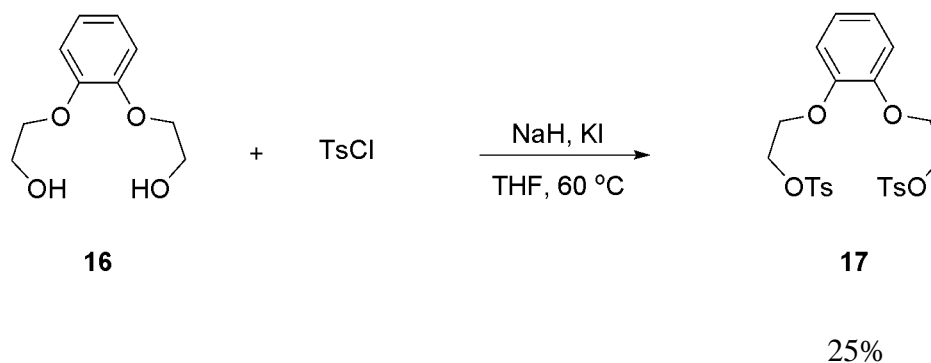
3.7.1 Synthesis of receptor 16



A mixture of pyrocatechol (1.00 g, 9.08 mmol), bromoethanol (4.00 mL, 56.7 mmol) and K_2CO_3 (12.55 g, 91.0 mmol) in CH_3CN (100 mL) was stirred and refluxed under nitrogen for 3 days. The color of the solution was changed from blue

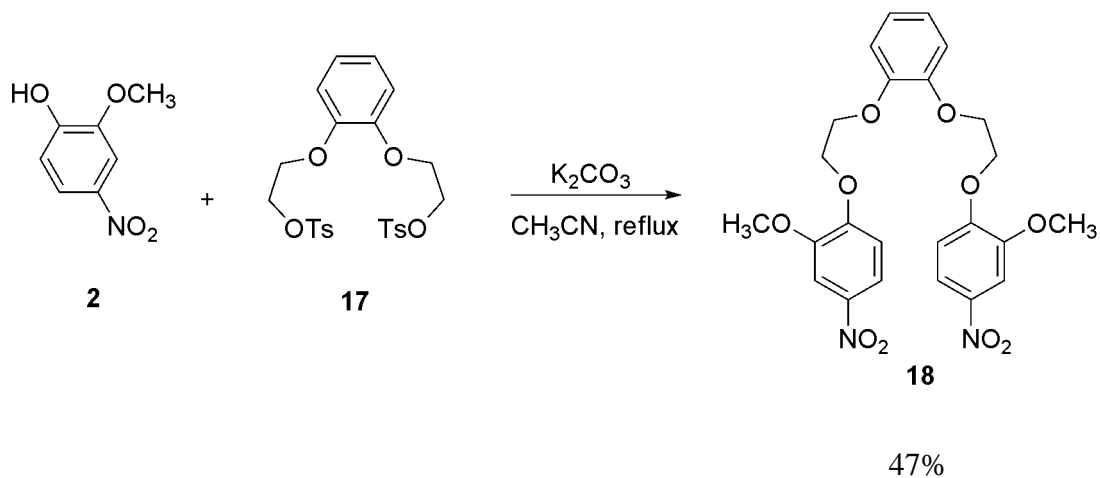
to brown. Then, the solvent was removed by evaporation. Then, 3M HCl was added to adjust pH = 1. The residue was extracted with CH₂Cl₂ (50×3 mL) and H₂O. The organic phase was collected and dried over anhydrous Na₂SO₄. The solvent was evaporated to dryness and dried under vacuum. The product was a brown oil in 1.05 g (58%). ¹H-NMR (400 MHz, CDCl₃) δ 7.0 – 6.8 (m, 4H), 4.1 – 3.9 (m, 8H).

3.7.2 Synthesis of receptor 17



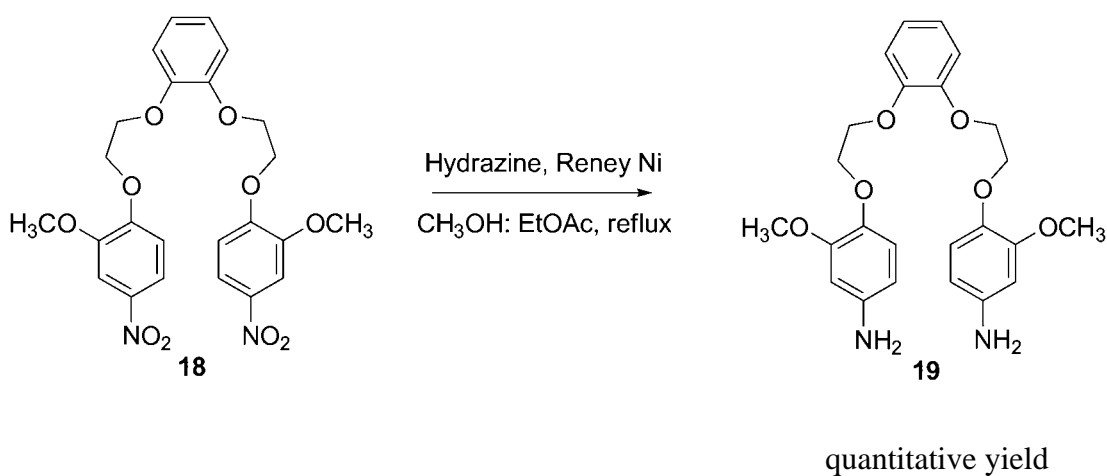
A mixture of compound **16** (0.10 g, 0.504 mmol), NaH (0.329 g, 13.7 mmol) and KI (0.20 g, 1.2 mmol) in THF (5 mL) was stirred under nitrogen at room temperature for 1 h. TsCl (0.23 g, 1.2 mmol) was dissolved in THF (5 mL) and added dropwise to the reaction. The mixture was stirred for 2 h at 60 °C. After cooling, the residue was extracted with CH₂Cl₂ (25 mL×3)/H₂O and brine. The organic phase was collected and dried over anhydrous Na₂SO₄. The reaction mixture was filtered, and the filtrate was evaporated to dryness. The crude product was purified by column chromatography using CH₂Cl₂ as eluant and a white solid was obtained in 0.06 g (25%). ¹H-NMR (400 MHz, CDCl₃) δ 7.80 (d, *J* = 8.4 Hz, 4H), 7.33 (d, *J* = 8.4 Hz, 4H), 6.91 – 6.80 (m, 4H), 4.32 (dd, *J* = 5.7, 3.8 Hz, 4H), 4.16 (dd, *J* = 5.7, 3.8 Hz, 4H), 2.43 (s, 6H).

3.7.3 Synthesis of receptor 18



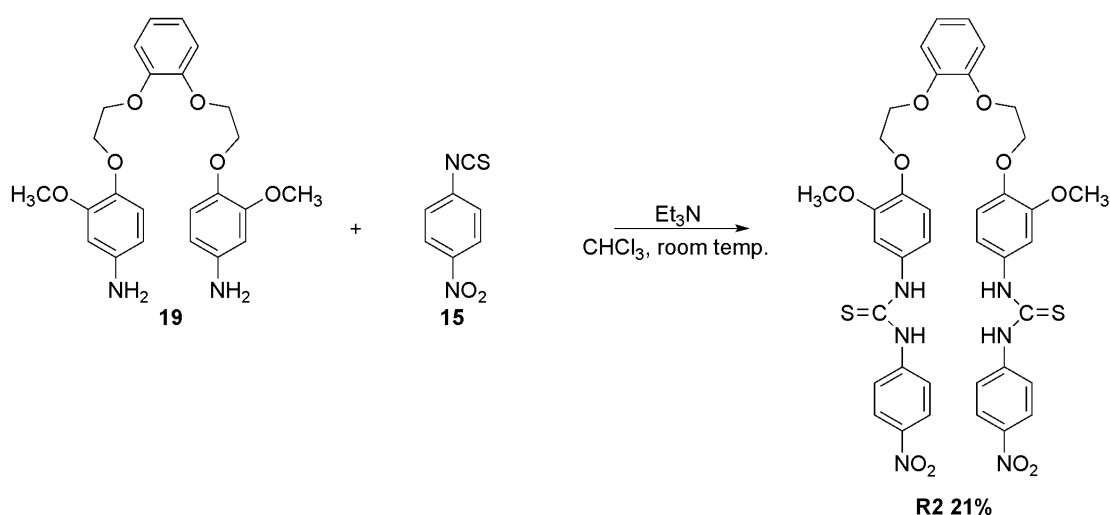
The mixture of compound **17** (0.06 g, 0.122 mmol), compound **2** (0.04 g, 0.242 mmol), K_2CO_3 (0.17 g, 1.22 mmol), tetrabutylammonium bromide in CH_3CN (50 mL) solution was stirred and refluxed under nitrogen. After 2 days, the solvent was removed and pH of the reaction mixture was adjusted to 1 with 3M HCl. The residue was extracted with CH_2Cl_2 (25×3 mL) and H_2O . The organic phase was collected and dried over anhydrous Na_2SO_4 . The solvent was removed and the product was then recrystallized with CH_3OH to yield 0.03 g (47%) of a yellow solid. $^1\text{H-NMR}$ (400 MHz, CDCl_3) δ 7.86 (dd, $J = 9.2, 2.0$ Hz, 2H), 7.72 (s, 2H), 7.04 – 6.98 (m, 6H), 4.45 (d, $J = 5.6$ Hz, 8H), 3.91 (s, 6H). $^{13}\text{C-NMR}$ (100 MHz, CDCl_3) δ 149.3, 148.8, 141.8, 122.4, 117.6, 115.6, 111.8, 106.9, 68.2, 68.0, 56.3, 29.7 ppm.

3.7.4 Synthesis of receptor 19



A mixture of compound **18** (0.03 g, 0.057 mmol) in CH₃OH (1.25 mL) and EtOAc (5.00 mL) was stirred with molecular sieve under nitrogen at room temperature. After 15 min, Raney Ni (1/4 spoon) and 0.50 mL of hydrazine hydrate were added and then refluxed for 1 hour. The molecular sieve and Raney Ni were removed by filtration. The residue was evaporated to dryness and extracted with CH₂Cl₂ (25 mL × 3) and H₂O. The organic phase was collected and dried over anhydrous Na₂SO₄. The solvent was evaporated to give a white solid as product in quantitative yield and the product was used in the next step without further purification.

3.7.5 Synthesis of receptor **R2**



In a similar procedure to the preparation of **L1**, **R2** was synthesized from compound **19** and 1-isothiocyanato-4-nitrobenzene. **R2** was obtained as yellow powders in 0.02 g (21%). MALDI-TOF (m/z) [M]⁺: calcd 800.19, found 823.73. ESI-HRMS: m/z calcd 823.1832 found 823.1689 for [$M+\text{Na}$]⁺. ¹H-NMR (400 MHz, d₆-DMSO) δ 10.22 (s, 2H), 10.14 (s, 2H), 8.18 (d, $J = 8.8$ Hz, 4H), 7.81 (d, $J = 9.2$ Hz, 4H), 7.14 - 6.92 (m, 10H), 4.30 - 4.28 (m, broad, 8H), 3.71 (s, 6H). ¹³C-NMR (100 MHz, d₆-DMSO) δ 179.1, 155.6, 148.2, 146.3, 145.5, 142.1, 135.6, 132.2, 126.3, 124.3, 121.5, 118.3, 116.4, 112.3, 110.0, 109.3, 67.5, 55.8, 55.5 ppm.

3.8 Complexation studies of ligands L1 – L4

The samples for $^1\text{H-NMR}$ titration were prepared in 10^{-2} - 10^{-3} M concentration in 5 mm NMR tubes. The UV-Vis spectra were measured using 10^{-5} M of ligands with quartz cuvette (path length = 1 cm) at room temperature. Fluorescence spectra were recorded at room temperature with the width of the excitation slit and the emission slit at 10 nm and excited at 340 nm. The fluorescence quantum yields, Φ_F , were estimated using the integrated emission intensity of anthracene as standard in ethanol via equation, $\Phi_F = \Phi'_{ST}(\text{Grad}_F/\text{Grad}_{ST})(\eta^2_F/\eta^2_{ST})$. Binding constants between the ligand and various ions were determined by linear equation of Benesi Hilderbrand plot.

3.8.1 Fluorescence titration

Fluorescence titrations of ligands **L1 – L4** were carried according to the following details.

1. Fluorescence titration of ligands L1 – L3 with various anions.

Solutions of ligands **L1 – L3** (5.0×10^{-6} M) were prepared in 10 mL of a volumetric flask and the 2 mL of each ligand was pipetted into a 1 cm pathlength quartz cuvette. The emission spectra were recorded in the range of 360 – 700 nm at room temperature by using the excitation wavelength at 340 nm, the width of excitation and emission slit was 10 nm, the smoothing factor was 15, the scan rate and the PMT voltage were medium. The solution of each anion (1.0×10^{-3} M) was prepared in 10 mL of a volumetric flask and transferred to microburette 2 mL. The anion solution was introduced in portion to the cuvette and stirred for 1 min prior to measurement. Amounts of added anions were listed in Table 3.1.

2. Fluorescence titration of ligand L4 with various anions.

Solution of ligand **L4** (5.0×10^{-5} M) was prepared in 10 mL of a volumetric flask and the 2 mL of this ligand was pipetted into a 1 cm pathlength quartz cuvette. The emission spectra were recorded in the same range as ligands **L1 – L3** at room temperature. The excitation wavelength, the width of excitation and emission slit, the smoothing factor, the scan rate and the PMT voltage were in the same condition with previous ligands. The concentration of each anion was 1.0×10^{-2} M and was prepared in 10 mL of a volumetric flask and was introduced in portion to the cuvette by microburette. The

solution mixture between ligand and anion was stirred for 1 min prior to measurement. Amounts of added anions were listed in Table 3.2.

Table 3.1 Amounts of anions (1.0×10^{-3} M) that added in 2 mL of ligands (L1 – L3 = 5.0×10^{-6} M) for complexation studies

Point	Equiv. of anion	Volume of anion (mL)
1	1.0	0.01
2	2.0	0.01
3	3.0	0.01
4	4.0	0.01
5	5.0	0.01
6	6.0	0.01
7	7.0	0.01
8	8.0	0.01
9	9.0	0.01
10	10.0	0.01
11	14.0	0.04
12	18.0	0.04
13	22.0	0.04
14	26.0	0.04
15	30.0	0.04
16	38.0	0.08
17	46.0	0.08
18	54.0	0.08
19	62.0	0.08
20	70.0	0.08
21	80.0	0.10
22	90.0	0.10
23	100.0	0.10

Table 3.2 Amounts of anions (1.0×10^{-2} M) that added in 2 mL of ligand **L4** (5.0×10^{-5} M) for complexation studies

Point	Equiv. of anion	Volume of anion (mL)
1	1.0	0.01
2	2.0	0.01
3	3.0	0.01
4	4.0	0.01
5	5.0	0.01
6	6.0	0.01
7	7.0	0.01
8	8.0	0.01
9	9.0	0.01
10	10.0	0.01
11	14.0	0.04
12	18.0	0.04
13	22.0	0.04
14	26.0	0.04
15	30.0	0.04
16	38.0	0.08
17	46.0	0.08
18	54.0	0.08
19	62.0	0.08
20	70.0	0.08
21	80.0	0.10
22	90.0	0.10
23	100.0	0.10

3. Fluorescence titrations of ligands L1 and L4 with sodium ion. The preparations of ligands were similar to the titration of anion. However, the sodium solution (1.0×10^{-3} M or 1.0×10^{-2} M) was prepared in CH_3CN and was introduced in portion to cuvette by microburette. The mixture between the ligand and sodium was stirred for 2 min prior to measurement. The titration procedure was similar to that of anion.

3.8.2 $^1\text{H-NMR}$ titration

From the fluorescence titration results, we chose the ligand **L1** and **L4** to study the complexation property with fluoride and sodium ions. $^1\text{H-NMR}$ titrations of ligands **L1** and **L4** were carried out as follows.

1. $^1\text{H-NMR}$ titrations of ligands L1 and L4 with fluoride anion. The solutions of ligands **L1** and **L4** (1.0×10^{-3} M) in CDCl_3 0.5 mL were prepared in a 5 mm of a NMR tube. The $^1\text{H-NMR}$ spectrum of each free ligand was recorded. The

solution of fluoride anion (1.0×10^{-2} M) in CDCl_3 was prepared in a vial and was added via a microsyringe (10 and 50 μL portions) to the free ligand solution. $^1\text{H-NMR}$ spectra were recorded after each addition. Amounts of added anions were listed in Table 3.3.

2. $^1\text{H-NMR}$ titrations of ligands L1 and L4 with sodium ion. The solution of ligands **L1** and **L4** (1.0×10^{-3} M) in $\text{CDCl}_3/\text{CD}_3\text{CN}$ (9/1 v/v) 0.5 mL were prepared in a 5 mm of a NMR tube. The $^1\text{H-NMR}$ spectrum of free ligand was recorded. The solution of sodium ion (1.0×10^{-2} M) in $\text{CDCl}_3/\text{CD}_3\text{CN}$ was prepared in a vial and was added via a microsyringe (10 and 50 μL portions) to the free ligand solution. $^1\text{H-NMR}$ spectra were recorded after each addition. The titration procedure was similar to that of fluoride anion.

Table 3.3 Amounts of fluoride (1.0×10^{-2} M) that added in 0.5 mL of ligands (**L1** and **L4** = 1.0×10^{-3} M) for complexation studies

Point	Equiv. of fluoride	Volume of fluoride (μL)
1	0.1	5
2	0.2	5
3	0.3	5
4	0.4	5
5	0.5	5
6	0.6	5
7	0.7	5
8	0.8	5
9	0.9	5
10	1.0	5
11	1.2	10
12	1.4	10
13	1.6	10
14	1.8	10
15	2.0	10
16	3.0	50
17	4.0	50

3.8.3 Determination of the stoichiometry of the L1·F complex by Job's method

Solutions of **L1** and fluoride in CHCl_3 (5.0×10^{-5} M) were prepared in a 20 mL of a volumetric flask. Solution of **L1** plus fluoride was pipetted to a 1 cm quartz cuvette to provide the total volume 2 mL according to Table 3.4. Emission spectrum of each addition was measured after stirred 2 min.

Table 3.4 Amounts of fluoride (5.0×10^{-5} M) and ligand **L1** (5.0×10^{-5} M) that added in cuvette for Job's method

Point	Volume of fluoride (mL)	Volume of L1 (mL)
1	0	2.00
2	0.20	1.80
3	0.40	1.60
4	0.60	1.40
5	0.80	1.20
6	1.00	1.00
7	1.20	0.80
8	1.40	0.60
9	1.60	0.40
10	1.80	0.20
11	2.00	0.00

3.9 Complexation studies of ligands R1 and R2

3.9.1 UV-vis titration with anion and cation

Solutions of ligands **R1** and **R2** (2.5×10^{-5} M) were prepared in 10 mL of a volumetric flask and the 2 mL of these ligands were pipetted into a 1 cm pathlength quartz cuvette. The absorption spectra were recorded in the range of 250 – 700 nm. The solution of anion or cation (5.0×10^{-3} M) was prepared in 10 mL of a volumetric flask and was introduced in portions to the cuvette by microburette. The solution mixture between ligand and anion was stirred for 2 min prior to measurement. Amounts of added anions were listed in Table 3.5.

Table 3.5 Amounts of anion or cation (5.0×10^{-3} M) that added in 2 mL of ligand (**R1** and **R2** = 2.5×10^{-5} M) for complexation studies

Point	Equiv. of anion or cation	Volume of anion or cation (mL)
1	0.1	0.01
2	0.2	0.01
3	0.3	0.01
4	0.4	0.01
5	0.5	0.01
6	0.6	0.01
7	0.7	0.01
8	0.8	0.01
9	0.9	0.01
10	1.0	0.01
11	1.2	0.02
12	1.4	0.02
13	1.6	0.02
14	1.8	0.02
15	2.0	0.02
16	2.4	0.04
17	2.8	0.04
18	3.2	0.04
19	3.6	0.04
20	4.0	0.04
21	4.8	0.08
22	5.6	0.08
23	6.4	0.08
24	7.2	0.08
25	8.0	0.08

3.9.2 $^1\text{H-NMR}$ titration with anion and cation

$^1\text{H-NMR}$ titration of **R1** had been carried out in d_6 -DMSO. However, we could not use this technique for following interactions between the receptor **R2** and various ions due to its low solubility in almost type of solvent. $^1\text{H-NMR}$ titration of ligand **R1** were carried out as follows

1. $^1\text{H-NMR}$ titration of ligand R1 with fluoride anion. The solution of ligand **R1** (1.0×10^{-2} M) in d_6 -DMSO 0.35 mL was prepared in a 5 mm NMR tube. The $^1\text{H-NMR}$ spectrum of free ligand was recorded. The solution of fluoride (0.1 M) in d_6 -DMSO was prepared in a vial and was added via a microsyringe (10 and 50 μL portions) to the free ligand solution. $^1\text{H-NMR}$ spectra were recorded after each addition. Amounts of added fluoride were listed in Table 3.6.

2.¹H-NMR titration of ligand R1 with sodium ion. The solution of ligand **R1** (1.0×10^{-2} M) in d_6 -DMSO 0.35 mL was prepared in a 5 mm NMR tube. The ¹H-NMR spectrum of free ligand was recorded. The solution of sodium (0.1 M) in d_6 -DMSO was prepared in a vial and was added via a microsyringe (50 μ L portion) to the free ligand solution. ¹H-NMR spectra were recorded after each addition. Amounts of added anions were listed in Table 3.7.

Table 3.6 Amount of fluoride (0.1 M) that added in 0.35 mL of ligand **R1** (1.0×10^{-2} M) for complexation studies

Point	Equiv. of fluoride	Volume of fluoride (μ L)
1	0.1	3.5
2	0.2	3.5
3	0.3	3.5
4	0.4	3.5
5	0.5	3.5
6	0.6	3.5
7	0.7	3.5
8	0.8	3.5
9	0.9	3.5
10	1.0	3.5
11	1.2	7.0
12	1.4	7.0
13	1.6	7.0
14	1.8	7.0
15	2.0	7.0

Table 3.7 Amount of sodium (0.1 M) that added in 0.35 mL of ligand **R1** (1.0×10^{-2} M) for complexation studies

Point	Equiv. of sodium	Volume of sodium (μ L)
1	0.5	18.0
2	1.0	18.0
3	1.5	18.0
4	2.0	18.0
5	3.0	36.0
6	4.0	36.0

3.10 Decomplexation studies of L1·F and L4·F

From complexation studies of various ligands, we chose ligands **L1** and **L4** to study the decomplexation property by adding some ion into the complex solution and followed the interaction by fluorescence and $^1\text{H-NMR}$ titration techniques.

3.10.1 Fluorescence titrations

The decomplexation of ligands **L1** and **L4** was studied in two processes. The first process was the study of each ligand in the presence of fluoride and then titrated with sodium ion, and vice versa in the last process.

1. Fluorescence titration of L1·100F (L4·100F) with sodium ion. The fresh solution of each ligand **L1** and **L4** ($\text{L1} = 5.0 \times 10^{-6} \text{ M}$, $\text{L4} = 5.0 \times 10^{-5} \text{ M}$) were prepared in 10 mL of a volumetric flask and the 2 mL of it was pipetted into a 1 cm pathlength quartz cuvette. The emission spectra were recorded in the range 360 – 700 nm at room temperature by using the excitation wavelength at 340 nm, the width of excitation and emission slit was 10 nm, the smoothing factor was 15, the scan rate and the PMT voltage were medium. The high concentration of 100 equiv. of fluoride was prepared and then added one portion into the ligand solution. The emission spectrum of ligand plus fluoride was recorded after stirring 60 sec. The sodium metal (1.0×10^{-2} and $1.0 \times 10^{-3} \text{ M}$ up to concentration of ligand) was prepared in a 10 mL of volumetric flask and transferred to microburette 2 mL. The metal solution was introduced in portion to the former cuvette and stirred for 60 sec. prior to measurement. Amounts of added Na^+ were shown in Table 3.8.

2. Fluorescence titration of L1·10Na (L4·10Na) with fluoride ion. A solution of ligands **L1** and **L4** ($\text{L1} = 5.0 \times 10^{-6} \text{ M}$, $\text{L4} = 5.0 \times 10^{-5} \text{ M}$) was prepared in 10 mL of a volumetric flask and was pipetted into a 1 cm pathlength quartz cuvette. The emission spectra were recorded in the range of 360 – 700 nm at room temperature by using the excitation wavelength at 340 nm, the width of excitation and emission slit was 10 nm, the smoothing factor was 15, the scan rate and the PMT voltage were medium. The high concentration of 10 equiv. (30 equiv.) of sodium was prepared and then added one portion into the ligand solution. The emission spectrum of ligand plus sodium was recorded after stirring for 1 min. Fluoride anion (1.0×10^{-2} and $1.0 \times 10^{-3} \text{ M}$

up to concentration of ligand) was prepared in a 10 mL of volumetric flask and transferred via microburette 2 mL. The fluoride solution was introduced in portion to the former cuvette and stirred for 60 sec. prior to measurement. The added cation and anion were listed in Table 3.9. The decomplexation study of L1·30Na and L4·30Na was also studied.

Table 3.8 Amounts of sodium that added in Ln·100F solution for decomplexation studies

Point	Equiv. of fluoride	Equiv. of sodium	Volume of sodium (mL)
1	100	1.0	0.01
2	100	2.0	0.01
3	100	3.0	0.01
4	100	4.0	0.01
5	100	5.0	0.01
6	100	6.0	0.01
7	100	7.0	0.01
8	100	8.0	0.01
9	100	9.0	0.01
10	100	10.0	0.01
11	100	14.0	0.04
12	100	18.0	0.04
13	100	22.0	0.04
14	100	26.0	0.04
15	100	30.0	0.04
16	100	38.0	0.08
17	100	46.0	0.08
18	100	54.0	0.08
19	100	62.0	0.08
20	100	70.0	0.08
21	100	80.0	0.10
22	100	90.0	0.10
23	100	100.0	0.10

Table 3.9 Amounts of fluoride that added in **Ln·10Na** solution for decomplexation studies

Point	Equiv. of sodium	Equiv. of fluoride	Volume of fluoride (mL)
1	10	1.0	0.01
2	10	2.0	0.01
3	10	3.0	0.01
4	10	4.0	0.01
5	10	5.0	0.01
6	10	6.0	0.01
7	10	7.0	0.01
8	10	8.0	0.01
9	10	9.0	0.01
10	10	10.0	0.01
11	10	14.0	0.04
12	10	18.0	0.04
13	10	22.0	0.04
14	10	26.0	0.04
15	10	30.0	0.04
16	10	38.0	0.08
17	10	46.0	0.08
18	10	54.0	0.08
19	10	62.0	0.08
20	10	70.0	0.08
21	10	80.0	0.10
22	10	90.0	0.10
23	10	100.0	0.10

3.10.2 ¹H-NMR spectroscopy of L1·4F (L4·4F) with sodium ion

The solution of each ligand (1.0×10^{-3} M) in $\text{CDCl}_3/\text{CD}_3\text{CN}$ (9/1 v/v) 0.5 mL were prepared in a 5 mm of a NMR tube. The ¹H-NMR spectrum of free ligand was recorded. The solution of fluoride ion (1.0×10^{-2} M) in $\text{CDCl}_3/\text{CD}_3\text{CN}$ was prepared in a vial. Its solution was added for 4 equiv. via a microsyringe to the free ligand solution and shook on it for 1 min. ¹H-NMR of ligand plus 4 equiv. of fluoride was recorded. The high concentration of sodium was also prepared in $\text{CDCl}_3/\text{CD}_3\text{CN}$ (9/1 v/v) and then excess added into the ligand solution. Its solution was shaken for 60 sec. ¹H-NMR spectrum of **Ln·4F·excessNa** was recorded.

3.11 Decomplexation studies of ligand **R1**

3.11.1 UV-vis titration of **R1**·4Anion with sodium ion

The solution of ligand **R1** (2.5×10^{-5} M) in DMSO was prepared in 10 mL of a volumetric flask and the 2 mL of it was pipetted into a 1 cm pathlength quartz cuvette. The absorption spectra were recorded in the range of 250 – 700 nm. The high concentration of 4 equiv. of each anion was prepared and then added one portion into the ligand solution. The absorption spectrum of ligand plus anion was recorded after stirring 2 min. The sodium metal (1.0×10^{-4} M) was prepared in a 10 mL of volumetric flask and transferred to microburette 2 mL. The metal solution introduced in portion to the former cuvette and stirred for 2 min. prior to measurement. Amounts of added Na^+ were listed in Table 3.10.

3.11.2 ^1H -NMR titration

The solution of ligand **R1** (1.1082×10^{-2} M) in d_6 -DMSO 0.35 mL was prepared in a 5 mm NMR tube. The ^1H -NMR spectrum of free ligand was recorded. The solution of anion was prepared in d_6 -DMSO in a vial for example the fluoride anion 0.08123 g (0.5149 M) was dissolved in d_6 -DMSO 0.5 mL. The solution of sodium ion (0.98818 M) in CD_3CN 0.5 mL was also prepared. The amount of fluoride solution 30 μL (4 equiv.) was added directly to the **R1** solution via a microsyringe and shook on it for 2 min. ^1H -NMR spectrum of **R1**·4F complex was recorded after addition. After that, the 40 μL of sodium solution (10 equiv.) was added. The ^1H -NMR spectrum of **R1**·4F·10Na was recorded. The fluoride anion was displaced by the other anions such as AcO^- , BzO^- and H_2PO_4^- and recorded the spectrum in the same procedure as **R1**·4F·10Na method.

Table 3.10 Amounts of sodium that added in **R1**·4Anion solution for decomplexation studies

Point	Equiv. of anion	Equiv. of sodium	Volume of sodium (mL)
1	4	0.1	0.01
2	4	0.2	0.01
3	4	0.3	0.01
4	4	0.4	0.01
5	4	0.5	0.01
6	4	0.6	0.01
7	4	0.7	0.01
8	4	0.8	0.01
9	4	0.9	0.01
10	4	1.0	0.01
11	4	1.2	0.02
12	4	1.4	0.02
13	4	1.6	0.02
14	4	1.8	0.02
15	4	2.0	0.02
16	4	2.4	0.04
17	4	2.8	0.04
18	4	3.2	0.04
19	4	3.6	0.04
20	4	4.0	0.04
21	4	4.8	0.08
22	4	5.6	0.08
23	4	6.4	0.08
24	4	7.2	0.08
25	4	8.0	0.08
26	4	9.0	0.10
27	4	10.0	0.10

3.12 Anion interference studies

The competitive experiments were carried out in the presence of 2 mL of ligand (**L1** – **L3** = 5.0×10^{-6} M and **L4** 5.0×10^{-5} M) and 100 equiv. of the anion mixture in CHCl_3 solution such as F^- , AcO^- , BzO^- , H_2PO_4^- , Cl^- , Br^- and I^- . The solution mixture between each ligand and these anions was stirred for 2 min. prior to measurement by a fluorescence spectrophotometer.

3.13 Principal component analysis (PCA) for R1 with ions

3.13.1 PCA for R1 with anions

The solution of ligand **R1** (2.5×10^{-5} M) in DMSO was prepared in a 100 mL volumetric flask, and 2 mL of the stock solution was pipetted into a 1 cm pathlength quartz cuvette. Solutions of ions (F^- , AcO^- , BzO^- , $H_2PO_4^-$, Na^+ , K^+) were prepared to have 4.0×10^{-2} M concentration, and 5 μ L of the ion solution and 5 μ L of DMSO were added into the ligand solution. The total volume of each sample was 2.01 mL. The absorption spectrum of **R1** + ion + DMSO was recorded in the range of 260 – 600 nm after stirring 1 min. Each ion was measured for 5 times. The UV-vis spectrum of the free **R1** solution and DMSO (10 μ L) was also recorded.

3.13.2 PCA for R1 with anions in the presence of cations

The solution of ligand **R1** (2.5×10^{-5} M) in DMSO was prepared in a 100 mL volumetric flask, and 22 mL of the stock solution was mixed with 55 μ L of each anion (4.0×10^{-2} M) and then was pipetted into a 1 cm pathlength quartz cuvette. A metal ion (Na^+ or K^+) solution (4.0×10^{-2} M) was added (5 μ L) into the mixed solution of the ligand and an anion. The absorption spectrum of the mixed solution was recorded in the range of 260 – 600 nm after stirring 1 min. Each experiment was repeated for 5 times.

CHAPTER IV

RESULTS AND DISCUSSION

4.1 Fluorosensor L1 – L4

4.1.1. Syntheses of L1 – L4

The fluorescent sensors **L1** – **L3** containing variable chain length of the polyethylene glycol and pyrene thiourea were synthesized by coupling reaction between 1-thiocyanatopyrene and the corresponding amino groups in a moderate yield as showed in this order, 48%, 38% and 52%, respectively. The reaction mechanism of all compounds proceeded via nucleophilic attack of nitrogen atom of amino group at carbon atom of 1-isothiocyanate in basic solution of triethylamine to give the thiourea moiety. The final products are in yellow solid. The monomeric pyrene model compound **L4** was also synthesized in 32% of white solid to compare the binding ability between in the presence and in the absence of polyethylene glycol chain. All synthesized compounds were good soluble in non-polar organic solvents such as dichloromethane, chloroform and polar organic solvent such as DMSO.

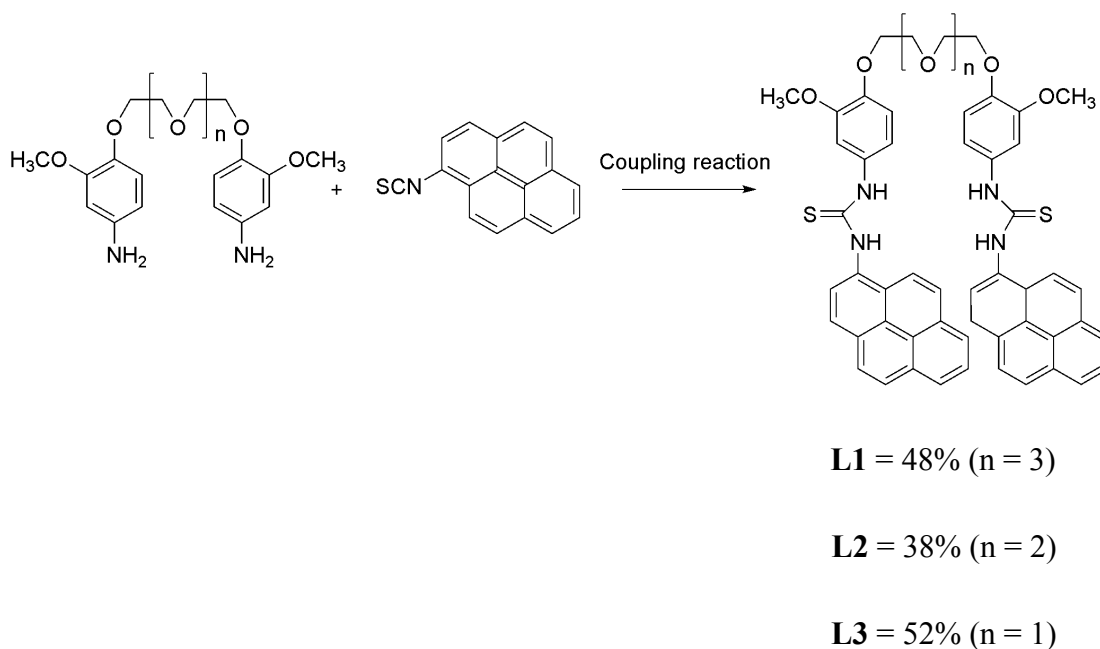


Figure 4.1 Syntheses of fluorescent sensors **L1** – **L3**

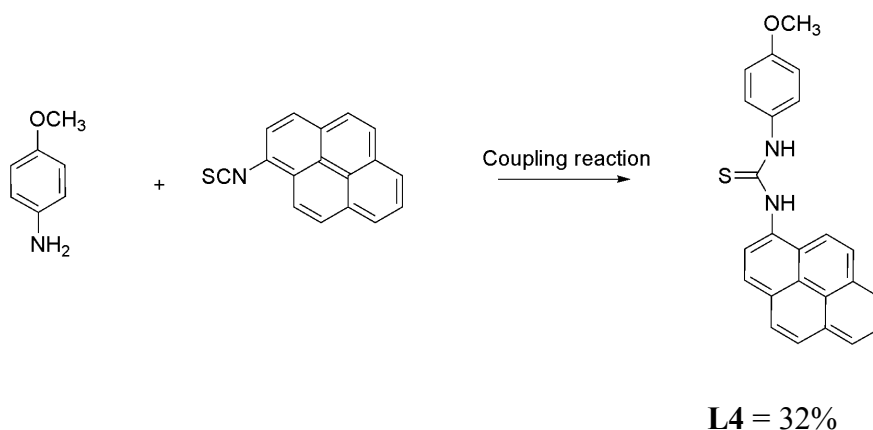


Figure 4.2 Syntheses of fluorescent sensor **L4**

4.1.2 Characterization of **L1** – **L4**

The UV-vis absorption spectra of all the sensors, **L1** – **L4**, were studied in CHCl_3 solution exhibiting two major absorption bands for the $\pi - \pi^*$ transition of aromatic hydrocarbons in the range 250 – 400 nm (Figure 4.3). These bands represent the characteristic shape of the pyrene group for $S_0 \rightarrow S_1$ and $S_0 \rightarrow S_2$ transitions [4]. The fluorescence emission spectra of **L1** – **L4** displayed only intense characteristic monomer bands of the pyrene in the same region between 390 – 410 nm (Figure 4.4). The fluorescence emissions of **L1** – **L3** were observed in an almost intensity at the same concentration, 5×10^{-6} M. However, the intensity of **L4** had a very weak monomer emission at this concentration therefore the emission of **L4** was measured at 5×10^{-5} M. The NMR spectroscopy was used to determine the structure of all receptors. ^1H -NMR spectra were recorded in CDCl_3 and ^{13}C -NMR spectra were prepared in d_6 -DMSO to increase the solubility. The ^1H -NMR data of the receptors **L1** – **L3** displayed no significant difference of their proton signals (Table 4.1). The polyethylene glycol protons, H_a , H_a' , H_b , H_c , showed the resonance signals around 3.6 – 4.1 ppm. The methoxy protons of H_d displayed at 3.8 ppm which observed at the same position with the H_b . The benzyl protons, H_e , of **L1** – **L3** receptors appeared as singlet peak at 7.0 ppm. The signals at 6.8 ppm, which corresponded to 4 protons, were assigned to the H_f and H_g . The two aromatic protons of **L4** were also observed as a doublet peak at 6.3 and 7.3 ppm. Moreover, the spectra of all the receptors showed a multiplet peak of pyrene signals in the range of 8.0 – 8.2 ppm, which was the characteristic peak of the aromatic pyrene protons. The protons of thiourea group

were overlapped with the pyrene proton when CDCl_3 was used as a solvent. However, the appearance of NH signals was observed in d_6 -DMSO solution (Figure A7, A11, A15, and A18). The ^{13}C -NMR data of **L1** – **L4** receptors were concluded in Table 4.2.

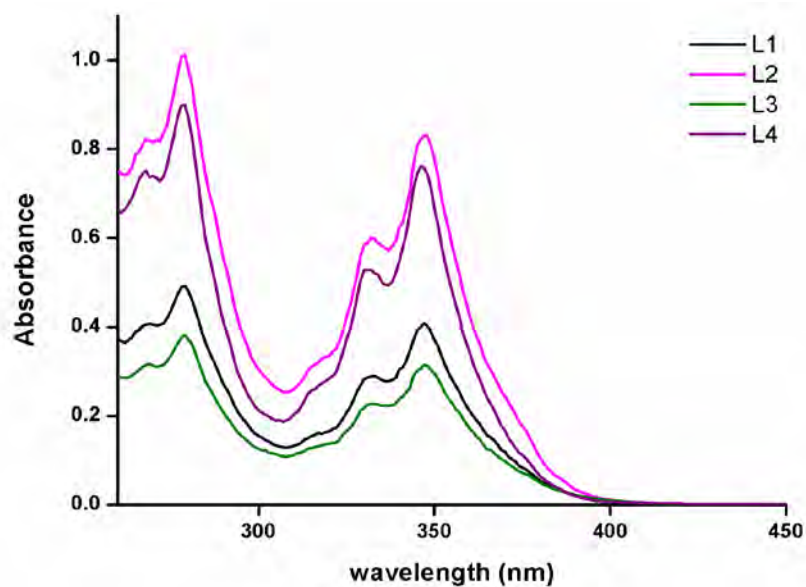


Figure 4.3 UV-vis absorption spectra of fluorescent sensors **L1** – **L4**

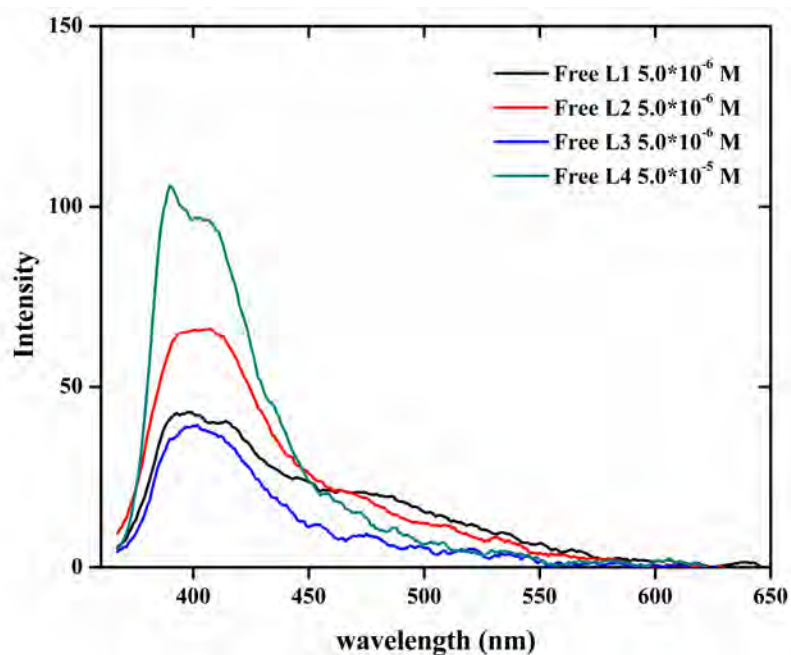
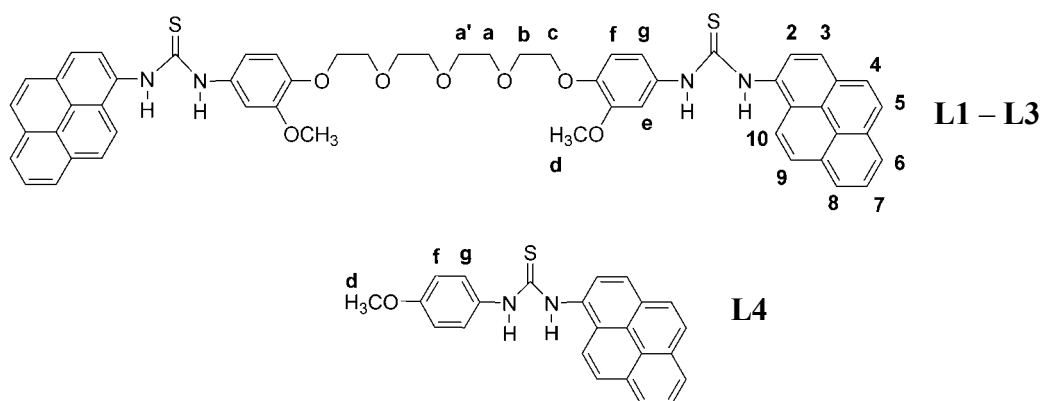


Figure 4.4 Fluorescence emission spectra of fluorescent sensors L1 – L4

Table 4.1 ¹H-NMR data for L1 – L4 in CDCl₃

H-Position	L1 (ppm)	L2 (ppm)	L3 (ppm)	L4 (ppm)
a'	3.6 (d)	-	-	-
a	3.6 (d)	3.7 (s)	-	-
b	3.8 (s)	3.8 (m)	3.9 (t)	-
c	4.1 (s)	4.1 (t)	4.1 (t)	-
d	3.8 (s)	3.8 (m)	3.8 (s)	3.8 (s)
f	6.8 (s)	6.8 (m)	6.8 (m)	6.9 (d)
g	6.8 (s)	6.8 (m)	6.8 (m)	7.3 (d)
e	7.0 (s)	7.0 (s)	7.0 (s)	-
pyrene	8.0 (m)	8.0 (m)	8.1 (m)	8.1 (m)
NH	8.0 (m)	8.0 (m)	8.1 (m)	8.1 (m)

Table 4.2 ¹³C-NMR data for L1 – L4 in d₆-DMSO

C-Position	L1 (ppm)	L2 (ppm)	L3 (ppm)	L4 (ppm)
a'	68.0	-	-	-
a	68.9	68.0	-	-
b	69.7	68.9	67.9	-
c	69.8	69.9	68.8	-
d	55.4	55.4	55.2	55.1
f	113.0	113.0	113.0	NA
g	109.7	109.7	109.5	113.5
e	116.7	116.8	116.6	-
C _{pyr}	130.6 - 122.7	130.6 - 122.7	130.4 - 122.5	130.6 - 122.6
C = S	181.2	181.2	181.0	181.6
C _{aro} - OCH ₃	145.3	145.3	145.1	156.6
C _{aro} - OCH ₂	148.5	148.5	148.4	-
C _{aro} - N	132.6	132.6	132.5	132.2
C _{pyr} - N	133.2	133.2	133.0	133.0

The fluorescence quantum yields of all synthesized receptors were calculated using the integrated emission intensity of anthracene as standard via equation (1). The anthracene standard should be chosen because its solution and all synthesized ligand solutions have identical absorbance at the same excitation wavelength (340 nm) to ensure their absorption of the same number of photons.

$$\Phi_F = \Phi_{ST}(\text{Grad}_F/\text{Grad}_{ST})(\eta^2_F/\eta^2_{ST}) \quad (1)$$

The subscripts *ST* and *F* denote standard and test, respectively. Φ is the fluorescence quantum yield. *Grad* is the gradient from the plot of integrated fluorescence intensity vs absorbance, and η is the refractive index of solvent ($\eta_{\text{EtOH}} = 1.3614$ and $\eta_{\text{CHCl}_3} = 1.4458$). The data were repeated and found the average value. From the data obtained, the fluorescence quantum yield increased with the chain length of the polyethylene glycol and no chain gave the lowest quantum yield. The differences in the quantum yields of **L1** - **L4** were attributed to the podand chain dependent fluorophore interaction [51] and dimeric pyrene in **L1** - **L3** gave higher quantum yield than monomeric pyrene in **L4**. The photophysical properties for all the sensors were summarized in Table 4.3.

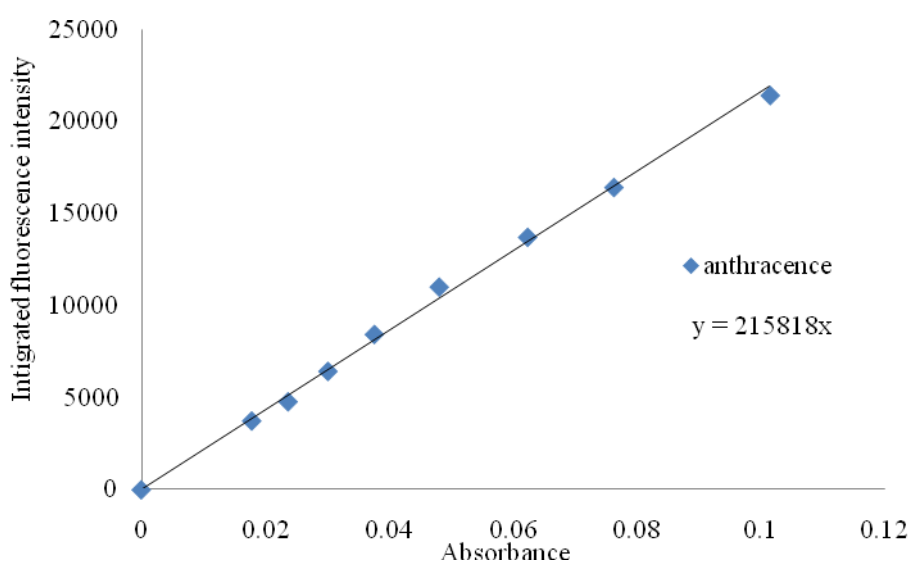


Figure 4.5 Linear plot for anthracene standard in EtOH (Grad = 215818)

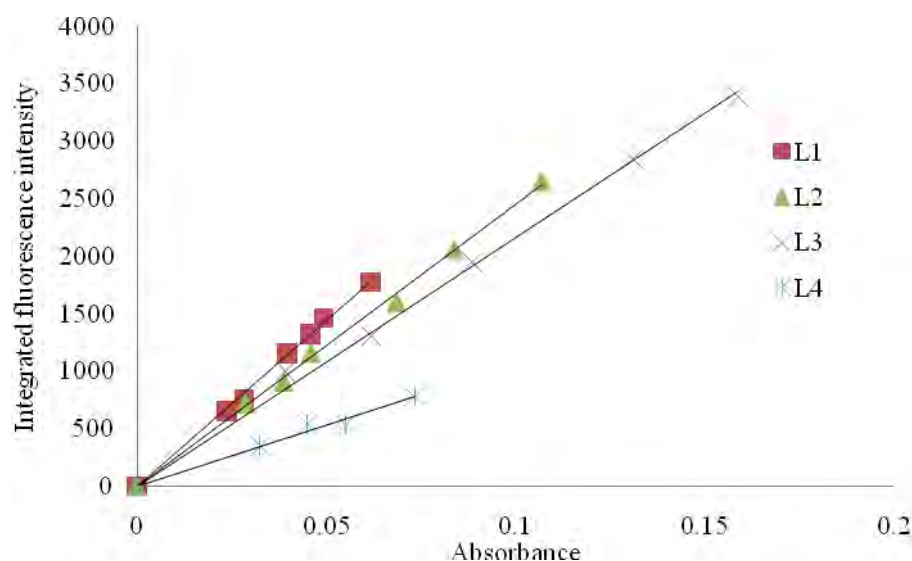


Figure 4.6 Linear plots for all synthesized ligands in CHCl_3 ($\text{Grad}_{\text{L1}} = 28872$, $\text{Grad}_{\text{L2}} = 24511$, $\text{Grad}_{\text{L3}} = 21654$, $\text{Grad}_{\text{L4}} = 10709$)

Table 4.3 The absorption and emission parameters for compound **L1** – **L4** in CHCl_3

Compound	Absorption		Emission	
	λ_{abs} (nm)	$\epsilon \times 10^4$ ($\text{mol}^{-1}\text{cm}^{-1}$)	λ_{em} (nm)	Φ_{F}^a (%)
L1	347	6.58	402	18.89
L2	347	6.60	407	11.85
L3	347	6.29	401	11.48
L4	346	3.04	393	5.60

^a Fluorescence quantum yield used anthracene as standard ($\Phi_{\text{ST}} = 0.27$ in EtOH)

4.1.3 Anion binding property

4.1.3.1 Photochemical studies

The anion binding properties of **L1** toward tetrabutylammonium anion salts were investigated in chloroform solution using fluorescence spectrophotometry. A solution of **L1** (5.0×10^{-6} M) was added 100 equiv. of F^- , OH^- , AcO^- , BzO^- , H_2PO_4^- , Br^- , Cl^- and I^- . The fluorescence spectrum of **L1**· F^- displayed pyrene excimer band at 500 nm when excited at 340 nm (Figure 4.7). However, no change was observed in the fluorescence spectra of **L1** in the presence of other salts. The order of intensity ratio between excimer and monomer bands ($I_{\text{E}}/I_{\text{M}}$) in **L1** varied as $\text{F}^- > \text{AcO}^- \approx \text{BzO}^- > \text{H}_2\text{PO}_4^- \approx \text{Cl}^- > \text{Br}^- \approx \text{I}^- > \text{OH}^-$ (Figure 4.8). The preference of fluoride to bind with –

NH of thiourea group through H-bond, was due to the highest basicity of fluoride. Moreover, the smallest atomic size of fluoride was suitable to encapsulate in the receptor molecule. Interestingly, the complexation of **L1** with OH^- displayed the minimum I_E/I_M ratio, even the OH^- was a high anion basicity. This confirmed that not only the basicity of anion but also the small size of anion was an important factor for binding with **L1** receptor.

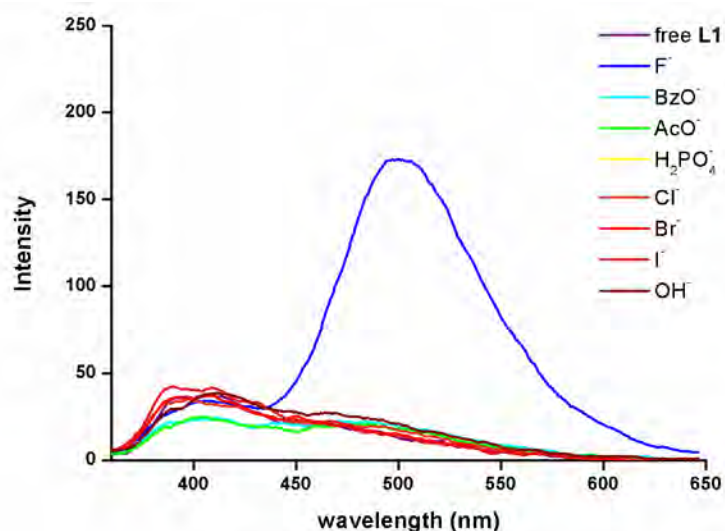


Figure 4.7 Fluorescence changes of **L1** with 100 equiv. of tetrabutylammonium anion salts in CHCl_3

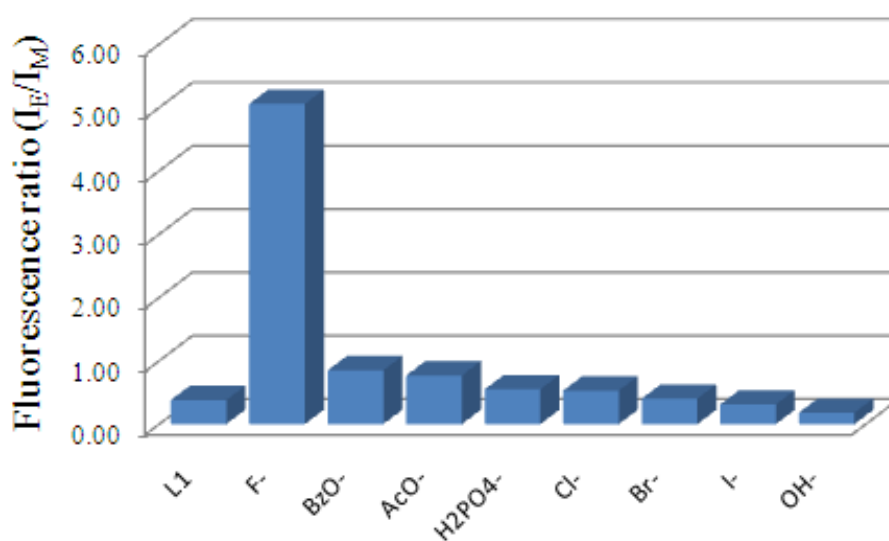


Figure 4.8 Plot of I_E/I_M (I_E : excimer fluorescence intensity at 500 nm; I_M : monomer fluorescence intensity at 398 nm)

Color changes were also observed after the addition of various anions to **L1** solution (Figure 4.9). The addition of fluoride ions into **L1** solution showed a color change from colorless to yellow. However, no color changes were observed by the addition of other anions. Therefore, the **L1** sensor can be used for the detection of fluoride by the naked eye. Moreover, the photograph under UV light showed strong emission of **L1** in the presence of fluoride.



Figure 4.9 (a) Color changes of **L1** ($5.0 \times 10^{-5} \text{M}$) in the presence and absence of 500 equiv. of anions (from left to right: **L1**, **L1**+ F^- , **L1**+ BzO^- , **L1**+ AcO^- , **L1**+ H_2PO_4^- , **L1**+ Cl^- , **L1**+ Br^- , and **L1**+ I^-) (b) Fluorescence changes of **L1** after addition fluoride (from left to right: **L1**, **L1**+ F^-) in CHCl_3

From the fluorescence titration spectra of **L1** with fluoride, the intensity enhancement of pyrene excimer band at 500 nm was gradually increased until the addition of fluoride anions into **L1** solution reached 100 equiv. However, there was a small change in monomer emission intensity at 398 nm (Figure 4.10). These confirmed that, the fluoride induced the formation of pyrene excimer interactions upon binding with fluoride resulting in the fluorescence enhancement of the excimer band. The single isoemissive point at 426 nm suggested the presence of only two species, free **L1** and **L1**· F^- in solution.

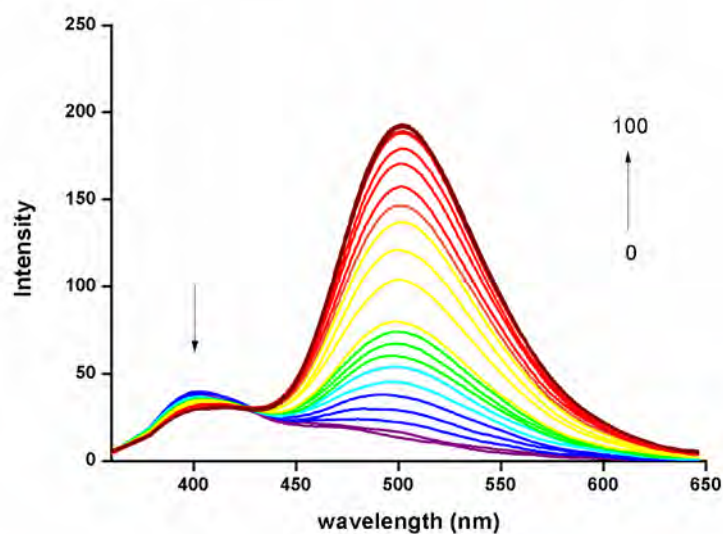


Figure 4.10 Fluorescence titration of **L1** with tetra-*n*-butylammonium fluoride in CHCl_3 ($[\text{L1}] = 5.0 \times 10^{-6} \text{ M}$, $\lambda_{\text{ex}} = 340 \text{ nm}$)

The Job's plot experiment of **L1** and fluoride displayed a maximum mole fraction of fluoride at 0.5 and supported the 1:1 or 2:2 complexation of **L1**: F^- fluoride ion (Figure 4.11). The proposed conformations of this complex in solution were a folded structure to make the intramolecular excimer formation and/or an unfolded structure to give the intermolecular excimer (Figure 4.12). Generally, the intramolecular reaction can proceed in good chemical yields only at very low concentration since it suffers from the competition of polymerization. The rate of polymerization is dependent on the monomer concentration [52]. In the case of free **L1** the ratios of fluorescence intensity between excimer and monomer were depended on the concentration of free **L1** ligand which gradually increased in the concentration range $5.0 \times 10^{-4} \text{ M}$ to $5.0 \times 10^{-7} \text{ M}$ and began to decrease when the concentration was too diluted at $5.0 \times 10^{-8} \text{ M}$ (Figure 4.13a and 4.13c). These results suggested that at the higher concentration of free **L1**, the aggregation led to lower monomer and excimer emission intensities of **L1** due to the self-quenching induced by interchain $\pi - \pi$ interactions [36]. In the presence of 100 equiv. of fluoride the intensity ratios were also dependent on the concentration of **L1** (Figure 4.13b and 4.13d), consisting of an enhancement of the excimer emission band. This suggested that the dimerization of **L1**: F^- complex proceeded *via* intermolecular interaction of pyrene molecule and

produced the unfolded structure [37]. This followed the definition of the rate of polymerization that described above. The unfolded structure of **L1** did not need to change the conformation for binding with fluoride anion and could reduce the steric hindrance within the receptor molecule. This may be affected the **L1**·F⁻ molecule preferring the unfolded structure.

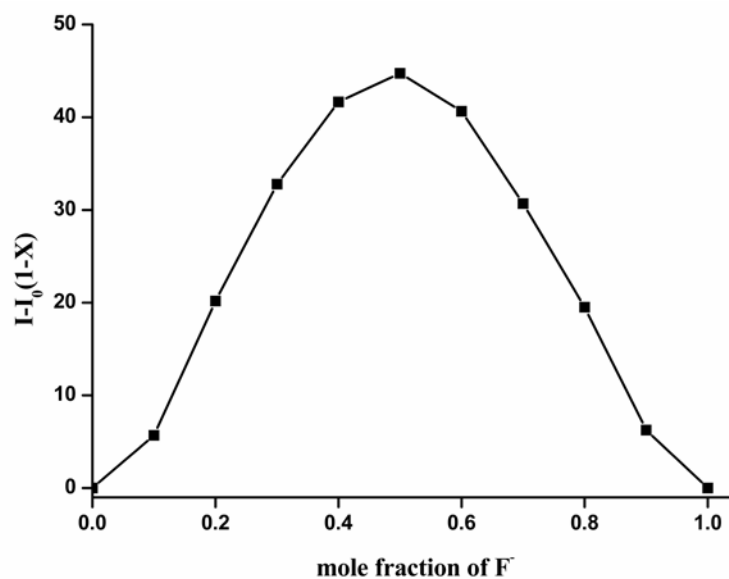


Figure 4.11 Job's plot of **L1** (5.0×10^{-6} M) with tetra-*n*-butylammonium fluoride in CHCl₃

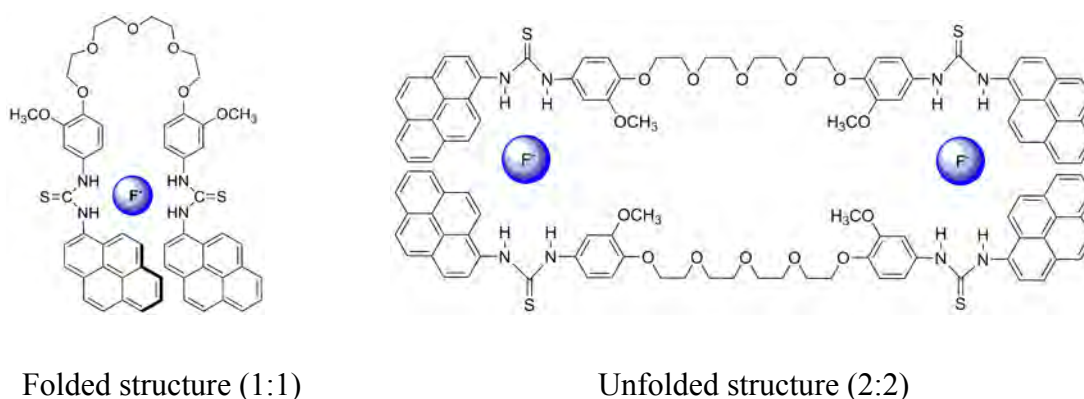


Figure 4.12 Proposed conformations of **L1** with fluoride ions in solution

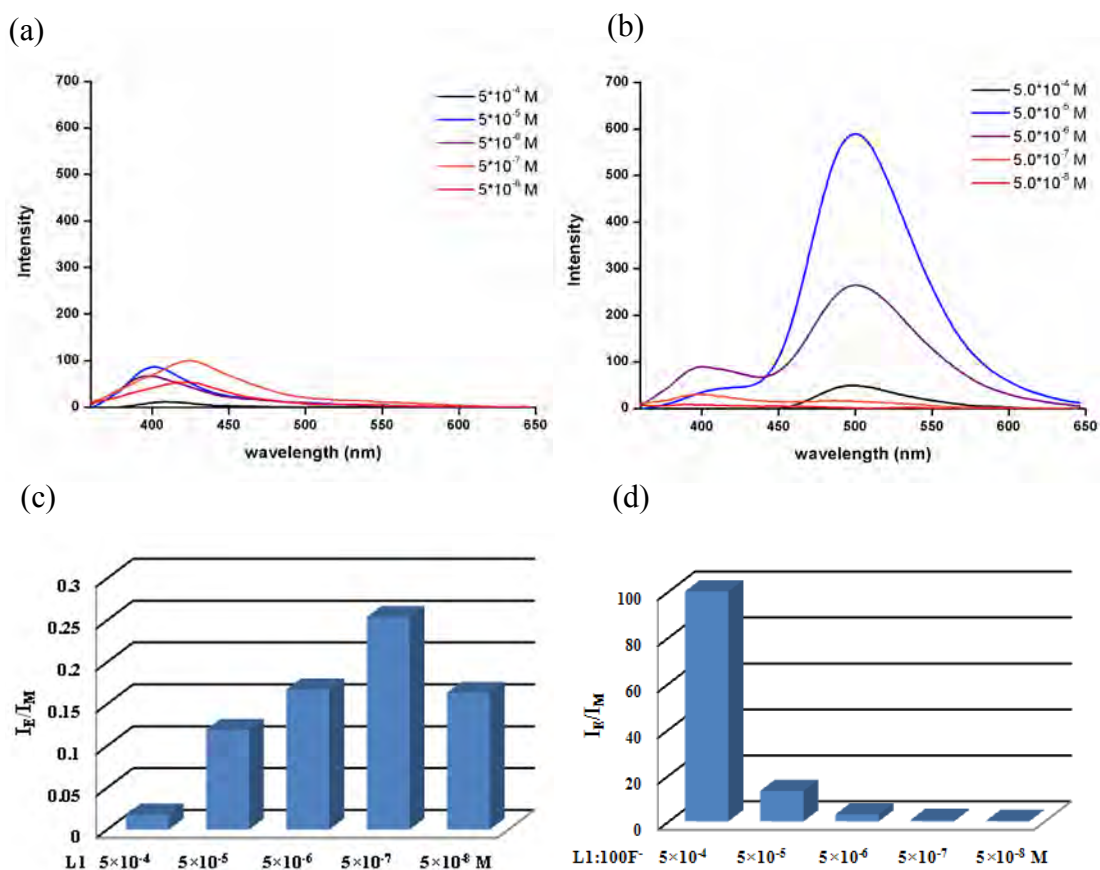


Figure 4.13 (a) Fluorescence emission of various concentration of **L1** (b) various concentrations of **L1** with fluoride (100 equiv.) (c) Plot of I_E/I_M of various concentrations of **L1** (b) various concentrations of **L1** with fluoride (100 equiv.)

From the fluorescence titration data, the binding constants (K_{ass}) for the formation of **L1** with tetrabutylammonium anions were calculated via a *Benesi-Hildebrand plot* [4] following equation (2) and the ratio of the interception at the origin to the slope yielded K_{ass} . The K_{ass} of **L1**·F⁻ was found to be higher than H₂PO₄⁻, BzO⁻ and AcO⁻, respectively (Table 4.4). Therefore, **L1** was selective toward only fluoride anions. This finding corresponded with previous research done by Gozen in 2007 in which the unfolded structure of pseudocyclic tris thiourea showed a common preference for F⁻ > H₂PO₄⁻ > AcO⁻ [28].

$$\frac{I_0}{I - I_0} = \frac{\alpha}{K_{ass} [M]} + \alpha \quad (2)$$

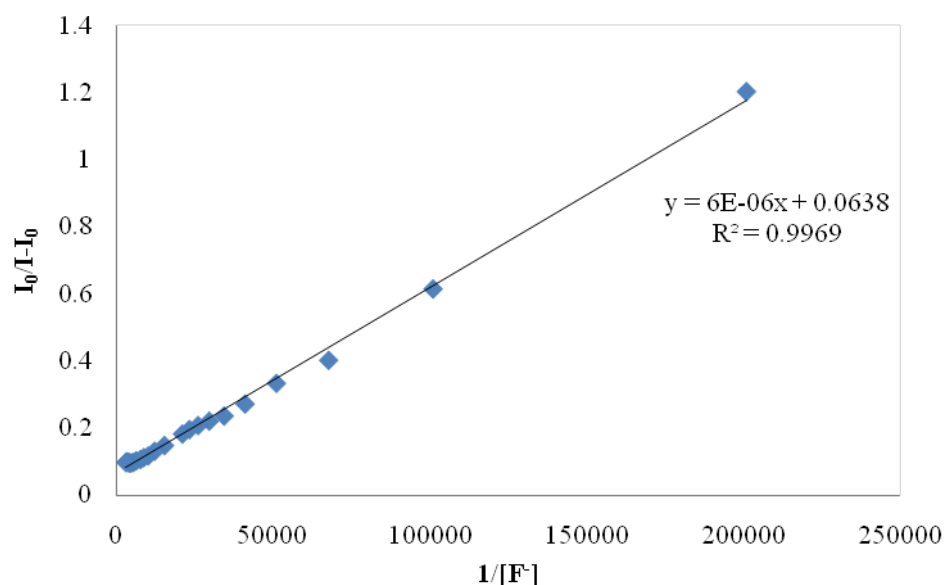


Figure 4.14 Example of Benesi-Hildebrand plot for calculation the binding constant of **L1** with fluoride anion

Table 4.4 The binding constants (M^{-1}) of receptor **L1** and various tetra-n-butylammonium anion salts in $CHCl_3$

L1·Anion	K_{ass}	R^2	Ratio	$\lambda_{ex}/\lambda_{em}$
F^-	1.0×10^4	0.9969	1 : 1	340/500
BzO^-	5.8×10^3	0.9918	1 : 1	340/408
AcO^-	4.2×10^3	0.9936	1 : 1	340/398
$H_2PO_4^-$	7.5×10^3	0.9991	1 : 1	340/391
Cl^-	ND ^a	ND ^a	ND ^a	340/412
Br^-	ND ^a	ND ^a	ND ^a	340/404
I^-	ND ^a	ND ^a	ND ^a	340/407
OH^-	ND ^a	ND ^a	ND ^a	340/400

^a ND = could not be determined due to there were small change in fluorescence emission

Besides **L1**, the anion binding properties of **L2** – **L4** with fluoride were also studied by fluorescence spectrophotometry. The fluorescence titration profiles of **L2**· F^- and **L3**· F^- complexes displayed the trend of the intensity enhancement at excimer band as same as **L1**· F^- complex (Figure 4.15 – 4.16). This finding difference with **L4**· F^- , the excimer emission band at ca. 500 nm was gradually increased accompany with the appearance of the new monomer band at ca. 420 nm (Figure 4.17). However, it was not clear that why did these new monomer bands increase accompany with the growth of the excimer bands?

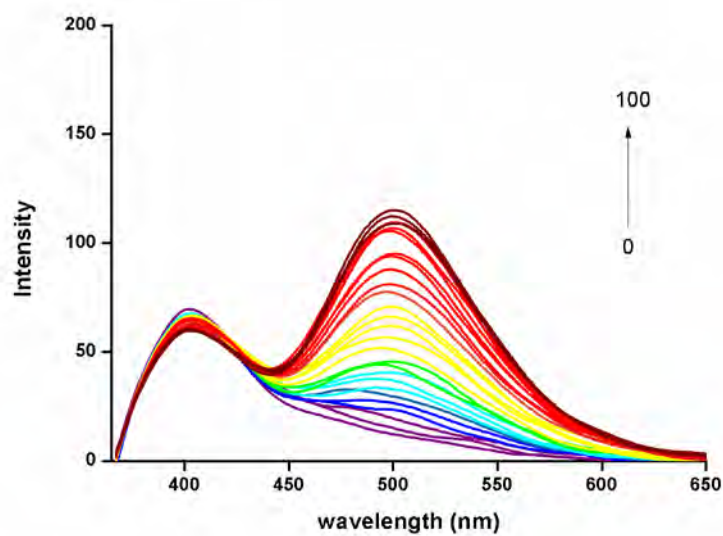


Figure 4.15 Fluorescence titration spectra of **L2** with tetra-*n*-butylammonium fluoride in CHCl_3 ($[\text{L2}] = 5.0 \times 10^{-6} \text{ M}$, $\lambda_{\text{ex}} = 340 \text{ nm}$)

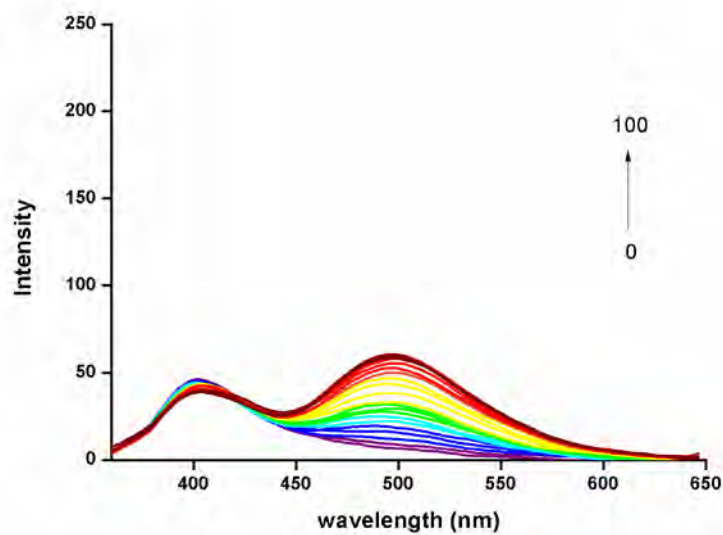


Figure 4.16 Fluorescence titration spectra of **L3** with tetra-*n*-butylammonium fluoride in CHCl_3 ($[\text{L3}] = 5.0 \times 10^{-6} \text{ M}$, $\lambda_{\text{ex}} = 340 \text{ nm}$)

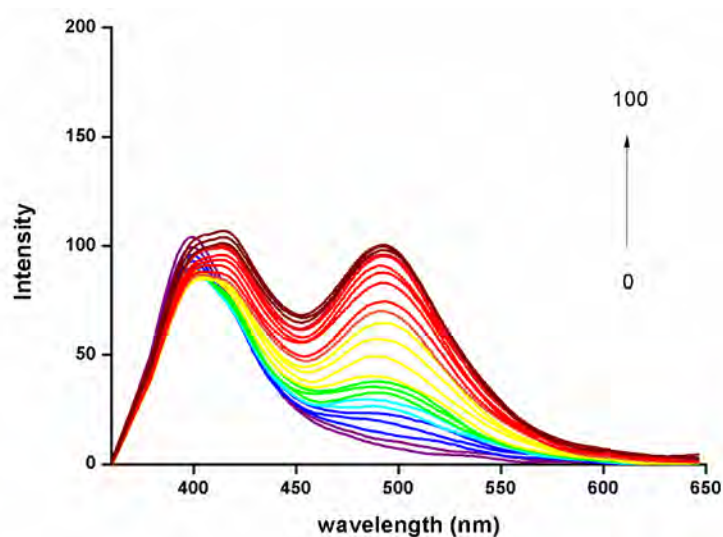


Figure 4.17 Fluorescence titration spectra of **L4** with tetra-*n*-butylammonium fluoride in CHCl_3 ($[\text{L4}] = 5.0 \times 10^{-5} \text{ M}$, $\lambda_{\text{ex}} = 340 \text{ nm}$)

The **L1**· F^- complex showed the highest binding constant and displayed the highest intensity ratio (Figure 4.18, Table 4.5). The difference in the binding properties of **L1** – **L4** with fluoride anion could be due to the effect of polyethylene glycol chain. Therefore, **L1** is the most efficient probe for detecting fluoride because a longer flexible polyethylene glycol chain may reduce the repulsion between the methoxy group and the oxygen of polyethylene glycol to provide more stable complex. In addition, F^- is the smallest anion and provides the least steric hindrance guests for **L1**. Moreover, the effect of dimerization on the sensitivity will be investigated by monitoring the fluoride induced an excimer emission at the minimum ligand concentrations. In the presence of 100 equiv. of fluoride, the minimum concentration of **L1** and **L4** for detection of the excimer emission band was $5 \mu\text{M}$ and $50 \mu\text{M}$, respectively. The fluorescence intensity at 500 nm of **L1**· F^- displayed 2 times higher fluorescence intensity than that of **L4**· F^- , even at lower concentration (Figure 4.19). Therefore, the excellent sensitivity of **L1** and weaker sensitivity of **L4** indicated that the dimer linkage on **L1** should improve the fluoride sensitivity. However, in the absence of fluoride the excimer bands were not observed. The fluorescence emission spectra of each free **L1** and **L4** displayed only the monomer band, even their concentration increased to $5.0 \times 10^{-4} \text{ M}$. This strongly supported fluoride was an important factor to induce the excimer formation.

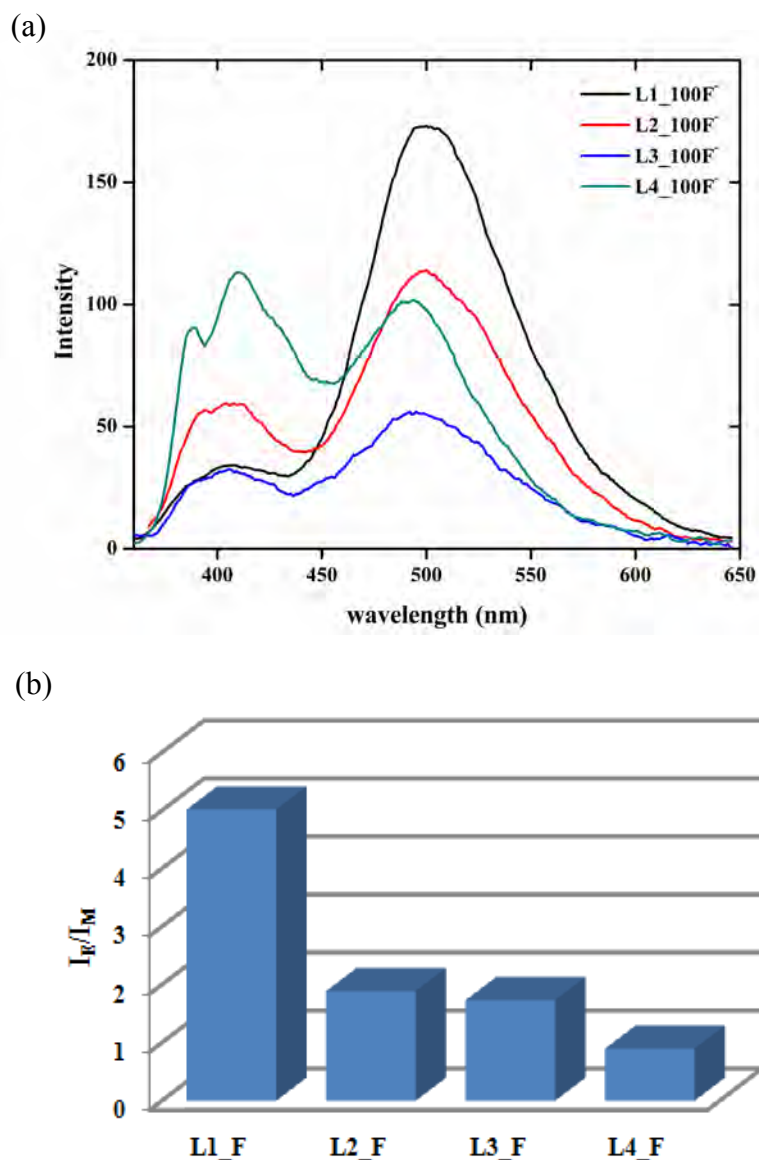


Figure 4.18 Fluorescence spectra of (a) **L1** – **L4** with 100 equiv. of tetra-*n*-butylammonium fluoride in CHCl_3 (b) plot of I_E/I_M ($[\text{L1}], [\text{L2}], [\text{L3}] = 5.0 \times 10^{-6} \text{ M}$, $[\text{L4}] = 5.0 \times 10^{-5} \text{ M}$, $\lambda_{\text{ex}} = 340 \text{ nm}$)

Table 4.5 The binding constants (M^{-1}) for complexation of all receptors, **L1** – **L4**, with tetra-*n*-butylammonium fluoride in CHCl_3

	L1·F⁻	L2·F⁻	L3·F⁻	L4·F⁻
LogK _{ass}	4.03	3.02	3.80	2.73

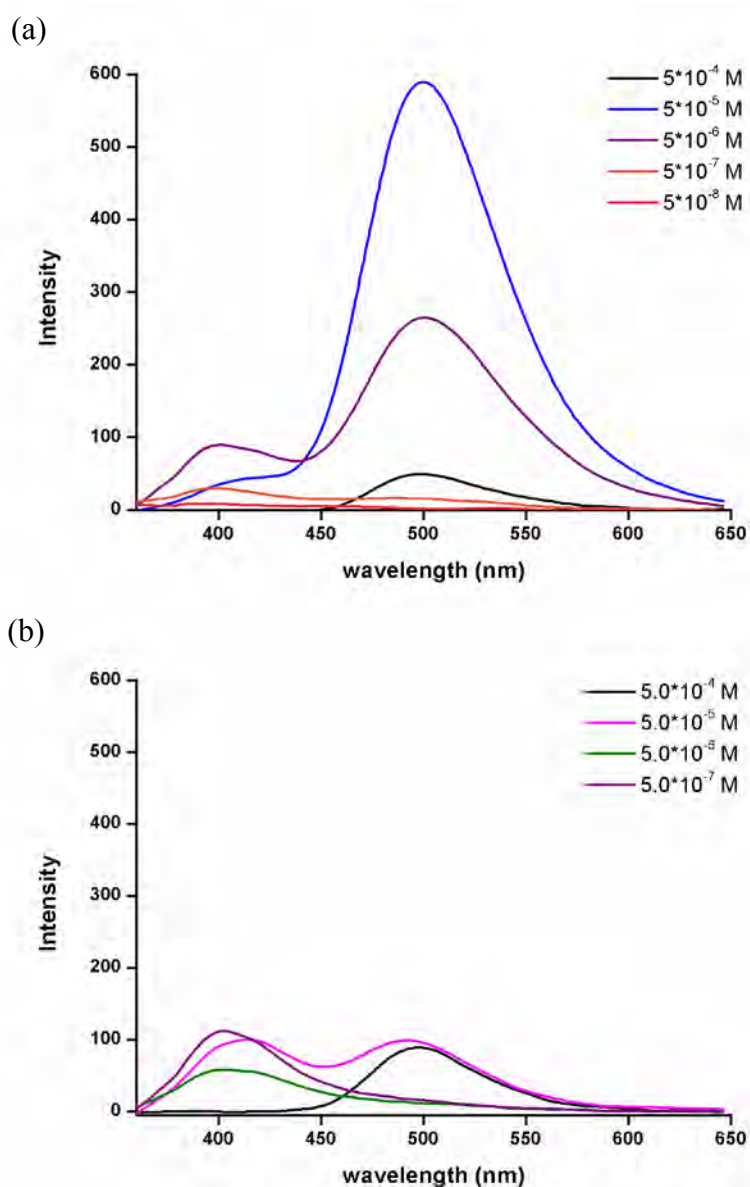


Figure 4.19 Fluorescence emission spectra of various concentrations of (a) **L1** and (b) **L4** with 100 equiv. of tetra-*n*-butylammonium fluoride in CHCl_3

The detection limit of **L1** was calculated by using three times the standard deviation (3SD) of the background noise to estimate the lowest concentration of fluoride that can be measured from the ratio between 3SD of the fluorescence intensity at 500 nm of free **L1** and slope of linear plot of fluorescence titration data of **L1** with fluoride at 500 nm (Table 4.6, Figure 4.20). [53] The detection limit of **L1** for minimum detection fluoride was found to be 2.43×10^{-6} M or 2.3 ppm in a non-polar organic solvent such as CHCl_3 .

Table 4.6 Fluorescence intensity data of free **L1** at 500 nm for repetition 10 times and its standard deviation

free L1	500 nm
1	68.92908
2	68.59905
3	68.91232
4	67.42912
5	68.24125
6	69.98227
7	69.38965
8	71.25394
9	71.17123
10	72.72158
SD	1.61875
3SD	4.8563

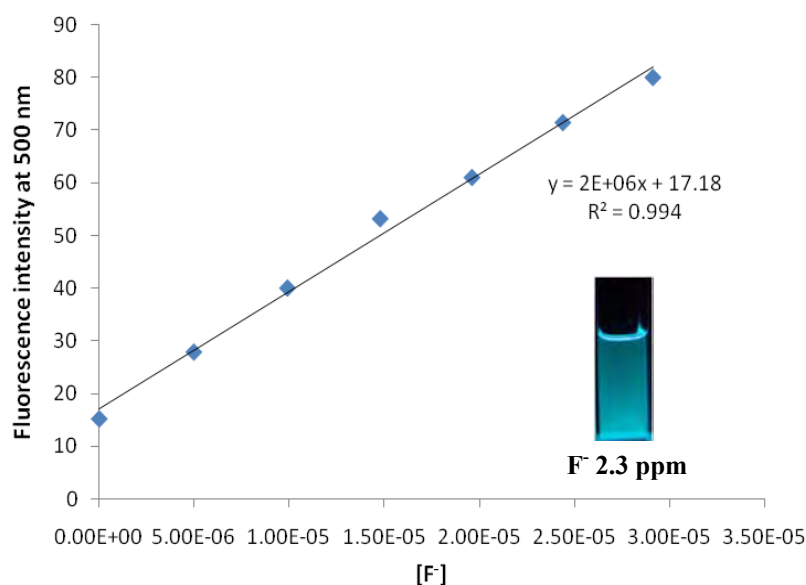


Figure 4.20 Plot of fluorescence intensity of **L1·F⁻** complex at 500 nm and fluorescence change of **L1** at 2.3 ppm of fluoride

It has been established that in nonpolar solvents (such as hexane) the oligo(ethyleneglycols) chain adopt disordered conformation due to their ethylene chain maintained favorable contact with hexane following the formation of excimer interaction [54]. Our studies found that the fluorescence spectra of **L1·F⁻** showed the intensity enhancement of the excimer band upon increasing the percentage of hexane in chloroform solution (Figure 4.21). Thus, the longer polyethylene glycol chain

provided higher binding constants. However, the excimer band intensity decreased upon adding only 5% of methanol in the $\mathbf{L1}\cdot\text{F}^-$ of chloroform solution. Therefore, not only the polyethylene glycol chain but also the non-polar solvent could increase the binding affinity of receptor with fluoride ion.

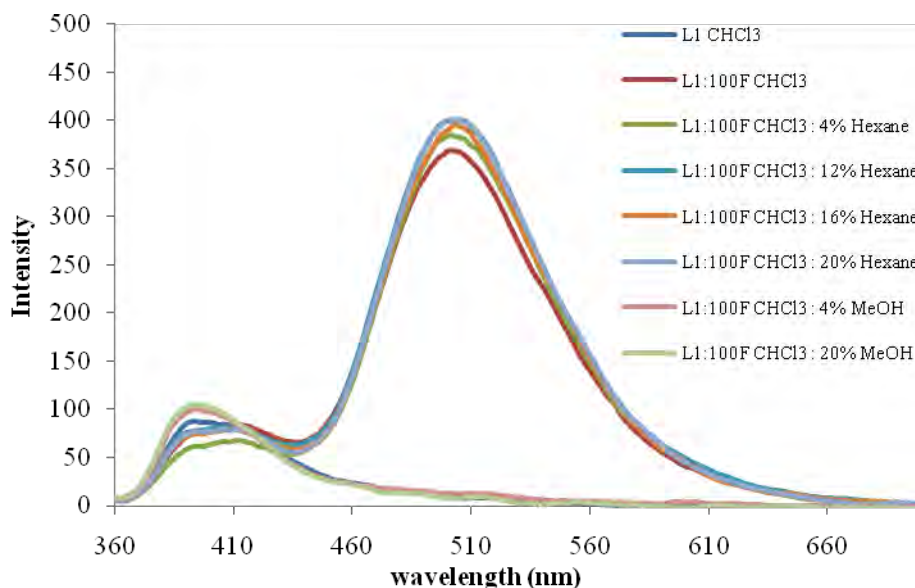


Figure 4.21 Fluorescence spectra of $\mathbf{L1}\cdot\text{F}^-$ in different mixtures of methanol or hexane in chloroform solution ($[\mathbf{L1}] = 5.0 \times 10^{-6}$ M, $[\text{F}^-] = 5.0 \times 10^{-4}$ M, $\lambda_{\text{ex}} = 340$ nm)

4.1.3.2 NMR studies

^1H -NMR titrations were used to support the result from fluorescence spectrophotometry. From the spectra obtained, there was a significant difference in the chemical shift of pyrene proton signals between free $\mathbf{L1}$ and $\mathbf{L1}\cdot\text{F}^-$ complex (Figure 4.22). Moreover, the signal of some pyrene protons became broad and shifted upfield concurrent with the downfield shift of some signals. The broadening and shielding of these signals stemmed from the anisotropic effect of the stacking-pyrene ring current induced by F^- [55 – 57]. This ring current caused some pyrene protons inside an anisotropic region to be shielded. This supported the pyrene fluorophore interaction as a result of fluoride induced $\pi - \pi$ stacking in $\mathbf{L1}\cdot\text{F}^-$ complex. The benzyl protons (H_e , H_g) displayed large downfield shift because of inductive effect from fluoride ion. All the polyethylene glycol protons (H_a , H_b , H_c) and the methoxy protons (H_d) were almost unchanged. Unfortunately, the protons of thiourea group were overlapped with the pyrene proton upon using CDCl_3 . Hence, we could not

follow a shift of NH protons which participated in hydrogen bonding interaction with fluoride ion. However, the appearance of NH signals was observed in DMSO-d₆ solution and disappeared completely upon addition of 4 equiv. of fluoride ion because the deprotonation of NH occurred in a very good proton acceptor solvent of DMSO [23].

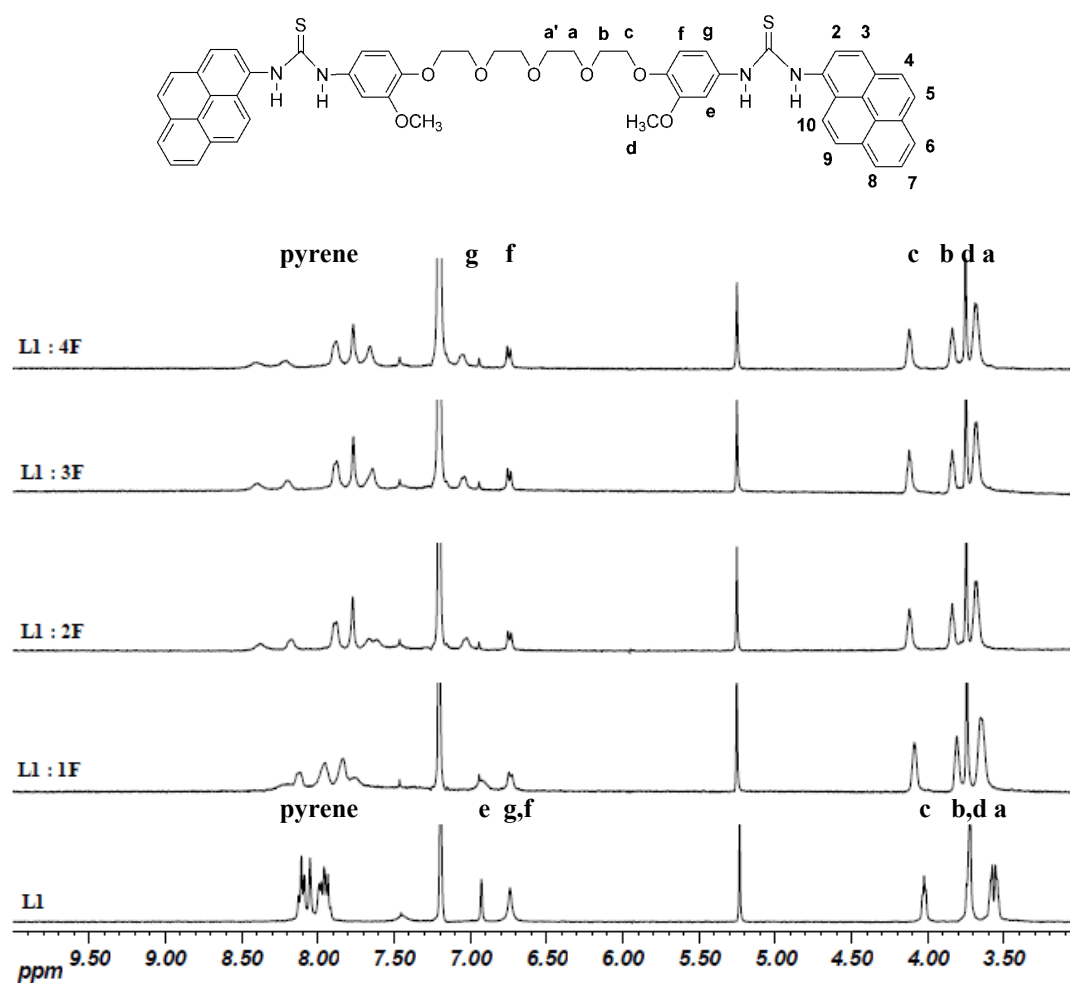
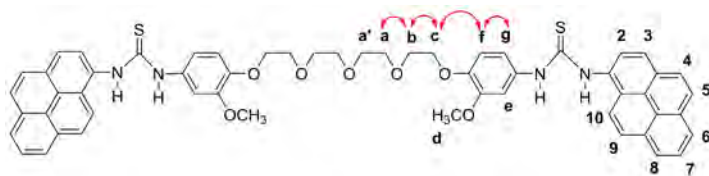


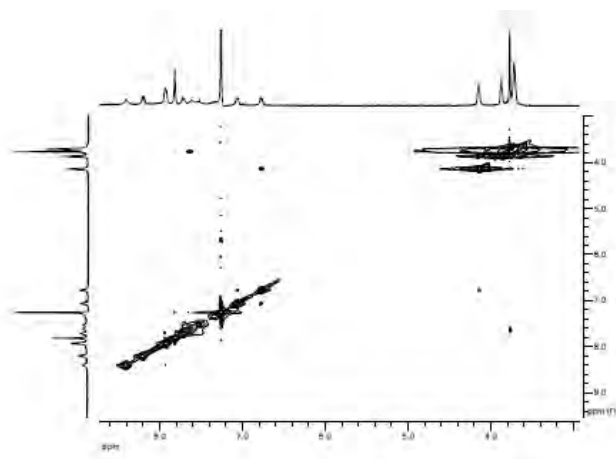
Figure 4.22 ¹H-NMR titration spectra of **L1**·F⁻ in CDCl₃ at 400 MHz

To describe the complicate conformation of **L1** and fluoride, the 2D NOESY technique was used to assign the correlation between protons in the space (Figure 4.23). The NOESY connection of the polyethylene glycol chain was clearly observed only the signal of adjacent protons, H_a and H_b, H_b and H_c, H_c and H_f, supporting these protons was in the same space. Unfortunately, the peaks of pyrene molecule could not be assigned by this technique due to overlapping of the

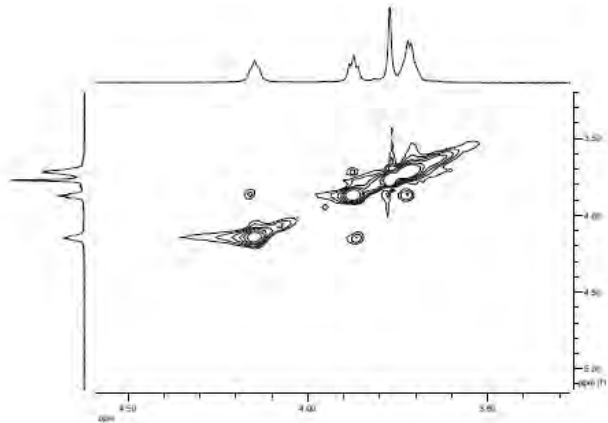
complicated proton signal. Therefore, this technique can not be differentiated the folded and the unfolded structures of $L1 \cdot F^-$ complex.



(a)



(b)



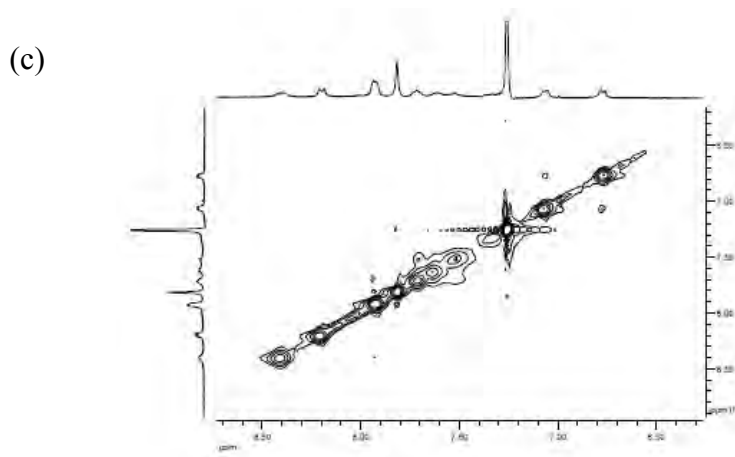


Figure 4.23 (a) Full 2D NOESY spectrum (b) zoom-in on the range of polyethylene glycol (c) zoom-in on the range of aromatic of $\mathbf{L1}\cdot\mathbf{F}^-$ in CDCl_3 at 400 MHz

The fluorescence spectra of $\mathbf{L1}$ in the presence of AcO^- , BzO^- and H_2PO_4^- provided small change of excimer band. These finding agreed with the result from ^1H -NMR spectroscopy in that, the signals of pyrene unit showed sharp peak in the presence of these anions whereas in the case of fluoride anion the pyrene protons became broad and more shift from the original free ligand (Figure 4.24). Therefore, the broad pyrene peak in the ^1H -NMR spectrum and the fluorescence intensity enhancement of excimer band of $\mathbf{L1}\cdot\mathbf{F}^-$ supported the excimer formation between two pyrene molecules.

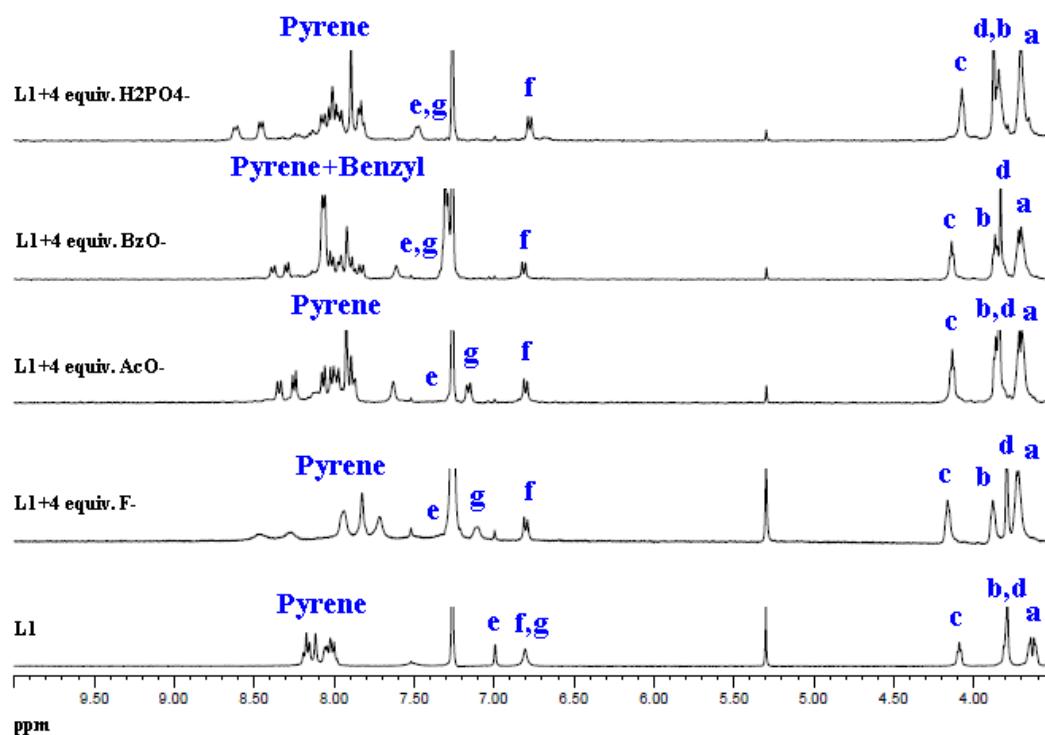


Figure 4.24 $^1\text{H-NMR}$ spectra of **L1** in the presence of 4 equiv. of tetrabutylammonium F^- , AcO^- , BzO^- and H_2PO_4^- in CDCl_3 at 400 MHz

Overall, we suggested that, the arrangement of the receptor **L1** was in unfolded form upon binding with fluoride because the fluorescence intensity ratios of excimer and monomer emission were depended on concentration of **L1** which implied the intermolecular excimer interaction of pyrene. Moreover, the fluorescence titration spectra exhibited the growth of excimer band upon the addition of fluoride and the $^1\text{H-NMR}$ titration spectra of **L1** and fluoride displayed the broad peak of pyrene proton signal. These supported that the fluoride can induce the $\pi - \pi$ stacking between the two pyrene molecules via the intermolecular excimer formation and gave the unfolded conformation of $\text{L1}\cdot\text{F}^-$ complex (Figure 4.25).

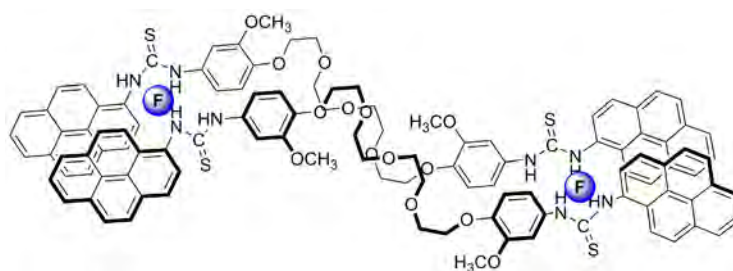


Figure 4.25 Unfolded structure of $\text{L1}\cdot\text{F}^-$ complex

The anion binding properties of **L1** – **L4** with 4 equiv. of fluoride were also studied and compared by ^1H -NMR spectroscopy. A broad multiplet peak of pyrene molecule of each ligand was clearly observed in the presence of fluoride. Especially, **L1** displayed a broader peak than other receptors (Figure 4.26). This supported that fluoride induced the $\pi - \pi$ stacking between the pyrene molecule and the longest polyethylene glycol chain in the **L1** had a great influence on the excimer formation efficiency.

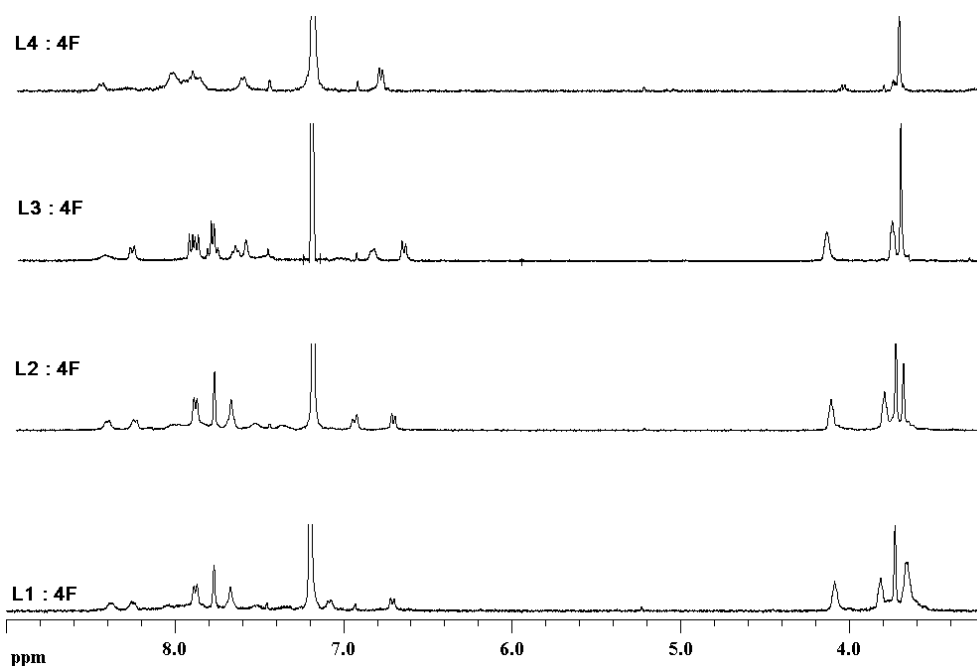


Figure 4.26 ^1H -NMR titration of all the synthesized receptors with F^- in CDCl_3 at 400 MHz

4.1.4 The cation binding and reversibility studies

L1 was the most selective sensor for fluoride among the synthesized receptors and consisted of tetraethylene glycol chain for binding with alkali metals (M^+). Therefore, it was chosen for studying the binding property with Na^+ by fluorescence and ^1H -NMR spectroscopy. We expected that the alkali metal should induce the conformational change of **L1** from linear structure to pseudo-crown ether and then $\text{L1}\cdot\text{M}^+$ could bind with various anions in different order (Figure 4.27). However, there was no significant difference between fluorescence spectra and ^1H -NMR spectra of free **L1** and its metal complexes (Figure A44, A45).



Figure 4.27 Expected structures of **L1·F·Na** or **L1·Na·F**

The fluorescence emission spectrum of **L1** was measured at different concentrations of sodium perchlorate monohydrate and tetra-*n*-butylammonium fluoride in mixed solvents between chloroform and acetonitrile (9:1 v/v). The ionic interactions between sodium and fluoride ions were strong and could induce the decomplexation of fluoride. Therefore, the excimer emission intensity at 500 nm was gradually quenched by titration with sodium ion (Figure 4.28). It was corresponded to the color of solution was changed from the yellow of **L1·F⁻** complex to the original color of **L1**.

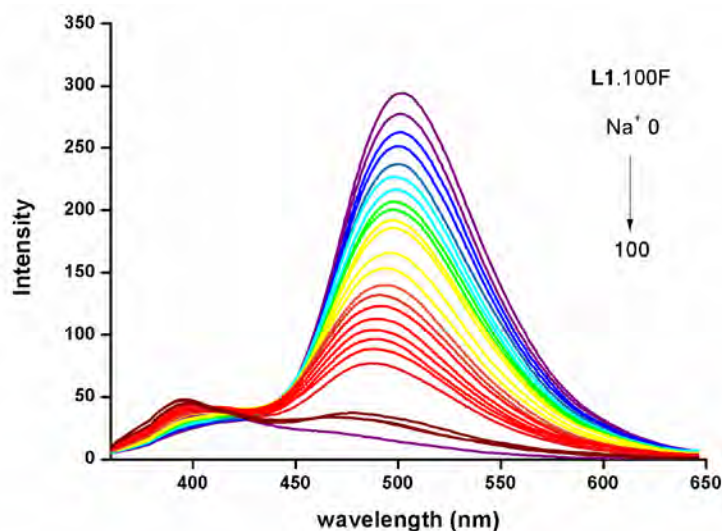


Figure 4.28 Fluorescence titration spectra of **L1·F⁻** complex with sodium perchlorate in $\text{CHCl}_3:\text{CH}_3\text{CN}$ (9:1 v/v)

On the other hand, the 100 equiv. of fluoride ion were added into **L1·30Na⁺** solution, the excimer emission band was not observed in the concentration

range of fluoride 0 – 30 equiv. and this band gradually increased until the concentration of fluoride was more than 30 equiv. or larger than amount of sodium ion (Figure 4.29). This confirmed that sodium ion preferred to form ion pair with fluoride.

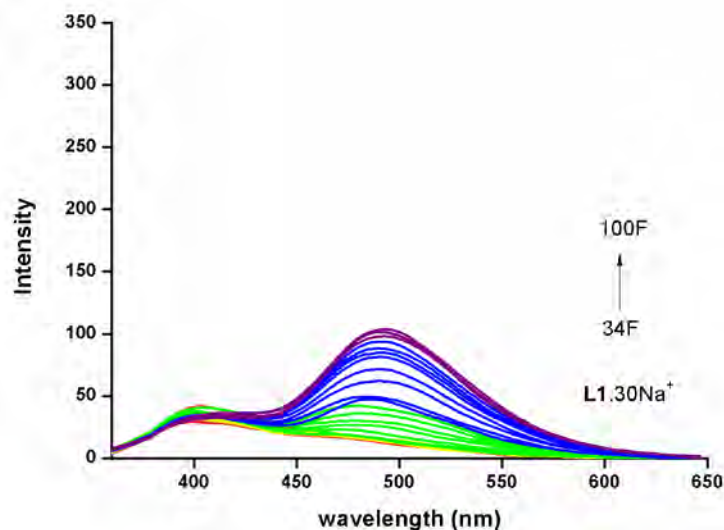


Figure 4.29 Fluorescence titration spectra of $L1 \cdot 30Na^+$ complex with tetra-n-butylammonium fluoride in $CHCl_3: CH_3CN$ (9:1 v/v)

For $L4 \cdot F^-$, the excimer emission intensity decreased by adding 100 equiv. of Na^+ into $L4 \cdot F^-$ solution while the monomer emission intensity completely increased. Interestingly, the intensity of the monomer band upon adding 100 equiv. of sodium was more than the original monomer band of **L4** (Figure 4.30).

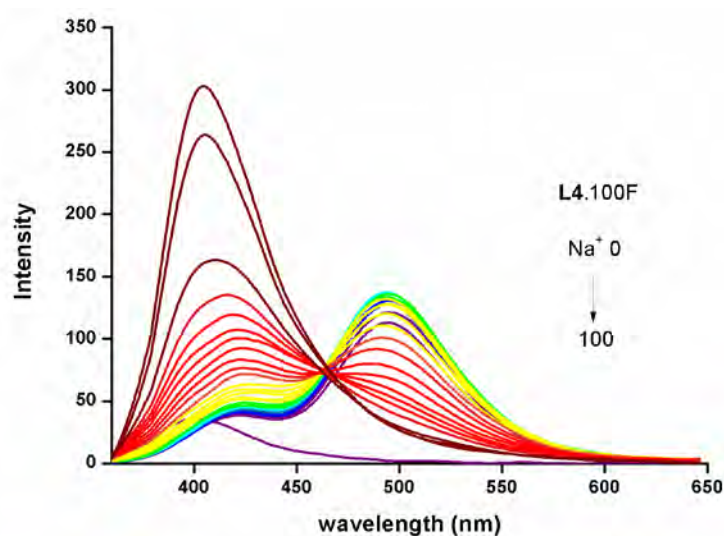


Figure 4.30 Fluorescence titration spectra of **L4**·F⁻ complex with sodium perchlorate in CHCl₃:CH₃CN (9:1 v/v)

The ¹H-NMR titration was also used to support the result from fluorescence spectrophotometry. We observed that, the ¹H-NMR spectrum of **L1**·4F in the presence of excess Na⁺ was similar to original free **L1** and showed the small change in pyrene characteristic peak Figure 4.31. This supported that sodium ion inhibited the π – π stacking interactions between the two pyrene molecules. In addition, the ¹H-NMR spectrum of **L4**·F in the presence of excess Na⁺ was the same as original **L4** (Figure 4.32). Because the **L4** had no polyethylene glycol chain for binding with sodium ion, this indicated that the ion pairs (NaF) were separated from **L4** and gave free **L4** in solution.

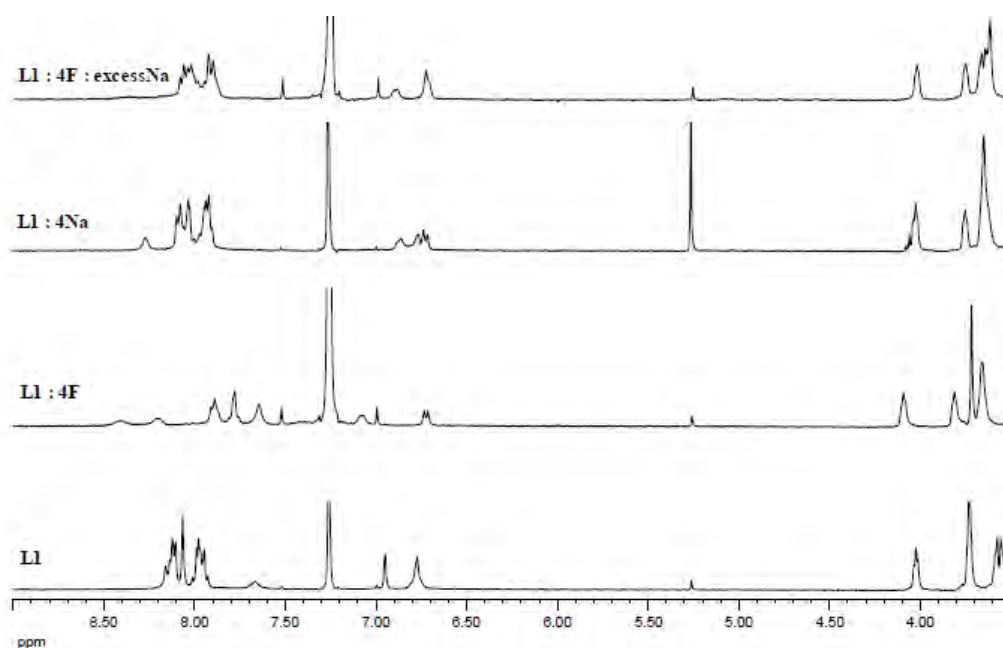


Figure 4.31 ¹H-NMR titration spectra of **L1**·F⁻ with sodium perchlorate monohydrate in CHCl₃:CH₃CN (9:1 v/v) at 400 MHz

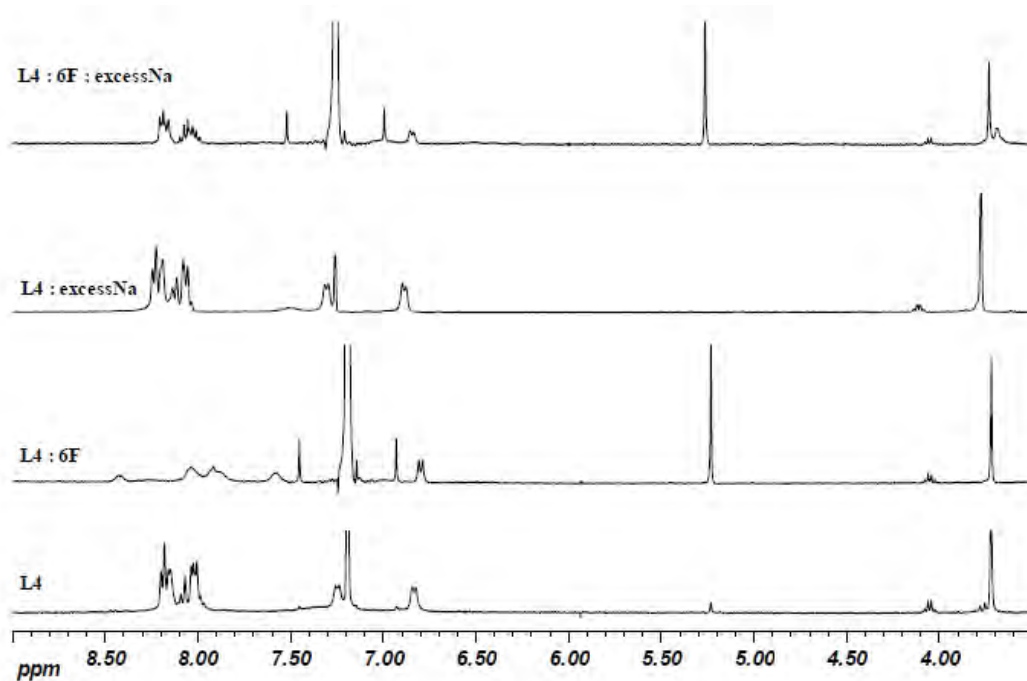
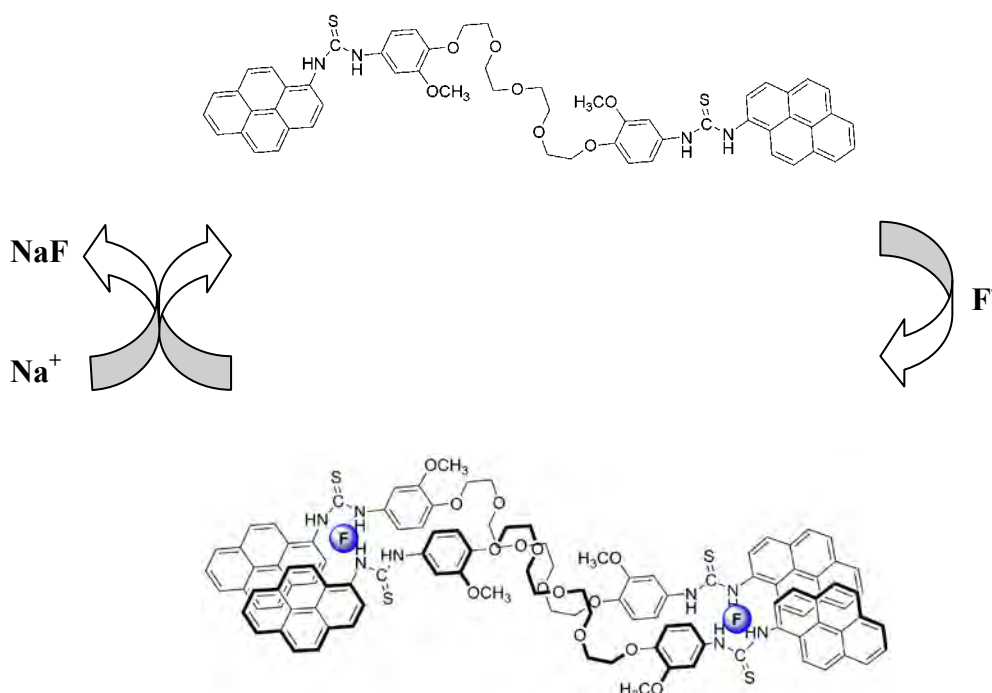


Figure 4.32 $^1\text{H-NMR}$ titration spectra of $\text{L4}\cdot\text{F}^-$ with sodium perchlorate monohydrate in $\text{CHCl}_3:\text{CH}_3\text{CN}$ (9:1 v/v) at 400 MHz

The results from fluorescence and $^1\text{H-NMR}$ could be concluded that the fluoride ion induced the intermolecular $\pi - \pi$ stacking of pyrene molecule in the unfolded structure of **L1** complex. However, Na^+ acted as an inhibitor for the pyrene stacking due to NaF formation as shown in Figure 4.33.



Intermolecular excimer of the unfolded structure

Figure 4.33 Proposed binding modes of **L1** with fluoride and sodium

4.1.5 Anion interference studies

To test the efficiency of all synthesized ligands for sensing fluoride, the competitive experiments were carried out in the presence of 100 equiv. fluoride mixed with AcO^- , BzO^- , H_2PO_4^- , Cl^- , Br^- and I^- at 100 equiv. as shown in Fig. 4.34 (last column). The ratios of excimer to monomer intensity change were compared between the ligands with each anion and with mixed anions. It can be concluded that AcO^- , BzO^- , H_2PO_4^- , Cl^- , Br^- and I^- can interfere the detection of fluoride anion for all the synthesized ligands by reducing the emission ratios (I_E/I_M). However, **L1**, **L2** and **L3** which possessed linking ethylene glycol chains preferred binding with fluoride in mixed anions as shown in the last column of Fig. 4.34. In case of the **L4** ligand with mixed anion, the fluorescence intensity showed completely quenching.

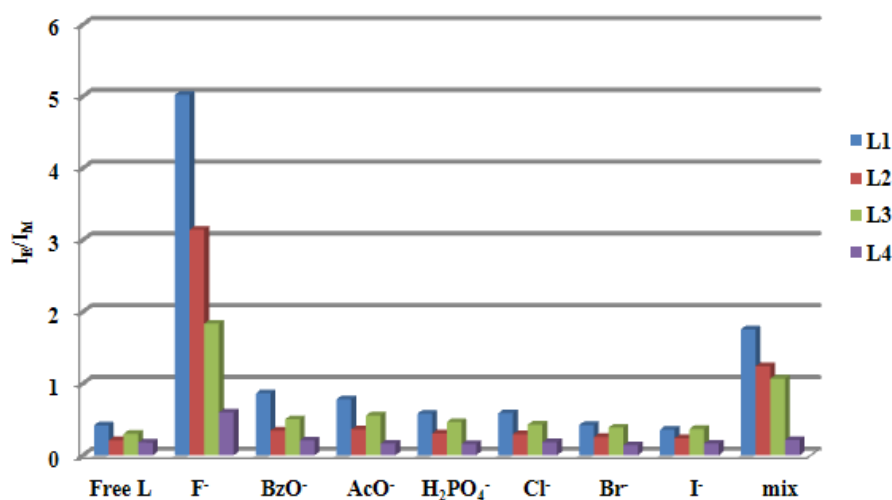


Figure 4.34 Selectivity of all the synthesized ligands toward each anion (100 equiv.) and the mixture of all anions

4.1.6 Application of L1

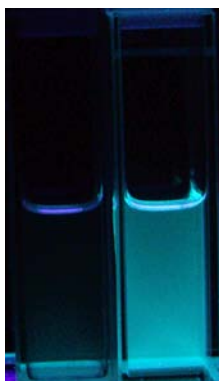


Figure 4.35 Fluorescence changes of **L1** (5.0×10^{-6} M) after addition 2.3 ppm fluoride (from left to right: **L1**, **L1**+2.3 ppm of F^-) in $CHCl_3$ under UV light.

Molecular sensing based on fluorescence emission of the artificial receptors has many applications for example the detection of anions (or cations) in water or in real life sample, for inexpensive disease screening as naked-eye sensor [58]. The heteroditopic receptors for anion and cation have been used as extraction or transport agents for ion pair species of environmental or biological importance [59]. Our sensor **L1** could detect fluoride in a non-polar organic solvent ($CHCl_3$) at concentration of fluoride as low as 2.3 ppm. The fluorescence change at detection limit could even be observed as a bright green color under UV light (Fig. 4.35).

4.2 Chromogenic sensors **R1** and **R2**

4.2.1 Syntheses of **R1** and **R2**

Chromogenic sensors **R1** and **R2** for anions have been synthesized. These molecules contained a nitrobenzene chromophore connecting to the thiourea receptors. The sensing mechanism upon binding with selective anions occurred by charge transfer (CT) between electron-rich anions and electron-deficient NO₂ moiety of nitrobenzene and this could be determined by UV-vis spectroscopy or naked-eye detection.

Flexible and semi-rigid thiourea nitrobenzene derivatives, **R1** and **R2**, have been synthesized by coupling the amino groups of the polyethylene glycol chain with *p*-isothiocyanatonitrobenzene in 57% and 21% yields, respectively (Figure 4.36). Final products were yellow solids. The receptor **R1** was well soluble in many non-polar and polar organic solvents such as dichloromethane, chloroform and DMSO. However, the receptor **R2** was slightly soluble in high polar solvent such as DMSO.

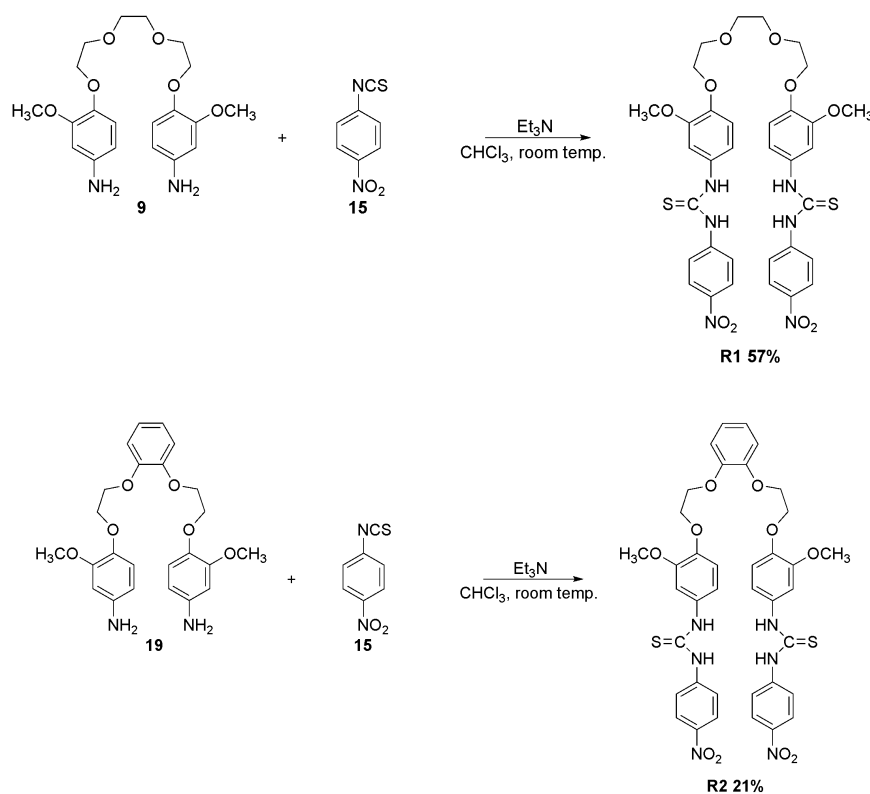


Figure 4.36 Syntheses of chemosensors **R1** and **R2**

4.2.2 Characterization of **R1** and **R2**

The receptors **R1** and **R2** were characterized by NMR and mass spectroscopy as well as elemental analysis. The receptor **R1** contained the flexible chain of triethylene glycol while the receptor **R2** consisted of the benzene ring connecting to both ethylene glycol chains to increase the rigidity of the synthesized receptor.

The UV-vis absorption spectra of all receptors were studied in DMSO solution exhibiting the absorption peak of the $\pi - \pi^*$ transition of aromatic hydrocarbons around 360 nm (Table 4.7). The molar absorptivity of the receptor **R1** containing flexible polyethylene glycol chain was higher than that of a more rigid molecule **R2**.

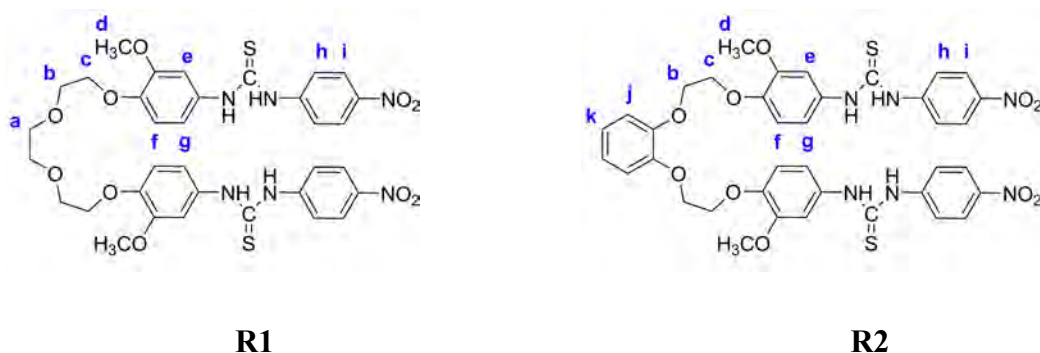
Table 4.7 The absorption and emission parameters for compounds **R1** and **R2** in DMSO

Receptors	Absorption
-----------	------------

	λ_{abs} (nm)	$\epsilon \times 10^4$ (mol ⁻¹ cm ⁻¹)
R1	369	3.13
R2	365	1.86

¹H and ¹³C-NMR spectroscopy were used to determine the structure of all receptors. The ¹H-NMR and ¹³C-NMR samples were recorded in d₆-DMSO. The triethylene glycol protons in the receptor **R1** (a, b and c positions) showed the resonance signals around 3.6 – 4.1 ppm. The methoxy protons of H_d displayed at 3.7 ppm. The benzyl protons, H_e, appeared as a singlet peak at 7.0 ppm. The signals at 6.9 ppm, which corresponded to 4 protons, were assigned to H_f and H_g. The two aromatic protons of the *p*-nitrophenyl rings were observed as a doublet peak at 7.8 and 8.2 ppm. The protons of thiourea group appeared as a singlet peak at 10.2 ppm. ¹H-NMR signals of the **R2** receptor was significantly different from the **R1** receptor. Especially, the proton signals of the diethylene glycol containing benzene ring displayed a doublet peak of 8H. Moreover, the protons j and k of the benzene ring were overlapped with the aromatic protons e, f and g appearing around 6.9 – 7.1 ppm. ¹H-NMR and ¹³C-NMR data of **R1** and **R2** receptors were concluded in Tables 4.8 and 4.9.

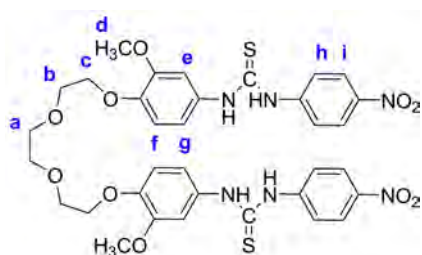
Table 4.8 ¹H-NMR data for **R1** and **R2** in d₆-DMSO



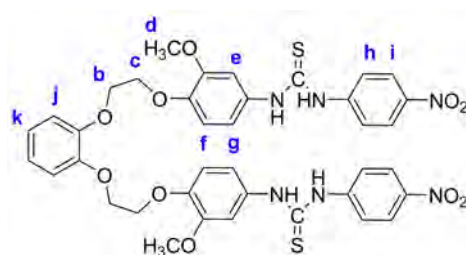
H-Position	R1 (ppm)	R2 (ppm)
a	3.6 (s, 4H)	-
b	3.7 (m, 4H)	4.30 – 4.28 (d, 4H)
c	4.1 (t, 4H)	4.30 – 4.28 (d, 4H)
d	3.7 (m, 6H)	3.7 (s, 6H)
e	7.1 (s, 2H)	7.1 – 6.9 (m, 2H)
f	6.9 (s, 2H)	7.1 – 6.9 (m, 2H)
g	6.9 (s, 2H)	7.1 – 6.9 (m, 2H)
h	7.8 (d, 4H)	7.8 (d, 4H)
i	8.2 (d, 4H)	8.2 (d, 4H)

j	-	7.1 – 6.9 (m, 2H)
k	-	7.1 – 6.9 (m, 2H)
NH	10.2 (s, 4H)	10.2 (s, 2H) 10.1 (s, 2H)

Table 4.9 ^{13}C -NMR data for **R1** and **R2** in d_6 -DMSO



R1



R2

C-Position	R1 (ppm)	R2 (ppm)
a	68.0	-
b	69.0	55.8
c	69.9	67.5
d	55.5	55.5
e	109.1	135.6 - 109.3
f	116.3	135.6 - 109.3
g	113.0	135.6 - 109.3
h	121.5	135.6 - 109.3

i	124.3	135.6 - 109.3
j	-	135.6 - 109.3
k	-	135.6 - 109.3
C = S	179.0	179.1
$\underline{C}_{\text{aromatic}} - \text{OCH}_3$	146.4	148.2
$\underline{C}_{\text{aromatic}} - \text{OCH}_2$	148.6	155.6
$\underline{C}_{\text{aromatic}} - \text{NH}$	142.1	145.5
$\underline{C}_{\text{aromatic}} - \text{NH}$	132.1	142.1
$\underline{C}_{\text{aromatic}} - \text{NO}_2$	145.6	146.3

4.2.3 Anion binding properties of R1 and R2

4.2.3.1 Photochemical studies of anion binding

Anion complexation studies were carried out in DMSO by UV-vis titrations of receptors **R1** and **R2** with tetrabutylammonium anion salts of F^- , AcO^- , BzO^- , H_2PO_4^- , Cl^- , Br^- and I^- . Upon addition of fluoride anion into **R1** solution, the absorption spectra at 369 nm decreased and an intense peak with shoulder around 472 nm was appeared (Figure 4.37). As amount of fluoride increased, the hydrogen bond interactions between fluoride and thiourea group accompanying with the formation of FHF^- ion which showed a charge transfer band at 472 nm [60]. In the case of the **R2**· F^- complex, the spectra around 369 nm disappeared gradually and a new peak without shoulder was observed around 472 nm (Figure 4.38). The change of **R2**· F^- spectra was attributed to deprotonation of NH to N^- in the thiourea fragments [61].

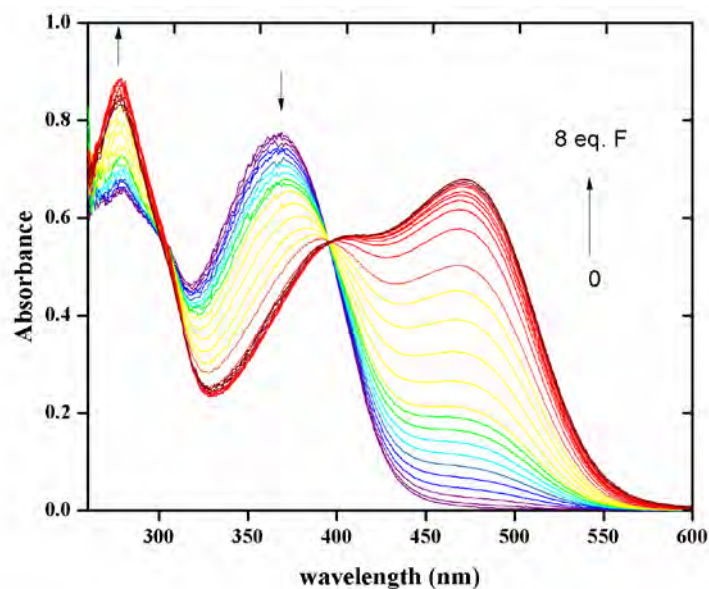


Figure 4.37 UV-vis titration spectra of **R1** (2.5×10^{-5} M) with fluoride in DMSO

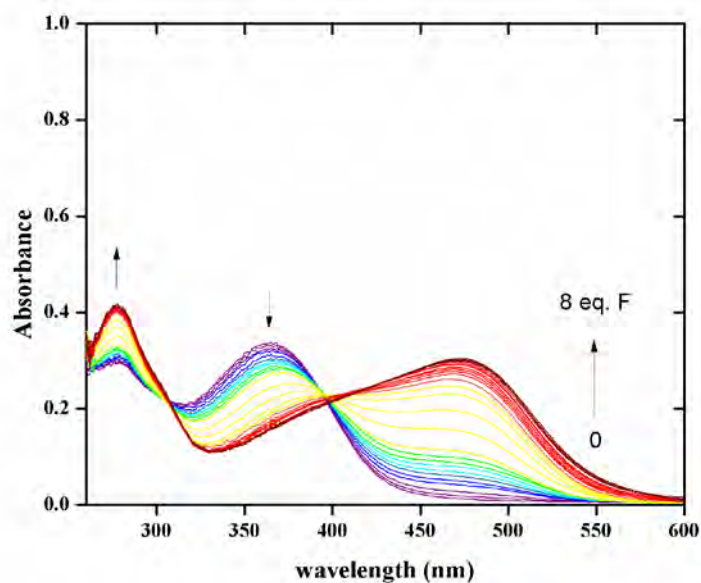


Figure 4.38 UV-vis titration spectra of **R2** (2.5×10^{-5} M) with fluoride in DMSO

Titration of AcO^- , BzO^- , H_2PO_4^- into the **R1** and **R2** solutions showed new bands around 380 – 400 nm because of the hydrogen bonding interactions as same as in the **R1**· F^- complex and displayed the charge transfer band around 460 – 470 nm (Figure 4.39, 4.40 and A46-A49). Therefore, the binding mechanisms in these cases were hydrogen-bonded complex accompanied with the deprotonation and the charge transfer processes.

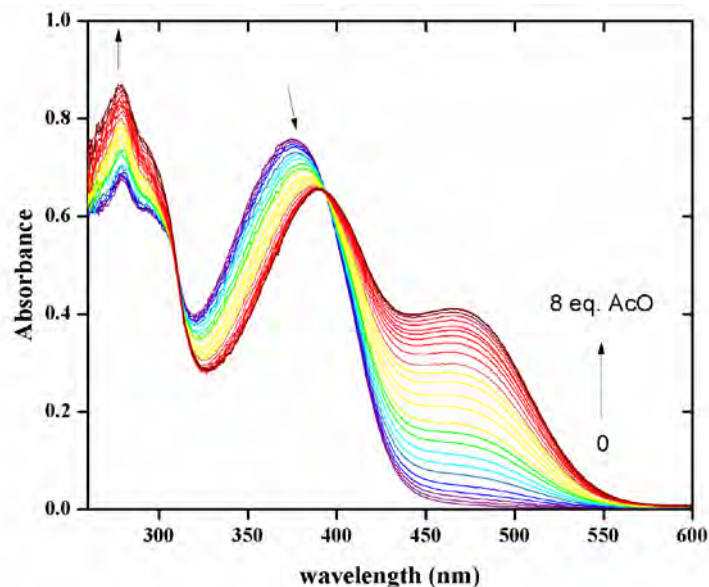


Figure 4.39 UV-vis titration spectra of **R1** (2.5×10^{-5} M) with AcO^- in DMSO

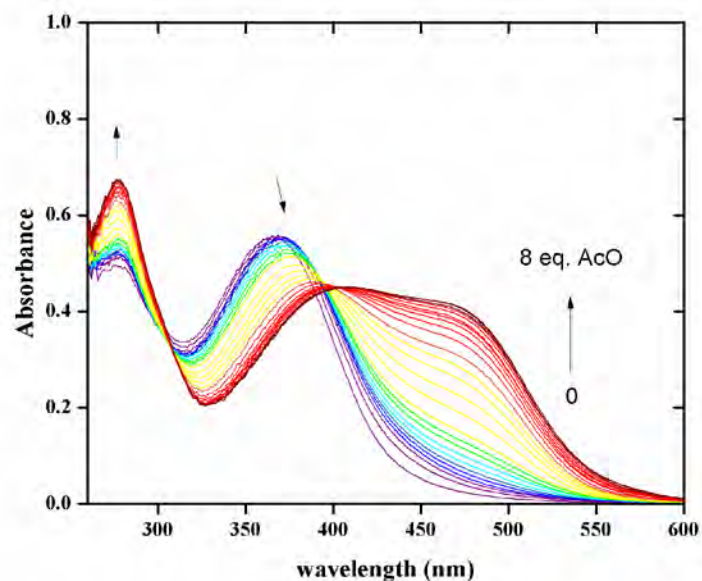


Figure 4.40 UV-vis titration spectra of **R2** (2.5×10^{-5} M) with AcO^- in DMSO

The stoichiometry of the host-guest complexes was obtained by the titration profile plots (Figure 4.41, 4.42 and A52-57). The stoichiometries of **R1** and **R2** with F^- , AcO^- and BzO^- were 1:2 for host:guest complexation and the binding constants were calculated by SPECFIT/32 software supporting the 1:2 complexation (Table 4.10) [62, 63]. The binding constants for **R1** were $\text{F}^- > \text{BzO}^- > \text{AcO}^-$. In addition, stoichiometries and binding constants of **R1** and **R2** with H_2PO_4^- could not

be determined by these methods because there was only small change in absorption peaks. In general, the selectivity for anions can be explained on the basis of the anion's basicity and the special interactions between the host and the anionic guests which depended on their size and shape [64, 65]. From the data obtained, all receptors were sensitive to addition of F^- , AcO^- , BzO^- and $H_2PO_4^-$. The binding constant of **R1** toward F^- was greater than that of **R2** toward F^- in an order of magnitude [66-69]. However, the selectivity trend with various anions and the stoichiometry of the flexible chain in **R1** was similar to the semi-rigid structure in **R2** ($F^- > BzO^- > AcO^- > H_2PO_4^-$). The possible structures of complexes of **R1** and **R2** with anions are shown in Figure 4.43. The absorption spectra of **R1** and **R2** displayed no charge transfer band in the presence of Na^+ or K^+ (Figure A50, A51).

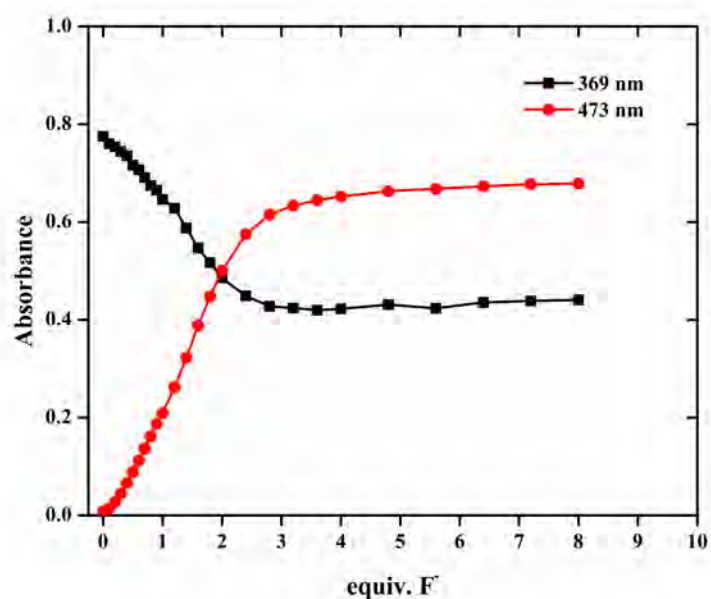


Figure 4.41 Titration profiles of **R1**· F^- at the wavelength 369 nm and 473 nm in DMSO show 1:2 for **R1**: F^- complexation

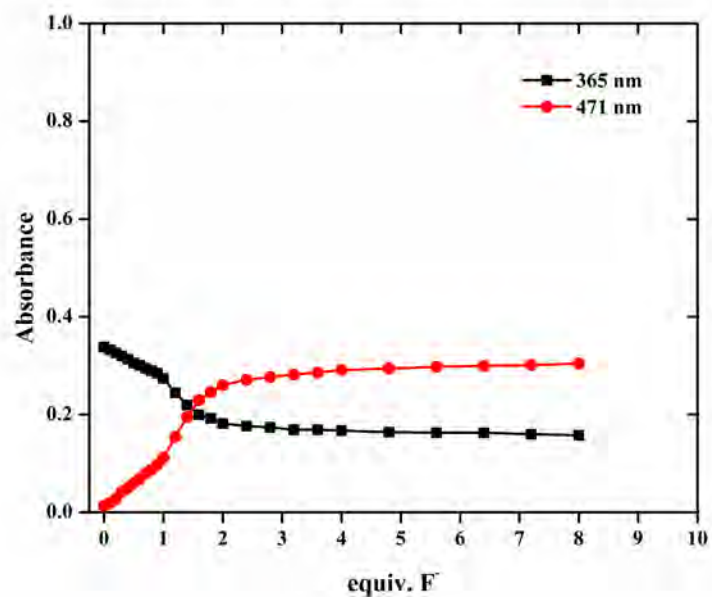


Figure 4.42 Titration profiles of $\mathbf{R2}\cdot\mathbf{F}^-$ at the wavelength 365 nm and 471 nm in DMSO show 1:2 for $\mathbf{R1}:\mathbf{F}^-$ complexation

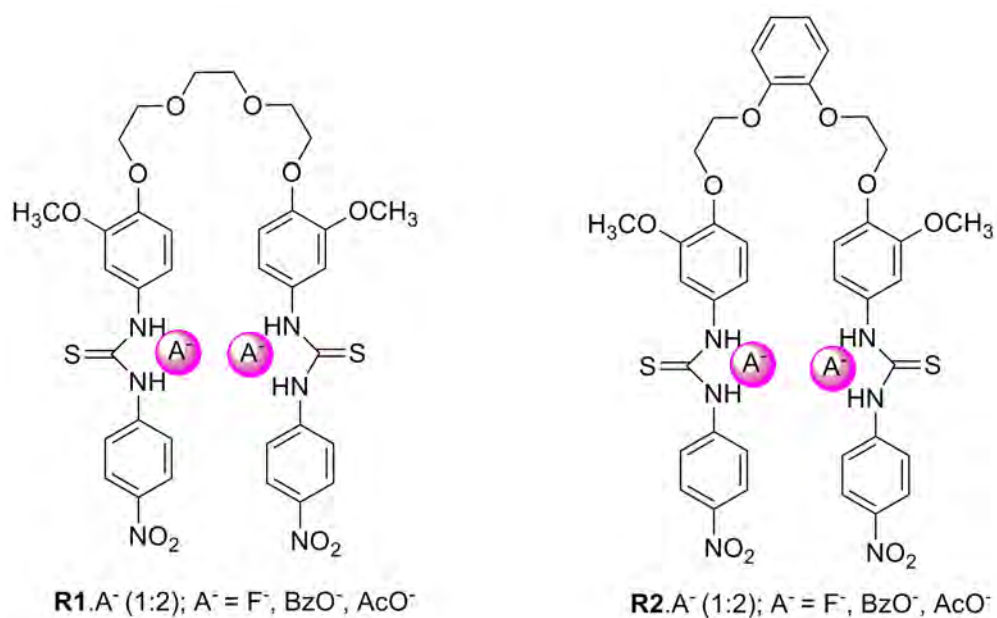


Figure 4.43 Proposed structures of the $\mathbf{R1}$ and $\mathbf{R2}$ complexes

Table 4.10 Binding constants of all receptors with tetrabutylammonium anion salts in DMSO

Receptor	Log K _a (S)			
	F ⁻	AcO ⁻	BzO ⁻	H ₂ PO ₄ ⁻
R1	8.71±0.07 (1:2)	6.84±0.08 (1:2)	7.04±0.03 (1:2)	NC ^a
R2	7.19±0.53 (1:2)	6.54±0.11 (1:2)	6.88±0.05 (1:2)	NC ^a

^a NC = cannot be calculated due to slight changes in absorption spectra.

To study properties of **R1** and **R2** as naked eye sensors for anions, the original color of the ligands and the colors of their complexes with ions are shown in Tables 4.11 and 4.12. The receptor **R1** exhibited the color change similar to that of **R2** (red) after adding F⁻ (column b). Upon addition of AcO⁻ into **R1** or **R2** solution, the color of solution changed from yellow to red in the same manner as F⁻ (column b). However, addition of BzO⁻ or H₂PO₄⁻ to **R1** and **R2** gave orange solutions (column b). When F⁻ was added into **R1** or **R2** solution and Na⁺ was subsequently added (column c), the color change from red to original yellow was observed due to the decomplexation of F⁻ anion while adding K⁺ gave no color change. In column c for AcO⁻ and BzO⁻, no color change was observed upon adding Na⁺ and K⁺. In contrast, adding Na⁺ or K⁺ gave the original color of **R1** and **R2** in the case of H₂PO₄⁻.

Table 4.11 Cations and anions response of compound **R1**

Anions (A ⁻)	Cations (M ⁺)	Color of the Solution		
		a	b	C
F ⁻	Na ⁺	●	●	●
	K ⁺	●	●	●
H ₂ PO ₄ ⁻	Na ⁺	●	●	●
	K ⁺	●	●	●
AcO ⁻	Na ⁺	●	●	●
	K ⁺	●	●	●
BzO ⁻	Na ⁺	●	●	●
	K ⁺	●	●	●

a = free **R1**, b = **R1** + 4 equiv. A⁻, c = b + 10 equiv. M⁺. All experiments were carried out in DMSO (5×10⁻³ M) at 298 K

Table 4.12 Cations and anions response of compound **R2**

Anions (A ⁻)	Cations (M ⁺)	Color of the Solution		
		a	b	C
F ⁻	Na ⁺	●	●	●
	K ⁺	●	●	●

H_2PO_4^-	Na^+	●	●	●
	K^+	●	●	●
AcO^-	Na^+	●	●	●
	K^+	●	●	●
BzO^-	Na^+	●	●	●
	K^+	●	●	●

a = free **R2**, b = **R2** + 4 equiv. A^- , c = b + 10 equiv. M^+ . All experiments were carried out in DMSO (5×10^{-3} M) at 298 K

4.2.3.2 NMR studies

Reversible complexation of **R1** with sodium ion was also studied by ^1H NMR spectroscopy. The decomplexation of **R1**· F^- occurred by adding 10 equiv. of sodium ion and showed the original spectrum of free receptor with the thiourea proton signals reappeared at a slightly downfield position of ^1H -NMR spectrum (Figure 4.44). This corresponded to the result from naked-eye detection in that the color of solution was changed from red to yellow (Table 4.11). However, the ^1H -NMR spectra of **R1**· AcO^- , **R1**· BzO^- and **R1**· H_2PO_4^- complexes remained to be found upon addition of sodium and the thiourea proton signals did not recover in these steps (Figure 4.45 and A58-59). This implied that the decomplexation occurred by adding sodium ion in **R1**· F^- case because sodium ion preferred to bind with fluoride in an ion pair fashion.

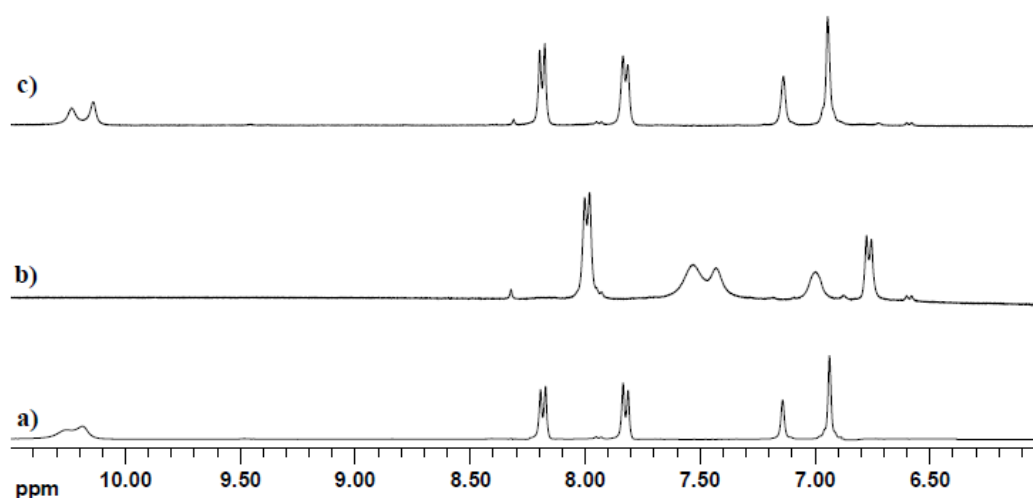


Figure 4.44 $^1\text{H-NMR}$ spectra of a) free **R1** b) **R1** + 4 equiv. F^- c) **R1** + 4 equiv. F^- + 10 equiv. Na^+ in $\text{d}_6\text{-DMSO}$ at 400 MHz

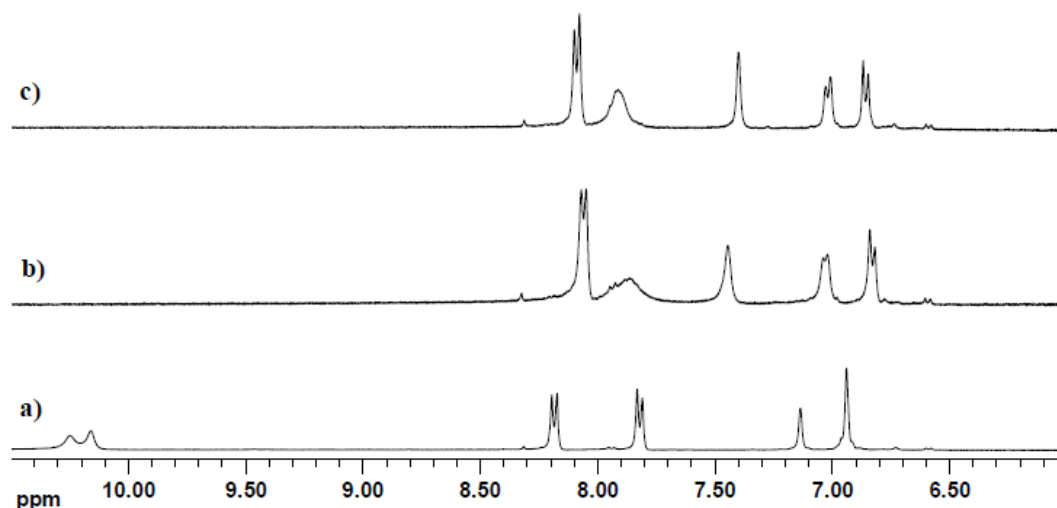


Figure 4.45 $^1\text{H-NMR}$ spectra of a) free **R1** b) **R1** + 4 equiv. AcO^- c) **R1** + 4 equiv. AcO^- + 10 equiv. Na^+ in $\text{d}_6\text{-DMSO}$ at 400 MHz

4.2.4 Principal components analysis (PCA)

From naked-eye sensing and UV-vis titration studies, we found that **R1** can possibly bind F^- , AcO^- , BzO^- and H_2PO_4^- to a different extent. In order to discriminate the sensing ability of **R1** toward these four anions, PCA was used to determine underlying information from UV-vis data. The PCA score plot of the first two principle components (PCs) for 25 samples of free **R1** and 4 anions (F^- , AcO^- , BzO^- and H_2PO_4^-) showed very high level of discrimination (98.7%) (Figure 4.46). Therefore, the clear clustering of the data was observed. These supported that, **R1** sensor could discriminate all 4 anions even the color of solution were not distinctively different. From the colorimetric response in Table 4.11, red solutions were obtained by addition F^- or AcO^- in **R1** solution. However, the PCA could separate F^- and AcO^- anions. H_2PO_4^- cluster appeared much closer to free **R1** cluster than other anions because **R1** sensor showed the less response with H_2PO_4^- anion.

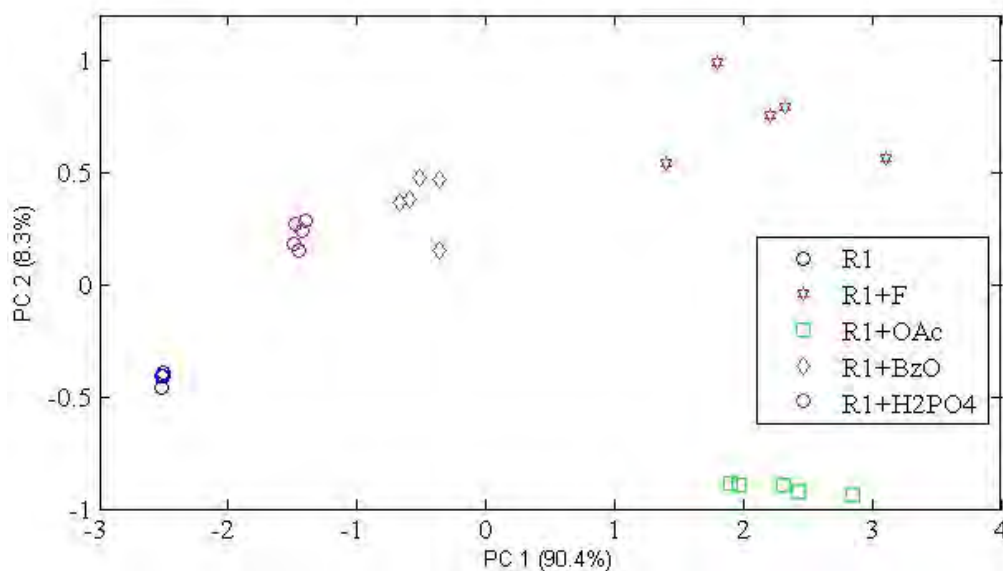


Figure 4.46 PCA score plot of the first two PCs for 25 samples of **R1** and 4 anions

The PCA score plot of the first two PCs for 10 samples of free **R1** and 2 ions such as Na^+ and K^+ in Figure 4.47 displayed low level of discrimination of 55.5% and could not separate any ions. Since, **R1** sensor was not selective for Na^+ and K^+ . However, in the presence of F^- , **R1** could separate Na^+ and K^+ as showed in Figure 4.48 and higher level of discrimination was obtained in 79%. This corresponded to the colorimetric response (Table 4.11) in that colors of solution were significantly difference between Na^+ (yellow) and K^+ (red). The PCA score plot of the first two PCs for 10 samples of **R1**· AcO^- sensor and 2 metals (Na^+ and K^+) in Figure 4.49 could not discriminate Na^+ and K^+ . However, the PCA results of **R1**· BzO^- and **R1**· H_2PO_4^- (Figures 4.50-4.51) appeared clear cluster.

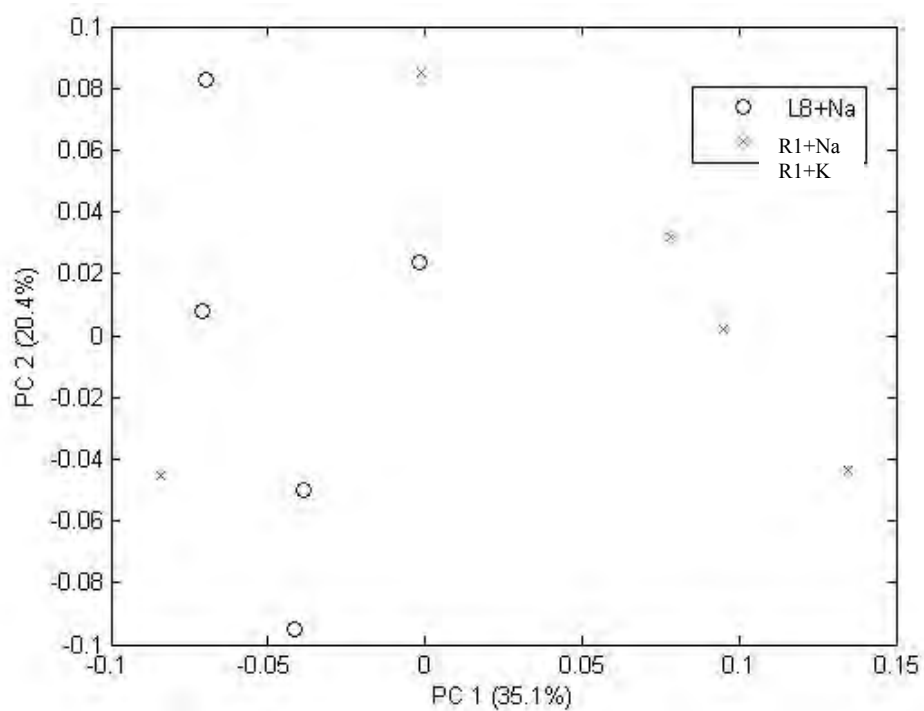


Figure 4.47 PCA score plot of the first two PCs for 10 samples of R1 and 2 metal ions

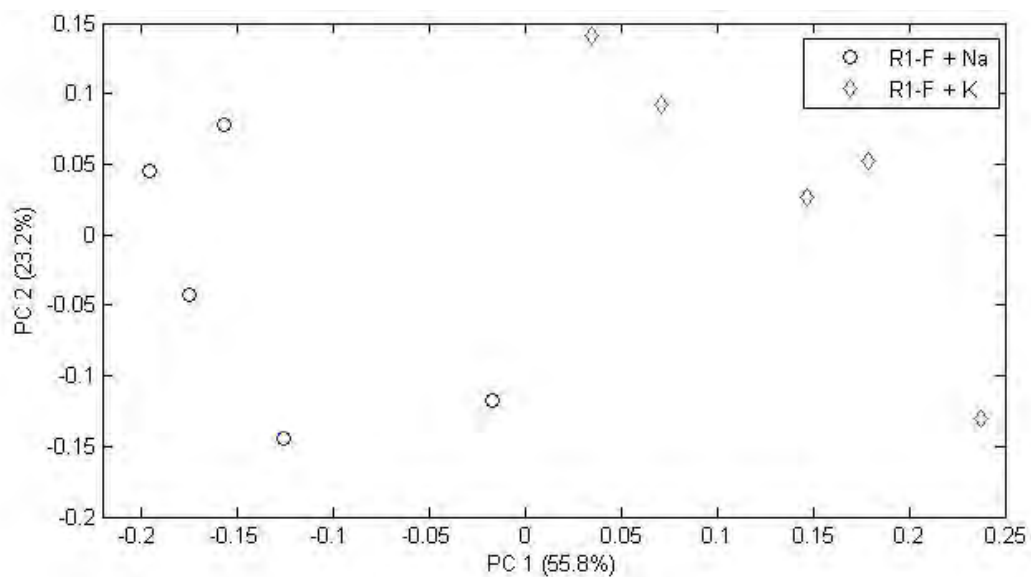


Figure 4.48 PCA score plot of the first two PCs for 10 samples of R1-F sensor and 2 metal ions

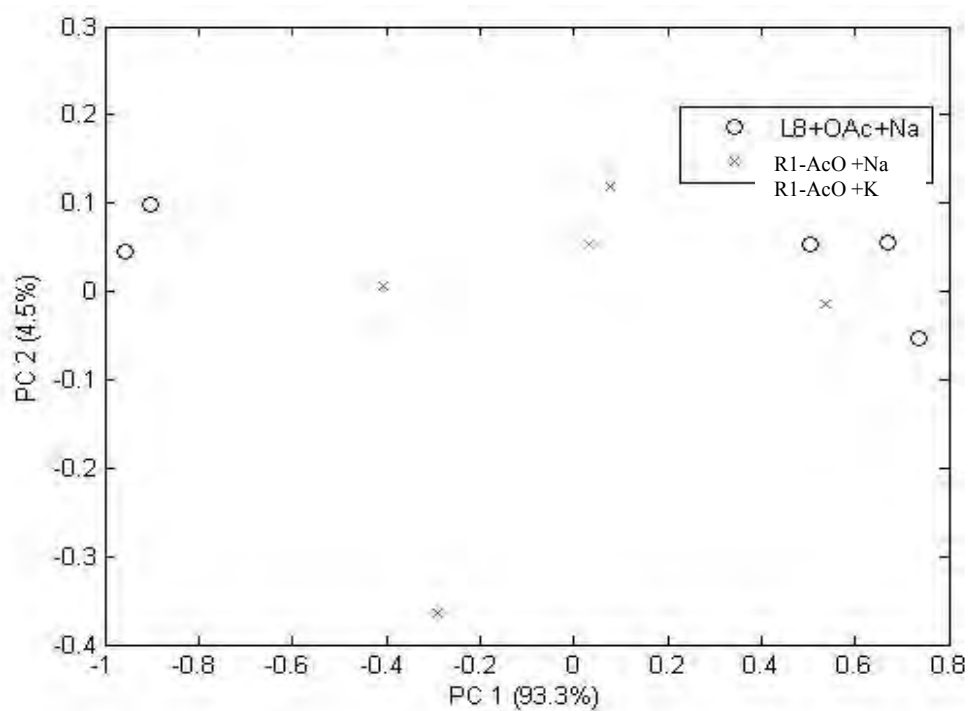


Figure 4.49 PCA score plot of the first two PCs for 10 samples of $R1 \cdot AcO^-$ sensor and 2 metal ions

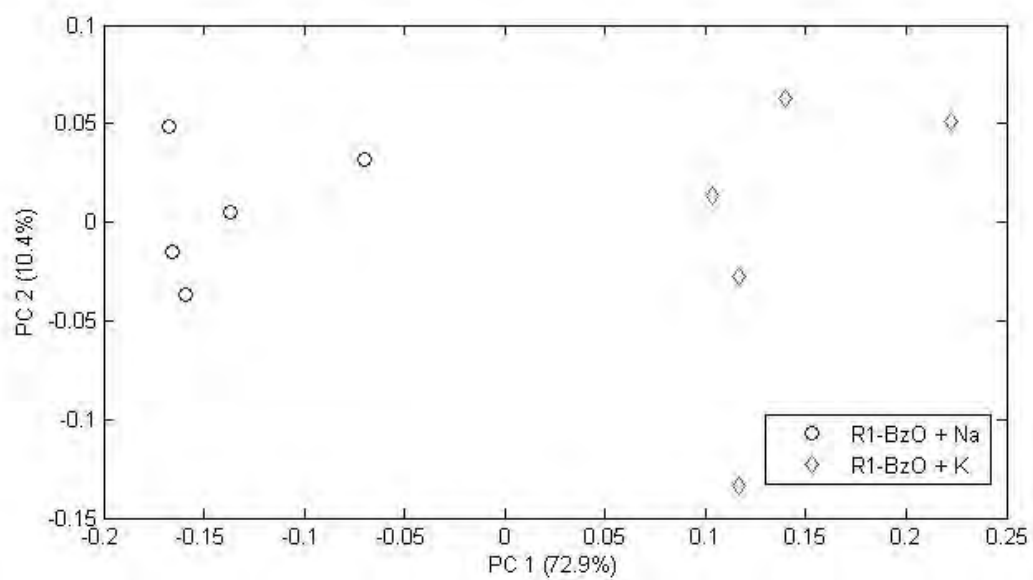


Figure 4.50 PCA score plot of the first two PCs for 10 samples of $R1 \cdot BzO^-$ sensor and 2 metal ions

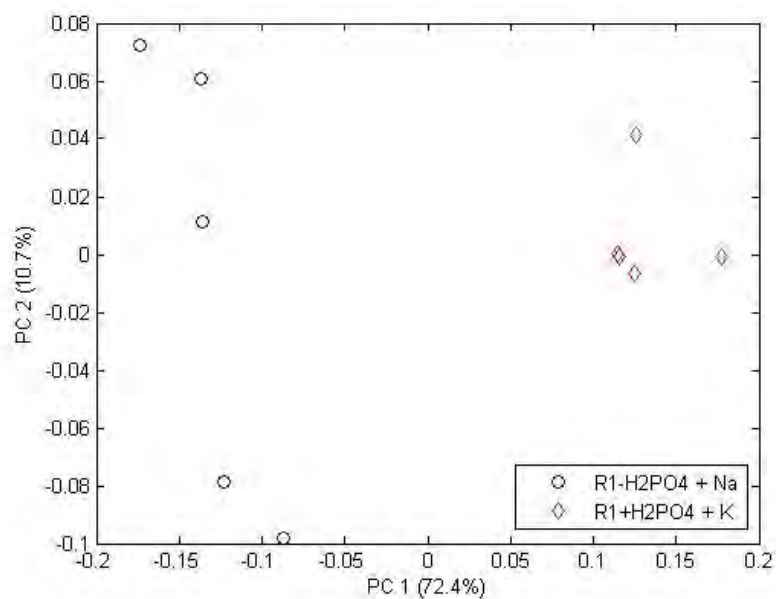


Figure 4.51 PCA score plot of the first two PCs for 10 samples of $\mathbf{R1}\cdot\mathbf{H}_2\mathbf{PO}_4^-$ sensor and 2 metal ions

The PCA score plot of the first two PCs for 10 samples of four-member array ($\mathbf{R1}\cdot\mathbf{F}^-$, $\mathbf{R1}\cdot\mathbf{AcO}^-$, $\mathbf{R1}\cdot\mathbf{BzO}^-$, $\mathbf{R1}\cdot\mathbf{H}_2\mathbf{PO}_4^-$) and 2 ions such as \mathbf{Na}^+ , \mathbf{K}^+ showed high level of discrimination (88.3%) (Figure 4.52). Therefore, the clear clustering of the data was observed. These supported that the sensor array could discriminate between \mathbf{Na}^+ and \mathbf{K}^+ .

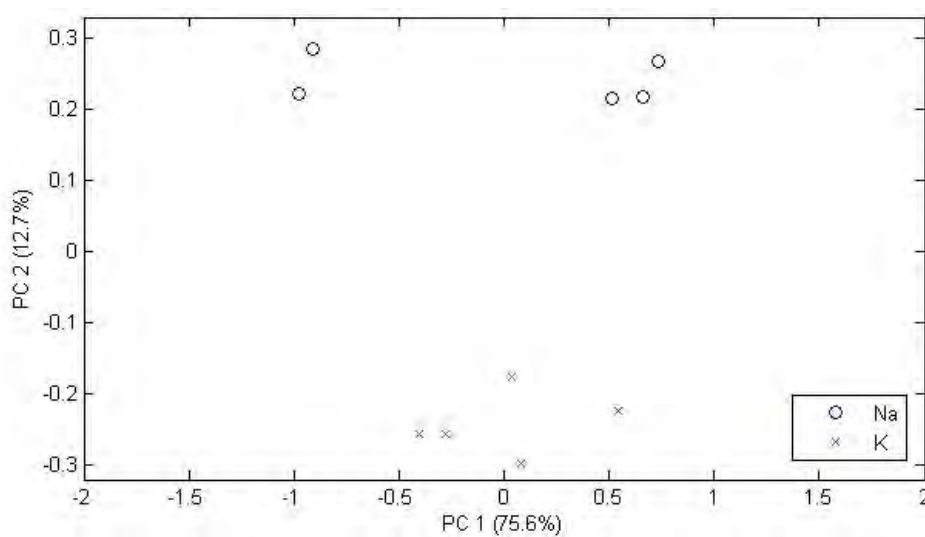


Figure 4.52 PCA score plot of the first two PCs for 10 samples of 4 sensors and 2 metal ions

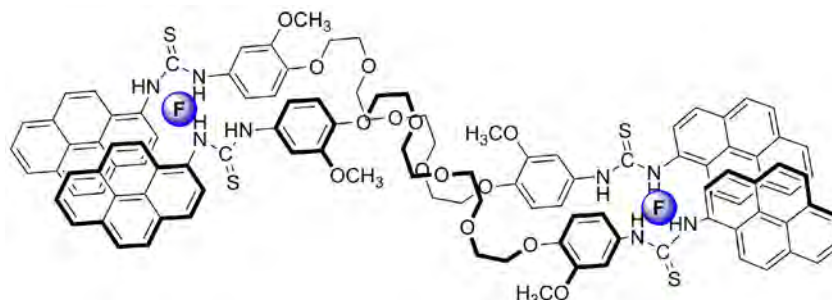
The PCA score plot for free **R2** and 4 anions (F^- , AcO^- , BzO^- and $H_2PO_4^-$) also displayed very high level of discrimination (Figure A68). These supported that, **R1** sensor could discriminate all 4 anions as same as **R1** receptor. Moreover, their sensor arrays (**R2**+ F^- , **R2**+ AcO^- , **R2**+ $H_2PO_4^-$) could discriminate between Na^+ and K^+ (Figure A69).

CHAPTER V

CONCLUSIONS

We have designed and synthesized the new dimeric pyrene thiourea molecules containing variable polyethylene glycol (PEG) chain lengths, **L1** – **L3**, and the monomeric pyrene thiourea, **L4** with no PEG chain. The fluorescence emission spectra of free **L1** – **L4** displayed intense characteristic monomer bands of the pyrene in the same region and no excimer emission band. The order of intensity ratios between excimer and monomer bands (I_E/I_M) in **L1** varied as $F^- > AcO^- \approx BzO^- > H_2PO_4^- \approx Cl^- > Br^- \approx I^- > OH^-$. The preference of fluoride to bind with $-NH$ of thiourea group through H-bonding, was due to the highest basicity of fluoride. Moreover, the smallest atomic size of fluoride was suitable to encapsulate in the receptor molecule. The fluorescence intensity of pyrene excimer band at 500 nm gradually increased upon the addition of fluoride anions into **L1** solution. However, there was a small change in monomer emission intensity at 398 nm. These suggested that fluoride induced the formation of pyrene excimer interactions resulting in the fluorescence enhancement of the excimer band. The Job's plot experiment of **L1** and fluoride displayed a maximum mole fraction of fluoride at 0.5 and supported the 1:1 or 2:2 complexation of **L1**: F^- . However, we proposed that in the presence of fluoride, the arrangement of **L1** was in the unfolded form because the ratios of excimer and monomer emission depended on concentration which implied the intermolecular excimer interaction of pyrene molecules. Moreover, 1H -NMR titrations of **L1** and fluoride displayed the broad peaks of pyrene proton signals and shifted upfield concurrent with downfield shift of some signals due to the $\pi - \pi$ stacking of the pyrene molecules and the anisotropic effect from their ring current, which supported the excimer formation. The binding property of **L1** with fluoride may be applied for detecting as low as 2.3 ppm of fluoride in organic media using fluorescence spectroscopy or under UV light. Results from fluorescence and 1H -NMR spectroscopy showed that decomplexation of **L1**: F^- occurred in the presence of sodium ion and implied the pyrene stacking by fluoride would be terminated when fluoride formed an ion pair with sodium ion.

Unfolded structure of L1·F complex



The flexible and the semi-rigid thiourea nitrobenzene derivatives of **R1** and **R2** have been synthesized. The UV-vis absorption spectra of all receptors exhibited the absorption peak of the $\pi - \pi^*$ transition of aromatic hydrocarbons around 360 nm. Upon addition of fluoride anion into **R1** solution, the absorption spectra at 369 nm decreased and an intense peak with shoulder around 472 nm appeared. As amount of fluoride increased, the hydrogen bond interactions between fluoride and thiourea groups were very strong leading to deprotonation and formation of FHF^- ion concurrent with the charge transfer band at 472 nm. In the case of the **R2**· F^- complex, the spectra around 369 nm disappeared gradually and a new peak was observed around 472 nm. We proposed that the change of **R2**· F^- spectra was attributed to deprotonation of NH to N^- in the thiourea fragments. UV-vis spectra of **R1** and **R2** upon adding AcO^- , BzO^- and H_2PO_4^- showed the first new peak around 380 – 400 nm due to hydrogen bonding interactions in a similar manner to the **R1**· F^- complex and displayed the charge transfer band around 460 – 470 nm. Stoichiometries of **R1** and **R2** with F^- , AcO^- and BzO^- were 1:2 (host:guest) ratios. K_{ass} was calculated by SPECFIT/32 software and the results also supported the 1:2 complexation model. The selectivity trend with various anions and the stoichiometry of the flexible chain in **R1** was similar to the semi-rigid structure in **R2** ($\text{F}^- > \text{BzO}^- > \text{AcO}^- > \text{H}_2\text{PO}_4^-$). Principal component analysis (PCA) was used to evaluate selectivity of **R1** and **R2** sensors for four anions (F^- , AcO^- , BzO^- , H_2PO_4^-) and two metal ions (Na^+ , K^+). Both sensors could discriminate all four anions and their arrays were found to be able to identify 2 metal analyses with high percentage accuracy.

Suggestions for future works

In this research, the selectivity of all synthesized receptors with various ions was studied in many organic solvents (CHCl_3 , CH_3CN and DMSO). However, there were no experiments doing in water because of the limitation of solubility. Our sensors might be studied in aqueous media by using mixed organic solvents with water or by using micelle to dissolve our host molecules. This result might be useful for real analytical applications.

REFERENCES

- [1] Steed, J. W., Turner, D. R., and Wallace, K. J. *Core Concepts in Supramolecular Chemistry and Nanochemistry*, John Wiley&Sons Ltd., 2007.
- [2] Kim, H. J. et al. *Org. Lett.* 2008, *10*, 1963 – 1966.
- [3] Bao, X., Yu, J., and Zhou, Y. *Sensor Actuat. B-Chem.* 2009, *140*, 467 – 472.
- [4] Valeur, B. *Molecular Fluorescence Principles and Applications*, Wiley-Vch, New York, 2001.
- [5] Tuntulani, T., and Suksai, C. *Top Curr Chem.* 2005, *255*, 163 – 198.
- [6] Zhou, Y., Zhu, C., Gao, X. S., You, X. Y., and Yao, C. *Org. Lett.* 2010, *12*, 2566 – 2569.
- [7] Hung, H., Cheng, C., Ho, I., and Chung, W. *Tetrahedron Lett.* 2009, *50*, 302 – 305.
- [8] Romero, T., Caballero, A., Tárraga, A., and Molina, P. *Org. Lett.* 2009, *11*, 3466 – 3469.
- [9] Jung, H. S. et al. *Org. Lett.* 2009, *11*, 3378 – 3381.
- [10] Chandrasekhar, V., Pandey, M. D., Bag, P., and Pandey, S. *Tetrahedron* 2009, *65*, 4540 – 4546.
- [11] Winnik, F. M. *Chem. Rev.* 1993, *93*, 587 – 614.
- [12] Brereton, R. G. *Applied Chemometrics for Scientists*, John Wiley & Sons, Ltd., 2007.
- [13] Palacios, M. A., Nishiyabu, R., Marquez, M., and Anzenbacher, P. *J. Am. Chem. Soc.* 2007, *129*, 7538 – 7544.
- [14] Saravanakumar, D., Devaraj, S., Iyyampillai, S., Mohandoss, K., and Kandaswamy, M. *Tetrahedron Lett.* 2008, *49*, 127 – 132.
- [15] Luxami, V., and Kumar, S. *Tetrahedron Lett.* 2007, *48*, 3083 – 3087.
- [16] Li, J., Lin, H., Jiang, P., and Lin, H. *J. Incl. Phenom. Macro.* 2008, *62*, 209 – 213.
- [17] Dydio, P., Zieliński, T., and Jurczak, J. *J. Org. Chem.* 2009, *74*, 1525 – 1530.
- [18] Li, J., Lin, H., Cai, Z., and Lin, H. *Spectrochim Acta A* 2009, *72*, 1062 – 1065.
- [19] Shao, J., Lin, H., and Lin, H. *Dyes Pigments* 2009, *80*, 259 – 263.
- [20] Qu, Y., Hua, J., and Tian, H. *Org. Lett.* 2010, *12*, 3320 – 3323.
- [21] Bao, X., Yu, J., and Zhou, Y. *Sensor Actuat. B-Chem.* 140, 2009, 467 – 472.

- [22] Kumar, M., Kumar, R., and Bhalla, V. *Tetrahedron* 2009, 65, 4340 – 4344.
- [23] Shao, J., Lin, H., and Lin, H. *Talanta* 2008, 75, 1015 – 1020.
- [24] Lin, C., Simov, V., and Drueckhammer, D. G. *J. Org. Chem.* 2007, 72, 1742 – 1746.
- [25] Chauhan, S. M. S., Bisht, T., and Garg, B. *Tetrahedron Lett.* 2008, 49, 6646 – 6649.
- [26] Lu, Q. et al. *Org. Lett.* 2009, 11, 669 – 672.
- [27] Tung, C., Yuan, Z., and Wu, L. *J. Org. Chem.* 1999, 64, 5156 – 5161.
- [28] Dahan, A. et al. *J. Org. Chem.* 2007, 72, 2289 – 2296.
- [29] Jung, H. S. et al. *Org. Lett.* 2009, 11, 3378 – 3381.
- [30] Abe, A. M. M., Helaja, J., and Koskinen, A. M. P. *Org. Lett.* 2006, 8, 4537 – 4540.
- [31] Hung, H., Cheng, C., Ho, I., and Chung, W. *Tetrahedron Lett.* 2009, 50, 302 – 305.
- [32] Zhou, Y., Zhu, C., Gao, X., You, X., and Yao, C. *Org. Lett.* 2010, 12, 2566 – 2569.
- [33] Xu, Y., Wang, G., Zhao, X., Jiang, X., and Li, Z. *J. Org. Chem.* 2009, 74, 7267 – 7273.
- [34] Monti, D., Monica, L. L., Scipioni, A., and Mancini, G. *New J. Chem.* 2001, 25, 780 – 782.
- [35] Hou, J., Jia, M., Jiang, X., Li, Z., and Chen, G. *J. Org. Chem.* 2004, 69, 6228 – 6237.
- [36] Varghese, R., George, S. J., and Ajayaghosh, A. *Chem. Commun.* 2005, 593 – 595.
- [37] Wu, X. et al. *J. Org. Chem.* 2008, 73, 491 – 494.
- [38] Palacios, M. A., Wang, Z., Montes, V. A., Zyryanov, G. V., and Anzenbacher, P. *J. Am. Chem. Soc.* 2008, 130, 10307 – 10314.
- [39] Rittikulsittichai, S. *Synthesis and binding properties of cation-templated Anion receptors*, Master of Science in Chemistry, Department of Chemistry, Faculty of Science, Chulalongkorn University, 2003.
- [40] Shao, J., Yu, X., Lin, H., and Lin, H. *J. Mol. Recognit.* 2008, 21, 425 – 430.
- [41] Upadhyay, K. K., Mishra, R. K., Kumar, V., and Chowdhury, P. K. R. *Talanta* 2010, 82, 312 – 318.

- [42] Suksai, C., and Tuntulani, T. *Chem. Soc. Rev.* 2003, 32, 192 – 202.
- [43] Han, F. et al. *Chem. Eur. J.* 2007, 13, 2880 – 2892.
- [44] Goswami, S., and Chakrabarty, R. *Tetrahedron Lett.* 2009, 50, 5910 – 5913.
- [45] Rocha, A., Marques, M. M. B., and Lodeiro, C. *Tetrahedron Lett.* 2009, 50, 4930 – 4933.
- [46] Monti, D., Monica, L. L., Scipioni, A., and Mancini, G. *New J. Chem.* 2001, 25, 780 – 782.
- [47] (a) Shao, J., Lin, H., and Lin, H. K. *Dyes and Pigments.* 2009, 80, 259 – 263, (b) Shao, J., Lin, H., and Lin, H. K. *Talanta.* 2008, 75, 1015 – 1020.
- [48] Kim, H. J., Kim, S. K., Lee, J. Y., and Kim, J. S. *J. Org. Chem.* 2006, 71, 6611 – 6614.
- [49] Kim, S. K. et al. *J. Am. Chem. Soc.* 2004, 126, 16499 – 16506.
- [50] Romero, T., Caballero, A., Tarraga, A., and Molina, P. *Org. Lett.* 2009, 11, 3466 – 3469.
- [51] Rocha, A., Marques, M. M. B., and Lodeiro, C. *Tetrahedron. Lett.* 2009, 50, 4930 – 4933.
- [52] Tung, C. H., Yuan, Z. Y., and Wu, L. Z. *J. Org. Chem.* 1999, 64, 5156 – 5161.
- [53] Ingle, Jr. J. D., and Wilson, R. L. *Anal. Chem.* 1976, 48, 1641 – 1642.
- [54] Zhong, Z., and Zhao, Y. *Org. Lett.* 2007, 9, 2891 – 2894.
- [55] Arunkumar, E., Chithra, P., and Ajayaghosh, A. *J. Am. Chem. Soc.* 2004, 126, 6590 – 6598.
- [56] Arunkumar, E., Ajayaghosh, A., and Daub, J. *J. Am. Chem. Soc.* 2005, 127, 3156 – 3164.
- [57] Nandy, R., Subramoni, M., Varghese, B., and Sankararaman, S. *J. Org. Chem.* 2007, 72, 938 – 944.
- [58] Magri, D. C., Brown, G. J., McClean, G. D., and de Silva A. P. *J. Am. Chem. Soc.* 2006, 128, 4950 – 4951.
- [59] de Silva, A. P., McClean, G. D., and Pagliari, S. *Chem. Commun.* 2003, 2010 – 2011.
- [60] Cui, Y. et al. *Inorg. Chem.* 2007, 46, 6427 – 6436.
- [61] Batista, R. M. F., Oliveira, E., Costa, S. P. G., Lodeiro, C., and Raposo, M. M. *M. Org. Lett.* 2007, 9, 3201 – 3204.

- [62] SPECFIT/32 Global Analysis System, v. 3.0.40, Spectrum Software Association.
- [63] Maeder, M., and Zuberbuhler, A. D. *Anal. Chem.* 1990, *62*, 2220 – 2224.
- [64] Devaraj, S., Saravanakumar, D., and Kandaswamy, M. *Sensor. Actuat. B.* 2009, *136*, 13 – 19.
- [65] Liu, B., and Tian, H. *J. Mater. Chem.* 2005, *15*, 2681-2686.
- [66] Hu, S., Guo, Y., Xu, J., and Shao, S. *Spectrochim. Acta. A.* 2009, *72*, 1043 – 1046.
- [67] Yeo, H. M., Ryu, B. J., and Nam, K. C. *Org. Lett.* 2008, *10*, 2931 – 2934.
- [68] Bao, X., Wang, L., Wu, L., and Li, Z. *Supramol. Chem.* 2008, *20*, 467 – 472.
- [69] Hisaki, I., Sasaki, S., Hirose, K., and Tobe, Y. *Eur. J. Org. Chem.* 2007, 607 – 615.

APPENDIX

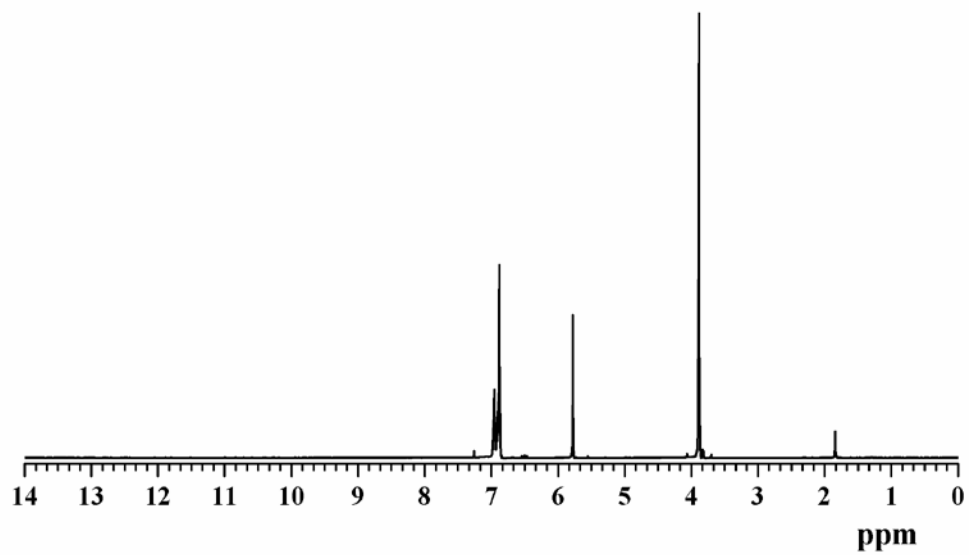


Figure A1 ^1H -NMR spectrum of **1** in CDCl_3 at 400 MHz

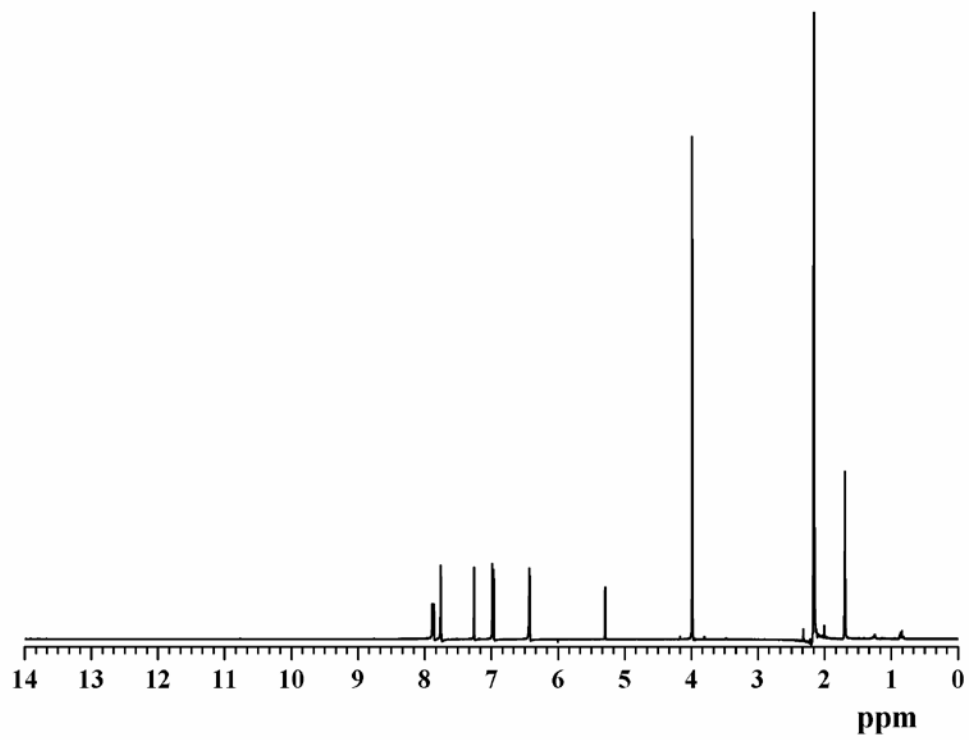


Figure A2 ^1H -NMR spectrum of **2** in CDCl_3 at 400 MHz

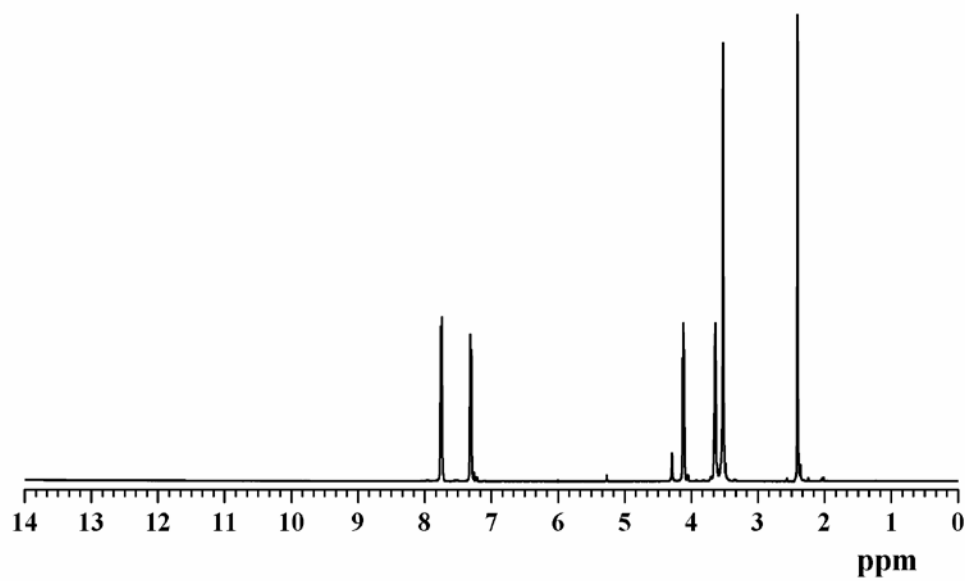


Figure A3 ¹H-NMR spectrum of **3** in CDCl₃ at 400 MHz

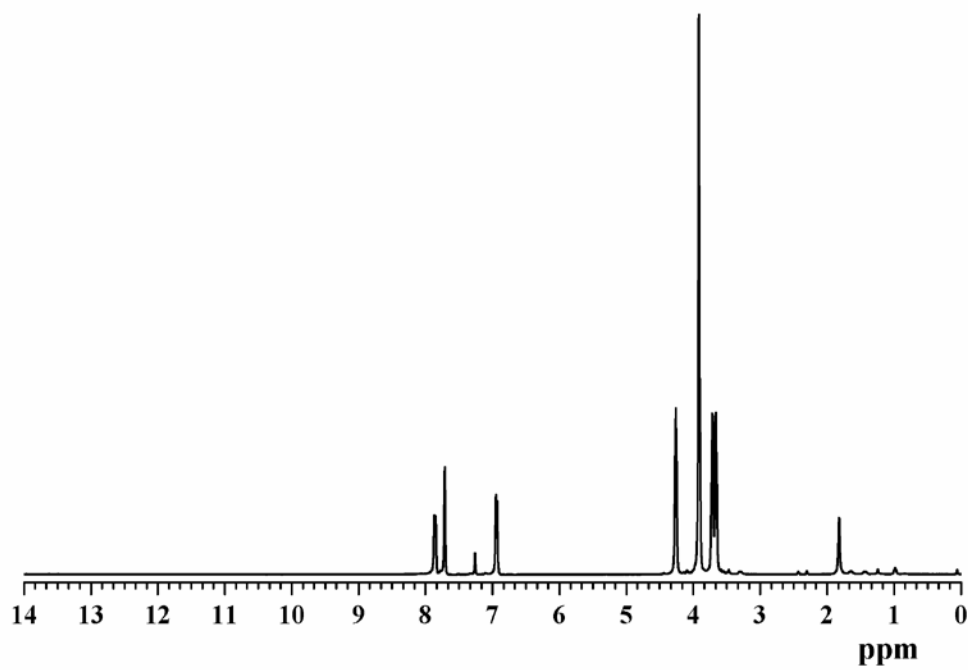


Figure A4 ¹H-NMR spectrum of **4** in CDCl₃ at 400 MHz

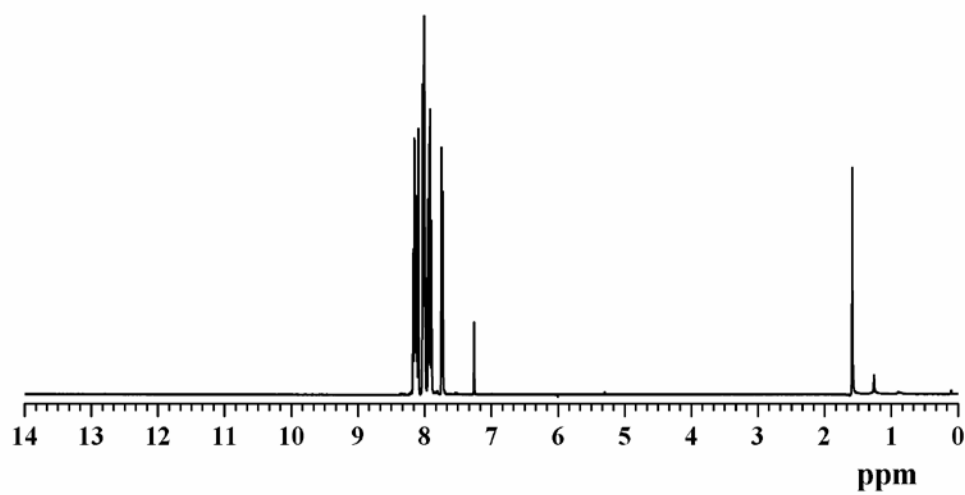


Figure A5 ¹H-NMR spectrum of **6** in CDCl₃ at 400 MHz

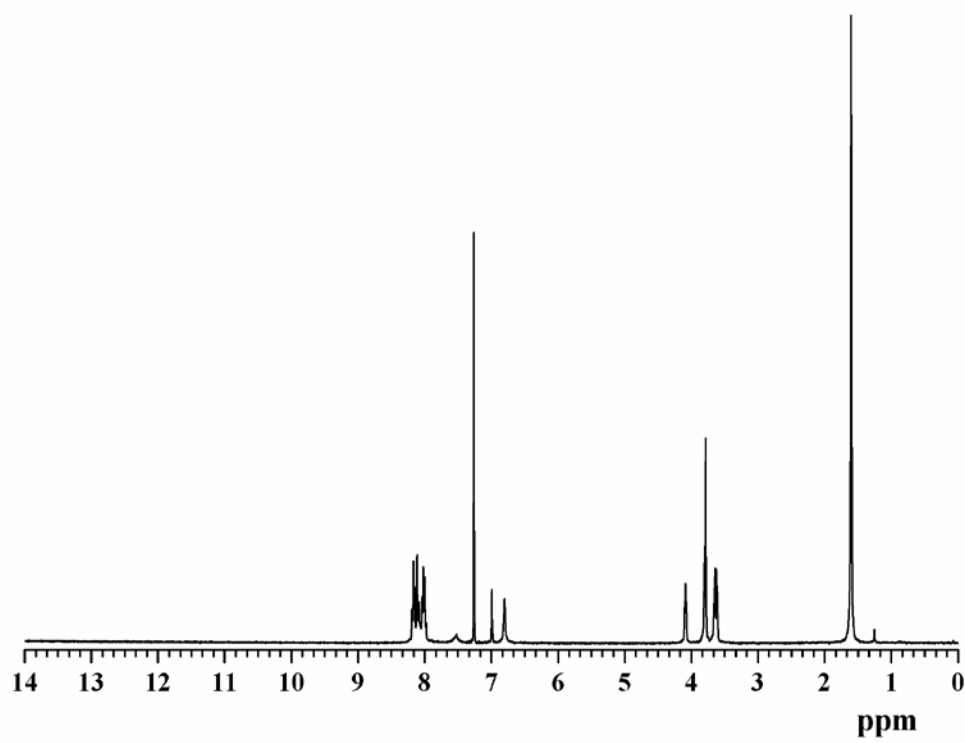


Figure A6 ¹H-NMR spectrum of **L1** in CDCl₃ at 400 MHz

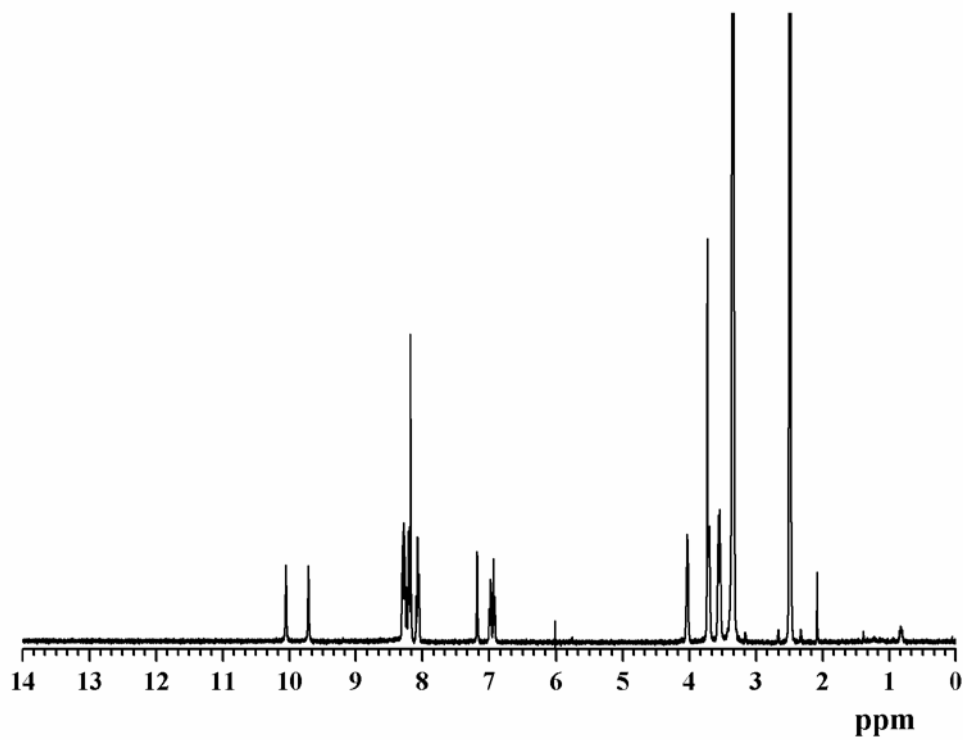


Figure A7 ¹H-NMR spectrum of **L1** in d₆-DMSO at 400 MHz

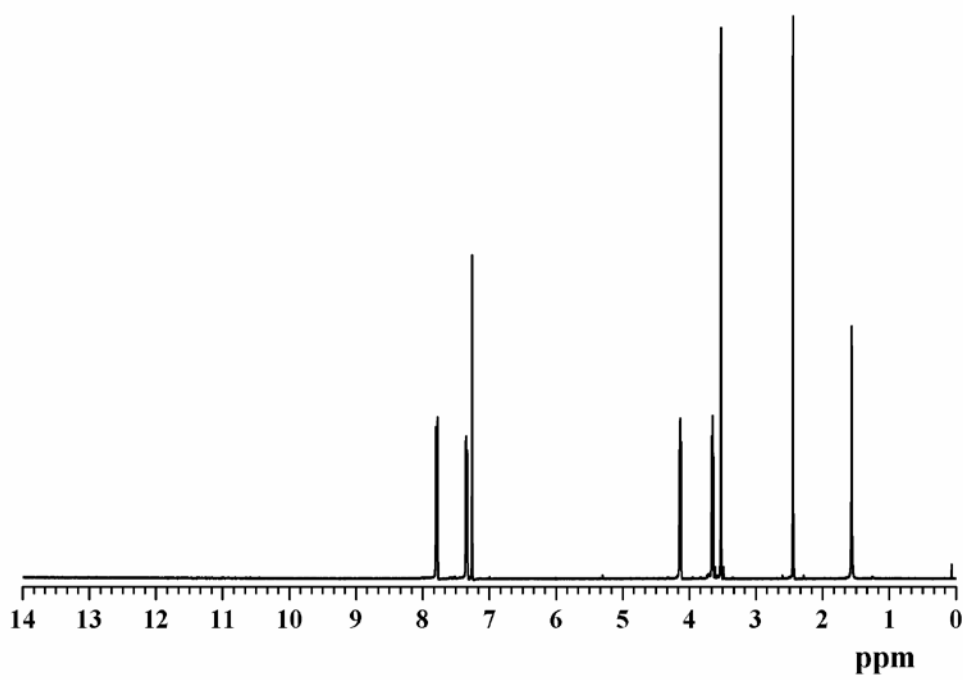


Figure A8 ¹H-NMR spectrum of **7** in CDCl₃ at 400 MHz

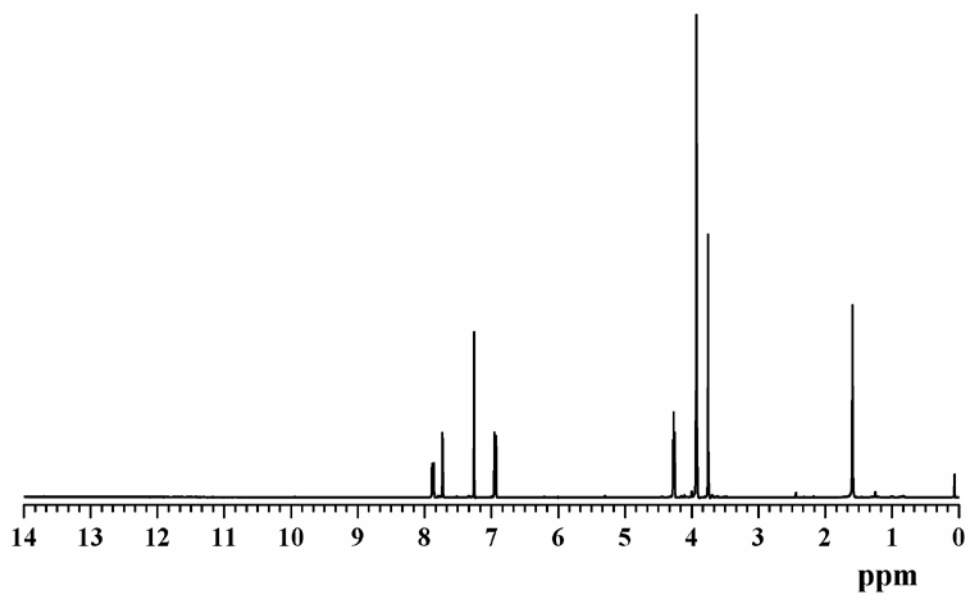


Figure A9 ¹H-NMR spectrum of **8** in CDCl₃ at 400 MHz

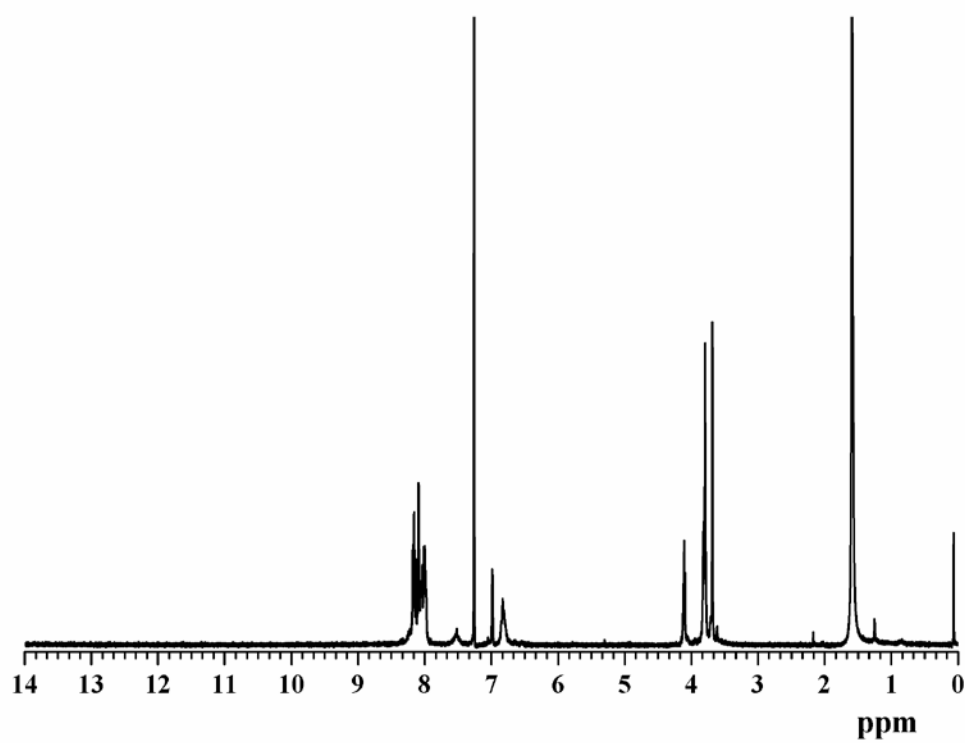


Figure A10 ¹H-NMR spectrum of **L2** in CDCl₃ at 400 MHz

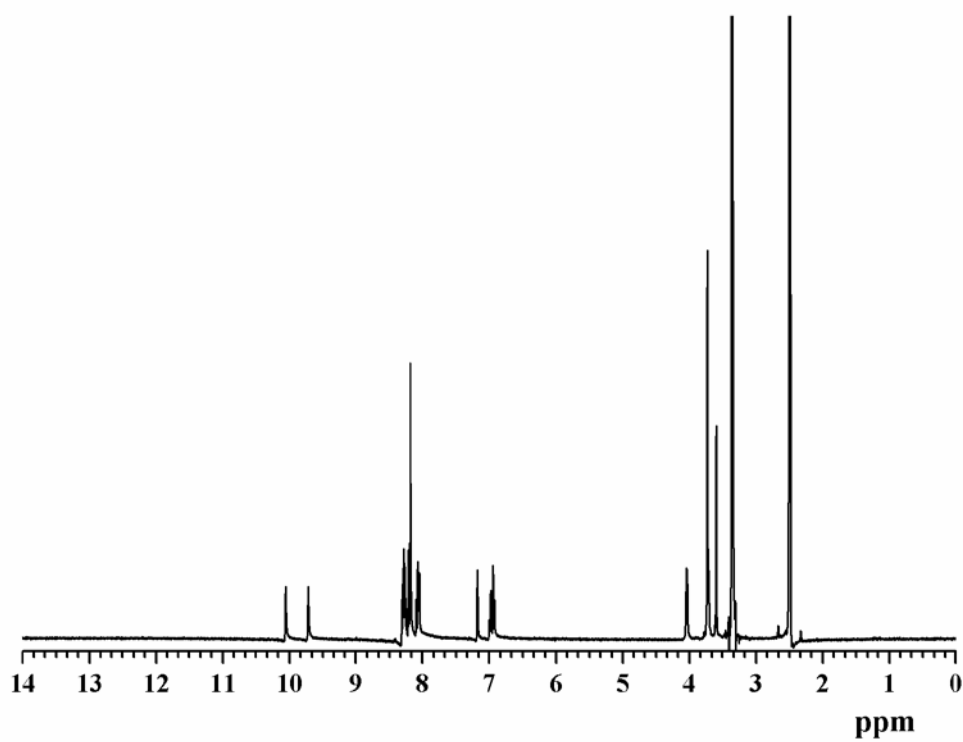


Figure A11 ¹H-NMR spectrum of **L2** in d₆-DMSO at 400 MHz

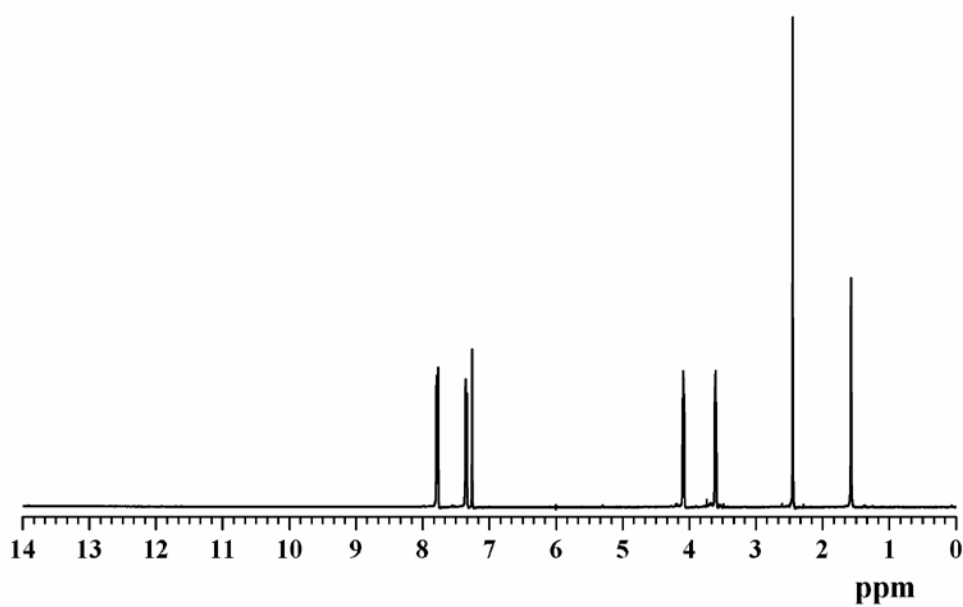


Figure A12 ¹H-NMR spectrum of **10** in CDCl₃ at 400 MHz

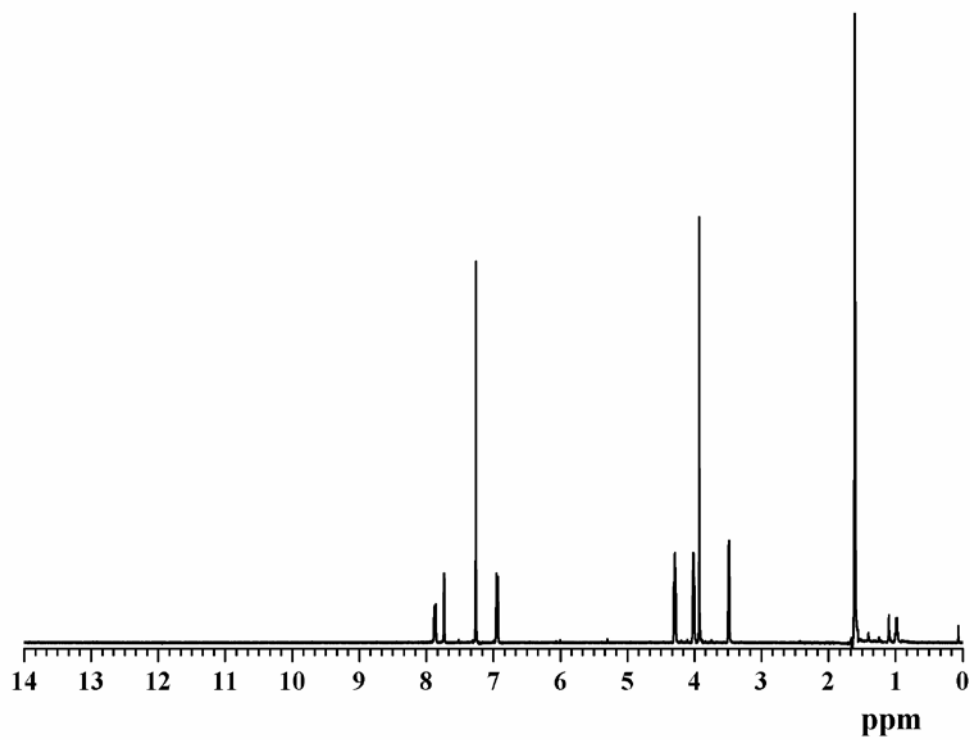


Figure A13 ¹H-NMR spectrum of **11** in CDCl₃ at 400 MHz

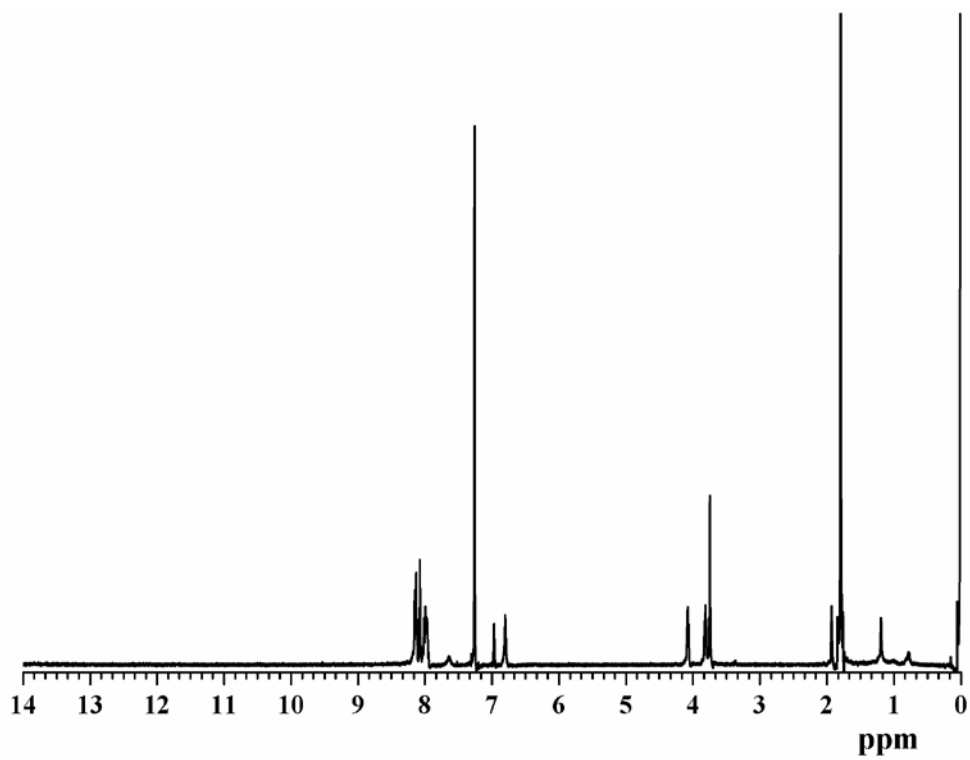


Figure A14 ¹H-NMR spectrum of **L3** in CDCl₃ at 400 MHz

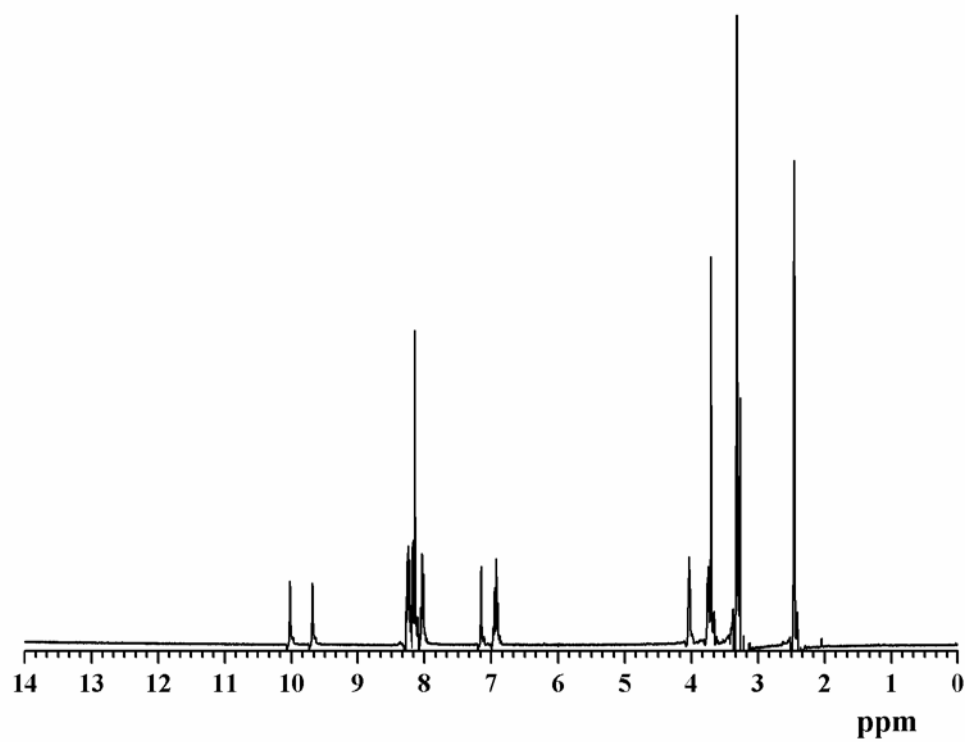


Figure A15 ¹H-NMR spectrum of **L3** in d₆-DMSO at 400 MHz

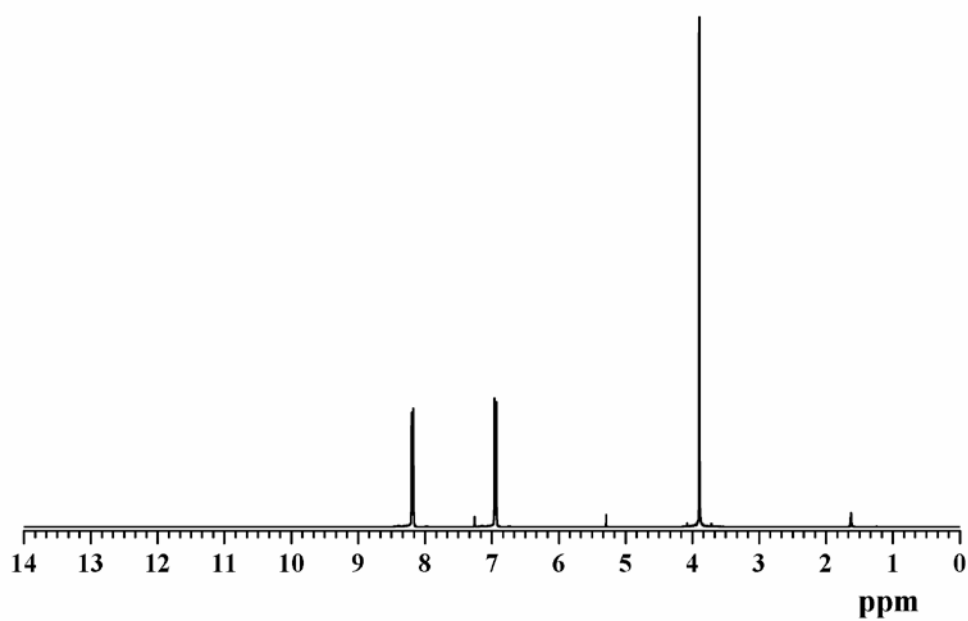


Figure A16 ¹H-NMR spectrum of **13** in CDCl₃ at 400 MHz

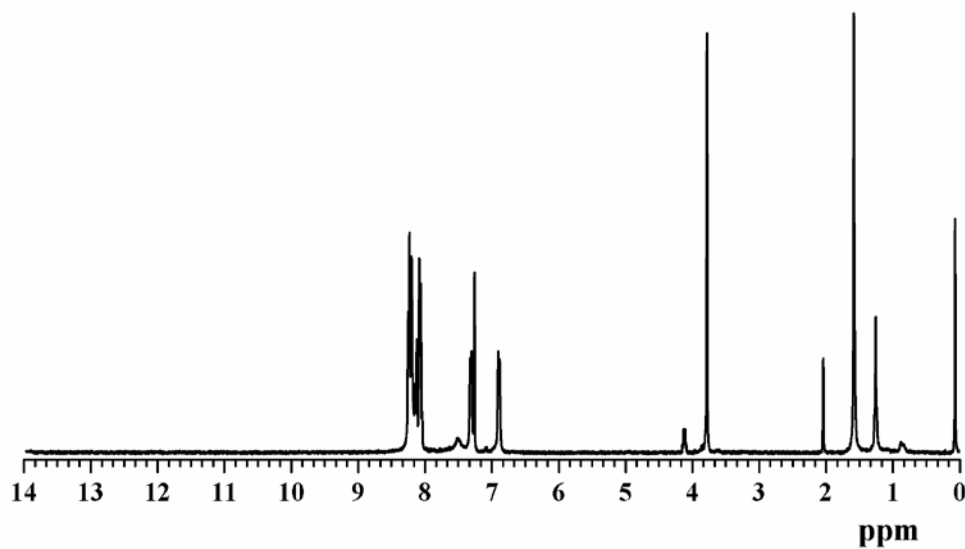


Figure A17 ¹H-NMR spectrum of **L4** in CDCl₃ at 400 MHz

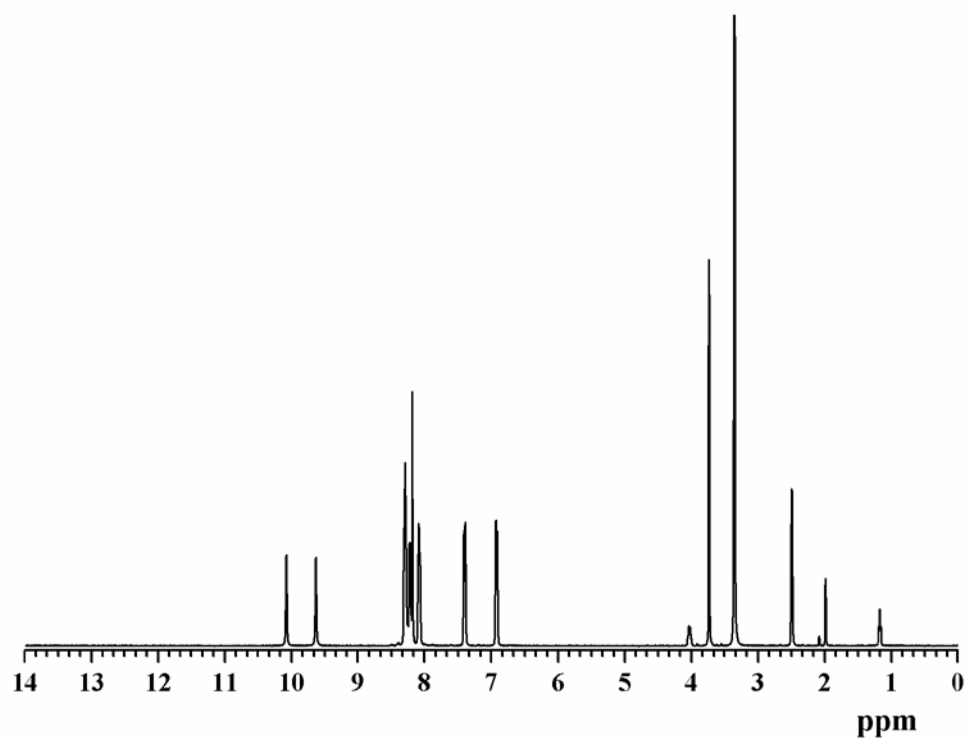


Figure A18 ¹H-NMR spectrum of **L4** in d₆-DMSO at 400 MHz

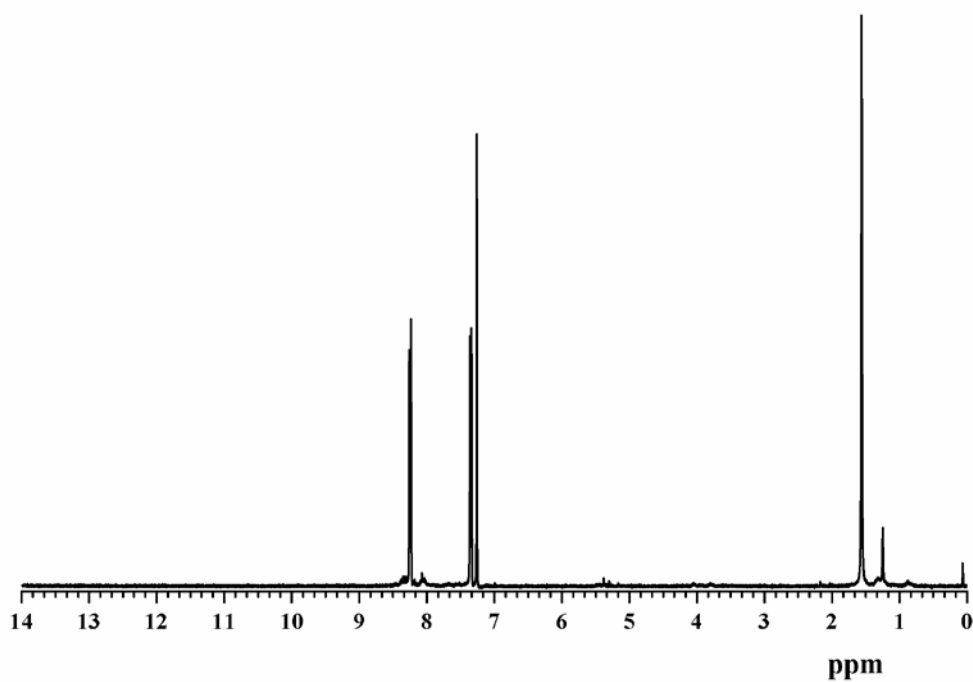


Figure A19 ¹H-NMR spectrum of **15** in CDCl₃ at 400 MHz

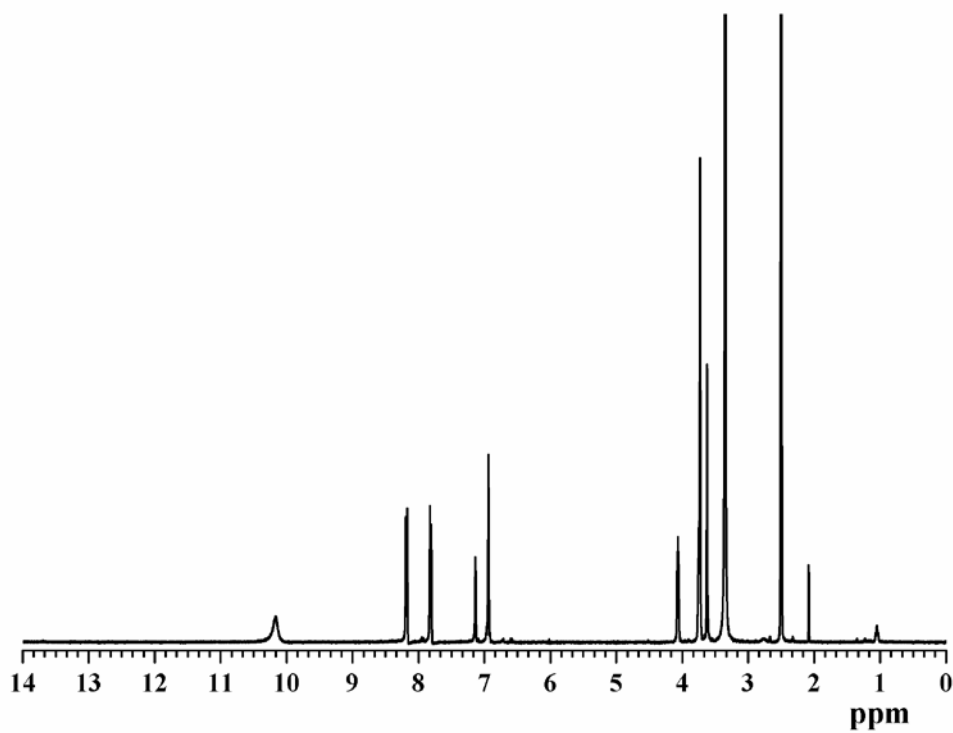


Figure A20 ¹H-NMR spectrum of **R1** in d₆-DMSO at 400 MHz

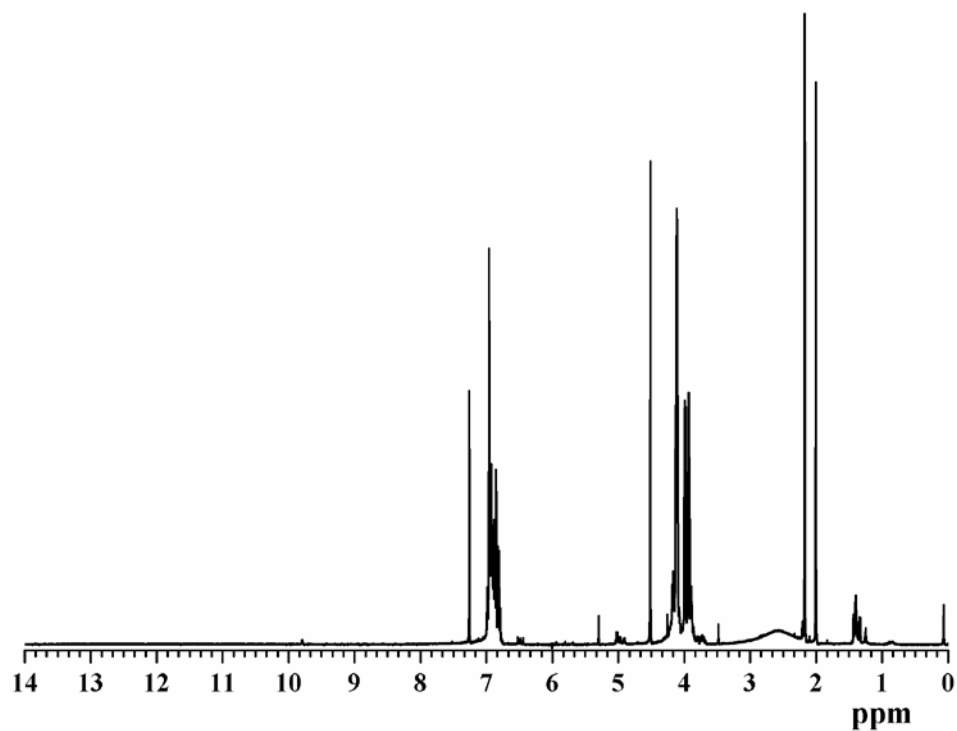


Figure A21 ^1H -NMR spectrum of **16** in CDCl_3 at 400 MHz

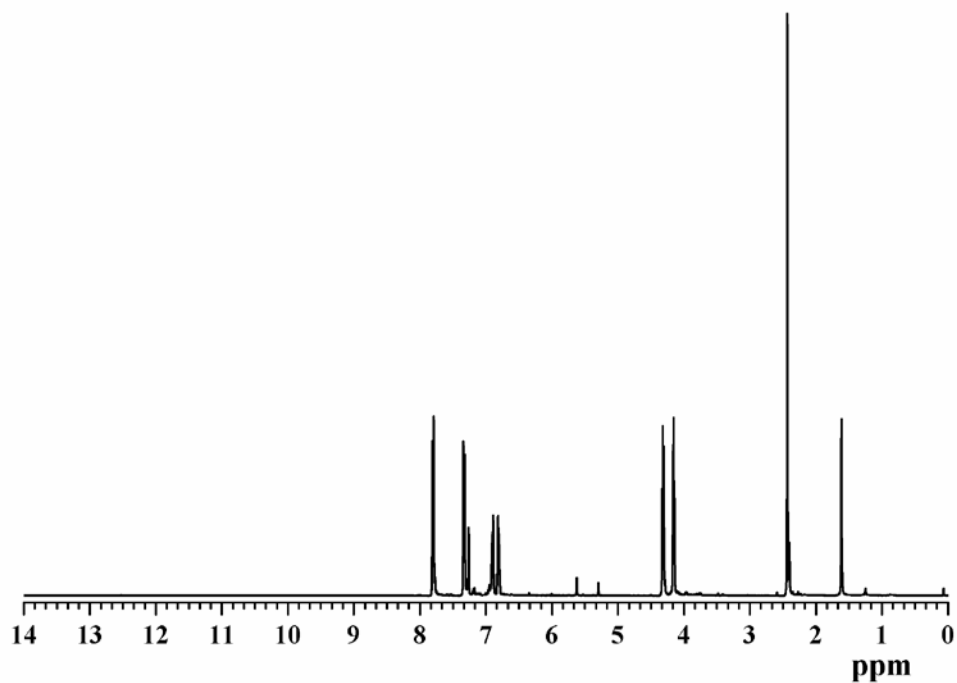


Figure A22 ^1H -NMR spectrum of **17** in CDCl_3 at 400 MHz

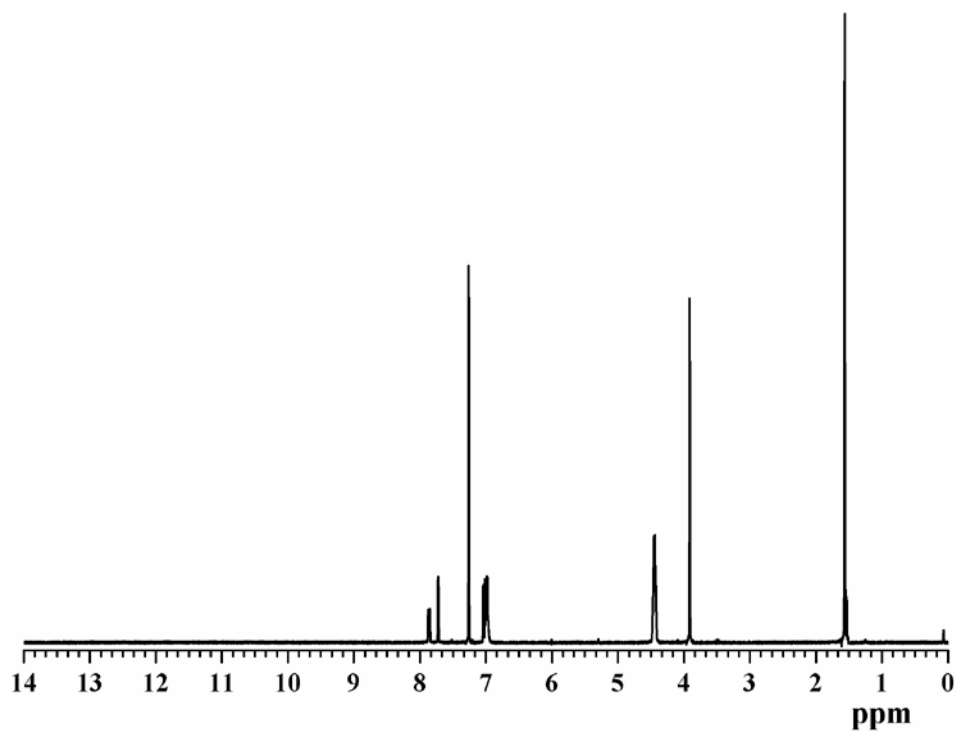


Figure A23 ¹H-NMR spectrum of **18** in CDCl₃ at 400 MHz

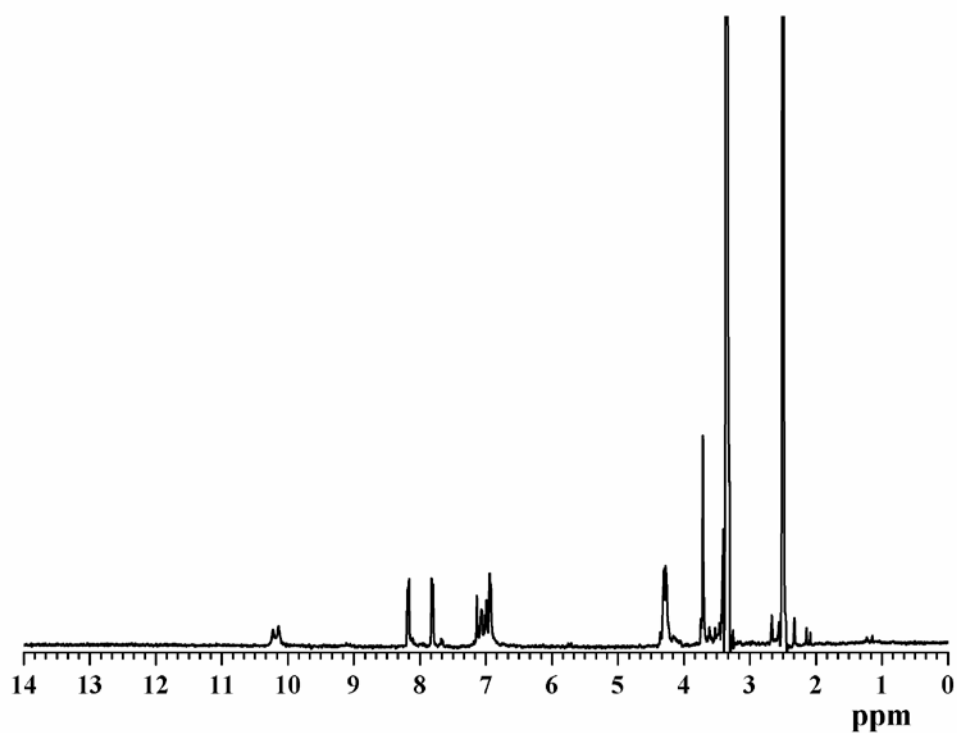


Figure A24 ¹H-NMR spectrum of **R2** in d₆-DMSO at 400 MHz

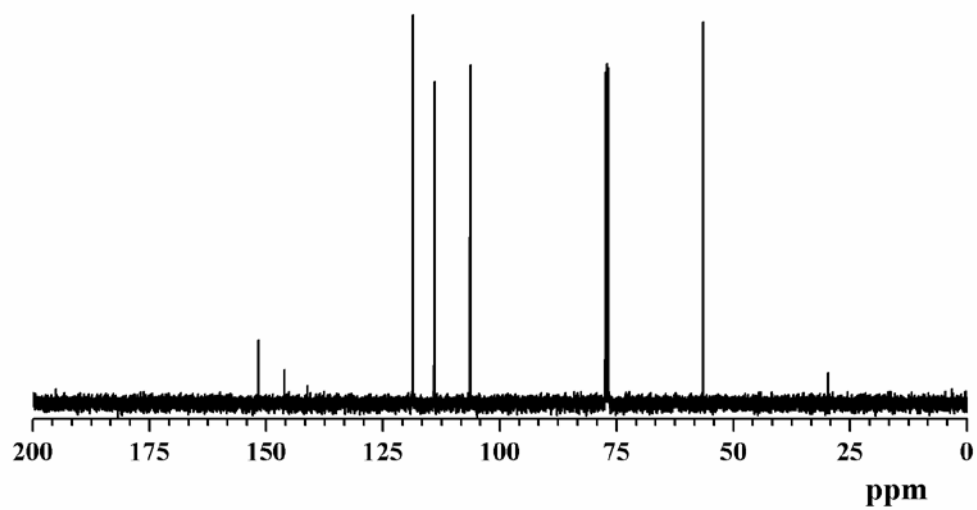


Figure A25 ^{13}C -NMR spectrum of **2** in CDCl_3 at 100 MHz

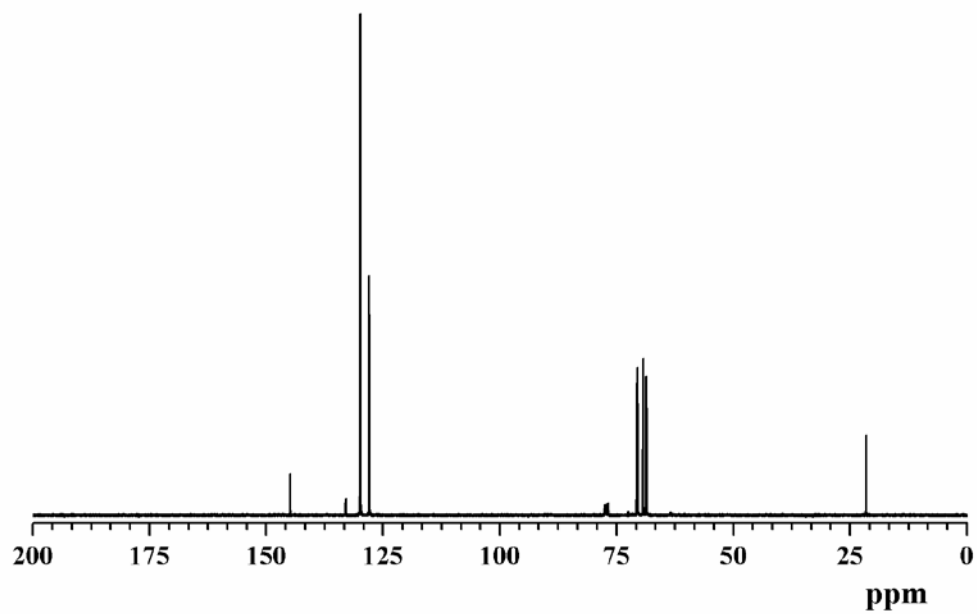


Figure A26 ^{13}C -NMR spectrum of **3** in CDCl_3 at 100 MHz

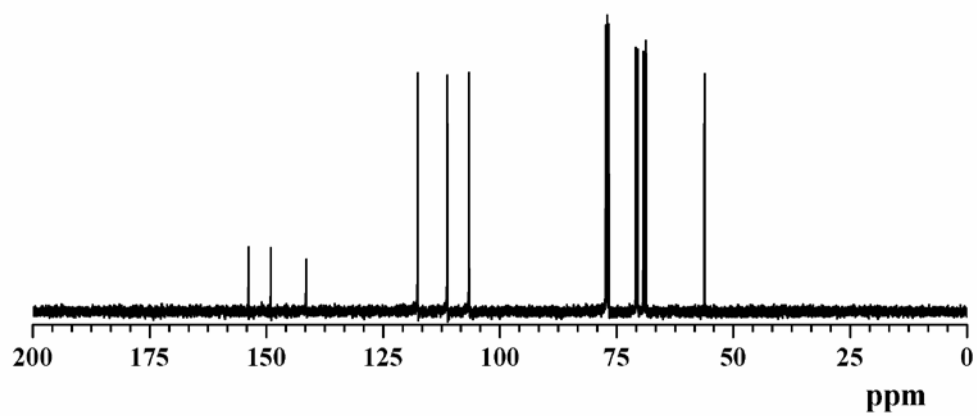


Figure A27 ^{13}C -NMR spectrum of **4** in CDCl_3 at 100 MHz

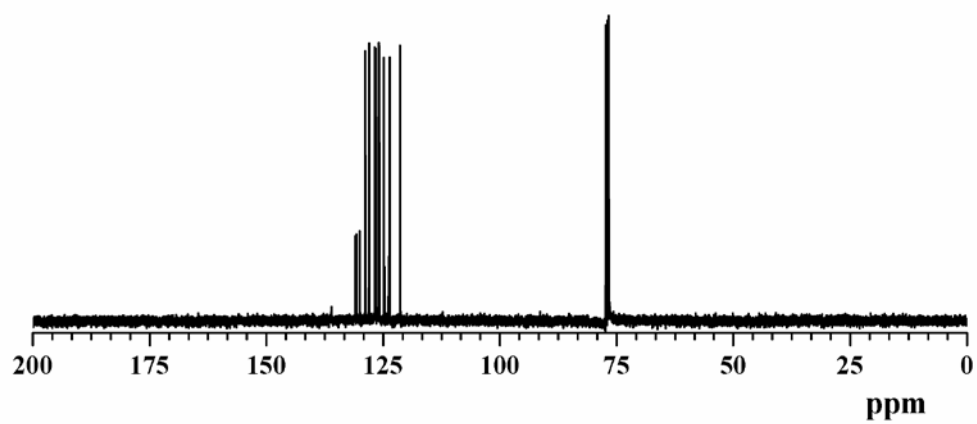


Figure A28 ^{13}C -NMR spectrum of **6** in CDCl_3 at 100 MHz

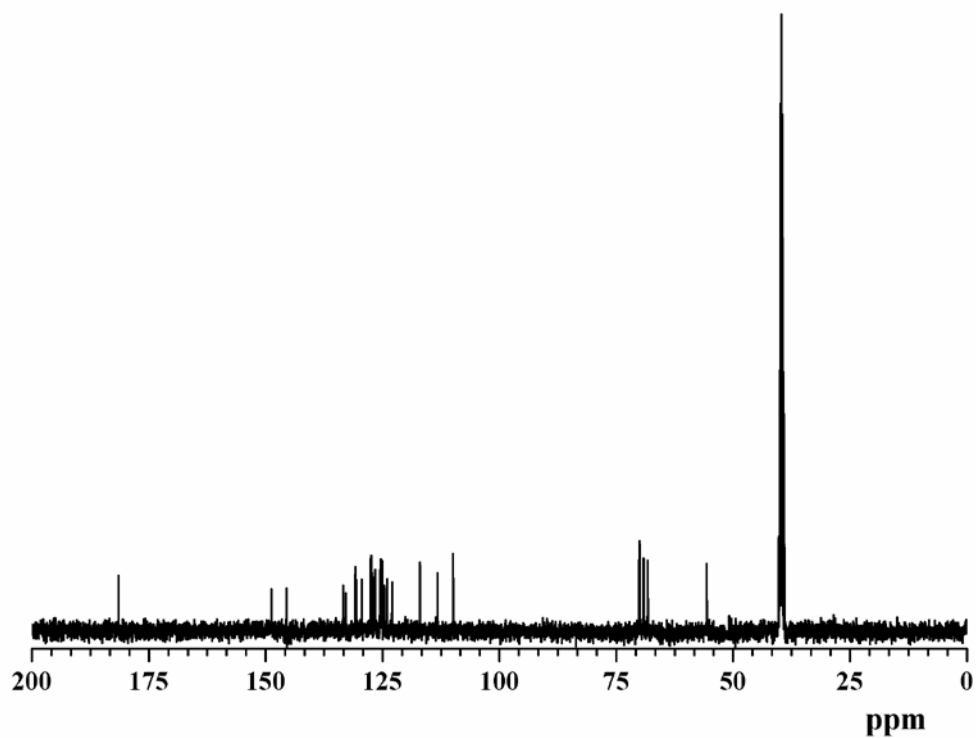


Figure A29 ^{13}C -NMR spectrum of L1 in d_6 -DMSO at 100 MHz

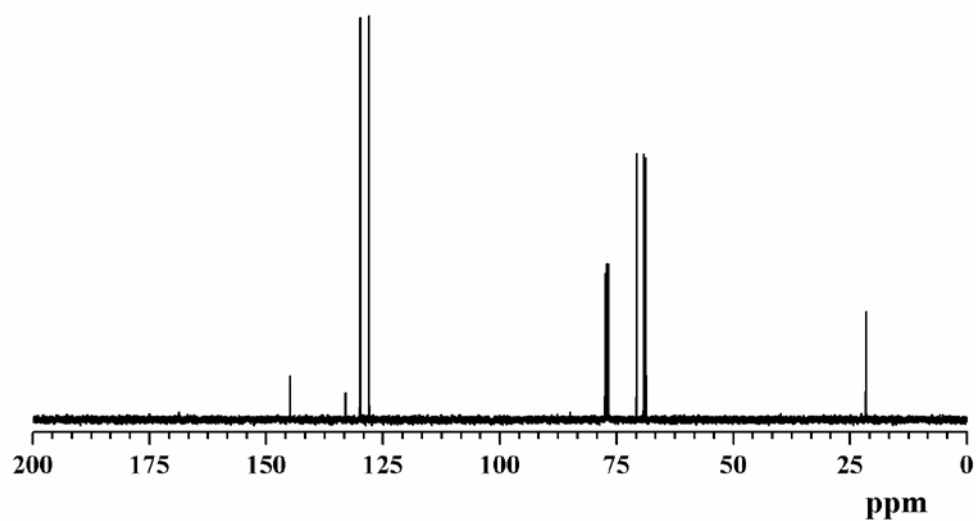


Figure A30 ^{13}C -NMR spectrum of 7 in CDCl_3 at 100 MHz

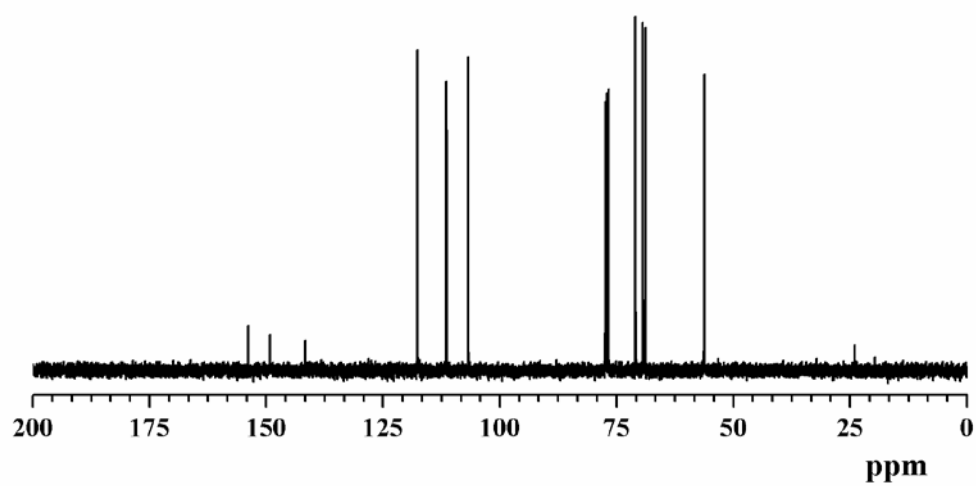


Figure A31 ^{13}C -NMR spectrum of **8** in CDCl_3 at 100 MHz

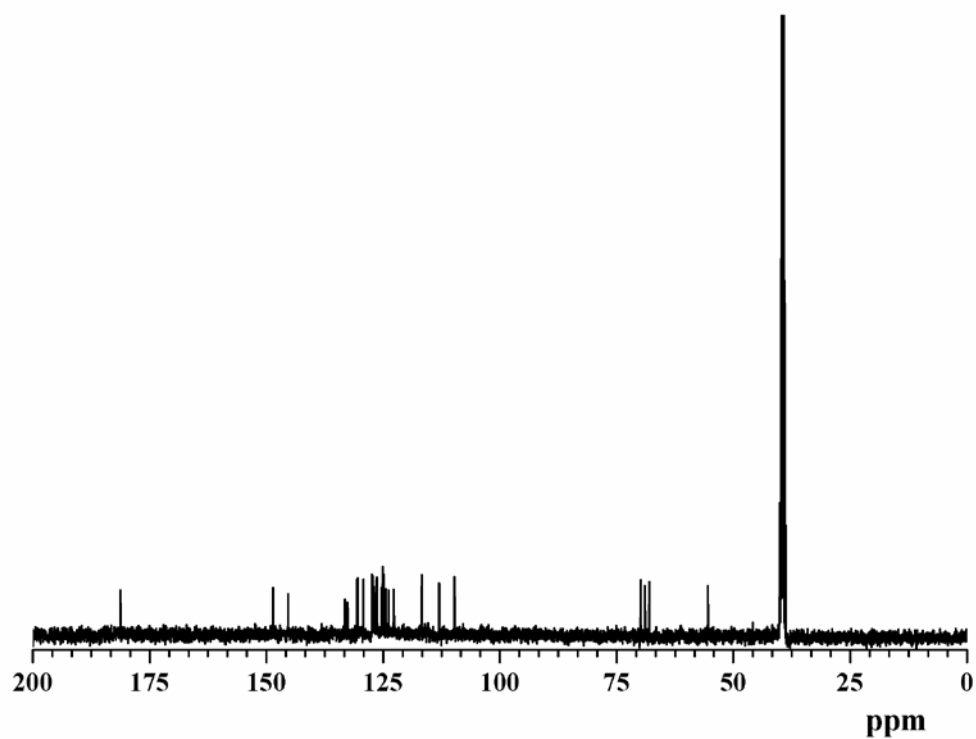


Figure A32 ^{13}C -NMR spectrum of **L2** in $d_6\text{-DMSO}$ at 100 MHz

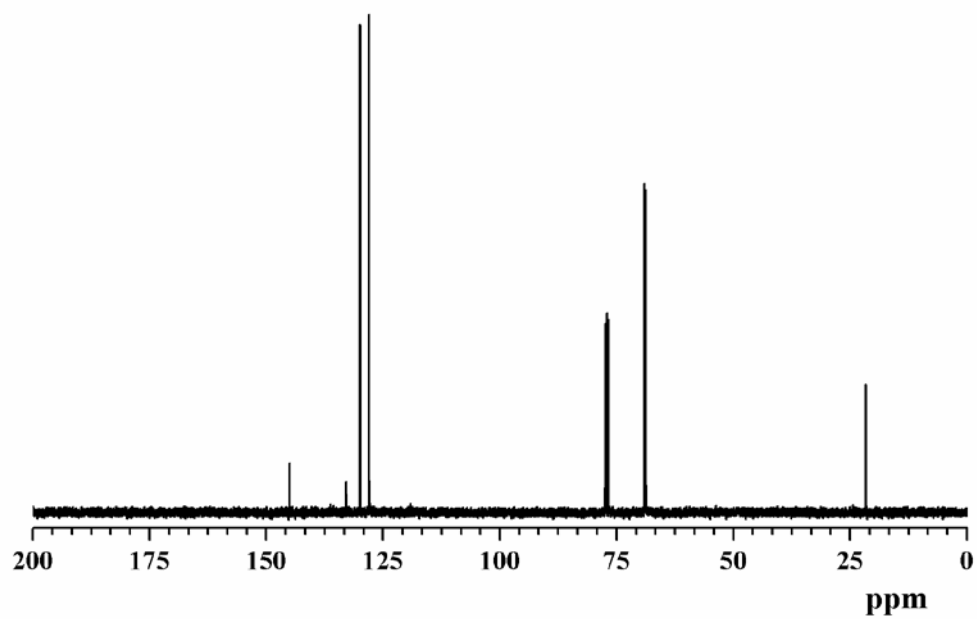


Figure A33 ^{13}C -NMR spectrum of **10** in CDCl_3 at 100 MHz

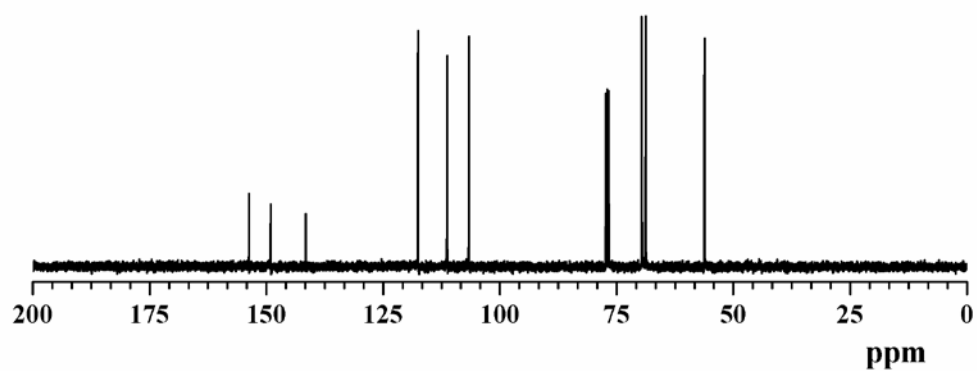


Figure A34 ^{13}C -NMR spectrum of **11** in CDCl_3 at 100 MHz

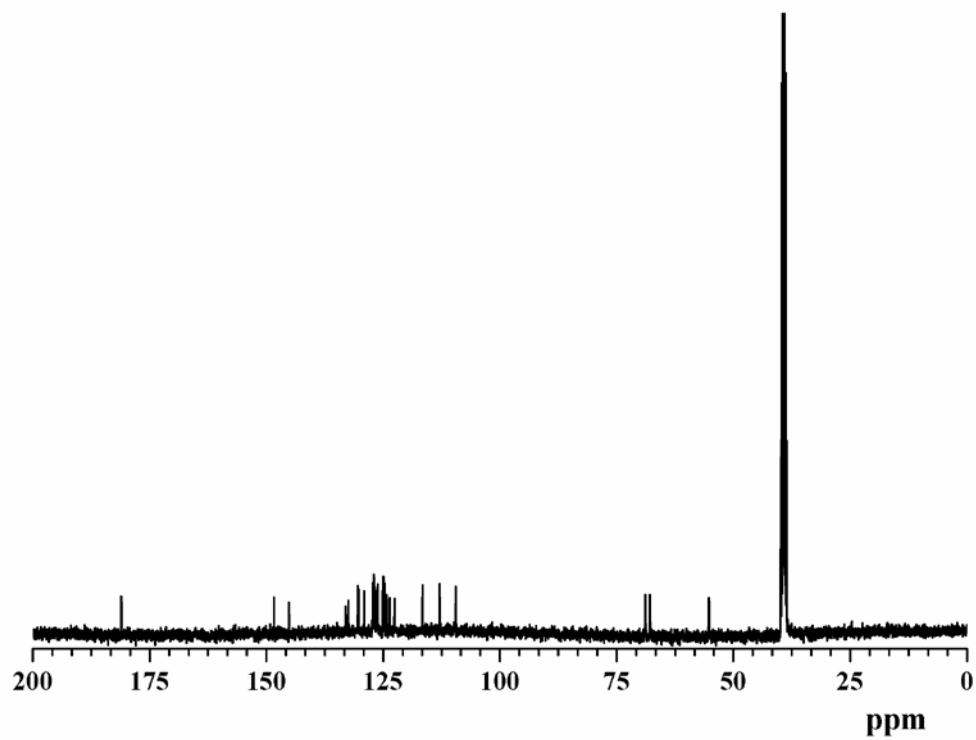


Figure A35 ^{13}C -NMR spectrum of **L3** in d_6 -DMSO at 100 MHz

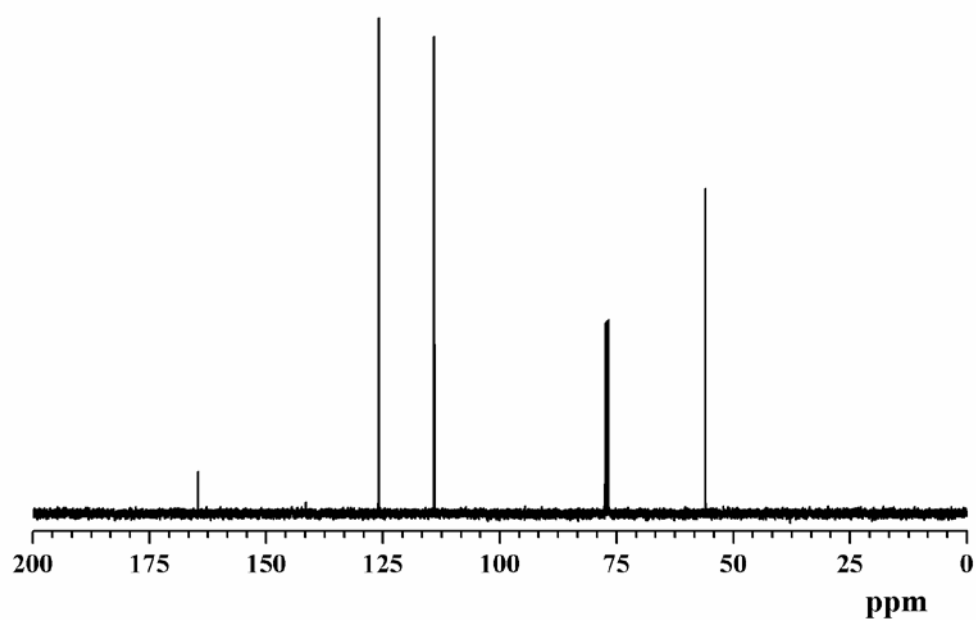


Figure A36 ^{13}C -NMR spectrum of **13** in CDCl_3 at 100 MHz

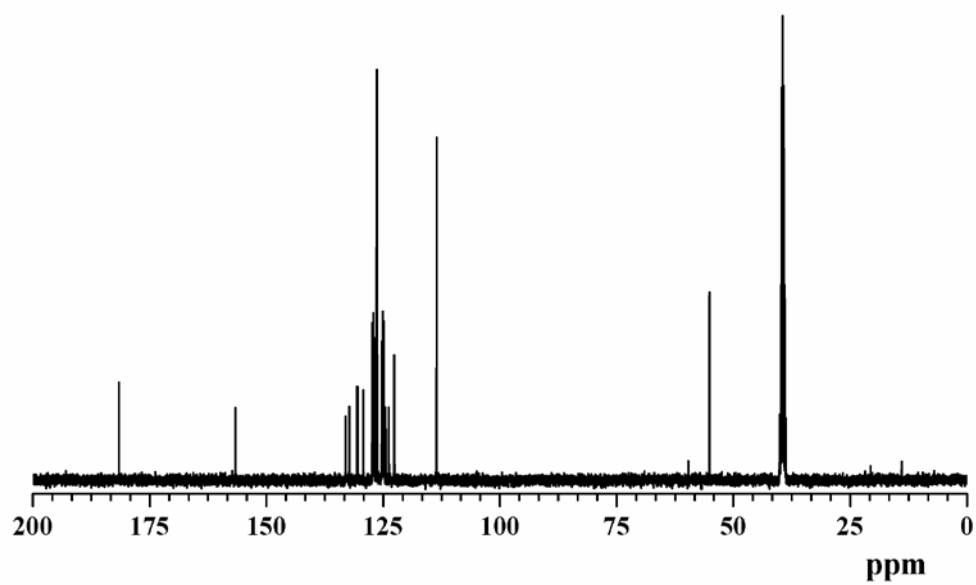


Figure A37 ^{13}C -NMR spectrum of **L4** in d_6 -DMSO at 100 MHz

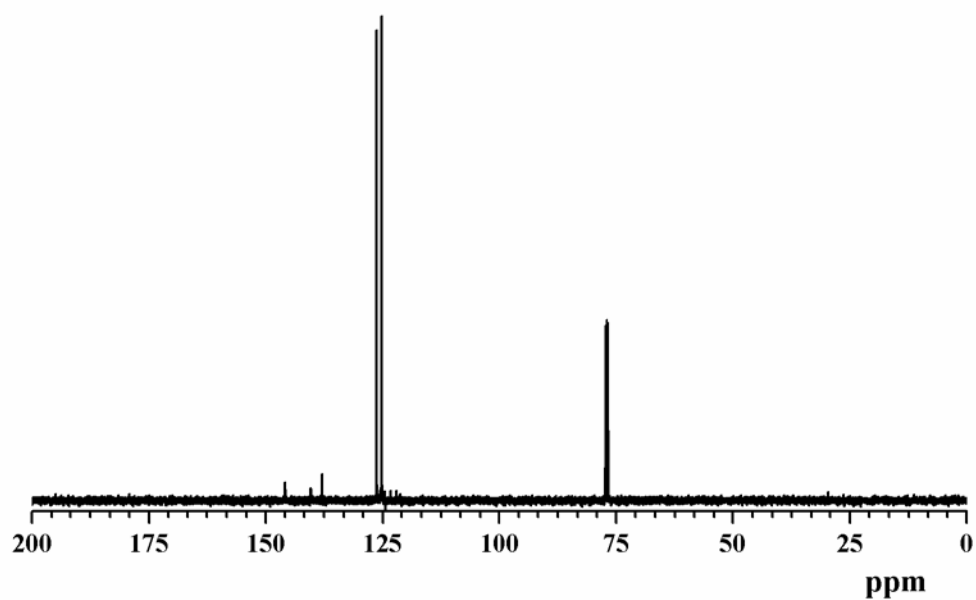


Figure A38 ^{13}C -NMR spectrum of **15** in CDCl_3 at 100 MHz

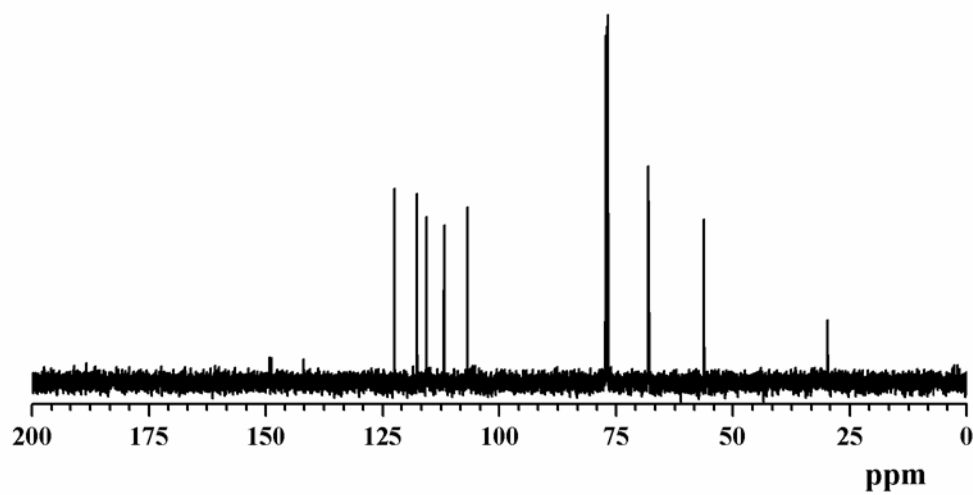


Figure A39 ^{13}C -NMR spectrum of **18** in CDCl_3 at 100 MHz

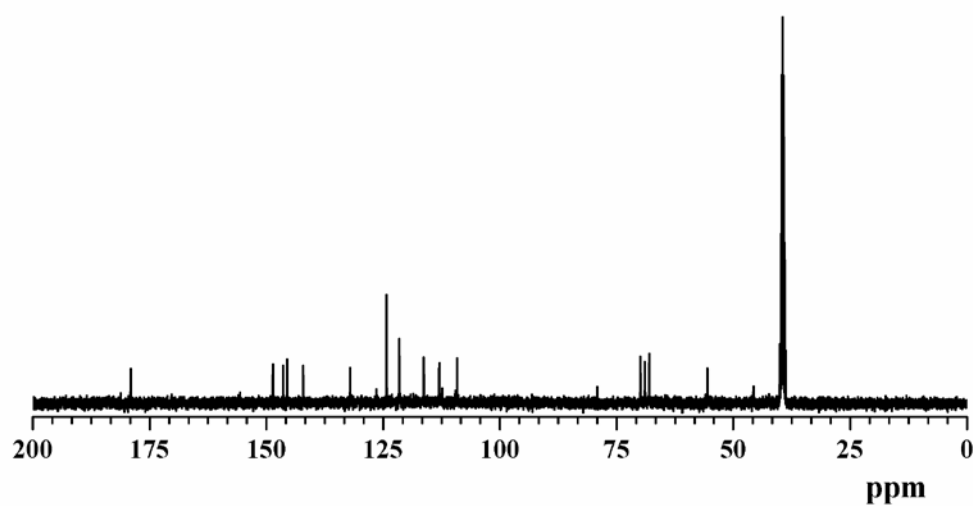


Figure A40 ^{13}C -NMR spectrum of **R2** in $d_6\text{-DMSO}$ at 100 MHz

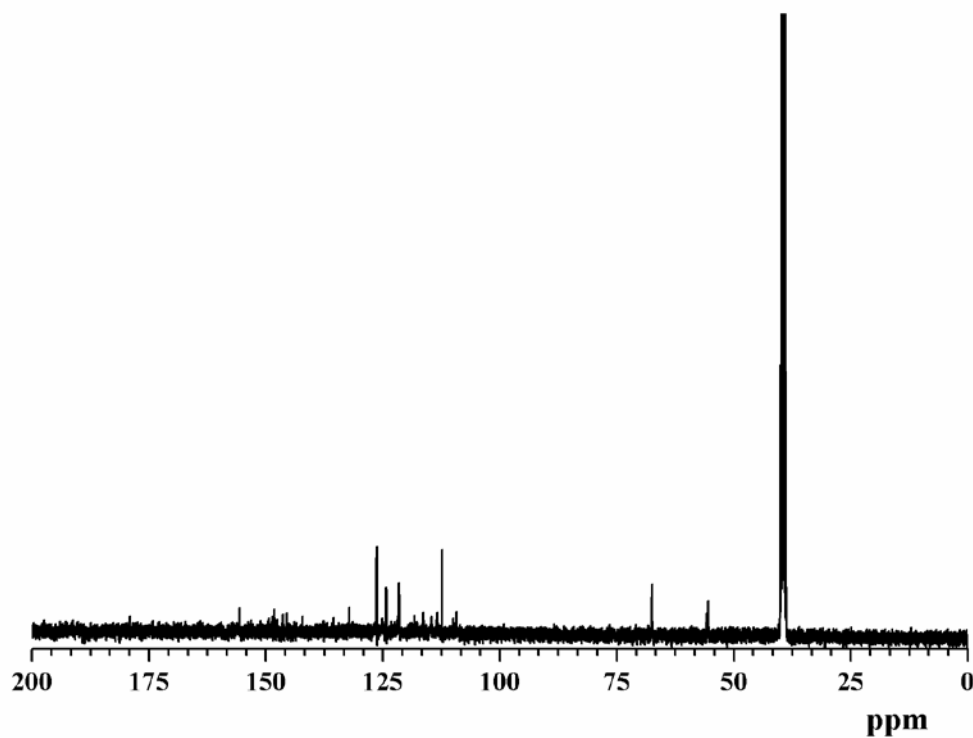


Figure A41 ^{13}C -NMR spectrum of R3 in d_6 -DMSO at 100 MHz

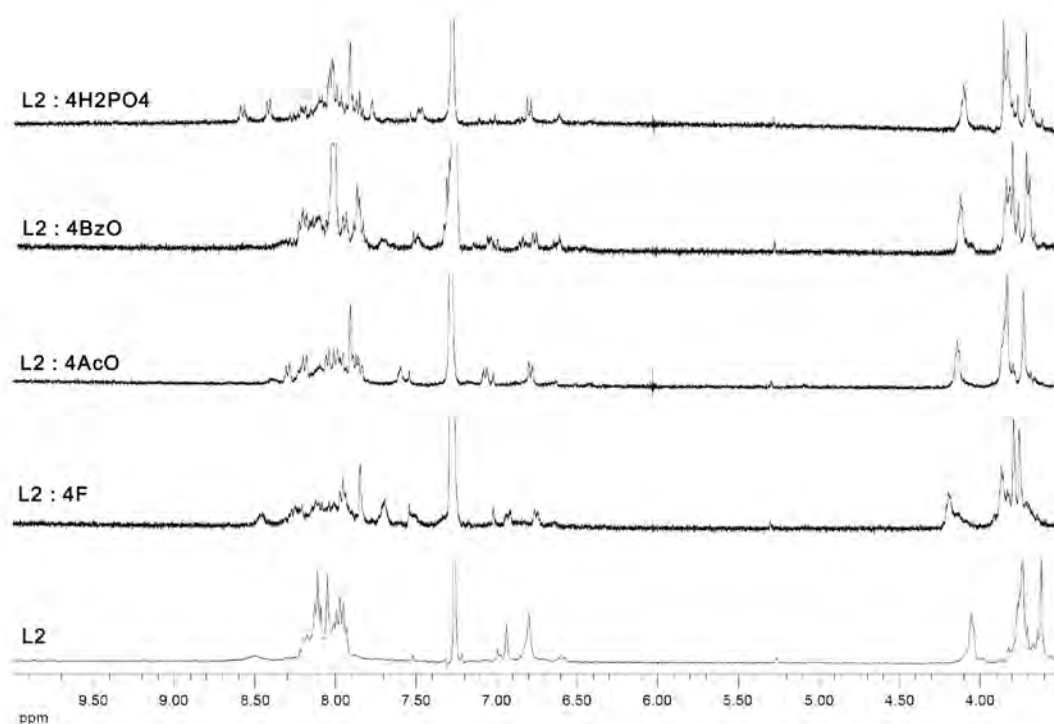


Figure A42 ^1H -NMR spectra of L2 with various TBA anions in CDCl_3 at 400 MHz

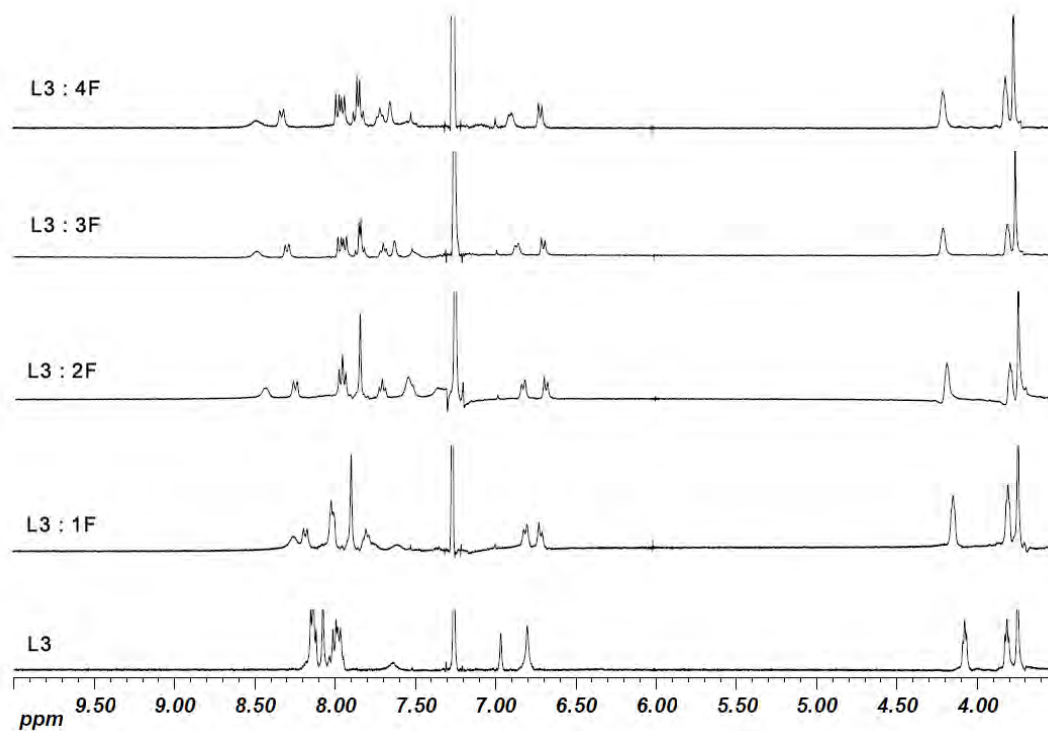


Figure A43 ¹H-NMR spectra of **L3** with various TBA anions in CDCl₃ at 400 MHz

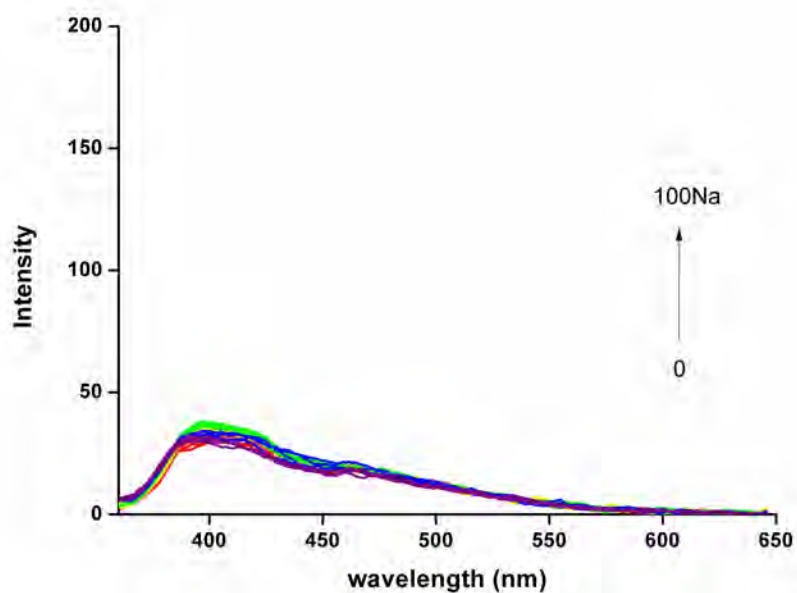


Figure A44 Fluorescence titration spectra of **L1** (5.0×10^{-6} M) with Na⁺ in CHCl₃/CH₃CN

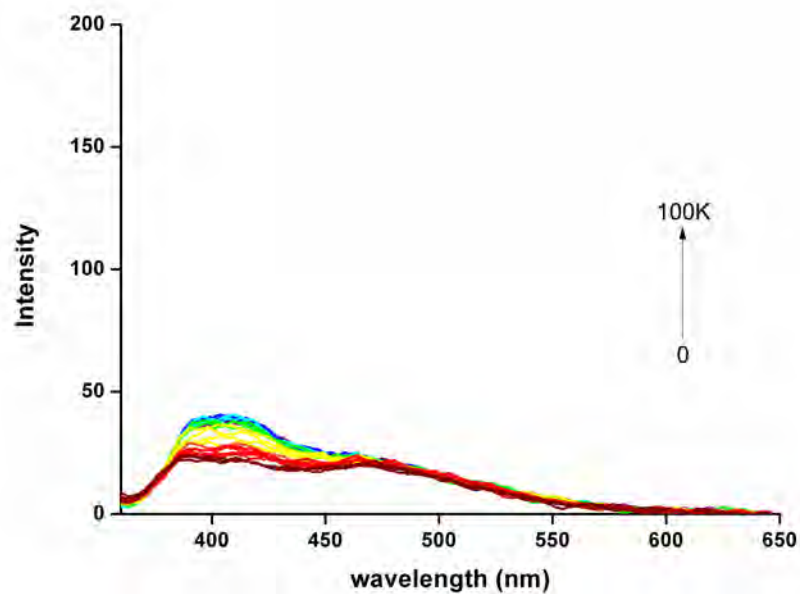


Figure A45 Fluorescence titration spectra of **L1** (5.0×10^{-6} M) with K^+ in $CHCl_3/CH_3CN$

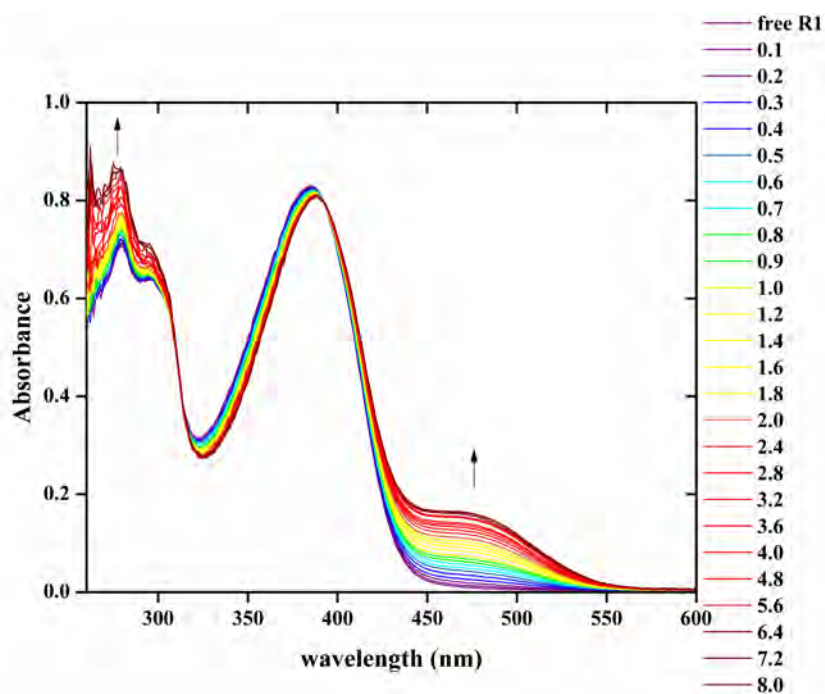


Figure A46 UV-vis titration spectra of **R1** (2.5×10^{-5} M) with BzO^- in DMSO

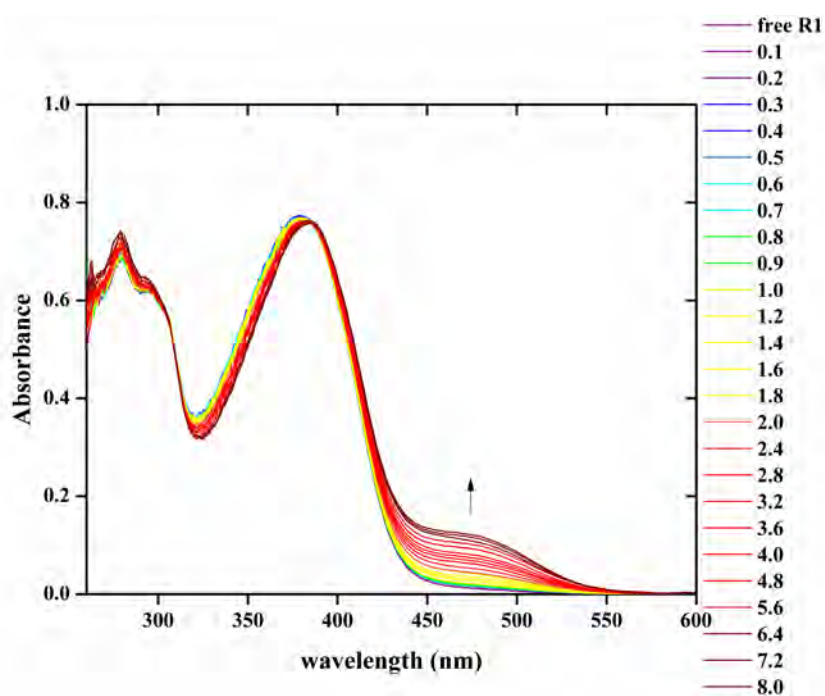


Figure A47 UV-vis titration spectra of R1 (2.5×10^{-5} M) with H_2PO_4^- in DMSO

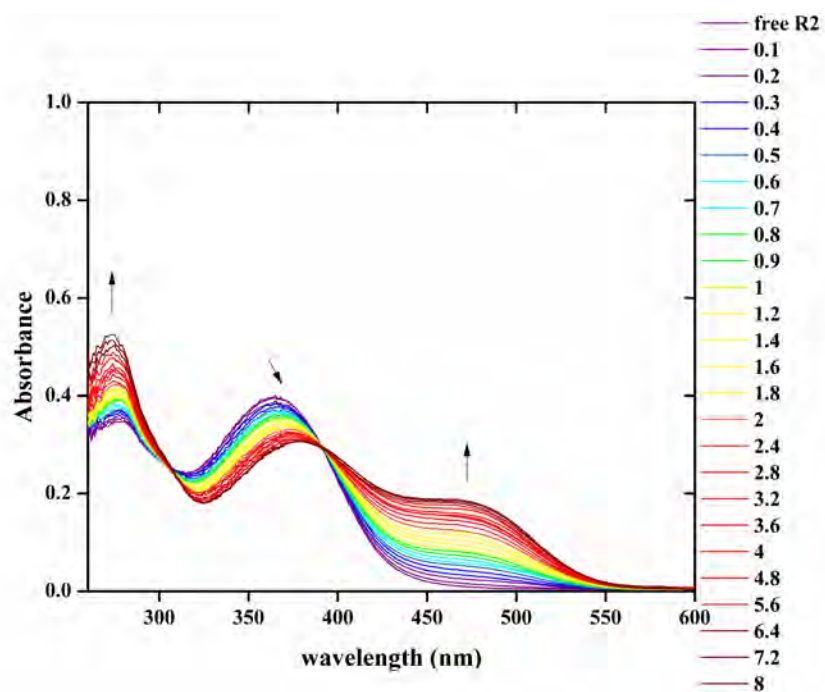


Figure A48 UV-vis titration spectra of R2 (2.5×10^{-5} M) with BzO^- in DMSO

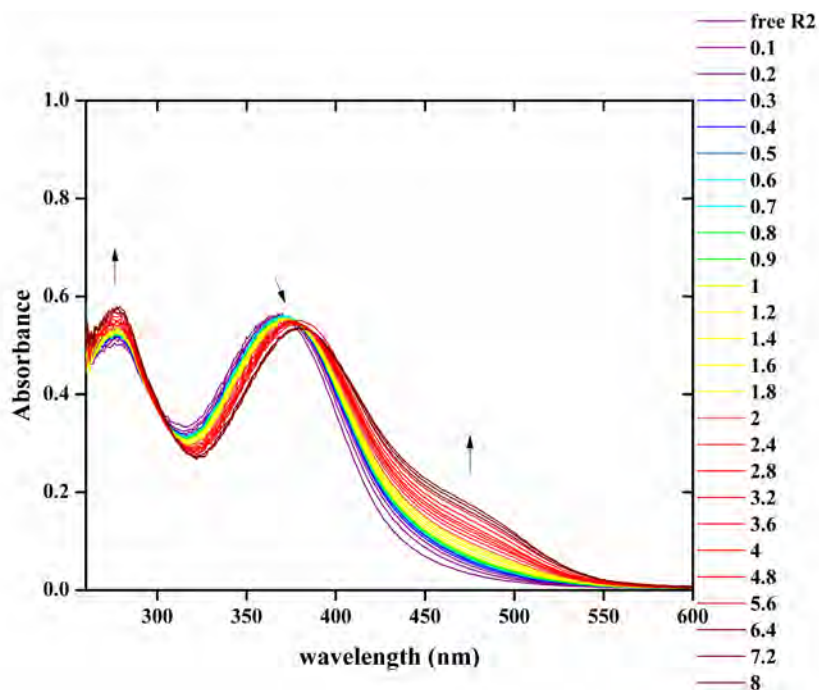


Figure A49 UV-vis titration spectra of **R2** (2.5×10^{-5} M) with H_2PO_4^- in DMSO

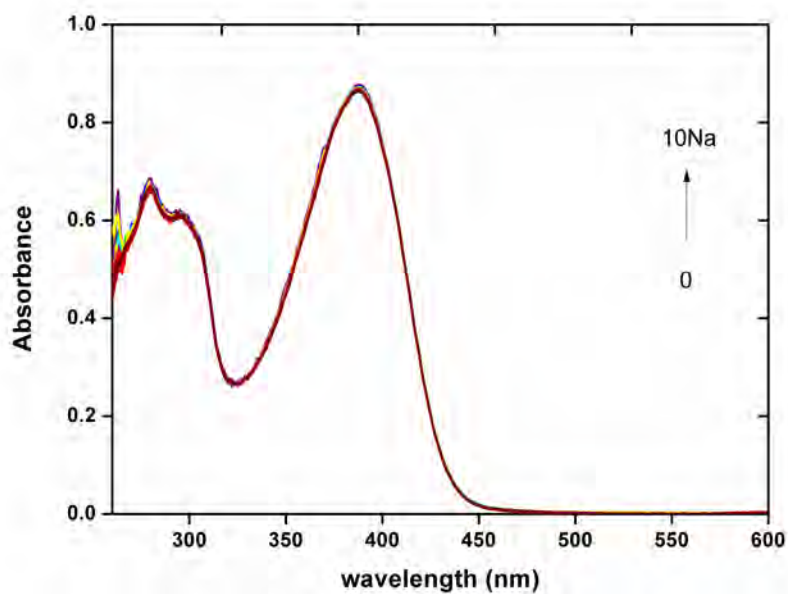


Figure A50 UV-vis titration spectra of **R1** (2.5×10^{-5} M) with Na^+ in DMSO

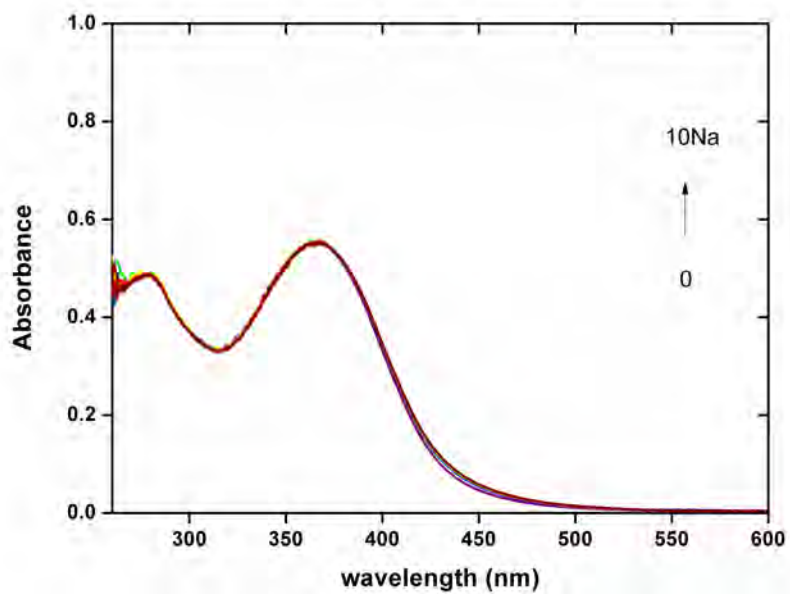


Figure A51 UV-vis titration spectra of **R2** (2.5×10^{-5} M) with Na^+ in DMSO

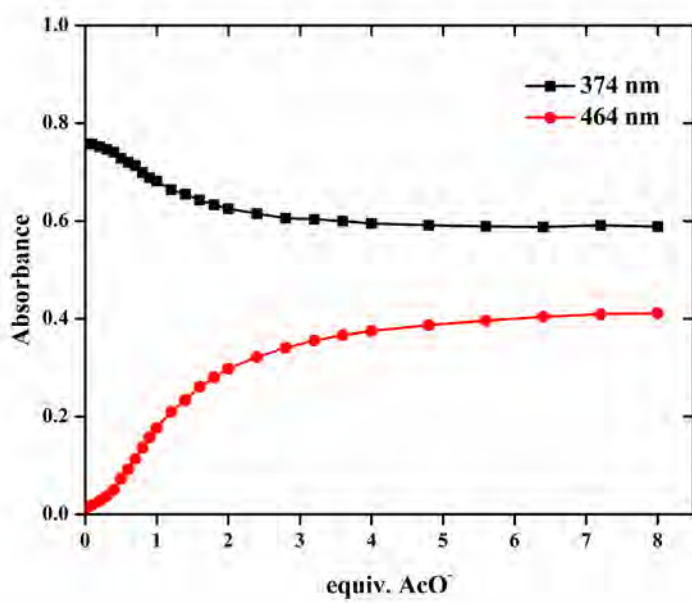


Figure A52 Titration profile of **R1·AcO⁻** at the wavelength 374 nm and 464 nm

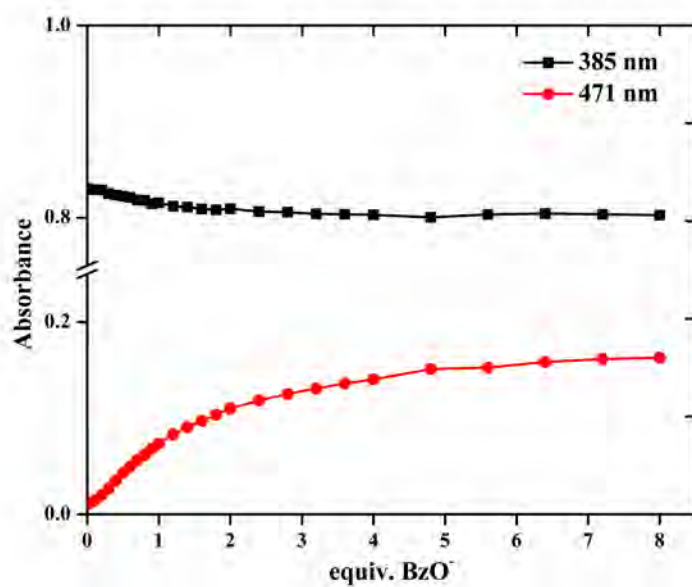


Figure A53 Titration profile of R1·BzO⁻ at the wavelength 385 nm and 471 nm

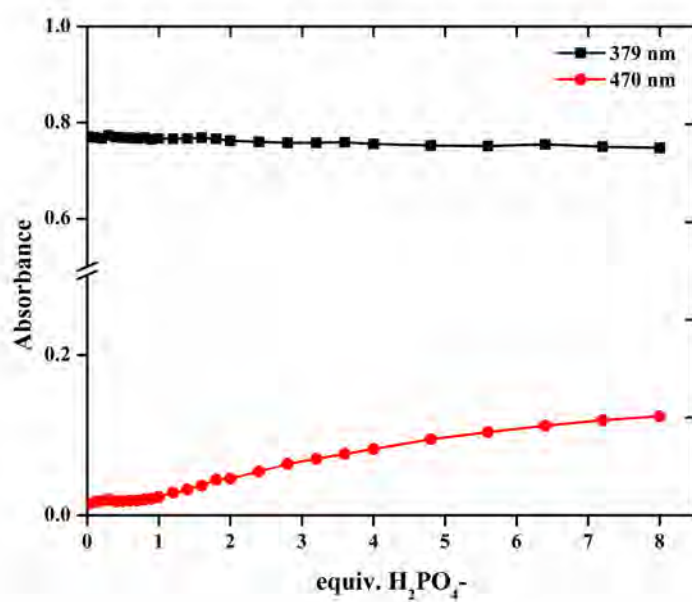


Figure A54 Titration profile of R1·H₂PO₄⁻ at the wavelength 379 nm and 470 nm

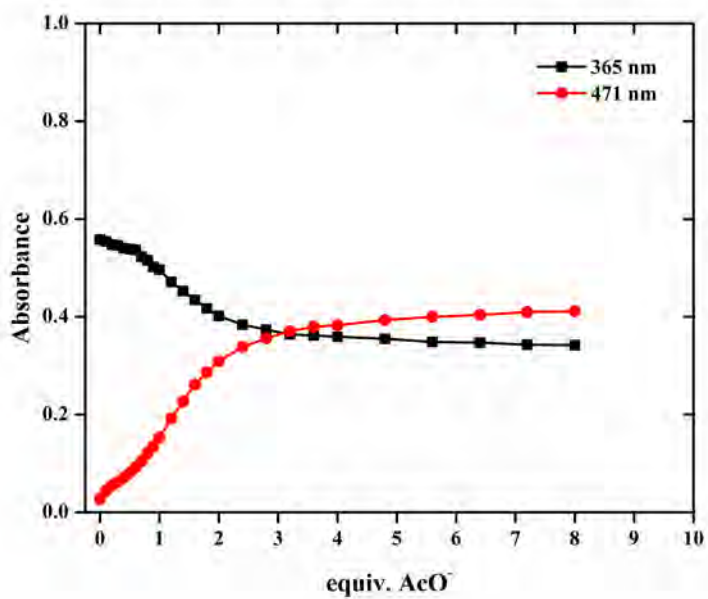


Figure A55 Titration profile of $R2 \cdot AcO^-$ at the wavelength 365 nm and 471 nm

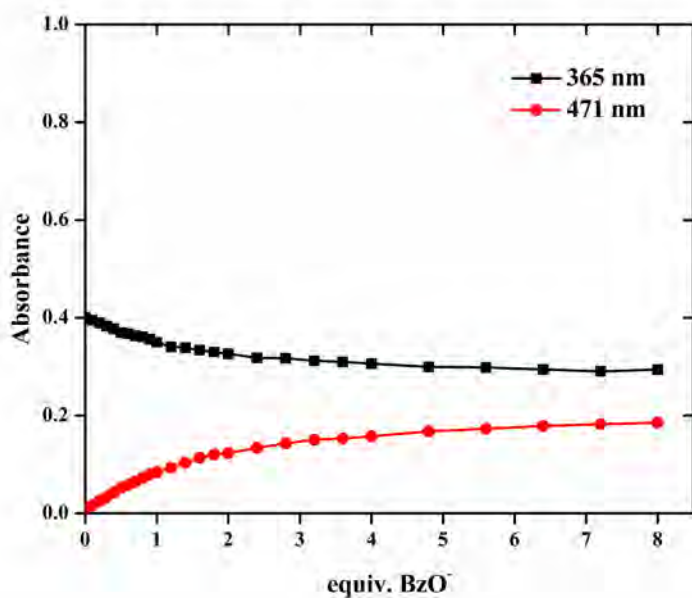


Figure A56 Titration profile of $R2 \cdot BzO^-$ at the wavelength 365 nm and 471 nm

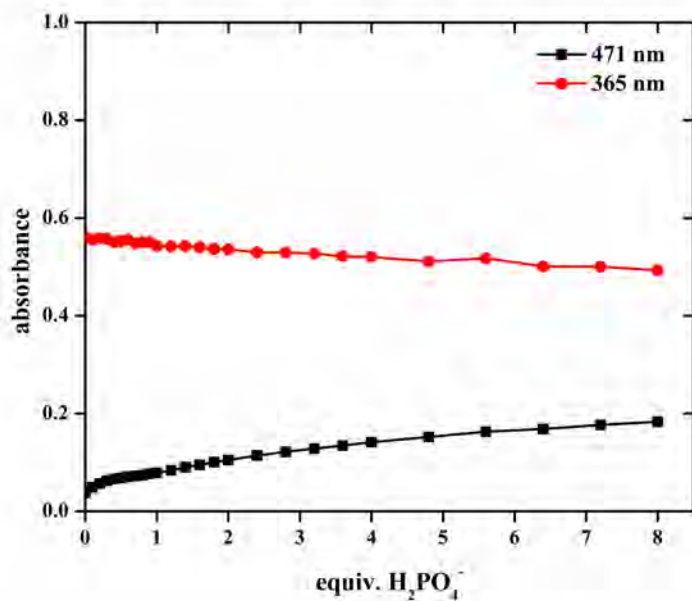


Figure A57 Titration profile of $\text{R2}\cdot\text{H}_2\text{PO}_4^-$ at the wavelength 365 nm and 471 nm

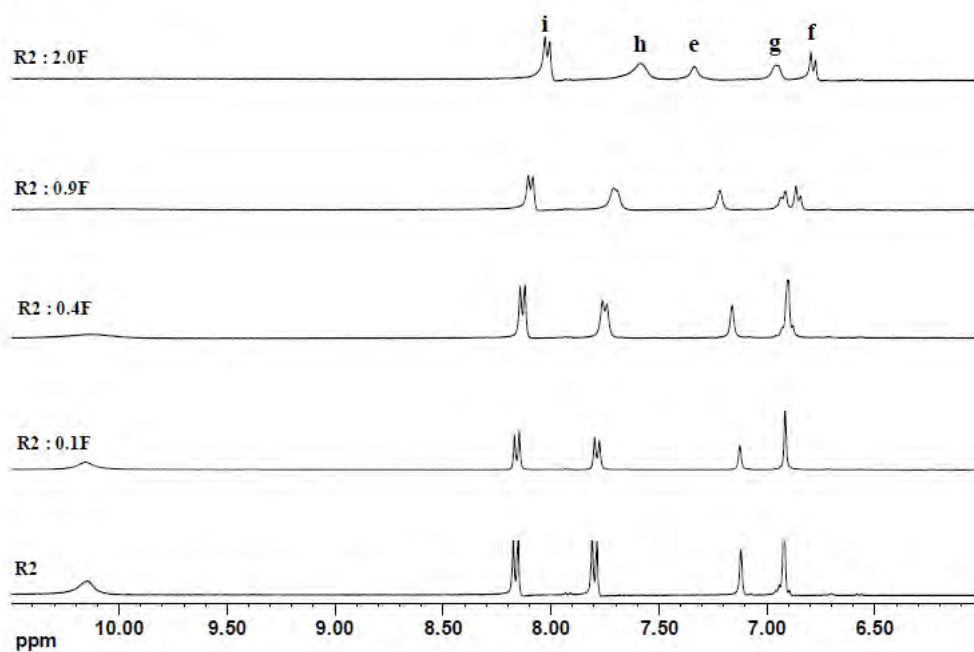


Figure 4.58 ^1H -NMR titration spectra of $\text{R1}\cdot\text{F}$ in d_6 -DMSO at 400 MHz

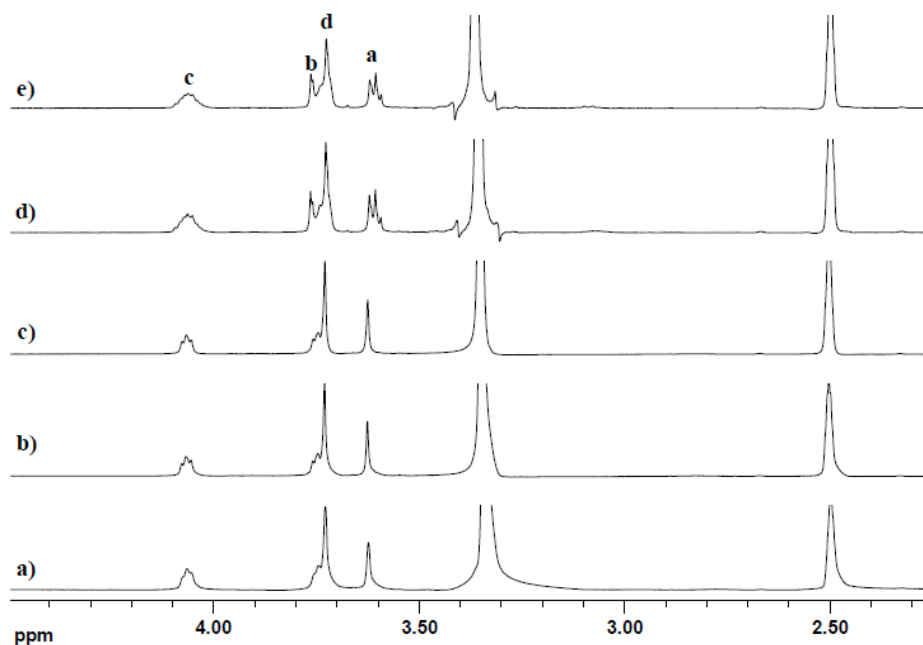


Figure 4.59 ^1H -NMR spectra of a) free **R1** b) **R1** + 2.0 equiv. Na^+ c) **R1** + 4.0 equiv. Na^+ d) **R1** + 4.0 equiv. Na^+ 7 days e) **R1** + 4.0 equiv. Na^+ 8 days in d_6 -DMSO at 400 MHz

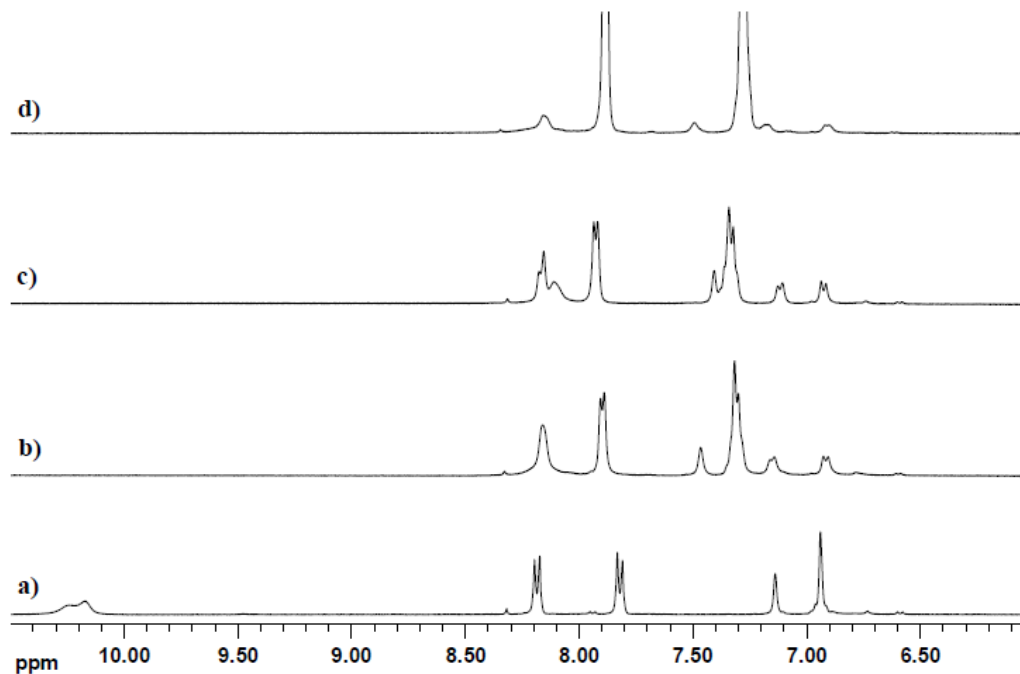


Figure A60 ^1H -NMR spectra of a) free **R1** b) **R2** + 4 equiv. BzO^- c) **R1** + 4 equiv. BzO^- + 10 equiv. Na^+ d) **R1** + 4 equiv. BzO^- + 10 equiv. Na^+ + excess BzO^- in d_6 -DMSO at 400 MHz

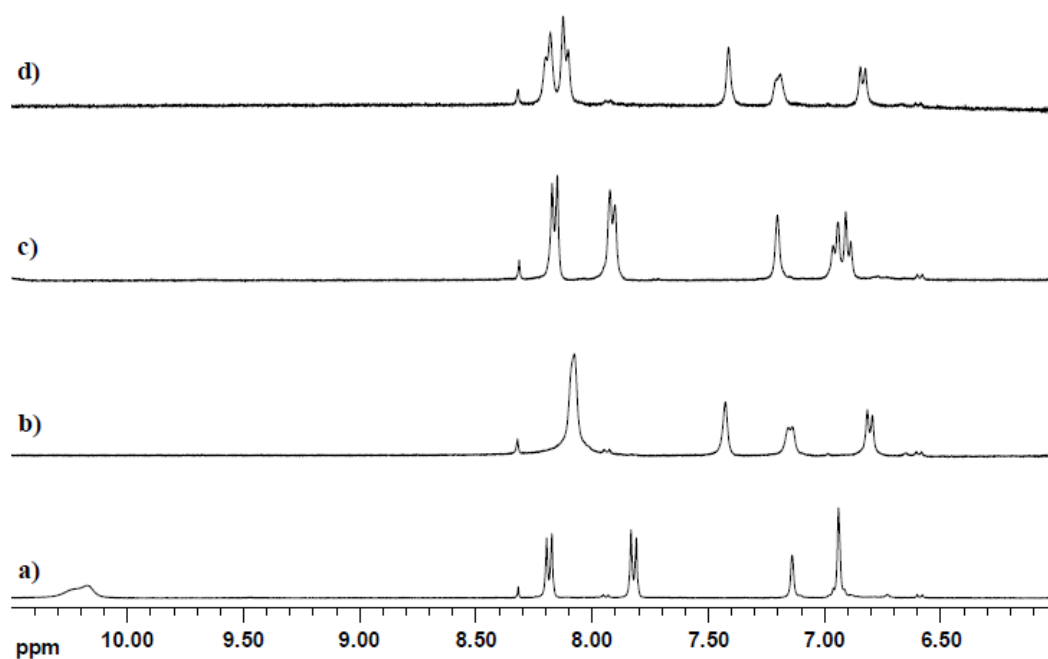


Figure A61 $^1\text{H-NMR}$ spectra of a) free **R1** b) **R1** + 4 equiv. H_2PO_4^- c) **R1** + 4 equiv. H_2PO_4^- + 10 equiv. Na^+ d) **R1** + 4 equiv. H_2PO_4^- + 10 equiv. Na^+ + excess H_2PO_4^- in $d_6\text{-DMSO}$ at 400 MHz

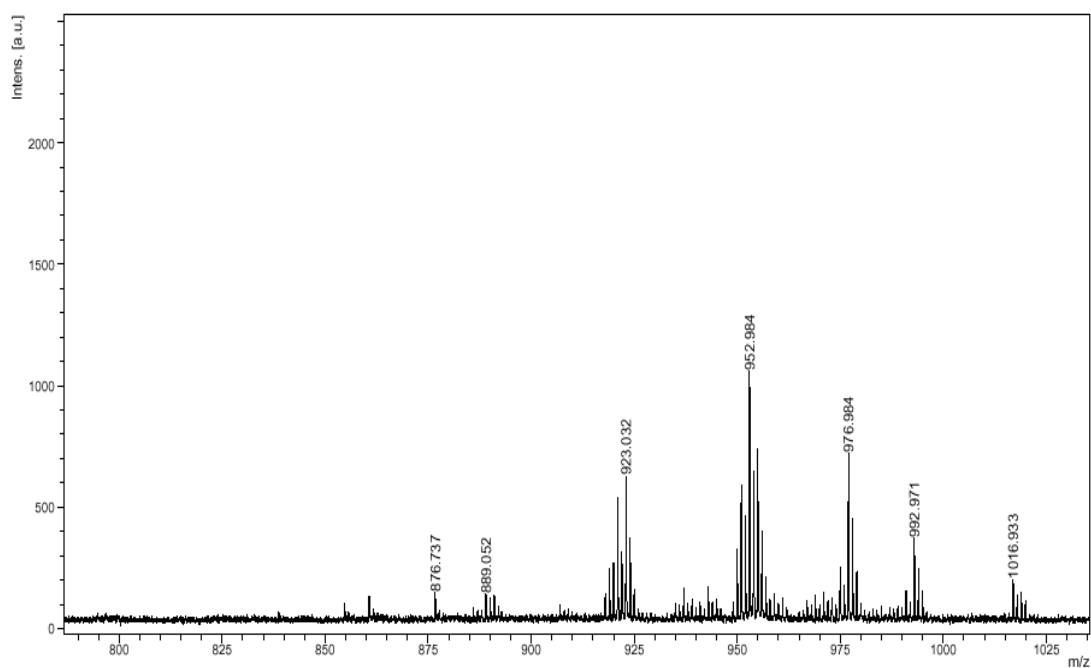


Figure A62 MALDI-TOF mass spectrum of **L1**

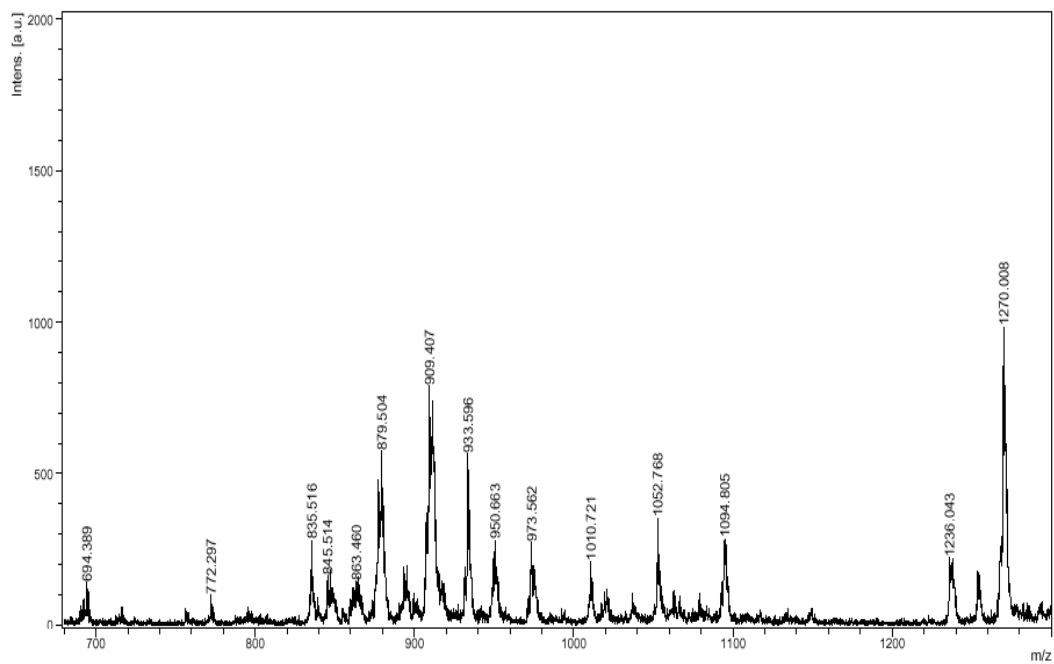


Figure A63 MALDI-TOF mass spectrum of L2

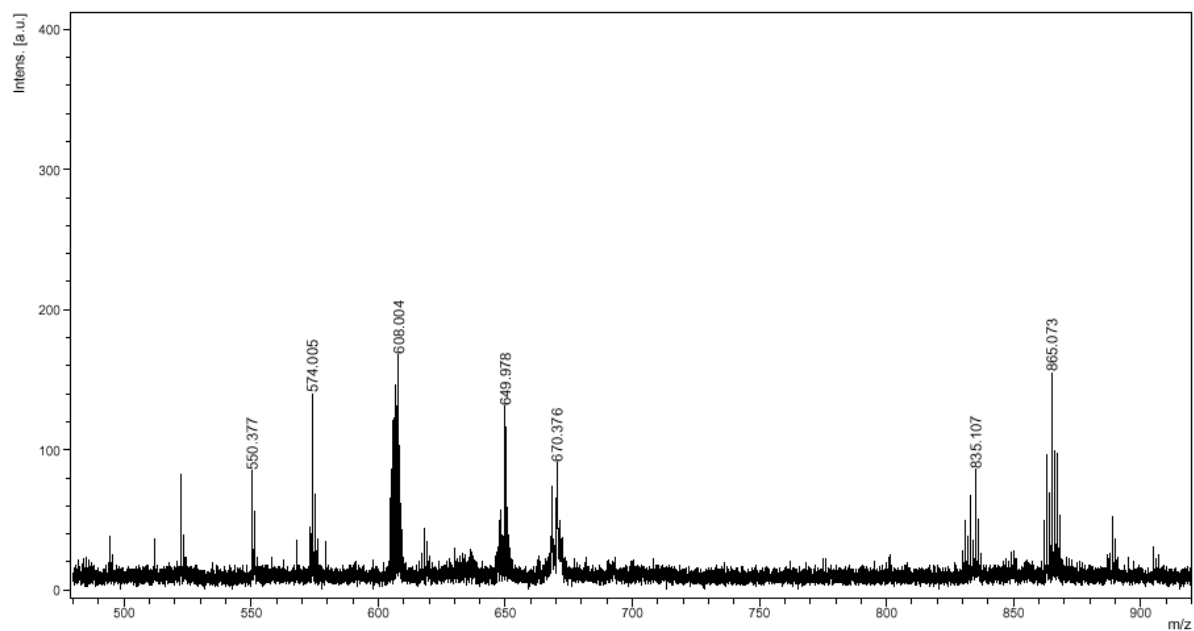


Figure A64 MALDI-TOF mass spectrum of L3

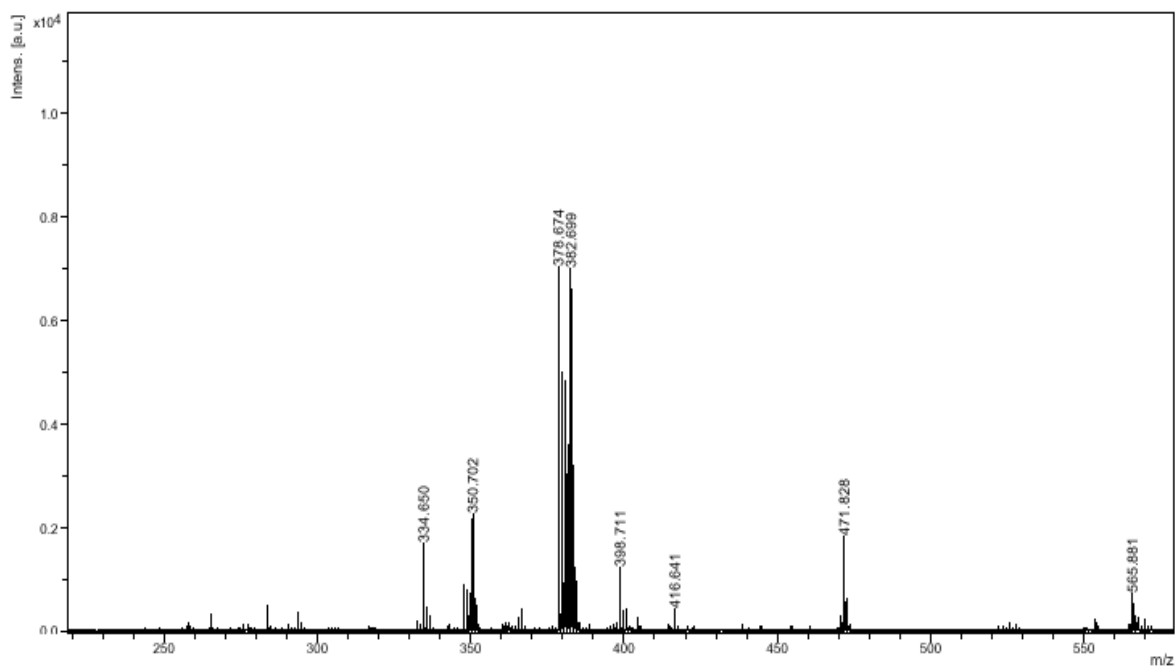


Figure A65 MALDI-TOF mass spectrum of **L4**

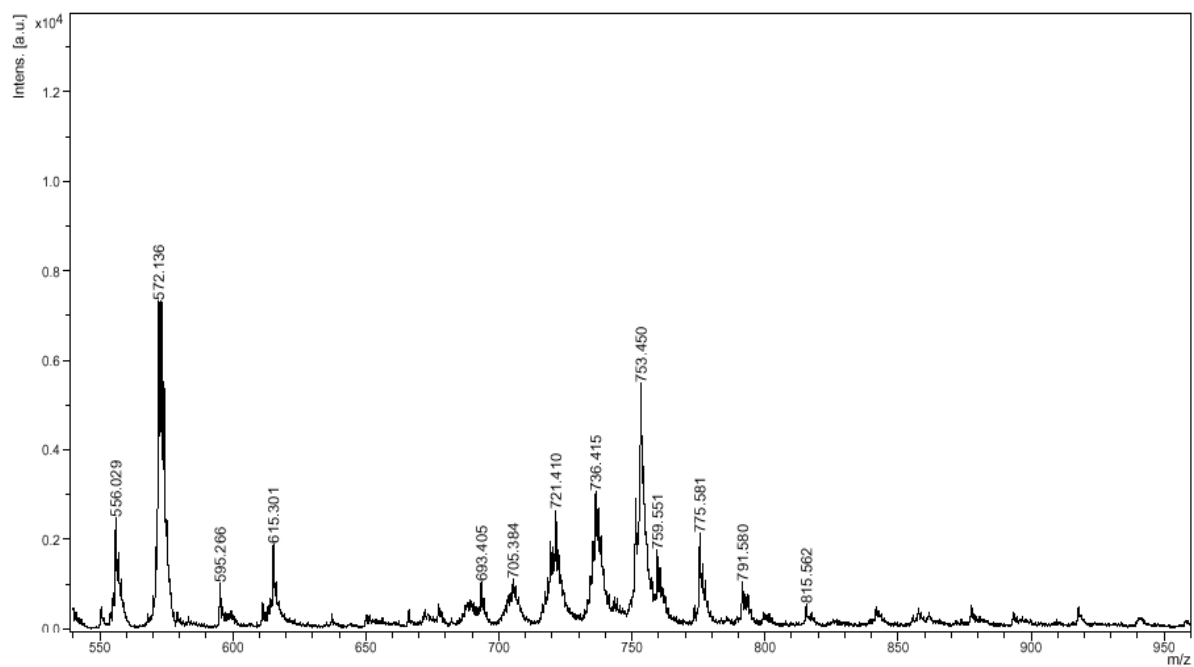


Figure A66 MALDI-TOF mass spectrum of **R1**

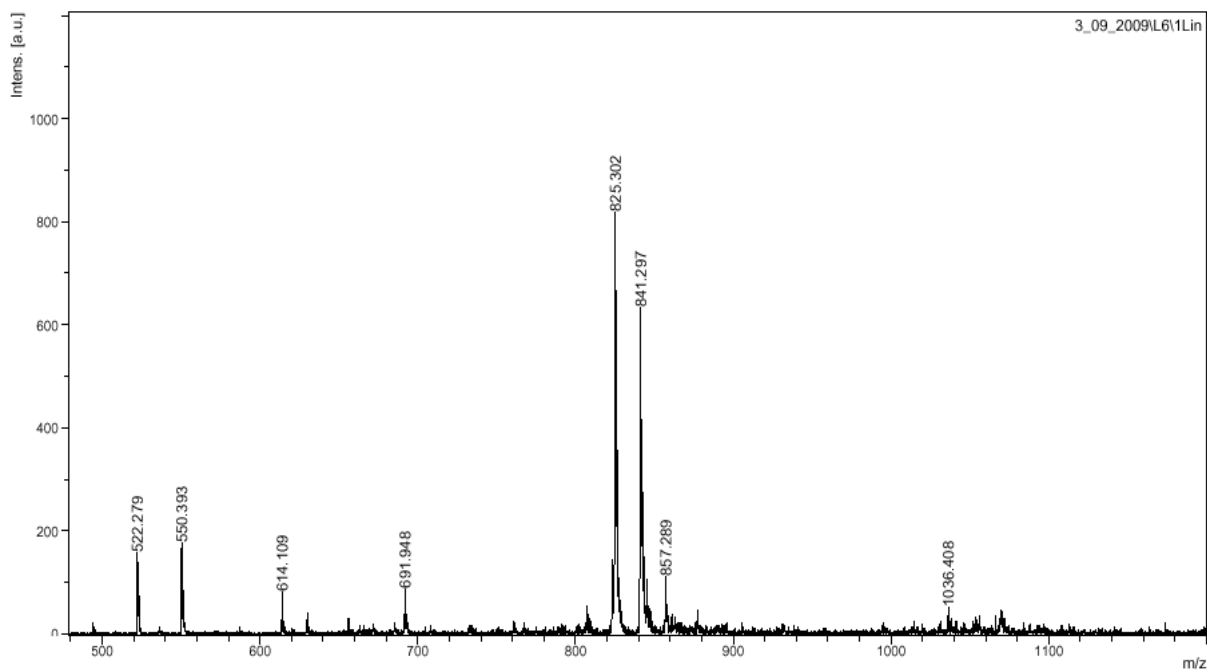


Figure A67 MALDI-TOF mass spectrum of **R2**

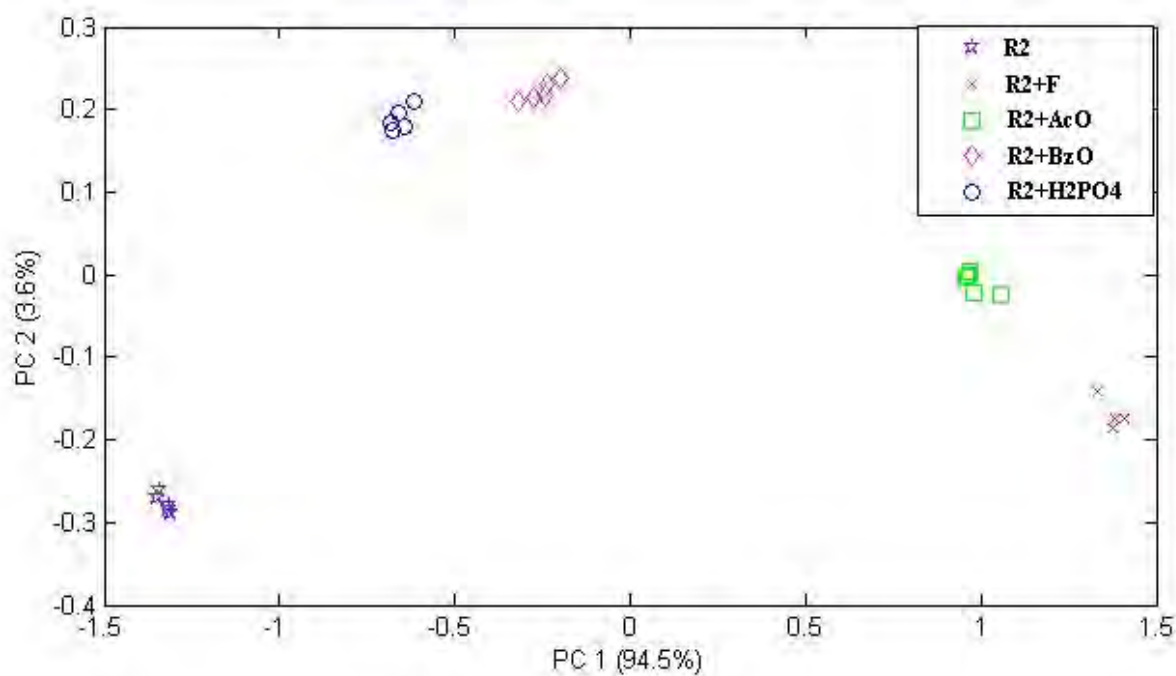


Figure A68 PCA score plot of the first two PCs for 25 samples of **R2** and 4 anions

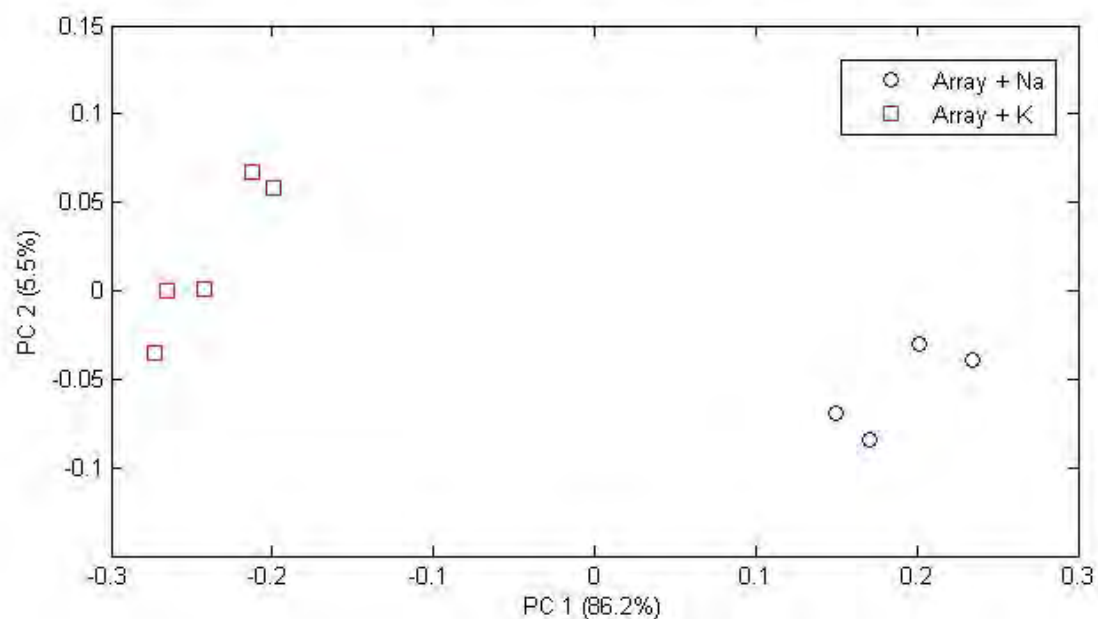


Figure A69 PCA score plot of the first two PCs for 3 sensor arrays ($\mathbf{R2+F^-}$, $\mathbf{R2+AcO^-}$, $\mathbf{R2+H_2PO_4^-}$) and 2 metal ions

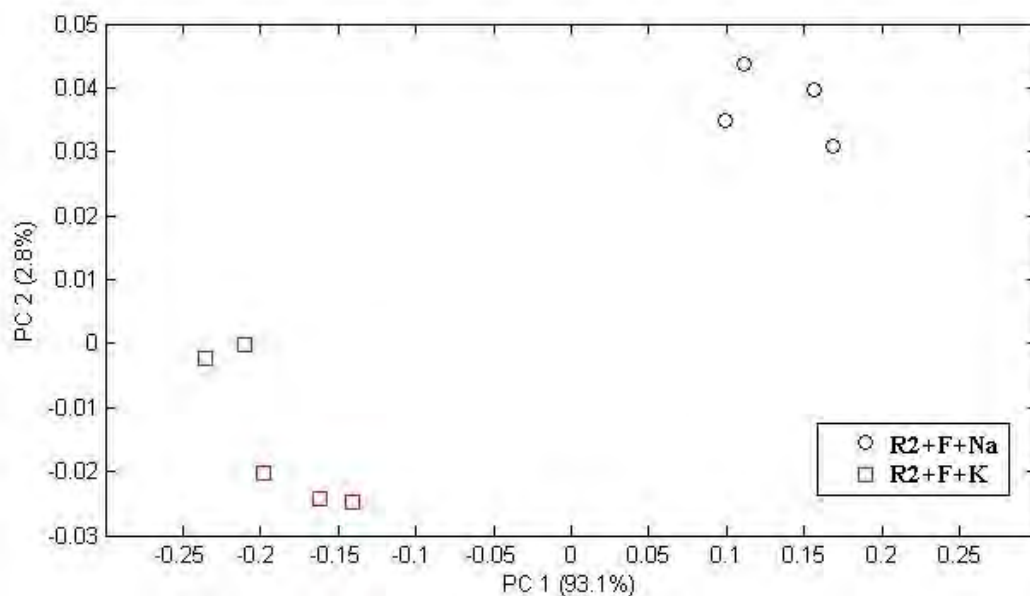


Figure A70 PCA score plot of the first two PCs for 10 samples of $\mathbf{R2 \cdot F^-}$ sensor and 2 metal ions

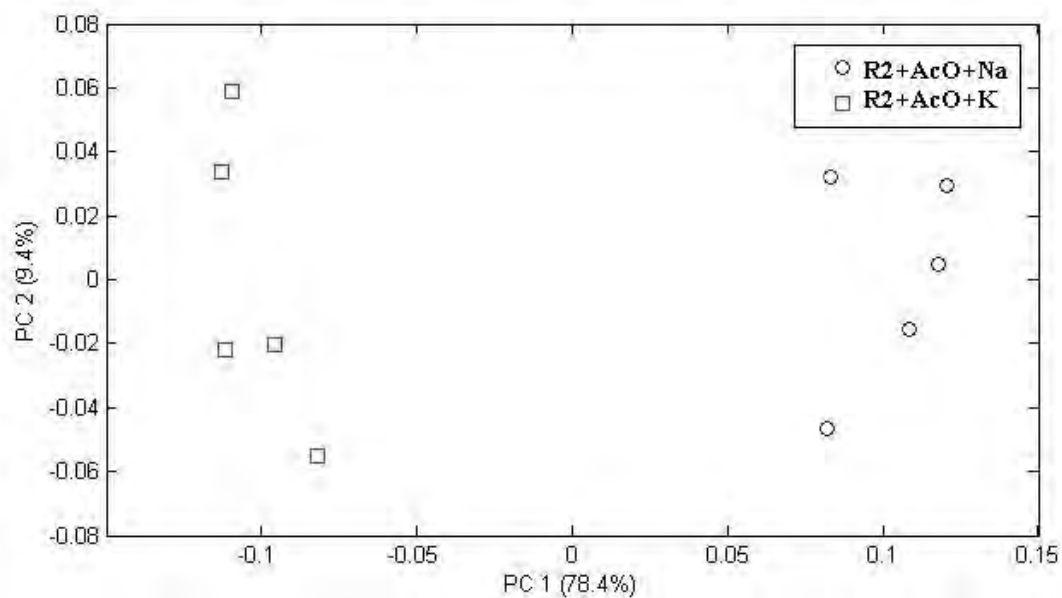


Figure A71 PCA score plot of the first two PCs for 10 samples of R2·AcO⁻ sensor and 2 metal ions

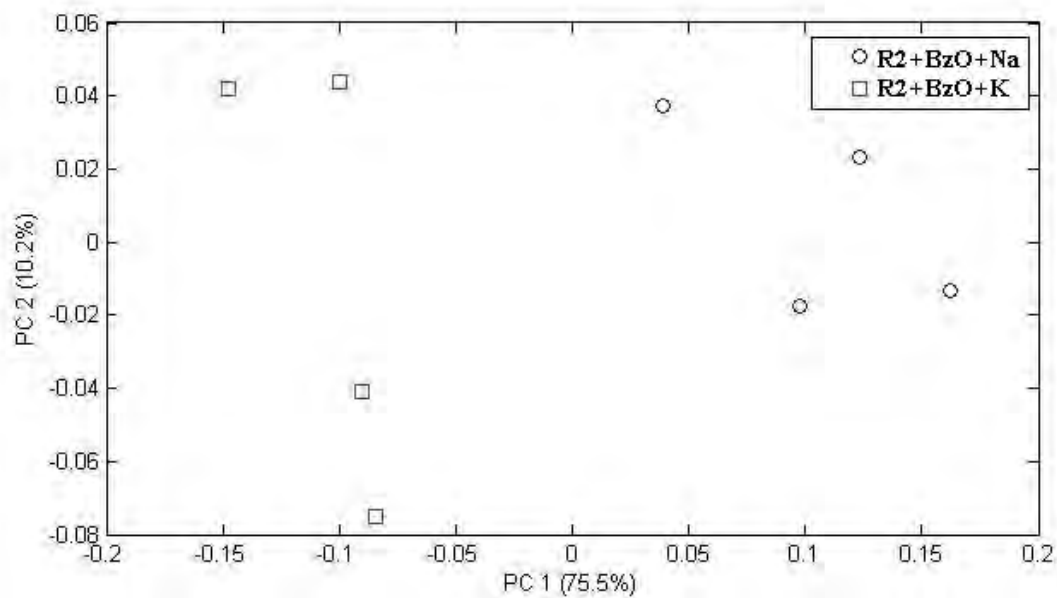


Figure A72 PCA score plot of the first two PCs for 10 samples of R2·BzO⁻ sensor and 2 metal ions

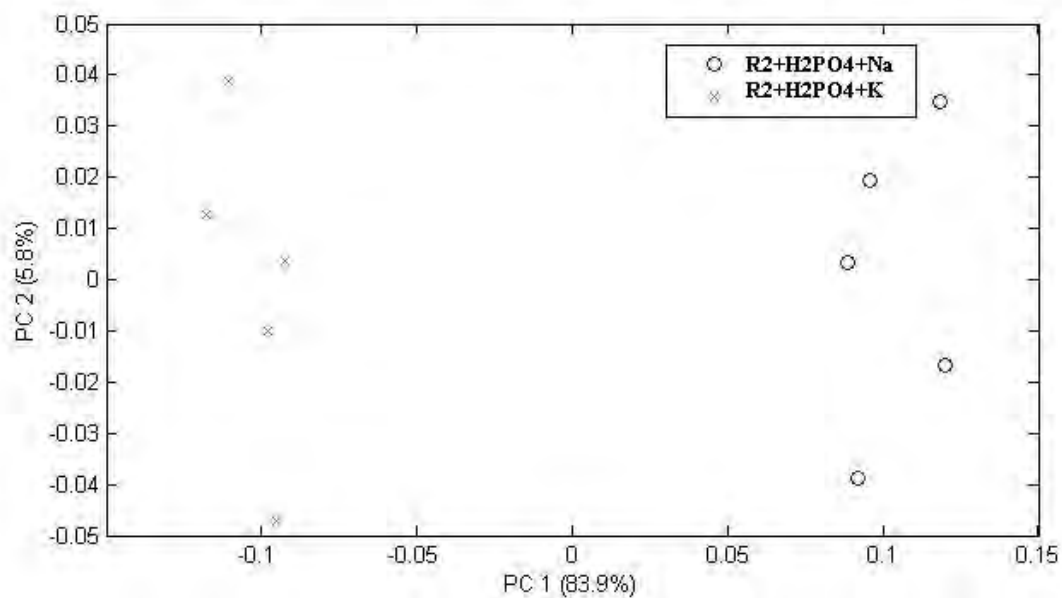


Figure A73 PCA score plot of the first two PCs for 10 samples of $R2 \cdot H_2PO_4^-$ sensor and 2 metal ions

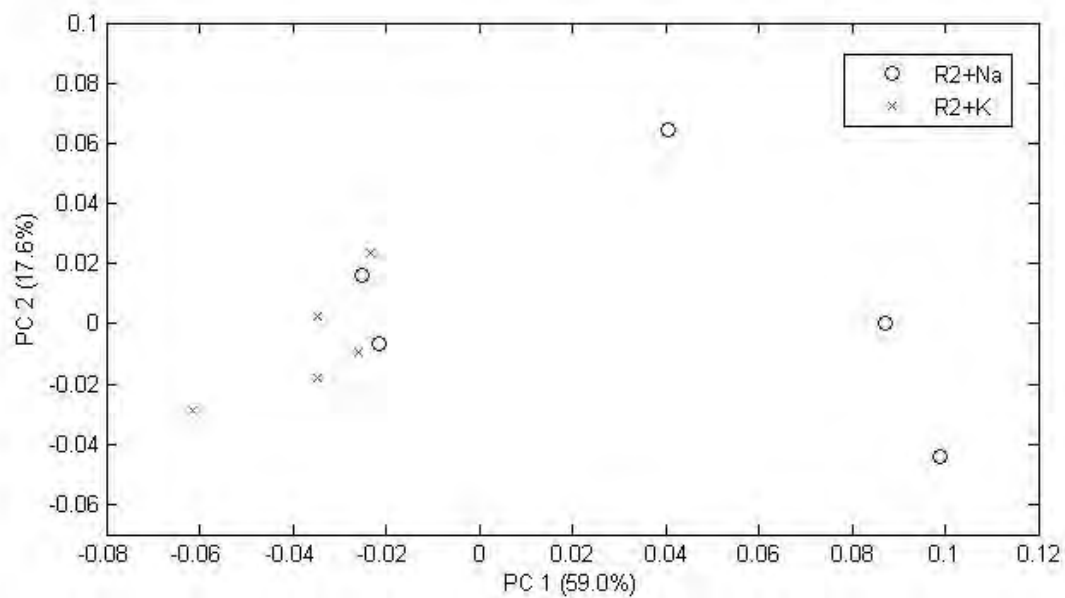


Figure A74 PCA score plot of the first two PCs for 10 samples of $R2$ and 2 metal ions

VITAE

Name: Miss Duangrat Thongkum

Date of Birth: September 19, 1979

Education:

- 2011 (being pursued) Ph.D. Candidate in Inorganic Chemistry
Chulalongkorn University, Bangkok, Thailand
Dissertation: Fluorescent sensors from pyrene excimer formation and colorimetric sensors from nitrobenzene for anion detection
Research Advisor: Prof. Dr. Thawatchai Tuntulani
- 2004 M.S. in Inorganic Chemistry
Prince of Songkla University, Songkla, Thailand
Dissertation: Synthesis and characterization of Ruthenium (II) complexes with 2-(phenylazo) pyrazine ligands
Research Advisor: Dr. Kanidtha Hansongnern
- 2002 B.S. in Chemistry
Prince of Songkla University, Songkla, Thailand

Professional experience: Inorganic Chemistry: Supramolecular Devices based on macrocyclic compounds

Grants:

- 2003 – 2004 Postgraduate Education and Research Program in Chemistry (PERCH)
- 2006 Teaching Assistant, Department of Chemistry, Faculty of Science, Chulalongkorn University
- 2006 – 2009 Commission on Higher Education

Presentations:

1. Synthesis of fluorescent chemosensors for detection of fluoride ion, **Oral presentation** in Commission on Higher Education Congress I University Staff Development Consortium, 5 – 7 September 2008, Ambassador City Jomtien Pattaya Chonburi.
2. Selective fluoride ion sensor based on pyrene excimer formation, **Oral presentation** in 34th Congress on Science and Technology of Thailand, 31 October – 2 November 2008, Queen Sirikit National Convention Center Bangkok.
3. Design and synthesis of pseudocyclic crown ethers as efficient fluorescence sensors for fluoride, **Oral presentation** in Pure and Applied Chemistry International Conference 2010, 21 – 23 January 2010, Sunee Grand Hotel and Convention Center Ubonratchathani.